UNIVERSITAT POLITÈCNICA
DE CATALUNYA
BARCELONATECH

# *Impact of solar PV plants with synchronous power controllers on power system stability*

**Daniel Remón Rodríguez**

Universidad del País Vasco Euskal Herriko Unibertsitatea



# PhD Thesis

# Impact of Solar PV Plants with Synchronous Power Controllers on Power System Stability

*Daniel Remón Rodríguez*

Barcelona, April 2017

# Impact of Solar PV Plants with Synchronous Power Controllers on Power System Stability

*Daniel Remón Rodríguez*

Dissertation submitted to the Doctorate Office of the Universitat Politècnica de Catalunya in partial fulfillment of the requirements for the degree of Doctor of Philosophy by the

**UNIVERSIDAD DE MÁLAGA**

**UNIVERSIDAD DE SEVILLA**

**UNIVERSIDAD DEL PAÍS VASCO/EUSKAL ERRIKO UNIBERTSITATEA**

**UNIVERSITAT POLITÈCNICA DE CATALUNYA**

**Joint Doctoral Programme in Electric Energy Systems**

Barcelona, April 2017

Impact of Solar PV Plants with Synchronous Power Controllers on Power System Stability


Printed by the UPC
Barcelona, April 2017

ISBN: –
Research Project: ENE2014-60228-R

UNIVERSITAT POLITÈCNICA DE CATALUNYA
Escola de Doctorat
Edifici Vèrtex. Pl. Eusebi Güell, 6
08034 Barcelona
Web: http://www.upc.edu

UNIVERSIDAD DE MÁLAGA
Escuela de Doctorado
Pabellón de Gobierno - Plaza el Ejido, s/n
29013 Málaga
Web: http://www.uma.es

UNIVERSIDAD DE SEVILLA
Escuela Internacional de Doctorado
Pabellón de México - Paseo de las Delicias, s/n
41013 Sevilla
Web: http://www.us.es

UNIVERSIDAD DEL PAÍS VASCO/EUSKAL ERRIKO UNIBERTSITATEA
Escuela de Máster y Doctorado
Edificio Aulario II - Barrio Sarriena, s/n
48940 Leioa (Bizkaia)
Web: http://www.ehu.eus/es

UNIVERSITAT POLITÈCNICA DE CATALUNYA
BARCELONATECH
Escola de Doctorat

## Assessment results for the doctoral thesis

**Academic year:**

Full name

Doctoral programme

Structural unit in charge of the programme

## Decision of the committee

In a meeting with the examination committee convened for this purpose, the doctoral candidate presented the topic of his/her doctoral thesis entitled _____

_____.

Once the candidate had defended the thesis and answered the questions put to him/her, the examiners decided to award a mark of:

☐ FAIL ☐ PASS ☐ GOOD ☐ EXCELLENT

| | | |
|---|---|---|
| (Full name and signature)<br>Chairperson | (Full name and signature)<br>Secretary | |
| (Full name and signature)<br>Member | (Full name and signature)<br>Member | (Full name and signature)<br>Member |

_____, _____

The votes of the members of the examination committee were counted by the Standing Committee of the Doctoral School, and the result is to award the CUM LAUDE DISTINCTION:

☐ YES ☐ NO

| | |
|---|---|
| (Full name and signature)<br>Chair of the Standing Committee of the Doctoral School | (Full name and signature)<br>Secretary of the Standing Committee of the Doctoral School |

Barcelona, _____

## International doctorate mention

- As the secretary of the examination committee, I hereby state that the thesis was partly (at least the summary and conclusions) written and presented in a one of the languages commonly used in scientific communication in the relevant field of knowledge, which must not be an official language of Spain. This rule does not apply to stays, reports and experts from a Spanish-speaking country.

| |
|---|
| (Full name and signature)<br>Secretary of the Examination Committee |

# Acknowledgements

Acknowledgement text.

Daniel Remón Rodríguez
Barcelona, Spain
April, 2017

# Abstract

The irruption of renewable energy sources with power electronics interfaces, such as wind energy and solar photovoltaics, is transforming power systems. These electricity networks have traditionally been designed to transmit electric energy, from centralized generating stations employing synchronous machines with a controllable production, to large consumption centers where the loads are distributed through different voltage levels. However, this landscape is modified by alternative generators with a power output that depends on weather conditions, and which are connected to different parts of the network, with a wide range of sizes, and employing new power conversion systems based on semiconductors.

As any technical evolution, this brings new challenges along, and modern power systems will have to overcome the issues related to the intrinsic variability of these energy sources, their limited contribution to the control of the grid, or the dynamics introduced by the alternative power conversion systems that replace synchronous generators, characteristics that threaten the stability of the network. To minimize the possible adverse effect on the power grid of generating systems connected through power electronics converters, transmission system operators define different strategies, such as increasing the active power reserves for frequency control and power balancing purposes, and require all connected systems to comply with various rules and regulations. In an effort to better integrate these renewable sources in power systems, some power converter controllers have been proposed that aim at reproducing certain features of conventional synchronous machines. This work deals with the

analysis of the impact that large power-electronics-based power plants, in the range of hundreds of megawatts, have on the stability of power systems.

First, the main characteristics of these advanced controllers, sometimes referred to as *virtual synchronous machines*, are reviewed, and their constituting blocks are systematically classified. This classification allows performing a detailed comparison of different aspects regarding their implementation and dynamics. Thus, the proposals usually found in the literature are compared in terms of their need for ancillary synchronization systems, their ability to energize a grid, their effectiveness to limit the current injected during a fault and keep the converters connected to the grid, their capability to limit active power injections and to control the converter capacitor voltage, or their performance regarding harmonic mitigation and voltage balancing. Additionally, time-domain simulations comparing the response of power converters employing these controllers are carried out and analyzed.

Afterwards, since the study of power system stability requires adequate models of the elements interacting with the system, the modeling of an actual 100 MW photovoltaic power plant, consisting of 100 power converters, is addressed. Thus, a detailed model of the power plant is developed in *DIgSILENT PowerFactory*®, considering a single-phase equivalent for transient stability studies in balanced systems. This model includes the internal network buses, cables, and transformers, and the power converters with their control systems and primary resources. Moreover, the model is implemented in a flexible way that allows considering power converters employing conventional controllers or *synchronous power controllers*, and the photovoltaic resource can be replaced by a storage system. Furthermore, a method to derive an equivalent model of power plants employing these advanced controllers is developed, and three equivalent models of the power plant, with different degrees of detail, are implemented employing this method. These models allow reducing the complexity of the original model and its associated computational burden, while reproducing its dynamics with accuracy, making them more suitable for the analysis of power systems with a large number of generating units, loads, passive elements, and controllers.

Finally, the stability of power systems integrating this type of generating stations is analyzed. A first analysis is carried out in a 12-bus test system, considering a

simpler model of the plant where the photovoltaic characteristics are modeled only through an active power limitation, and comparing the impact of these plants as the solar penetration grows, up to a 50% level. This is followed by the analysis of the power system of northern Chile, considering the actual location of the power plant previously modeled, and including the full detail of the photovoltaic resource. Lastly, the impact of hybrid power plants consisting of a synchronous generator and a photovoltaic system, with different configurations with the possibility of curtailing the solar production or employing a storage system, is assessed. These analyses comprise the study of the eigenvalues of the system and its response to different types of events through time-domain simulation, and prove the ability of the studied controllers to increase the damping of the system, to reduce the oscillations suffered by other generators, and to limit maximum frequency deviations.

# Contents

# List of Figures

# List of Tables

# Nomenclature

**Acronyms / Abbreviations**

| | |
|---|---|
| ac | Alternating Current |
| BESS | Battery Energy Storage System |
| dc | Direct Current |
| DSPF | DIgSILENT PowerFactory |
| EMT | ElectroMagnetic Transient |
| FACTS | Flexible Alternating Current Transmission System |
| FLL | Frequency-Locked Loop |
| HVDC | High-Voltage Direct Current |
| IPT | Instantaneous Power Theory |
| LVRT | Low-Voltage Ride-Through |
| MV | Medium Voltage |
| p.u. | Per unit |
| PI | Proportional-Integral |

| | |
|---|---|
| PLL | Phase-Locked Loop |
| POI | Point Of Interconnection |
| PSS | Power System Stabilizer |
| PV | Photovoltaic |
| PWM | Pulse Width Modulation |
| RMS | Root Mean Square |
| SG | Synchronous Generator |
| SING | Sistema Interconectado del Norte Grande |
| SOC | State Of Charge |
| SOGI | Second-Order Generalized Integrator |
| SPC | Synchronous Power Controller |
| SRF | Synchronous Reference Frame |
| VSC | Voltage Source Converter |
| VSG | Virtual Synchronous Generator |
| VSM | Virtual Synchronous Machine |

Chapter
1.

# Introduction

*This chapter summarizes the main challenges that power systems are currently facing, focusing on the integration of renewable energy sources and other distributed energy resources as one of the main drivers of an unprecedented paradigm shift in the electricity sector. This establishes a framework for this thesis, which addresses the impact that renewable energy sources using power electronics have on power system stability. The chapter concludes with the objectives and contributions of the thesis.*

## 1.1 Background

The first power systems were built during the last decades of the 19th century. Since then, the expansion of power systems, and the construction of new ones, have gone hand in hand with social and economic progress, and these systems have been providing industries, public buildings, and households with electricity, which has become an indispensable good for most human activities. During all these years, power systems have been in constant evolution, developing safe, reliable, and efficient electricity networks. However, the main principles that define how power systems are designed and operated have not changed much. Namely, large power stations produce most of the electricity requested by all types of consumers, which

is transported by a robust high-voltage grid through long distances from generation to consumption centers. There, the power is distributed radially, with decreasing voltage levels, supplying the connected loads. In addition, the control of the system relies on generators, which must track demand variations and correct deviations from the rated operated conditions, in order to achieve an acceptable quality of supply.

Nowadays, this power system picture is changing, driven by a global effort to establish a more sustainable energy system, employing cleaner, renewable sources which are expected to be more profitable than conventional ones in the long run. The conventional generation mix, dominated by coal-fired power plants, natural gas combined cycles, nuclear power stations, and hydro generators, is turning towards a more diverse landscape, where it is possible to see wind and solar generation, among other renewable sources. As technology matures, the installed capacity and the annual generation by these sources is expected to increase, as can be seen in Fig. 1.1, which shows the world annual electricity generation from alternative energy sources forecast by the U.S. Energy Information Administration for the period 2020–2040 [1]. The growing importance of these sources, whose characteristics differ substantially from those of conventional resources, poses new challenges on power systems, as discussed in the following.

### 1.1.1 Challenges of modern power systems

This change in the generation mix, which is nonetheless beneficial from the point of view of carbon emissions and sustainability, also raises several issues for power systems and their traditional control schemes, due to the nature of the resources employed and the characteristics of the power conversion systems.

The main difference with respect to conventional generators, or at least the one which affects electricity markets and bulk generation the most, is that the commonest sources, i.e., wind and solar energy, are inherently variable. Their maximum energy production depends to a large extent on weather conditions, like the average wind, wind gusts, the relative position of the sun, and the presence of clouds; and this makes their power generation variable when they operate at their maximum power point, which is the usual strategy. Thus, these sources are not fully con-

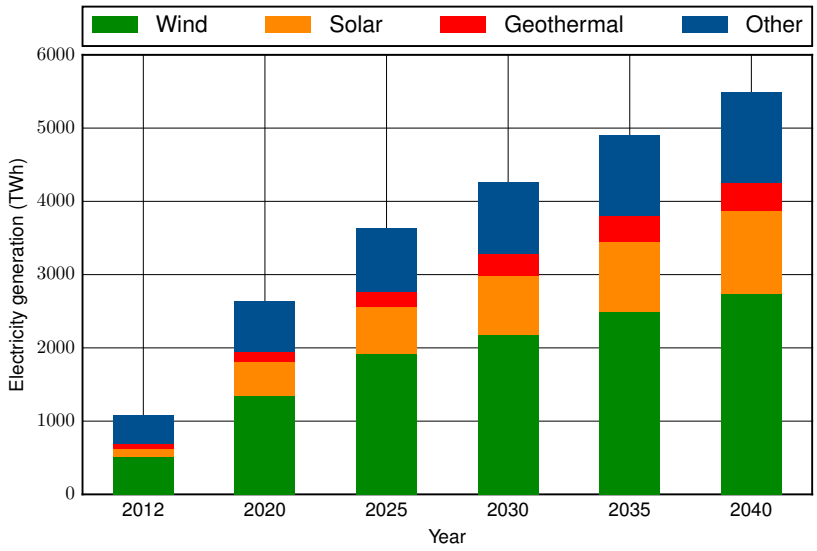


Fig. 1.1. World electricity generation from non-hydro renewable energy sources forecast by the U.S. Energy Information Administration [1].

trollable, or *dispatchable*, as conventional generators are. This works against the traditional conception of power systems, where controllable generators maintain the balance with a variable demand. In fact, many analyses consider these sources as negative loads, and their variability must be compensated by the remaining conventional generators.

Another important difference is the location of the generating plant. Conventional generating units can concentrate a large amount of generation in a reduced area, and can be located optimally taking into account the demand to be supplied, the characteristics of the grid, and the availability of fuel. However, wind and solar energy spread across regions, with a relatively low intensity, and sometimes the best locations are far away from the main consumption zones or the existing transmission infrastructure.

This has led to two main types of renewable generation systems. The first one consists in the connection of a small generating unit to the distribution grid, injecting the power produced in a limited area. Obviously, many power system users can opt for this solution, resulting in a significant amount of generating units be-

ing connected to distribution grids. This is the case of residential photovoltaic (PV) systems connected to the low voltage network, or small plants consisting of some PV modules or a small wind turbine which can be connected at the medium voltage grid. The other type includes power plants that harvest energy from a wide area and inject it into the power network through a single point, handling powers like those of conventional generators. Typical examples of this are wind farms with many wind turbines, concentrated solar power plants using a large steam turbine, or large PV plants formed by a number of power converters, which can reach a rated power in the range of 100 MW.

These two features of wind and solar resources have an impact on the way in which power systems are controlled and operated. Their limited controllability affects not only the longer-term balance between generation and demand, but also the regulation of the power system frequency, which is achieved through active power variations. Moreover, the installation of many small generating devices at distribution systems alters their traditional operation with a unidirectional power flow, which is the basis for their design, and may affect voltage profiles and protection schemes.

An additional remarkable fact about wind energy and PV generation concerns the power conversion technology. Nuclear, fossil-fuel-fired, and hydro power plants employ Synchronous Generators (SG) to inject power into the grid. These machines are able to operate in synchronism naturally, behave as voltage sources able to create and maintain a working a grid, and withstand large short-circuit currents, among other characteristics that shape the dynamics of power systems. On the other hand, wind turbines and PV systems employ power electronic converters, with a very fast response and able to synthesize alternating voltages, whose interaction with the grid greatly depends on their control systems, and may be counterproductive if not correctly designed.

Apart from new renewable energy sources, power systems are also changing due to the irruption of other technologies. Some of them are related to the integration of renewable sources, and are meant to solve some of the issues introduced by them. For instance, a solution to reduce the impact of the variability associated to these sources, and make a better utilization of the available resources, is to reinforce the

interconnection of power systems. This is done both with conventional ac lines and with High-Voltage Direct Current (HVDC) links, which enable long-distance power transmission in an efficient way not subject to the stability concerns of ac lines. Furthermore, HVDC systems offer a new area for the evolution of power systems, with multi-point systems where renewable generators can be directly connected, and open a broad range of questions about their control and their interaction with neighboring ac systems.

Another complementary technology is energy storage, which could compensate the variability of renewable sources and enable more flexible power systems. Moreover, these systems can be installed close to areas with overproduction during certain intervals of the day, or in regions where there is an intensive consumption during certain hours, so congestion issues are mitigated. In fact, the electric vehicle, whose penetration is growing as more drivers turn towards electric mobility on similar grounds as those investing on renewable generation, could be considered a particular case of storage system, with its own additional complexity. If properly employed, storage systems and electric vehicles managing energy smartly can alleviate the stress introduced by renewable production variations during some periods of the day. Moreover, these systems share some characteristics with renewable generators, like their generally distributed nature, and the grid-interface technology employed.

The proliferation of distributed energy resources at all voltage levels of subtransmission and distribution grids calls for a more detailed monitoring of these networks, which raises new concerns about data privacy, and different operation strategies that coordinate these agents and preserve the quality of supply. Thus, distribution systems take some characteristics of transmission systems, which opens the door to considering the figure of distribution system operators in charge of the control of the grid while other agents participate in the competitive energy business. In any case, another challenge related to these distributed energy resources is their integration in energy markets so power systems are operated efficiently. Markets will have to enable the participation of a large number of small agents, perhaps integrating more regions as the level of interconnection increases, and the importance of ancillary markets like those related to firm capacity, energy balancing, or conges-

tion management could rise, while the energy market could be severely affected by a large amount of suppliers with a near-zero marginal cost of energy.

### 1.1.2 Evolution of the integration of renewable energy sources in power systems

The requirements for renewable generators have evolved with the development of new technology and the penetration of more renewable units in power systems, especially in the case of low-power installations employing power electronic converters. Initially, these small generating units were connected to distribution systems without many concerns. They had to fulfill requirements similar to those demanded from loads connected to these systems, i.e., adequate protection of equipment and persons, limits on the harmonic currents injected or absorbed by the devices, and, in some cases, constraints on the exchanged reactive power or the installation of capacitor banks for reactive power compensation. The control of these first grid-feeding devices consisted basically of a fast current control loop and a maximum power point tracking algorithm that ensured the injection of as much active power as available from the source, and the minimum reactive power injection or absorption allowed, in order to reduce the size of the power conversion system and the losses.

As their penetration grew, so did the concern about safety. This led to discussion about the behavior that these devices should have under abnormal grid conditions; namely, when its frequency or voltage deviate from their rated values. In the case of voltage, this gave rise to the definition of Low-Voltage Ride-Through (LVRT) requirements [2, pp. 21–23], which define how long a power converter must remain connected during a voltage sag, depending on the depth of the sag and the evolution of the voltage, as depicted in Fig. 1.2. Similar operation regions have also been defined for the case of voltage surges. Nonetheless, the limited current characteristic of power converters has required the upgrade of some short-circuit protections that were not sensitive enough to detect faults fed only by these more moderate currents.

Additionally, when the generation from distributed sources in some parts of the system became sufficient to maintain a portion of the grid in operation for a certain period of time despite losing the connection from the main grid, new concerns were

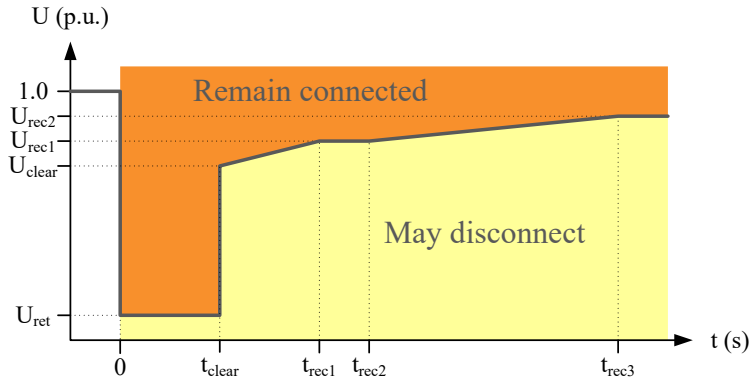


Fig. 1.2. Voltage versus time curve describing low-voltage ride-through requirements in [2].

raised, especially about the safety of operation and maintenance teams. Thus, anti-islanding schemes were defined so these devices would be disconnected from the grid upon the detection of abnormal conditions, so that the grid would remain deenergized [3, 4]. However, distributed resources have also been considered a solution to enhance the reliability of certain parts of the grid that are subject to disconnections from the main energy supply. This has encouraged the study of control systems able to maintain those portions of the grid in operation, or to reenergize them, until they can be reconnected.

Besides, system operators and regulators have realized that distributed generation may play a beneficial role in the control of voltage in distribution feeders, so new standards modify the way in which reactive power is controlled, allowing distributed power converters to regulate the voltage [4, 5]. Something similar happens with the regulation of frequency in the case of larger power plants connected at higher voltage levels. In many countries, renewable generators are required to participate in frequency regulation when frequency increases, decreasing their active power proportionally to the frequency error, as a conventional generator would do [2, p. 19]. In fact, some grid codes consider the participation of renewable units in frequency regulation in both senses if they operate with a small active power margin [2, p. 26]. Additionally, it has been proposed that these generators provide a synthetic inertial response, emulating the behavior of synchronous machines that naturally limits frequency deviations.

Therefore, the requirements for renewable generators tend to be similar to the requirements for conventional generators based on synchronous machines, especially for systems above a certain power rating. Except for the possibly limited availability of the resource, this should not be an issue for renewable generating systems employing synchronous machines, like hydro or concentrated solar power plants, but requires a careful design of the controllers of power electronic converters, the usual interface of the booming PV and wind energy.

### 1.1.3 Challenges of the integration of variable energy sources using power electronics

Besides the constrained *dispatchability*, and the reserve and balancing requirements due to the variability inherent to many renewable sources, most wind and solar PV generating systems present new control challenges in the range of a few seconds and below. This is due to the fact that their grid interface consists of power electronic devices, whose dynamics are completely different from those of synchronous machines, which play a crucial role in the design of power systems and their control layers. If not correctly addressed, these differences in the dynamics may affect the stability of the system.

First, it is worth noting that the fast response of power electronic devices allows power converters to synthesize a voltage reference almost instantaneously, and to control the injected current in a few milliseconds. Therefore, the dynamics of the interaction between a power converter and the grid to which it is connected depend fundamentally on the power converter control layers above the current control loop. The final output of these layers is precisely a current reference correctly synchronized with the grid and fulfilling the control objectives of the power conversion system, that is to say, following a given power or voltage reference, and maintaining the dc voltage, and the ac voltage and current magnitudes within safe operation limits.

Contrary to synchronous machines, which naturally synchronize themselves with the power grid, power converters require a synchronization system, which is usually implemented as an ancillary block that extracts information about the phase of the voltage at the point of connection of the converter. This kind of system is sub-

ject to errors induced by noise, but especially by abnormal grid conditions. This is the case when the system is tuned for a particular frequency and the grid frequency diverges from this reference value or, more commonly, by grid faults that involve a voltage sag or a phase jump.

Additionally, this lack of natural synchronization results in a lack of inertial contribution when there is a frequency event. Synchronous generators naturally contribute to limiting the frequency deviation, releasing or absorbing energy stored as rotational kinetic energy in their rotors in opposition to the frequency deviation. Power converters, unless explicitly designed to do so, are insensitive to this kind of disturbance.

Going further, the friction of mechanical parts, and the addition of damper windings are able to increase the damping of the response of a synchronous machine to a certain extent, which, together with other controllers, can contribute to the reduction of harmful power and frequency oscillations. Once again, power converters will have a similar effect on the power system only as a consequence of their controller dynamics.

Power system stability is also favored by an adequate regulation of frequency and voltage. Due to their fast and flexible response, power converters have a large potential capability to contribute to the regulation of both magnitudes, only limited by the maximum power available from the resource in the case of underfrequency events. But, as in the case of conventional generators, the corresponding control systems must be installed and properly tuned.

Finally, it is worth noting the significant differences in the short-circuit capability of synchronous machines and power converters. In this case, the constraints are physical and the behavior of a synchronous machine cannot be reproduced with a power converter. The reason for this is that the power electronic devices usually employed in these systems cannot withstand more than twice their rated current for a few seconds without being damaged, whereas a synchronous generator is able to inject currents over five times its rated current.

Taking all these facts into account, the provision of synchronous generator services by power-electronics-based renewable systems requires a sound design of their controllers and, in most cases, a design tradeoff between sizing all the elements of

the power conversion system only for maximum power generation and letting the power converter inject greater currents and keep an active power reserve, which is more expensive but more useful for the power grid. In any case, some features could only be reproduced by power converters at a extraordinary cost, like the injection of large short-circuit currents, so the design of the whole power conversion system must consider which features of synchronous machines are essential, or more valuable, for a correct integration of this energy resources.

## 1.2 Objectives and outline of the thesis

This thesis presents the most relevant work carried out during my enrollment in the PhD Programme in Electric Energy Systems at the Universitat Politècnica de Catalunya - BarcelonaTech (UPC) between 2014 and 2017. My PhD project was defined as an industrial PhD project in collaboration with Abengoa, Seville, Spain, where I carried out most of the research presented here. In addition, I visited the University of Waterloo, Ontario, Canada, during the period from September 2015 to June 2016. During my PhD, I participated in several research projects related to the control of renewable power plants employing power electronics and their impact on power systems. Namely, Abengoa's *PV síncrona* and *Power analysis* projects, and the UPC Renewable Electric Energy Systems group *Control of virtual synchronous photovoltaic power plants with energy storage* project.

The definition of the PhD project took into account Abengoa's interest in PV plants able to provide the services of conventional generators, and focused on the analysis of the impact of this kind of plants on the stability of power systems. Furthermore, it considered the utilization of the Synchronous Power Controller (SPC) to embed certain characteristics of synchronous generators in power converters, and a 100-MW PV power plant actually being built in Chile. Thus, the objectives of the PhD project included the study of the SPC and similar controllers, the modeling of this PV plant, and the assessment of the impact of the plant on the Chilean system, as well as the analysis of the impact of similar PV plants in standard test power systems considering scenarios with different solar penetration levels, or different plant configurations with storage or an adjacent synchronous generating unit.

This document is structured as follows. Chapter 2 describes the state of the art on some topics of interest for the PhD project. First, an introduction to power converters and the basic controllers that enable an adequate connection of these devices to the grid is presented. This is followed by a summary of the characteristics of controllers that aim at reproducing the dynamics of synchronous generators, based on the droop or the virtual synchronous machine concept. Afterwards, the problem of power system stability is presented, including a description of the types of stability usually studied. Then, the prior art on wind farm and solar plant modeling is reviewed, with emphasis on the development of equivalent models for power system analysis. Finally, the previous work on the analysis of the impact of renewable energy sources on power systems is reviewed.

The following two chapters deal with aspects of the control and modeling of PV plants like the studied one. Chapter 3 presents a classification of droop controllers and virtual synchronous machines. It includes a comparison of their implementation details and dynamic responses. Then, Chapter 4 details the model of the PV plant employed, as well as its implementation in the power system analysis software *DIgSILENT PowerFactory*®. This chapter also includes the derivation of equivalent models of the PV plant with different degrees of aggregation, and the modeling of other types of resources like supercapacitors or batteries.

The remaining chapters address the analysis of the impact of these PV plants. Thus, Chapter 5 presents the analysis of the impact of PV plants with synchronous power controllers on a 12-bus test system for three different penetration levels. Chapter 6 includes the analysis of the impact of the actual PV plant being built in Chile on this system, and the study of a future scenario with an increased solar penetration level. As an introduction to this study, two other scenarios are analyzed in the 12-bus system. And Chapter 7 is devoted to the analysis of the impact of power plants considering a PV generation system and other elements. Namely, the capabilities of battery energy storage systems to reproduce the response of larger PV plants, and the interaction with synchronous machines forming a hybrid power plant with the PV system are studied in different test power systems.

Finally, Chapter 8 draws the main conclusions of this work, and identifies those areas where more research is needed, proposing several options for future work.

## 1.3 List of publications and contributions

This section lists the main contributions of the PhD project, classified as journal or conference papers, and contributions on related topics that deviate slightly from the main theme of the thesis.

The selected journal papers present the main results of this thesis. Their topics range from the study of the SPC and similar controllers to the analysis of their impact on large power systems, including also the development of adequate models for this analysis. The theory and the results presented in these papers are discussed in detail in the following chapters. Additionally, the conference papers listed here provide additional insight on these and similar topics, presenting partial results of the study of the SPC, the development of power plant models, and the impact of power converters using the SPC on small power systems.

The remaining contributions address different aspects of the control of power converters for renewable energy sources and their impact on power systems, which have been studied in collaboration with other PhD students and researchers in an interdisciplinary work environment. Several of these publications focus on the study of the current control loop of power converters, whose correct operation is essential for a good performance of the SPC and higher-level controllers. Other contributions, including two patents, are devoted to the control of different renewable resources, as is the case of wave energy, and to the control of power systems involving different generating units and loads; whereas other papers analyze the impact of HVDC links emulating inertia on power systems.

Journal papers:

1. **D. Remon**, C. A. Cañizares, and P. Rodriguez, "Impact of 100-MW-scale PV plants with synchronous power controllers on power system stability in northern Chile," accepted for publication in *IET* Generation, Transmission & Distribution, May 2017.

2. **D. Remon**, A. M. Cantarellas, J. M. Mauricio, and P. Rodriguez, "Power system stability analysis under increasing penetration of photovoltaic power plants with synchronous power controllers," *IET Renewable Power Genera-*

*tion*, vol. 11, no. 6, pp. 733–741, May 2017.

3. **D. Remon**, A. M. Cantarellas, and P. Rodriguez, "Equivalent model of large-scale synchronous photovoltaic power plants," *IEEE Transactions on Industry Applications*, vol. 52, no. 6, pp. 5029–5040, Nov.–Dec. 2016.

4. W. Zhang, **D. Remon**, and P. Rodriguez, "Frequency support characteristics of grid-interactive power converters based on the synchronous power controller," *IET Renewable Power Generation*, vol. 11, no. 4, pp. 470–479, March 2017.

Conference papers:

5. **D. Remon**, A. M. Cantarellas, J. Martinez-Garcia, J. M. Escaño, and P. Rodriguez, "Hybrid solar plant with synchronous power controllers contribution to power system stability," accepted in *IEEE Energy Conversion Congress and Exposition (ECCE)*, Cincinnati, OH, 2017.

6. W. Zhang, **D. Remon**, J. Rocabert, A. Luna, I. Candela, and P. Rodriguez, "Frequency support properties of the synchronous power control for grid-connected converters," in *IEEE Energy Conversion Congress and Exposition (ECCE)*, Milwaukee, WI, 2016, pp. 1–8.

7. **D. Remon**, A. M. Cantarellas, W. Zhang, I. Candela, and P. Rodriguez, "Enhancement of the stability of a distribution system through synchronous PV," in *IEEE PES General Meeting*, Boston, MA, 2016, pp. 1–5.

8. **D. Remon**, A. M. Cantarellas, M. A. A. Elsaharty, C. Koch-Ciobotaru, and P. Rodriguez, "Equivalent model of a synchronous PV power plant," in *IEEE Energy Conversion Congress and Exposition (ECCE)*, Montreal, QC, 2015, pp. 47–53.

9. **D. Remon**, A. M. Cantarellas, M. A. A. Elsaharty, C. Koch-Ciobotaru, and P. Rodriguez, "Synchronous PV support to an isolated power system," in *IEEE Energy Conversion Congress and Exposition (ECCE)*, Montreal, QC, 2015, pp. 1982–1987.

10. W. Zhang, **D. Remon**, A. M. Cantarellas, A. Luna, J. Rocabert, I. Candela, and P. Rodriguez, "Comparison of different power loop controllers for synchronous power controlled grid-interactive converters," in *IEEE Energy Conversion Congress and Exposition (ECCE)*, Montreal, QC, 2015, pp. 3780–3787.

11. **D. Remon**, A. M. Cantarellas, J. D. Nieto, W. Zhang, and P. Rodriguez, "Aggregated model of a distributed PV plant using the synchronous power controller," in *IEEE International Symposium on Industrial Electronics (ISIE)*, Buzios, Brazil, 2015, pp. 654–659.

12. **D. Remon**, A. M. Cantarellas, E. Rakhshani, I. Candela, and P. Rodriguez, "An active power self-synchronizing controller for grid-connected converters emulating inertia," in *International Conference on Renewable Energy Research and Applications (ICRERA)*, Milwaukee, WI, 2014, pp. 424–429.

13. **D. Remon**, A. M. Cantarellas, E. Rakhshani, I. Candela, and P. Rodriguez, "An active power synchronization control loop for grid-connected converters," in *IEEE PES General Meeting*, National Harbor, MD, 2014, pp. 1–5.

Other contributions:

14. A. Mir Cantarellas, **D. Remón Rodríguez**, and P. Rodríguez Cortés, "Competitive power controller and method for distributed power systems," Patent P201531918EN, Priority date: 20 Dec. 2015.

15. A. M. Cantarellas, **D. Remon,** W. Zhang, and P. Rodriguez, "An adaptive vector control based wave-to-wire model of wave energy converters," accepted in *IET Power Electronics*, March 2017.

16. A. M. Cantarellas, **D. Remon,** and P. Rodriguez, "Adaptive vector control of wave energy converters," *IEEE Transactions on Industry Applications*, vol. 53, no. 3, pp. 2382–2391, May–June 2017.

17. W. Zhang, **D. Remon**, A. M. Cantarellas, A. Luna, and P. Rodriguez, "Dynamics estimation and generalized tuning of stationary frame current controller for grid-tied power converters," *EPE Journal*, vol. 26, no. 3, pp. 85–95, 2016.

18. W. Zhang, **D. Remon**, A. M. Cantarellas, and P. Rodriguez, "A unified current loop tuning approach for grid-connected photovoltaic inverters," *MDPI Energies*, vol. 9, no. 9, 723, September 2016.

19. E. Rakhshani, **D. Remon**, A. M. Cantarellas, J. M. Garcia, and P. Rodriguez, "Virtual synchronous power strategy for multiple HVDC interconnections of multi-area AGC power systems," *IEEE Transactions on Power Systems*, vol. 32, no. 3, pp. 1665–1677, May 2017.

20. E. Rakhshani, **D. Remon**, A. Mir Cantarellas, and P. Rodriguez, "Analysis of derivative control based virtual inertia in multi-area high-voltage direct current interconnected power systems," *IET Generation, Transmission & Distribution*, vol. 10, no. 6, pp. 1458–1469, 4 21 2016.

21. A. M. Cantarellas, **D. Remon**, J. Martinez-Garcia and P. Rodriguez, "Competitive control of wave power plants through price-signal optimum allocation of available resources," accepted in *IEEE Energy Conversion Congress and Exposition (ECCE)*, Cincinnati, OH, 2017.

22. E. Rakhshani, H. Mehrjerdi, **D. Remon**, A. M. Cantarellas, and P. Rodriguez, "Frequency control of HVDC interconnected system considering derivative based inertia emulation," in *IEEE PES General Meeting*, Boston, MA, 2016, pp. 1–5.

23. E. Rakhshani, **D. Remon**, A. M. Cantarellas, H. Mehrjerdi, and P. Rodriguez, "Derivative based inertia emulation of interconnected systems considering phase-locked loop dynamics," in *IEEE PES General Meeting*, Boston, MA, 2016, pp. 1–5.

24. A. M. Cantarellas, **D. Remon**, C. Koch-Ciobotaru and P. Rodriguez, "Adaptive power control of wave energy converters for maximum power absorption under irregular sea-state conditions," in *IEEE Energy Conversion Congress and Exposition (ECCE)*, Montreal, QC, 2015, pp. 6655–6659.

25. J. D. Nieto, **D. Remon**, A. M. Cantarellas, C. Koch-Ciobotaru, and P. Rodriguez, "Overview of intelligent substation automation in distribution sys-

tems," in *IEEE International Symposium on Industrial Electronics (ISIE)*, Buzios, Brazil, 2015, pp. 922–927.

26. W. Zhang, A. M. Cantarellas, **D. Remon**, A. Luna, and P. Rodriguez, "A proportional resonant controller tuning method for grid connected power converters with LCL+trap filter," in *International Conference on Renewable Energy Research and Applications (ICRERA)*, Milwaukee, WI, 2014, pp. 445–450.

27. E. Rakhshani, **D. Remon**, A. M. Cantarellas, K. Rouzbehi, and P. Rodriguez, "Integration of renewable generation for frequency support of HVDC/AC interconnected systems under power market scenario," in *IEEE PES General Meeting*, National Harbor, MD, 2014, pp. 1–5.

28. W. Zhang, C. Citro, A. M. Cantarellas, **D. Remon**, A. Luna, and P. Rodriguez, "Tuning of proportional resonant controllers for three phase PV power converters with LCL+trap filter," in *IEEE PES T&D Conference and Exposition*, Chicago, IL, USA, 2014, pp. 1–5.

Chapter
2.

# State of the art

*This chapter presents an overview of several topics of interest for this thesis. The first section summarizes the main aspects of power converters and their control are summarized, whereas the second section introduces new control approaches designed to achieve a harmonious interaction between these devices and the power grid. This is followed by an overview of power system analysis, including the main aspects of power system stability. Finally, the last two sections present a literature review of renewable power plant modeling and the analysis of power system stability under the presence of this kind of generators, respectively.*

## 2.1 Power converters for renewable generation

An important fraction of renewable energy sources and storage systems operate in dc. Therefore, they are connected to the ac grid through conversion systems based on power electronics. These conversion systems differ substantially from synchronous machines, which have traditionally been the interface between energy sources and power systems. Thus, they introduce different dynamics, and also new control capabilities, that must be taken into account when the impact of these sources on power systems is analyzed.

### 2.1.1 Power converter hardware

Power converters consist of a set of switches that connect different electrical points. The devices acting as switches are normally thyristors or transistors.

Thyristor technology was developed first and became widespread for many applications. Their behavior shares several similarities with diodes, but a thyristor is turned on only when it receives a turn-on signal while the voltage drop across the device is positive; it is turned off when the current reverses. A particular type, gate turn-off thyristors, can be turned off by an additional signal. To operate properly, thyristors require a current source, whose current is forced into another circuit. Therefore, converters employing thyristors are usually referred to as current source converters. They are able to handle large currents and power flows, but they lack reactive power control, and their switching frequency is of the order of the grid frequency, which results in harmonic currents or voltages, and large filters are required.

Converters based on transistors work differently. Transistors can be switched on and off by a gate signal, and they require a voltage source, forming then Voltage Source Converters (VSC). Although some converters may use metal-oxide-semiconductor field-effect transistors, with switching frequencies over tens of kilohertz, insulated-gate bipolar transistors are preferred in power applications because they can handle relatively large power flows with moderate switching frequencies around a kilohertz. The principle of operation of a VSC is to connect a point of the circuit to different voltages in such a way that the average value is equal to a reference. Their increased switching frequency reduces the harmonic injection and the size of filters, and the switching flexibility allows the bidirectional transfer of active and reactive power. The following discussion will focus on this type of converters. More details about the devices forming power converters can be found in [6, pp. 16–32].

Depending on the application, different converter topologies are employed. It is possible to build single-phase converters, and use three of them to obtain a three-phase converter, but it is also possible to build a three-phase converter, with a single dc bus capacitor and requiring less switches. Three-phase converters may allow connecting three or four wires if a neutral conductor is required. However, two basic VSC topologies must be remarked. One of them is the half-bridge topology, shown in Fig. 2.1a, which consists on a voltage source and two switches that determine

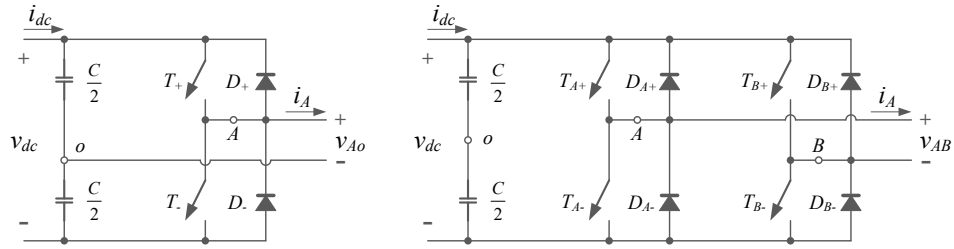


(a) Half-bridge. (b) Full-bridge.

Fig. 2.1. Basic converter topologies [6].

whether their midpoint is connected to the positive or the negative terminal. A very simple three-phase converter is obtained when three half-bridge branches are used. The other one is the full-bridge topology, depicted in Fig. 2.1b, which is able to force a positive, negative or zero voltage between the midpoints of both branches. Reference [7] presents several topologies for wind and PV systems which are based on these basic two.

Other configurations, with more than two levels, have also been studied. They allow increasing the power rating of the converter with the same kind of transistors, at the expense of a greater number of devices. Moreover, they reduce the harmonic content for the same switching frequency because the voltage steps are shorter than in the case of a two-level converter. Common examples are diode-clamped, flying capacitors and cascaded converters [8], or a generalized topology based on cells constituted by half-bridge converters [9]. In recent years, modular multilevel converters are gaining research interest, especially in their application to HVDC links, where large voltages and currents must be managed. They are formed by different cells, each of which is itself a VSC with a capacitor, usually with a full-bridge or half-bridge topology [10, 11]. Apart from their ability to handle large powers, this topology is of special interest because the cell capacitors can be used to store energy.

### 2.1.2 Power converter control

The control architecture of a VSC for renewable generation is usually divided in several layers, controlling different magnitudes in different ranges of time.

#### 2.1.2.1 Modulation

The modulation constitutes the lowest control layer of a converter. It is an algorithm that transforms a voltage reference into on and off signals for the switches. The switching signals are calculated in such a way that the average voltage synthesized by the power electronics devices during a switching period is equal to the specified reference, taking into account the time that the output terminal is connected to each dc terminal and the voltage of each of these dc terminals.

The commonest modulation technique applied to VSC is Pulse Width Modulation (PWM) [12]. It defines a fixed switching frequency, and, during a switching period, the output terminal is connected to each dc voltage level for the adequate time to obtain the desired average. This strategy enables a fast control of the power converter voltage, and it results in signals with low distortion, except at frequencies around multiples of the switching frequency, which can be easily filtered.

#### 2.1.2.2 Voltage controller

Although a modulation algorithm allows tracking a voltage reference, it operates in open loop. Therefore, the control system can be subject to steady-state errors, and it cannot control any variable other than the voltage at the internal converter terminals.

A first solution to these problems is the use of a closed-loop voltage controller that feeds back a voltage measurement, which can be taken at different points of the power conversion system, and generates a reference for the modulation aiming to correct the measured error. This controller allows identifying the power converter with a controlled voltage source, and can be useful for certain applications where the power converter is the only electrical source. However, this control strategy does not have any control on the current circulating through the power electronics devices, which will cause the activation of overcurrent protections and the disconnection of the converter when there is a fault in the system to which the converter is connected. Additionally, when the converter is connected to a power system with other voltage sources or to a strong grid, there may be undesired interactions among different elements trying to control the same magnitude.

#### 2.1.2.3 Current controller

Alternatively, taking into account that the controller immediately above the modulation establishes an equivalence between the converter and a controlled source, the controlled variable should be defined by the type of source that the power conversion system represents in the power system. For a converter associated to a generating unit, and connected in parallel to a working grid, the simplest option is to connect it as a current source, so as not to compete with the grid voltage. Moreover, using adequate higher level controllers, this option can also be adapted to the case of isolated operation.

The objective of a current controller is thus to generate voltage references for the modulation block such that the current injected by the converter follows a given reference. The following description will be oriented to the control of three-phase converters, since these are the ones used in the plants studied in this thesis.

The simplest controller that can be included in the control loop is a Proportional-Integral (PI) controller [12, pp. 25–30], [7, pp. 317–318]. It uses as input the instantaneous current error, and it generates the references for the modulation. These controllers can have a fast response, automatically compensate any dead time effects and their performance can be easily enhanced by anti-windup systems. However, due to the sinusoidal nature of the reference, they are not able to reproduce it exactly, and thus they cannot make the steady-state error zero, as shown in Fig. 2.2. Additionally, their ability to reject disturbances is limited.

Three-phase four-wire systems can directly apply independent single-phase current controllers, but three-phase three-wire systems have to ensure a zero sum of the phase currents. The commonest current control strategies for that case are based on $\alpha\beta$ and $dq$ frames, which are explained in the following.

These reference frames are useful because they take profit of the fact that the sum of three-phase currents is zero for three-wire systems, which allows reducing the number of variables to control to two. The principle behind this reduction is to consider currents and voltages in three-phase systems as three-dimensional vectors with coordinates $x_{abc} = (x_a, x_b, x_c)$, and projecting them onto a plane.

The $\alpha\beta$ frame is based on projecting the vectors directly on the plane defined by (2.1), which represents all three-phase signals whose sum is equal to zero. Further,

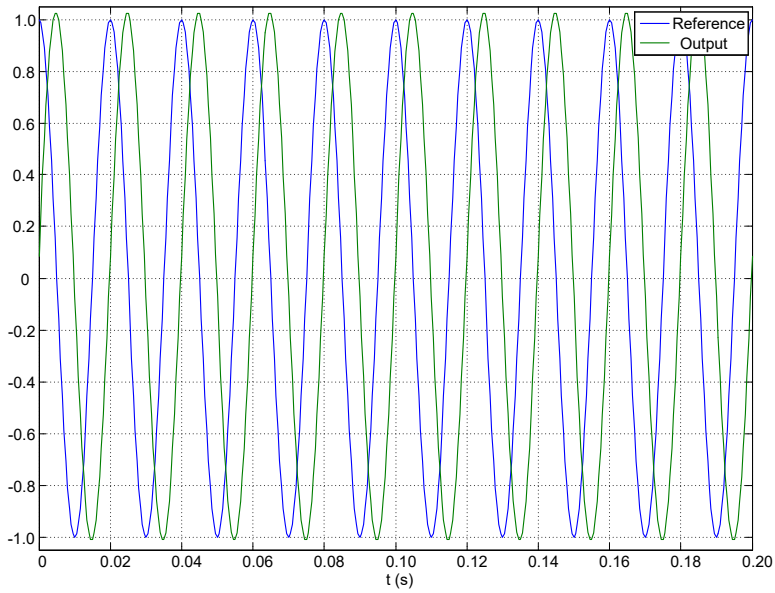


Fig. 2.2. Sinusoidal reference tracking by proportional-integral controller.

two axes are defined on this plane, the $\alpha$ axis has the same direction and sense as the projection of the $a$ axis onto the plane, and the $\beta$ axis leads the latter by 90°, which means that a set of direct-sequence voltages or currents will pass over the $\beta$ axis a quarter of a cycle after passing over the $\alpha$ axis. A third axis can be defined perpendicular to the plane and such that the resulting reference frame is positively oriented, in order to obtain an equivalent three-dimensional reference frame; this allows studying systems with nonzero homopolar components. The corresponding transform is defined by the orthogonal matrix in (2.2) and the relationships in (2.3).

$$\pi_{\alpha\beta} : x_a + x_b + x_c = 0 \tag{2.1}$$

$$T_{\alpha\beta 0} = \sqrt{\frac{2}{3}} \begin{pmatrix} 1 & -\frac{1}{2} & -\frac{1}{2} \\ 0 & \frac{\sqrt{3}}{2} & -\frac{\sqrt{3}}{2} \\ \frac{1}{\sqrt{2}} & \frac{1}{\sqrt{2}} & \frac{1}{\sqrt{2}} \end{pmatrix} \tag{2.2}$$

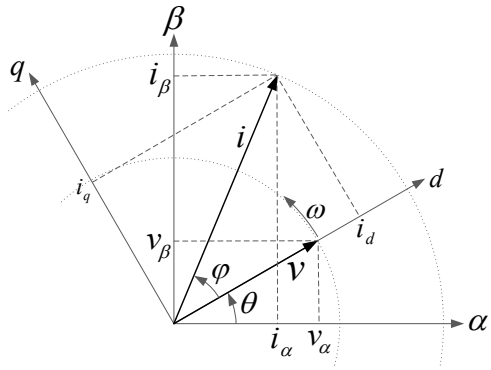


Fig. 2.3. $\alpha\beta$ and $dq$ frames.

$$\begin{aligned} x_{\alpha\beta 0} &= T_{\alpha\beta 0}\, x_{abc} \\ x_{abc} &= T_{\alpha\beta 0}^{T}\, x_{\alpha\beta 0} \end{aligned} \tag{2.3}$$

This transform maintains the magnitude of the vectors and the expression of the active power as a scalar product. Moreover, the projection onto this plane allows considering the current vector as the sum of its projection on the direction of the voltage and its projection on the perpendicular direction. These projections generate active and reactive power respectively.

Three-phase direct-sequence sinusoidal signals rotate in this plane at their angular frequency, and they define sinusoidal signals, with a phase-shift of 90°, on each axis. In some cases, it might be interesting to consider a new reference frame where they are stationary, which leads to the widespread $dq$ frame, whose relation with the $\alpha\beta$ frame is shown in Fig. 2.3. It is defined subtracting the turn caused by the angular frequency from the $\alpha\beta$ signals, as shown by (2.4) and (2.5), and can be obtained directly from the three-phase signals using (2.6) and (2.7).

$$T_{dq0} = \begin{pmatrix} \cos(\theta) & \sin(\theta) & 0 \\ -\sin(\theta) & \cos(\theta) & 0 \\ 0 & 0 & 1 \end{pmatrix} \tag{2.4}$$

$$\begin{aligned} x_{dq0} &= T_{dq0}\, x_{\alpha\beta 0} \\ x_{\alpha\beta 0} &= T_{dq0}^{T}\, x_{dq0} \end{aligned} \tag{2.5}$$

$$T_\theta = \sqrt{\frac{2}{3}} \begin{pmatrix} \cos(\theta) & \cos\left(\theta - \frac{2\pi}{3}\right) & \cos\left(\theta + \frac{2\pi}{3}\right) \\ -\sin(\theta) & -\sin\left(\theta - \frac{2\pi}{3}\right) & -\sin\left(\theta + \frac{2\pi}{3}\right) \\ \frac{1}{\sqrt{2}} & \frac{1}{\sqrt{2}} & \frac{1}{\sqrt{2}} \end{pmatrix} \tag{2.6}$$

$$\begin{aligned} x_{dq0} &= T_\theta \, x_{abc} \\ x_{abc} &= T_\theta^T \, x_{dq0} \end{aligned} \tag{2.7}$$

There is a degree of freedom in the choice of the rotation angle $\theta$, which can be modified by a constant, and it is normally chosen to be related to the voltage phase-angle, in such a way that the voltage is aligned to the $d$ axis or the $q$ axis. In this case, the current components in each axis will be associated to active or reactive power. In Fig. 2.3, the voltage defines the $d$ axis.

Taking into account that for constant power references and voltage, the current references in $dq$ will also be constant, current controllers in the $dq$ frame can use a simple PI controller, which can be tuned with conventional methods [12, pp. 93–98], [7, pp. 319–320], [13]. Controllers defined in the $dq$ frame are called synchronous controllers.

However, the equations describing the current produced by the converter are coupled in the $dq$ frame, as obtained in (2.8), which correspond to a converter with a simple filter formed by a resistance $R$ and an inductance $L$, and where $v$ refers to the voltage at the point of connection, $u$ indicates the voltage at the converter terminals, and $\omega$ is the pulsation of the grid voltage. Because of this coupling, it is necessary to include two decoupling branches in the block diagram of the controller, as shown in Fig. 2.4.

$$\frac{d}{dt} i_{dq}(t) = \begin{pmatrix} -\frac{R}{L} & \omega \\ -\omega & -\frac{R}{L} \end{pmatrix} i_{dq}(t) + \frac{1}{L}\left(u_{dq}(t) - v_{dq}(t)\right) \tag{2.8}$$

Additionally, in a real implementation, it is necessary to estimate the angle of the voltage in order to apply the $dq$ transform and obtain constant signals. This is done through a synchronization block, like the widely used Phase-Locked Loop (PLL) included in Fig. 2.4. The phase-angle of the voltage is continuously varying and its estimation is subject to the PLL dynamics, which have some influence on the

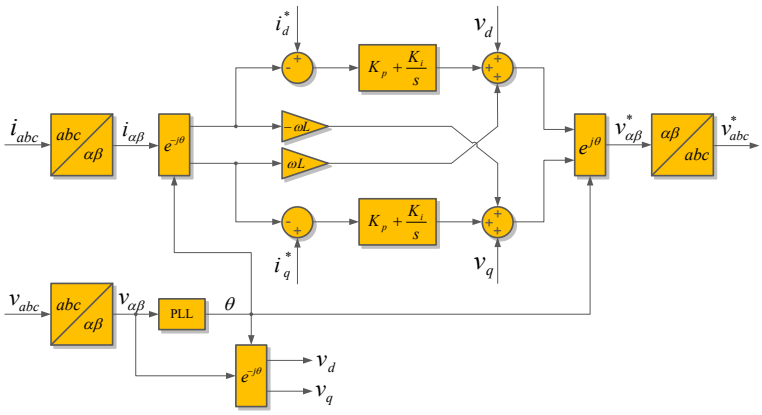


Fig. 2.4. Proportional-integral current controller in the *dq* frame.

controller performance [7, 14].

In the previous discussion, only the case of perfectly sinusoidal signals has been considered. However, real systems must take into account the negative sequence and harmonics. To control each of these currents, an additional control loop analogous to the fundamental frequency controller, must be introduced.

In order to simplify the resulting control diagram, and to reduce the influence of the phase-angle estimation dynamics, the controllers can be translated to the $\alpha\beta$ frame, dividing the integral term in two branches, one controlling the positive sequence and another taking care of the negative, as considered in Fig. 2.5a in the *dq* frame. Utilizing (2.9), where $f$ is a time-domain function and $\mathscr{L}$ is the Laplace operator, and considering $\theta = \omega t$, the integral terms become first order transfer functions with conjugate poles $\pm j\omega$ in the $\alpha\beta$ frame, as in Fig. 2.5b.

$$\mathscr{L}\left[f(t)e^{at}\right](s) = \mathscr{L}\left[f(t)\right](s-a) \tag{2.9}$$

Adding the effect of both integral controllers, a single transfer function that controls both the positive and the negative sequence is obtained, as shown in (2.10). This leads to a much simpler control diagram that corresponds to a resonant controller [13, 15, 16]. Moreover, this controller only needs an estimation of the system frequency, and the phase-angle is not required. This estimation can be obtained from a Frequency-Locked Loop (FLL), whose effect on the controller dynamics is

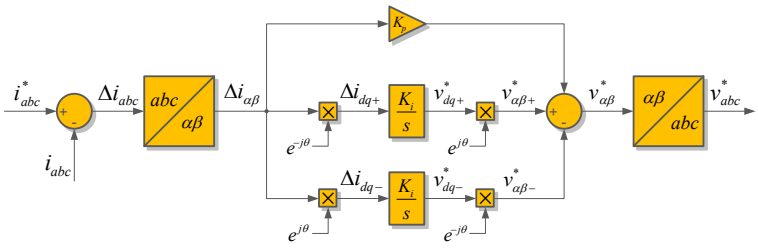


(a) $dq$ frame.

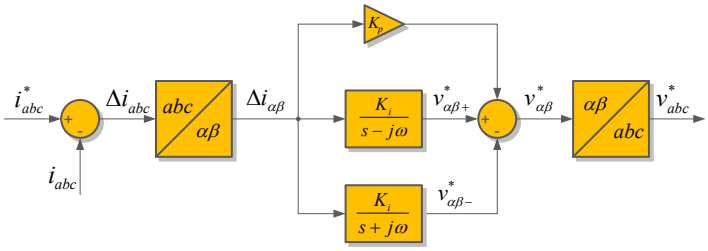


(b) $\alpha\beta$ frame.

Fig. 2.5. Equivalence between current controllers in different frames.

smaller than in the case of using a PLL [7, pp. 80–89, 194–202], [17, 18].

$$C_r(s) = \frac{K_i}{s+j\omega} + \frac{K_i}{s-j\omega} = \frac{2K_i s}{s^2+\omega^2} \tag{2.10}$$

The ability of this resonant controller to track sinusoidal references follows the internal model principle, which states that including a model of the reference in the feedback loop ensures the reference is correctly tracked. Additional information on this kind of notch filter can be found on many references [7, pp. 74–80, 326–329, 381–384], [16], and its discrete-time implementation is discussed in [19]. The same controller can be applied in parallel for different harmonics, by simply replacing the resonance frequency [7, p. 331], [13, 16], and phase-delays can be included to increase the damping of the response for some frequencies [12, pp. 103–106].

#### 2.1.2.4 Cascaded voltage and current controllers

A solution to control the three-phase voltage at a particular electrical point without losing the capability to limit the injected current is to define a voltage controller that

works above the current controller, generating the current reference to be tracked. In this case, if there is a fault that would require a large current injection in order to maintain the reference voltage, the current reference can be limited taking into account the power converter rating and avoiding an undesired trip.

Nevertheless, a careful design of the whole control loop is necessary, since the voltage controller must be several times as slow as the current controllers in order to avoid any coupling between the dynamics of both controllers. And, as any other voltage controller, it may suffer some instability issues when it is connected to a strong grid and tries to control the grid voltage.

#### 2.1.2.5 Other low-level control techniques

Other strategies have been applied to the control of the basic magnitudes that can be handled by a power converter, especially the current.

A deadbeat controller, which belongs to the family of predictive controllers, is one such strategy that has been applied to the control of converter currents [12, pp. 64–78], [7, pp. 320–325]. The principle of operation of this kind of controllers is to predict the evolution of the controlled quantity in order to determine the required average voltage at the converter terminals, i.e., the modulation reference. Deadbeat controllers are able to cancel the error at the end of the following sampling period, and it can be proved that they are the fastest current controllers that achieve zero error in two sampling periods. To predict the behavior of the controlled variable, these controllers are designed using a model of the filter and the grid. Therefore, they are sensitive to any variations in the parameters, but an observer can be added to reduce the derived problems.

A different approach is hysteresis control [12, pp. 30–31]. This controller generates the switching signals directly, without using a modulation algorithm. This is a type of bang-bang nonlinear control and has a very fast response because the state of the switches is directly determined by the comparison of the converter current with its reference. However, its use is not widespread in converters connected to power systems, mainly because this strategy results in a variable switching frequency, which increases the cost of the filtering equipment and can result in undesired resonances.

#### 2.1.2.6 Synchronization systems

Like any other generator connected to the grid, power converters have to be synchronized with the grid voltage. Therefore, they usually incorporate a grid synchronization block that supports the operation of the other blocks forming the control system of the power converter. Grid synchronization techniques can be based on frequency-domain methods, or, more commonly, on time-domain methods. The latter is the case of phase-locked loops used in most applications, and also of frequency-locked loops. The following summarizes the aspects of interest of these two types of synchronization system from the point of view of this thesis, following [7, ch. 4 and 8].

The basic structure of a PLL consists of a phase detector, a filter and an oscillator. The phase detector generates an error signal that is proportional to the phase difference between the input signal and the oscillator output signal. This error is then filtered, and the output modifies the frequency of the oscillator. Canceling this error ensures that the oscillator is correctly tracking the input signal.

For grid-connected applications, the cut-off frequency of a PLL is close to the grid frequency to be detected, and thus the phase detector is key to remove errors and oscillations in the output. For single-phase systems, phase detectors based on a quadrature signal generator are common, ranging from a simple delay of $\frac{1}{4}$ cycle to the use of the inverse Park transform. Additionally, adaptive filters can be employed to facilitate the phase detection. A special case is the use of a Second-Order Generalized Integrator (SOGI), whose bandwidth is not affected by the frequency being detected, and can be used in conjunction with the Park transform to define a SOGI-based PLL with very good performance. A schematic of a SOGI-based PLL is presented in Fig. 2.6.

In three-phase systems, a similar approach can be taken, without the need for a quadrature signal generator, given the fact that the Park transform can be applied directly to the set of three-phase voltages. However, the straightforward application of the transform to translate the signals into the Synchronous Reference Frame (SRF) gives rise to an SRF-PLL that is subject to large detection errors when the input signal is distorted. In order to overcome the issues introduced by this distortion, the design of the PLL can take into account the SRF corresponding to different se-

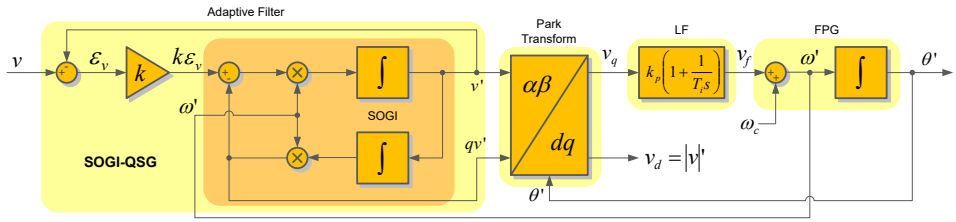


Fig. 2.6. SOGI-based PLL [7].

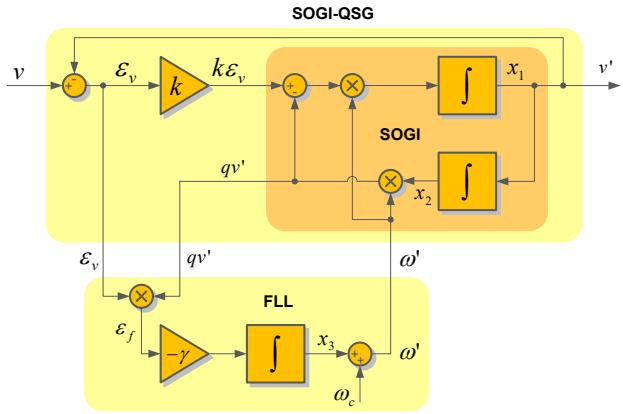


Fig. 2.7. SOGI-FLL diagram [7].

quences and harmonics, and include decoupling networks to remove the distortion. This results in a Decoupled Double Synchronous Reference Frame PLL (DDSRF-PLL) with improved performance.

On the other hand, FLLs only have to detect the grid frequency, which is more stable than its phase, and can fully exploit the characteristics of the SOGI. Namely, as shown in Fig. 2.7 a SOGI-FLL uses the SOGI both as a quadrature signal generator and as an oscillator, thus reducing the complexity of the synchronization system and improving its transient response. In a three-phase system, a structure employing two SOGIs, each of them acting on one of the $\alpha\beta$ components of the voltage, can be employed to obtain a robust estimation of the grid frequency, constituting a Double SOGI FLL (DSOGI-FLL).

Further details about PLLs and FLLs, and their dynamic response to different events and grid conditions, are presented in [7, 14, 17, 18].

#### 2.1.2.7 Power controller

The active and reactive power injected by power converters are usually controlled by simple techniques based on the Instantaneous Power Theory (IPT). Many of these techniques are based on, or derived from, voltage oriented control, i.e., defining a synchronous reference frame whose $d$ axis is aligned with the grid voltage vector [7, p. 219].

In general, in the $dq$ frame, the instantaneous active and reactive power are given by:

$$\begin{aligned} P &= v_d i_d + v_q i_q \\ Q &= v_q i_d - v_d i_q \end{aligned} \tag{2.11}$$

When the $d$ axis is aligned with the grid voltage, $v_q = 0$ and the expressions of active and reactive power are simply:

$$\begin{aligned} P &= v_d i_d \\ Q &= -v_d i_q \end{aligned} \tag{2.12}$$

This type of control can also be applied in the $\alpha\beta$ frame, considering the corresponding expressions, which are analogous to (2.11):

$$\begin{aligned} P &= v_\alpha i_\alpha + v_\beta i_\beta \\ Q &= v_\beta i_\alpha - v_\alpha i_\beta \end{aligned} \tag{2.13}$$

In this case, the expressions cannot be simplified because $v_{\alpha\beta}$ has oscillating components.

Given active and reactive power references and a voltage measurement, (2.11) and (2.13) allow defining the current reference that the power converter should follow in order to inject those active and reactive power respectively as:

$$\begin{pmatrix} i_d^{ref} \\ i_q^{ref} \end{pmatrix} = \frac{1}{v_d^2 + v_q^2} \begin{pmatrix} v_d & -v_q \\ v_q & v_d \end{pmatrix} \begin{pmatrix} P^{ref} \\ Q^{ref} \end{pmatrix} \tag{2.14}$$

$$\begin{pmatrix} i_\alpha^{ref} \\ i_\beta^{ref} \end{pmatrix} = \frac{1}{v_\alpha^2 + v_\beta^2} \begin{pmatrix} v_\alpha & -v_\beta \\ v_\beta & v_\alpha \end{pmatrix} \begin{pmatrix} P^{ref} \\ Q^{ref} \end{pmatrix} \tag{2.15}$$

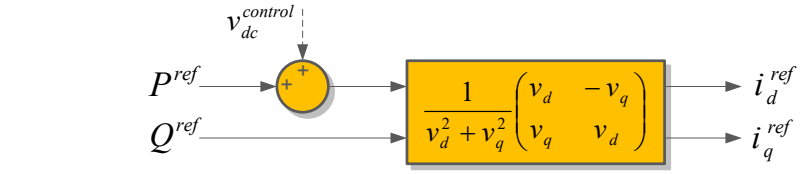


(a) Open loop.

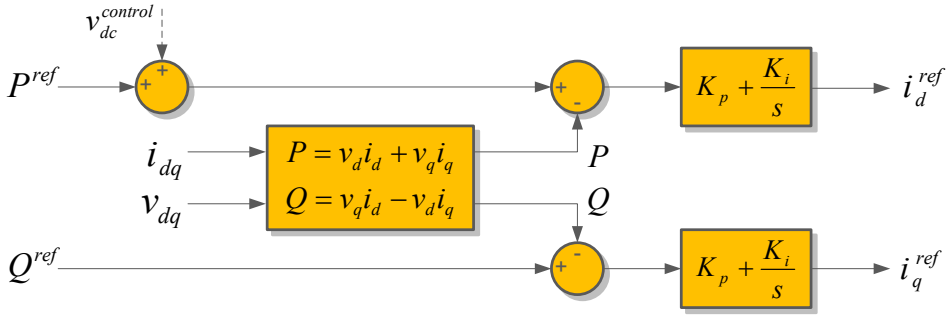


(b) Closed loop.

Fig. 2.8. Active and reactive power controllers based on vector oriented control.

Employing these references, it is possible to define open-loop controllers of active and reactive power, like the one shown in Fig. 2.8a, in both reference frames. These controllers respond instantaneously and do not allow controlling the active and reactive power dynamics. Alternatively, closed-loop controllers can be defined. The simplest approach that guarantees zero steady-state error consists on two PI controllers, acting on the active and reactive power error. In the $dq$ frame, as indicated in Fig. 2.8b, they directly generate the $i_{dq}$ references, whereas in the $\alpha\beta$ frame they generate the current magnitude and phase-shift with respect to the voltage, whose phase-angle is then required to compute the total phase-angle of the current and the reference components [7, pp. 221–225].

Other power control techniques employ virtual flux to achieve synchronization, or direct power control to compute the switching signals. In the latter case, a hysteresis controller can be applied to directly compute these signals from the active and reactive power errors, or a conventional controller like a PI can be used to generate the voltage reference for a modulation algorithm.

#### 2.1.2.8 DC voltage controller

Voltage source converters must keep their dc link voltage within a given range in order to operate adequately. Excessively low voltages result in high dc currents and may give rise to overmodulation, which reduces the quality of the synthesized signals. On the other hand, very high voltages may damage the insulation and harm the equipment.

Therefore, a dc voltage controller is usually included in the control system of a power converter. The simplest approach consists of a proportional-integral controller acting on the voltage error and generating a signal that should modify the active power reference of the converter, as shown in Fig. 2.8. In this way, through modifying the exchange of power between the converter and the grid, it is possible to charge and discharge the dc link capacitor until the objective voltage is attained.

Alternatively, if the power generated by the resource feeding the converter is controllable, as would be in the case of a battery, the active power reference of the resource can be used for this purpose, thus not affecting the active power interaction between the converter and the grid.

## 2.2 Grid-friendly power converter controllers

The conventional power converter controllers presented in the previous section are useful to inject the maximum power available from the renewable resource at any time, which is usually the objective of renewable power plants. In addition to them, ancillary loops can be included to improve the power quality of the grid; for instance, regulating the voltage at the point of connection, or reducing the harmonic content in the grid voltage, as active filters do. However, this is not enough when the penetration of generating units based on power electronics becomes important in a power system. Like other generators, these units should contribute to the control and stability of the system, but this is not possible if they inject power regardless of the system state, and if their dynamics differ from those traditionally taken into account in the design of the controllers that guarantee the stability of the power system. Among these differences, it is possible to cite the lack of mechanical inertia, which may result in larger frequency excursions for a given power imbalance

as more conventional generating units are replaced by this kind of generators; and their strong dependence on the dynamics of their synchronization systems, which are not based on a natural synchronization system that automatically contributes to the power system balance.

Therefore, research efforts have been directed at the design of power controllers that emulate the behavior of synchronous generators during the last years. The objective of these controllers is to make power converters participate in the control of the system and react to disturbances in the grid like synchronous machines. Synchronous generators are naturally synchronized with the grid when frequency variations occur, and their inertia contributes to frequency stability, limiting its variations. Moreover, a synchronous machine behaves as a voltage source behind an impedance, and can therefore form a grid from a deenergized system. Taking this into account, the converter controller system should emulate the inertia of a synchronous machine and make the converter behave as a voltage source behind an impedance.

### 2.2.1 Droop controllers

A first step in this direction is taken by droop controllers. The objective of this type of controllers is to participate in primary frequency regulation, or load sharing, in the same way as synchronous generators do through their droop characteristics, i.e., modifying the active power they inject proportionally to the frequency deviation. Therefore, inertia emulation is not considered in their design, although the response obtained with some implementations is equivalent to emulating inertia, as proven in [20].

Two main classes of droop controllers can be identified. The first one is basically a conventional power converter controller, with an additional block that modifies the active power reference of the converter through a proportional action that uses the frequency deviation as an input. Taking this approach, a grid-feeding converter with controllable active and reactive power can become a grid-supporting converter [21], with external droops determining its power references, as depicted in Fig. 2.9.

The other approach makes the converter behave as a voltage source whose frequency is determined by the active power error, as shown in Fig. 2.10. The resulting

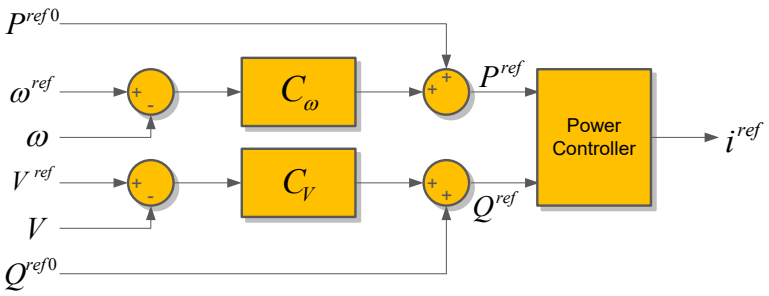


Fig. 2.9. Conventional droop controller based on a grid-feeding converter [21].

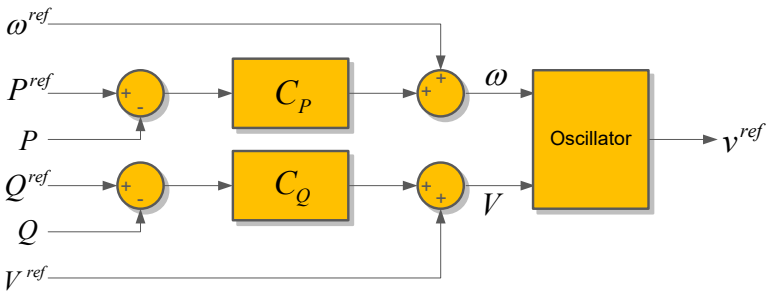


Fig. 2.10. Droop controller defining a voltage source [21].

voltage can then be reproduced by conventional converter inner controllers as explained in Subsection 2.1.2, directly or after being modified by a virtual impedance [21], and the voltage source frequency and angle can be used for synchronization purposes. In this way, the electrical model consists of a voltage source behind an impedance, and no additional synchronization system is necessary, which are features of synchronous machines. However, the dynamics are significantly different due to the lack of inertia.

This type of droop controller has been widely studied in the literature, with many applications in microgrids. Some examples can be [22], which is one of the first proposals and combines the droop with flux control, or [23–26], which address different aspects of the controller and its implementation in detail. Apart from these, it is possible to observe that other controllers, which are not usually classified as droop controllers, give rise to equivalent dynamics, like the Power-Synchronization Control in [27, 28].

### 2.2.2 Virtual synchronous machines

The goal of reproducing other features of synchronous generators, with special attention to their inertia, is sought by other controllers that incorporate more complex dynamics in their control loops than droop controllers. Authors have proposed different implementations and given them different names, like Virtual Synchronous Machine (VSM), Virtual Synchronous Generator (VSG), synchronous converter, or Synchronous Power Controller (SPC), but it is possible to identify common features among them.

Some designs aim only at emulating the inertial response of a synchronous machine, which is defined by its swing equation [29, pp. 128–131]:

$$2Hf\frac{df}{dt} = P_{mech} - P_{elec}, \tag{2.16}$$

where $H$ is the inertia constant of the machine in seconds, and the frequency $f$ and input and output power $P_{mech}$ and $P_{elec}$ are expressed in per unit (p.u.). Taking this into account, the active power reference of a conventional power converter controller can be modified in the following way:

$$P_{ref} = P_{ref0} - 2Hf\frac{df}{dt} \tag{2.17}$$

This is the approach taken in [30], where a *virtual synchronous generator* is presented. This idea is expanded in [31], where the energy and the inertia of a virtual rotating mass are considered and some simulation results are presented, and [32], where the converter PLL is modified to include inertia and emulate the behavior of a synchronous generator, also including a damping coefficient. This controller was developed within a 6th EU-Research Framework project, which led to additional developments and results: real-time simulation [33, 34], experimental results [35, 36], study of measurement systems [37], and an implementation based on an energy storage system [38]. This controller is also applied to the control of a battery energy storage system by other authors in [39], and the contribution of that system to the frequency stability of an autonomous grid is documented in [40].

This type of controller, usually named simply *inertia emulation controller*, has been applied to the control of wind turbines, and has reached commercial uses in

grid-connected wind power plants. One of these commercial implementations is presented in [41–43] and analyzed in [44, 45].

However, power converters that use this controller do not reproduce other features of synchronous machines, especially their voltage source behavior. An opposite approach leads to the *virtual synchronous machine* presented in [46]. In this case, the authors embed a complete model of a synchronous machine in the control of the converter. On the one hand, a virtual rotating mass is considered and its angle and angular speed depend on the active power balance. The virtual inertia effect of this mass, and the resulting energy variations, are supported by a storage system connected to the dc bus of the power converter. On the other hand, a virtual excitation system is included to control the reactive power injection. As explained in more detail in [47], the model considers, not only the swing equation of the machine, but also the flux linkage equations, including damper windings. This requires setting a large set of parameters, mainly consisting of resistance and inductance values, as those defining the dynamics of actual synchronous machines.

Therefore, in addition to the complexity of the controller, the converter dynamics inherit other features of synchronous machines, including their weakly damped nature. Further work by the same authors, included in [48, 49], considers a simpler model, shown in Fig. 2.11, where the excitation and flux linkage equations are replaced by a voltage source corresponding to the electromotive force and a virtual impedance. The resulting current reference, as in the original implementation in [46], is fed to a hysteresis controller that does not require a modulation block. The ability of this controller to operate in island mode is studied in [50], and this implementation is compared with another one that provides voltage references for a modulation algorithm in [51].

Most proposals follow this intermediate approach, considering the swing equation of the synchronous machine and a simplified model where it is represented only as a voltage source. The main differences reside in how this voltage is synthesized, and whether an ancillary synchronization block is used or not.

The *virtual synchronous generator* in [52] uses the voltage signals obtained from the virtual electromotive force directly as the input of the modulation block. Its swing equation includes a damping term, considering the frequency deviation with

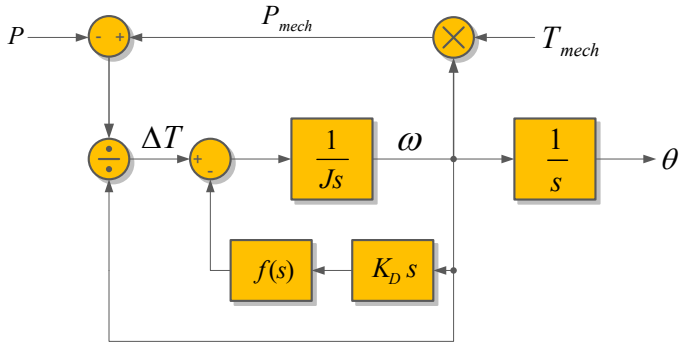


(a) Electromechanical model.

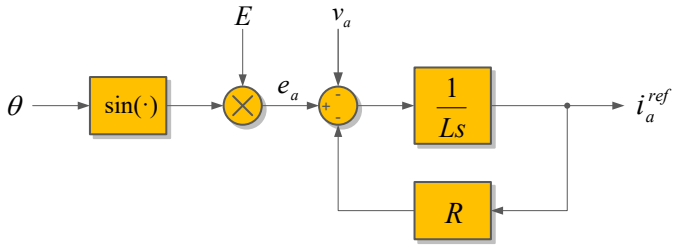


(b) Phase *a* voltage source model.

Fig. 2.11. Simplified version of the virtual synchronous machine presented in [48].

respect to the grid frequency, which is estimated with a PLL. Moreover, it uses an external frequency droop that modifies the active power reference in order to participate in primary regulation. This structure is extended to include a reactive power control loop in [53], and a scheme with variable inertia is considered in [54]. The contributions to stability and power oscillation damping of this controller are studied, respectively, in [55, 56].

A similar approach is followed by the *synchronverter* presented in [57, 58]. In this case, the voltage is also directly fed to the modulation, but the damping term in the swing equation is calculated with respect to the rated frequency. However, the controller still uses a PLL in order to achieve the initial synchronization between the converter and the grid. As shown in Fig. 2.12, no external droop loop is considered, so the contribution to frequency regulation depends directly on the damping coefficient, leading to a tradeoff between a sufficiently damped response and a natural participation in the control of frequency. This controller is applied to control, not

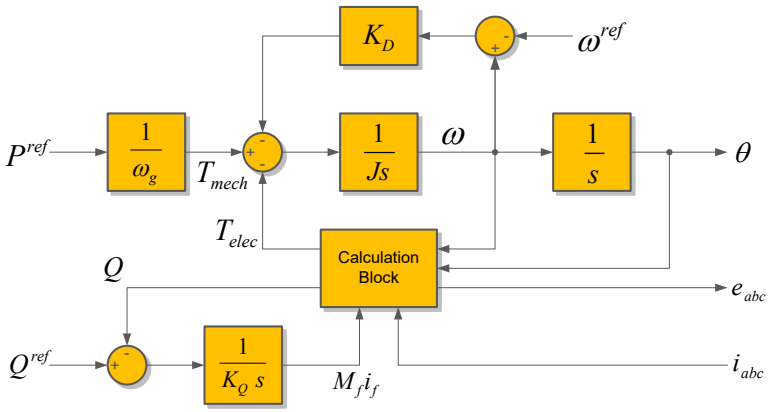


Fig. 2.12. Main *synchronverter* diagram [57].

only generating units, but also a STATCOM, in order to reproduce the behavior of a synchronous condenser [59]. Further developments include a virtual impedance that is used during the initial synchronization, thus removing the need for a PLL [60], and the performance of this controller is compared with a synchronous generator in [61].

A different structure is used by the *virtual synchronous machine* proposed in [62]. Instead of directly employing the voltage as a reference for the modulation, the control system includes a voltage and a current controller. The virtual machine voltage is thus used to generate a current reference, which the current controller tracks by sending the right reference to the modulation block. Thanks to this scheme, the current to be injected by the converter can be limited, avoiding undesired trips. Furthermore, the controller flexibility is enhanced with a virtual impedance block in [63]. In this case, a PLL is also used to determine the frequency deviation damping the response defined by the swing equation. Further developments of this controller include a synchronization controller to be used during the initialization [64], and an adaption to single-phase systems [65].

A third alternative implementation of the voltage source is introduced with the *synchronous power controller* in [66–68]. This controller does not aim at controlling the voltage directly with the modulation or through a voltage controller. Instead, it considers the current induced through the virtual machine impedance due to the

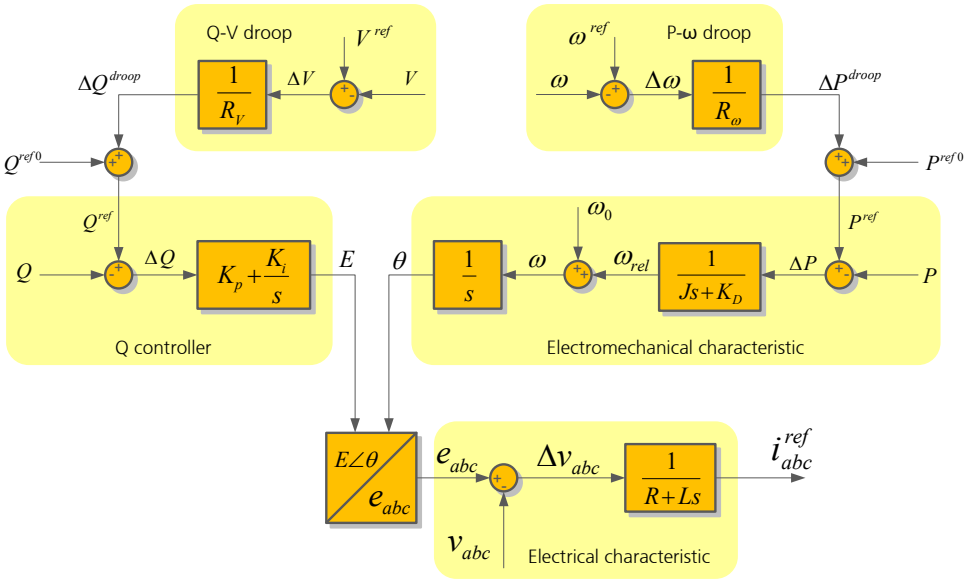


Fig. 2.13. General SPC diagram.

voltage difference between the virtual electromotive force and the grid voltage. In fact, this impedance works as a virtual admittance, with the form of a first-order low-pass filter that processes the voltage error, as in Fig. 2.13. The current reference thus generated, which can be easily limited, is sent to the converter inner controllers, avoiding control issues related to the control of voltage in strong grids, and enabling the simple inclusion of this controller as an outer layer for commercial converters. Furthermore, different virtual admittances can be considered for different frequencies and sequences, allowing the converter to perform functions of an active filter [66]. The SPC can use the virtual frequency as an input for the external droop loop, and the synchronization of the converter with the grid can be achieved through the modification of the virtual admittance, so no additional synchronization systems are required either during normal operation or during the initialization of the system.

Many other contributions related to virtual synchronous machines and similar controllers can be found in the literature. For instance, [69] studies the control of a full-converter wind turbine where the generator side converter emulates the

turbine of a conventional plant, and the grid side converter reproduces the associated synchronous generator, whereas the DC link acts as a virtual transmission shaft. Other examples include the study of the low-voltage ride-through capability of this type of controllers [70], their application in a microgrid [71], and inertia emulation for HVDC controllers [72]. And it is also possible to find overview papers that compare some of these controllers, like [73, 74].

Finally, it is worth noting that most of these controllers focus on controlling the active and reactive power injected by the power converter. If the dc link voltage must be controlled while using one of these controllers, two main alternatives arise. One of them is to modify the active power generated by the primary source, which is analogous to modifying the mechanical power produced by the turbine associated to an actual synchronous machine, but this requires an independent controller for this primary source. The other one would be to modify the active power reference of the converter, which may interact with the dynamics defined by the virtual synchronous machine, but does not require an additional controller. Other strategies can be designed to share the contribution to dc link voltage control among different devices, especially in the case of HVDC.

## 2.3 Power system analysis

The analysis of power systems involves a wide range of topics related to the correct operation of these systems. These topics range from the determination of the system state in static conditions to the assessment of its ability to withstand certain disturbances, also including the quality of the electricity service, the correct operation of the power and protection equipment, and the optimal utilization of power. This thesis focuses on the analysis of the stability of power systems with large penetrations of renewable generators employing power electronics, and the present section will focus on this kind of analysis. This involves mainly the study of the system in dynamic conditions, but it is also necessary to take into account some steady-state analyses that are employed when the stability of a power system is analyzed.

### 2.3.1 Static analyses

The objective of static analyses is to determine or estimate the state of a power system at a given point of time. In a real power system, this time can be in the present for monitoring and operation purposes, in the past in order to study the evolution of the system during a given period, or in the future for scheduling and planning purposes.

The *state* of a power system usually refers to a set of voltage magnitudes and angles, currents, active and reactive power flows, or injections that describe the system under study completely. Strictly speaking, the state of a power system is constantly changing due to connections, disconnections, variations in the power exchanged by the elements connected to the system, or changes in the external conditions. However, most of these disturbances are sufficiently small to consider that the power system operates normally in steady-state conditions, that is to say, with negligible state variations during short time intervals. This justifies the use of static models to determine the state of the system under normal operation, i.e., when the system is not subject to an important disturbance [75, p. 1].

#### 2.3.1.1 Power flow

The basic power system analysis tool is *power flow* analysis, sometimes also referred to as *load flow* analysis. Its goal is to determine the voltage magnitude and angle at all the nodes in a given power system, given the voltage magnitude at some of these buses, the active power generated by each generating unit, and the active and reactive power consumed by all the loads in the system. The data allow writing a system of nonlinear equations with as many equations as unknown variables. In its most conventional form, this requires that the active power generated by one unit is not taken into account, and its voltage angle is fixed instead; this bus becomes then the *slack bus*. Other implementations allow using a distributed slack bus, which shares the possible active power imbalance among selected generators, and also different types of data, like current injections, or voltage-dependent power consumption.

Power flow equations correspond to the active and reactive power balance at each node between flows through lines and injections, and have a characteristic

shape given by the equations describing the power flows through lines and transformers. In the case of a line connecting nodes $k$ and $m$, described by a $\pi$ model with line admittance $y_{km} = g_{km} + jb_{km} = y_{mk}$, and shunt admittances $y^{sh}_{km} = g^{sh}_{km} + jb^{sh}_{km}$ at the $k$ node and $y_{mk} = g^{sh}_{mk} + jb^{sh}_{mk}$ at the $m$ node, the equations would look like:

$$\begin{aligned} P_{km} &= U_k^2 \left(g_{km} + g^{sh}_{km}\right) - U_k U_m g_{km} \cos\left(\theta_{km}\right) - U_k U_m b_{km} \sin\left(\theta_{km}\right) \\ Q_{km} &= U_k^2 \left(b_{km} + b^{sh}_{km}\right) + U_k U_m b_{km} \cos\left(\theta_{km}\right) - U_k U_m g_{km} \sin\left(\theta_{km}\right) \end{aligned} \tag{2.18}$$

Where $U_k$ and $U_m$ stand for the voltage magnitude at buses $k$ and $m$, respectively, and $\theta_{km} = \theta_k - \theta_m$ is their phase-angle difference.

These equations can be generalized to include the effect of tap-changing and phase-shifting transformers, and the admittances connected at and incident to a given bus can be grouped in a generalized term $Y_{km} = G_{km} + jB_{km}$ that allows writing the power balance at node $k$ as:

$$\begin{aligned} P_k &= U_k \left[\textstyle\sum_m U_m \left(G_{km} \cos\left(\theta_{km}\right) + B_{km} \sin\left(\theta_{km}\right)\right)\right] \\ Q_k &= U_k \left[\textstyle\sum_m U_m \left(G_{km} \sin\left(\theta_{km}\right) - B_{km} \cos\left(\theta_{km}\right)\right)\right] \end{aligned} \tag{2.19}$$

This results in a clearly nonlinear problem with a product of two voltage variables multiplied by a trigonometric function of the difference between two angle variables. Nevertheless, a classical method like Newton-Raphson's can solve power flow problems in most situations. In fact, simplified versions of this method are usually employed to speed up the calculation process. In ill-conditioned cases, where the solution lies in a narrow region, far from the initial guess, or is a bifurcation point, robust methods can be employed. Details about power flow models and solution methods can be found in power system books; as concise summaries, [75, pp. 1–66] and [76, pp. 61–101] may be cited.

#### 2.3.1.2 Continuation power flow

Continuation power flow methods are employed to determine how far a power system is from its maximum loadability limit. They are based on a homotopy function of which this loadability limit is a variable, and obtain solution curves through a predictor-corrector method.

These methods allow identifying limit-induced bifurcations, operation points that may lead to a collapse because the operating limit of a device is reached; saddle-node bifurcations, at the maximum loadability point; and other bifurcations. Furthermore, continuation power flows based on homotopy allow calculating the power curve beyond the saddle-node bifurcation. A detailed explanation of continuation power flows methods can be found in [76, pp. 103–130].

#### 2.3.1.3 Optimal power flow

The power flow equations are usually combined with optimization problems in order to determine optimal operation actions. For instance, a power system operator may want to reduce the system losses through a correct setting of voltage references, or the amount of power to be generated by the generating units in the system may be scheduled for the following day, or week, in an economically optimal way taking into account technical constraints. Furthermore, this operation might take into account security constraints that increase the robustness of the system, for instance, fulfilling the *N-1* criterion that guarantees the devices in the system will continue working in their safe operation area in steady state even if any other device is disconnected from the grid. This means that any solution must fulfill the power flow equations for all the considered scenarios.

Therefore, this usually results in an optimization problem with a large number of nonlinear equations and, very often, also with integer variables, which requires specific optimization methods and a large computation capability. The complexity of this problem, its formulation, and some solution methods are discussed in [76, pp. 131–153].

#### 2.3.1.4 State estimation

The objective of state estimation is similar to the power flow problem, i.e., to determine the voltage magnitude and angle at all the buses in the system, and all the magnitudes that can be calculated from them, like power flows. However, state estimation methods take into account that, in transmission systems, there are usually many more measurements than unknown variables, and that these measurements

are subject to certain error. Therefore, the state obtained from a power flow problem may inherit the error in the data, and is not taking profit of the available redundancy.

State estimation methods [77–79], on the other hand, consider all the available data, which results in an overdetermined problem. This problem can be solved by a least squares method in order to obtain the approximate solution that minimizes the total error of the available measurements, which in fact is a more reliable solution than one obtained from a power flow if there is uncertainty in the measurements. Furthermore, this error can contain weight coefficients that take into account the reliability of each measurement, and the results of the estimation may give hints about errors in the measurements, the parameters defining some elements of the power system, or even the state of some elements like switches.

#### 2.3.1.5 Short-circuit analysis

Despite short circuits cause large disturbances in electrical systems, followed by appreciable transients, usually they are studied in a planning stage, and their objective is to determine the rating of different elements and how protections must be coordinated. In these studies, only particular values of the resulting currents are of interest, such as their peak value, and they can be obtained with simplified methods that do not consider the dynamics of the power system. These methods are usually defined in standards, which may have different applications. An introduction to the theory underlying these methods can be found in [75, pp. 57–76].

#### 2.3.1.6 Other analyses

Many other analyses are carried out in power systems considering it is in a steady state, especially for planning purposes. This is the case, for instance, of protection coordination, or harmonic analysis and mitigation.

### 2.3.2 Power system stability

The stability of a power system is the property that enables the system to remain in a state of operating equilibrium under normal operating conditions and to reach an acceptable state of equilibrium after a disturbance [29, p. 17]. Due to the importance

of power systems in everyday life, maintaining them in a stable operating point is one of the main concerns of their operators.

Instability may arise in weak systems, especially when a large generation or load area is connected to the rest of the system by a reduced number of long lines. However, it may also occur in totally developed and well interconnected systems which are operated close to their limits for economic reasons. Therefore, prevention of instability is a task that must be carried out during the planning stage. Nonetheless, serious events leading to the loss of supply or other malfunctions of the power system are normally caused by disturbances in the grid, and the response of the system control elements and operators can contribute to the stability of the system after the disturbance, so stability must also be taken into account at the operation stage.

The stability of conventional power systems has been deeply studied. Adequate models of power system elements and the response of the main types of power plants are widely known (see, for instance, [76]). Moreover, past power system events have been analyzed in detail. With this knowledge and experience, power systems are planned to fulfill security constraints, controllers are tuned to keep the system in a safe operating point, and operators are trained to react properly to disturbances, which results in a high degree of security and reliability of power systems.

Nevertheless, the inclusion of new power sources and generation technologies might modify this picture. First, some sources depend on weather conditions and are therefore variable and not fully controllable, opposite to conventional power plants, which usually employ a fuel that can be stored and spent as necessary. Secondly, the systems employed to generate electric power are in many cases power converters, whose natural behavior is different from that of synchronous generators. Thirdly, in many cases, the resource is dispersed and electricity is injected into the grid by small generating units in distribution networks, which are designed only to deliver power to customers and may behave strangely if power flows are reversed. Fourthly, in other cases, the resource is located far away from consumption centers, requiring long transmission lines, for which HVDC, also employing power converters, is becoming a common technology. These characteristics, if not correctly taken into account, may generate problems for conventional power systems, but they can also enhance system performance if they are managed properly, due to the increased con-

trol flexibility of power converters, and the benefits that moving generation closer to consumption has.

Until recently, this kind of new systems used to have a negligible impact on the grid because of their limited penetration. However, their growth during the last years, which is expected to continue, has made this impact significant. Therefore, the concern about the effects that these systems have on power systems is increasing, which reflects on a larger number of reports being published, and more stringent connection requirements being set by system operators.

The increase of distributed generation and nonlinear loads has led to a growing trend in the study of distribution systems. The typical concerns of these studies are power quality, voltage profiles, phase imbalances, current and voltage harmonics, protections, and islanded operation of some parts of the grid, which may be unplanned and become dangerous for power system users and workers.

Despite the interest for the impact on distribution systems, power system stability is understood as a transmission system issue, concerning the ability of all generators to maintain synchronism and the capability of the power system to maintain adequate values of voltage and frequency throughout, and it is also affected by the connection of new generating units based on power electronics at all voltage levels. A basic introduction to each of these different aspects of power system stability follows.

#### 2.3.2.1 Angle stability

Angle stability is the ability of synchronous machines connected to a power system to remain in synchronism [29, p. 18]. The principle underlying the synchronous operation of these machines is the relation between the electrical power output and the angle difference between the machine and the grid, and between this electrical power output and the machine speed.

When a machine accelerates with respect to the grid, its relative angle increases, and so does its electrical power output. In turn, this output increase tends to decelerate the machine. In a stable case, the machine eventually reaches a new equilibrium for which the input and output powers are equal, and the machine speed remains constant and equal to the grid frequency. However, in an unstable case, the increase

in the power output of the accelerated machine may not be enough to counter the initial acceleration and get the machine back to an equilibrium point, so its rotor angle continues increasing until synchronism is lost. This phenomenon can be experienced both by one machine against the rest of the power system, and by different groups of synchronous machines against each other.

To study angle stability, the variations in the electrical torque that acts as a braking torque on the rotor of a synchronous machine are usually split into two components. One of them is in phase with rotor angle variations and is called synchronizing torque, whereas the other one is in phase with the speed deviation and is called damping torque. For stable operation, it is necessary that both components of the braking torque are positive. Otherwise, instability will occur in the form of an aperiodic drift if synchronizing torque is not enough, and through growing oscillations if there is a lack of damping torque. Examples of these different cases can be seen in Fig. 2.14.

Furthermore, angle stability phenomena are classified taking into account the characteristics of the disturbance originating them, which defines the analysis techniques that can be used. Small-disturbance phenomena are those that involve small deviations from a base operating point, and they can be analyzed employing a linearized system; whereas large-disturbance phenomena comprise large or sudden variations, and the analysis cannot neglect the nonlinearities in the equations.

Namely, in small-disturbance angle stability analyses, the perturbations that alter the system performance are considered small enough to linearize the system around an initial point of operation, and small-signal techniques can be applied. In practical power systems, this instability usually arises as a problem of insufficient damping of oscillations [29, p. 25]. These oscillations are normally classified in four types: local modes, interarea modes, control modes, and torsional modes. The main differences among them are their origin and their frequency.

To analyze the dynamics of a system, it can be described by its state space, which consists of a set of differential and algebraic equations that define the evolution of the state of the system from a given initial state with given inputs. For small disturbances, these equations can be linearized and written in matrix form, and the eigenvalues of the state matrix determine the natural response of the system. In

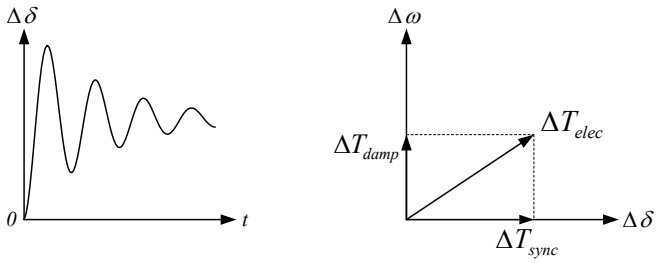


(a) Stable evolution.

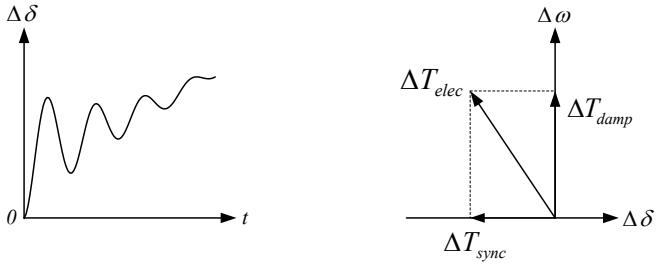


(b) Non-oscillatory instability.

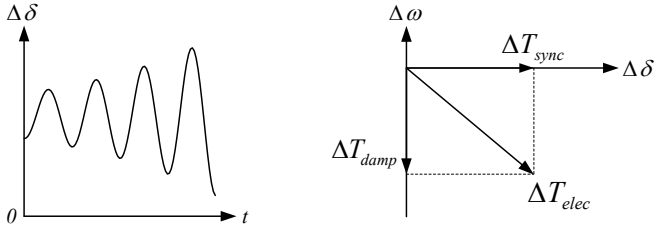


(c) Unstable oscillations.

Fig. 2.14. Time-domain evolution of the angle of a synchronous machine depending on the synchronizing and damping torque [29].

general, these eigenvalues are complex numbers. Eigenvalues whose imaginary part is not zero give rise to oscillations, whereas real eigenvalues correspond to non-oscillatory responses. The real part of the eigenvalues determines their damping. If it is positive, the response will grow indefinitely, leading to instability, whereas for negative values the associated response will decay until it has no influence on the system.

On the other hand, when large disturbances, like a short circuit, a line trip, the loss of a big generator, or the loss of a large amount of load, are considered, large

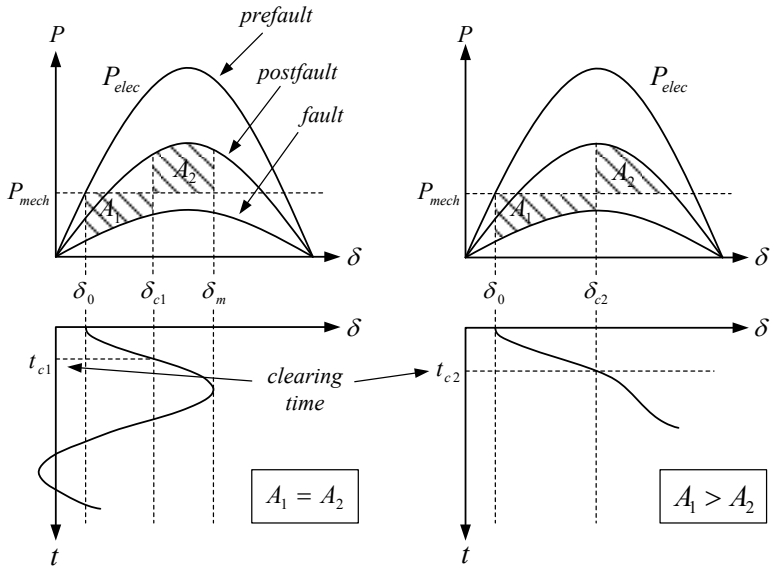


Fig. 2.15. Equal area criterion application example [29]. When area $A_1$ is greater than area $A_2$, the system may experience first-swing instability. Otherwise, the area equality determines an upper bound for the maximum angle deviation.

currents, torque values, or rotor angle deviations are involved, and the result depends on the nonlinear behavior of the power system. A simplified approach to the study of the stability after a fault usually considers a synchronous machine connected to an infinite bus, and the balance between its mechanical input and its electrical output. The stability of this system can be assessed with the equal-area criterion [29, pp. 831–835], an example of which can be seen in Fig. 2.15, or more advanced direct methods based on Lyapunov theory [80, pp. 222–237].

However, direct methods only determine whether the stability of a system is guaranteed or not, and they provide very limited information about the reasons for instability, or the available stability margin. An alternative strategy to analyze this type of stability is based on simulating the system behavior by numerically integrating the constituting equations. First, it overcomes the main drawback of direct methods, since simulations always show if the system is stable or unstable, as long as the model is accurate. Secondly, the results of the simulations include data about the speed, the angle and the voltage of the machines, which can be more useful to

determine the causes for instability or to prevent it.

#### 2.3.2.2 Frequency stability

The study of frequency stability is concerned with large imbalances in generation and consumption within a power system. The origin of these imbalances might be the sudden connection of a large load, the unplanned disconnection of an important generating unit, or the separation of the system into different electrical islands after a fault.

The time constants involved in these phenomena may range from several seconds to hours. Therefore, the models that might be required to simulate this kind of events would include the energy supply systems, and the protections and controls that are activated under these circumstances [29, pp. 1085–1086], in addition to the models used to study angle stability, which are normally designed to study contingencies in the range of a few seconds.

The analysis of the response of a power system to a large energy imbalance that originates a frequency deviation can be divided in four stages taking into account the nature and the duration of the different contributions to the system response [80, pp. 350–357]. The first stage corresponds to the rotor swings that generators suffer when their mechanical input or the characteristics of their electrical output change suddenly after an event. These variations modify the equilibrium point of each generator, but their load angle cannot change instantaneously. If the generators are able to remain in synchronism and they have enough damping, they reach the new equilibrium point after a few seconds, as shown in Fig. 2.16. Then, a second stage can be identified where the mechanical input and electrical output mismatch affecting the generators causes them to accelerate or decelerate as a result of their torque balance and their moment of inertia.

The resulting frequency deviation activates turbine governors and other primary controllers, so a third stage begins where the input power is modified according to the action of these controllers, usually following a droop curve. This action establishes a new equilibrium point for which the frequency is stabilized, but not at the rated value in general. Finally, the fourth stage comprises the activation of secondary controllers to restore the frequency to its rated value, through the variation

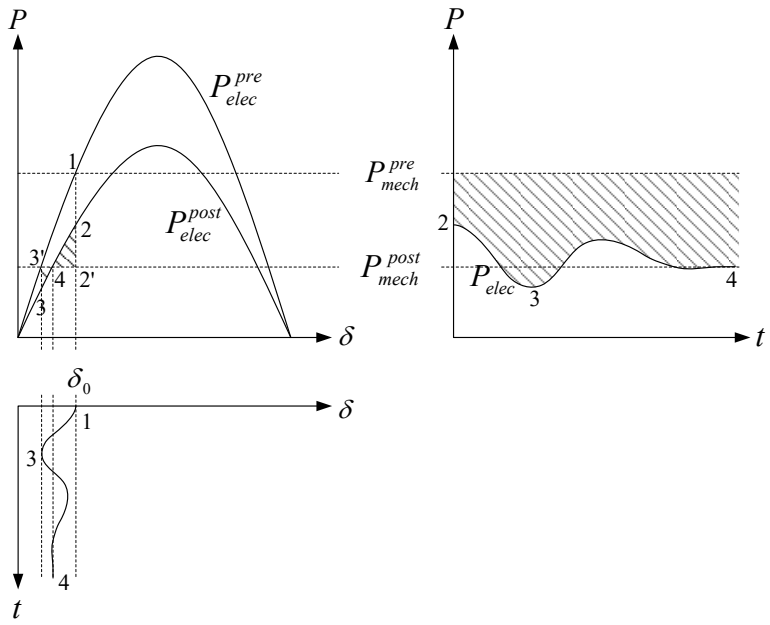


Fig. 2.16. Rotor swings after the disconnection of a neighboring generator [80].

of the power references of selected generators. Furthermore, in interconnected systems, it is important to control the power flows through the tie-lines in addition to the frequency. This requires setting appropriate values for the secondary control parameters, as discussed in [29, pp. 601–610] and [80, pp. 364–368].

This allows identifying several factors that affect frequency stability. On the one hand, during the second stage, the frequency deviation is mainly influenced by the inertia of the machines in the system. Therefore, a system with a large inertia constant will suffer limited frequency deviations, reducing the stress set on primary and secondary controllers. In modern power systems, the inclusion of power generation based on converters may have therefore a detrimental effect. On the other hand, primary control is fundamental during the third stage, and the influence of generator limits must be considered. In this stage, defense plans based on load shedding can play a crucial role to avoid a frequency collapse, and they must take into account that some generators may be tripped by underfrequency protections.

#### 2.3.2.3 Voltage stability

Voltage stability is the ability of the power system to maintain all the bus voltages within a given operating range, and it can be affected by short-term or long-term phenomena.

The commonest short-term phenomena are voltage sags, i.e., short duration voltage reductions. They are usually the result of connecting large loads or electric motors, energizing transformers, or power system faults. The reverse phenomenon can also happen, normally after the disconnection of a large load. Due to the large magnitude and short duration of the transients involved, the study of this type of events requires electromagnetic models that take into account the interaction of inductors and capacitors, whereas the output of slow controllers can be considered constant. Additionally, it is often necessary to use multi-phase models since the event may affect only one or two phases, or do it in different degrees for each one.

When such contingencies are analyzed, the main objective is to assess the ability of generators and other power system elements to withstand the disturbance without being damaged or being disconnected from the grid. Therefore, emphasis is set on calculating maximum currents and verifying the fault ride-through capability of devices.

Long-term phenomena include brownouts and voltage collapses. A brownout is a reduction of voltage that lasts for several minutes or even hours, and it can be caused by a problem in a power system lacking reactive power resources or transmission capacity, or induced by the system operator in order to reduce the total power demand. A voltage collapse is the worst outcome of a lack in reactive power generation and transmission capacity, and it may end up in the disconnection of loads and generators, and even a total blackout. The classical study of voltage stability focuses on this type of phenomenon, assessing the distance to the instability and the mechanisms leading to it.

This classical analysis considers the characteristics of power transmission, i.e., the relation between the power transmitted through one line and the voltage at the end of that line is studied. Due to the quadratic form of the associated curve, shown in Fig. 2.17, the same amount of active power can be transmitted for two different voltage values. However, only the highest one allows a stable operation, and power

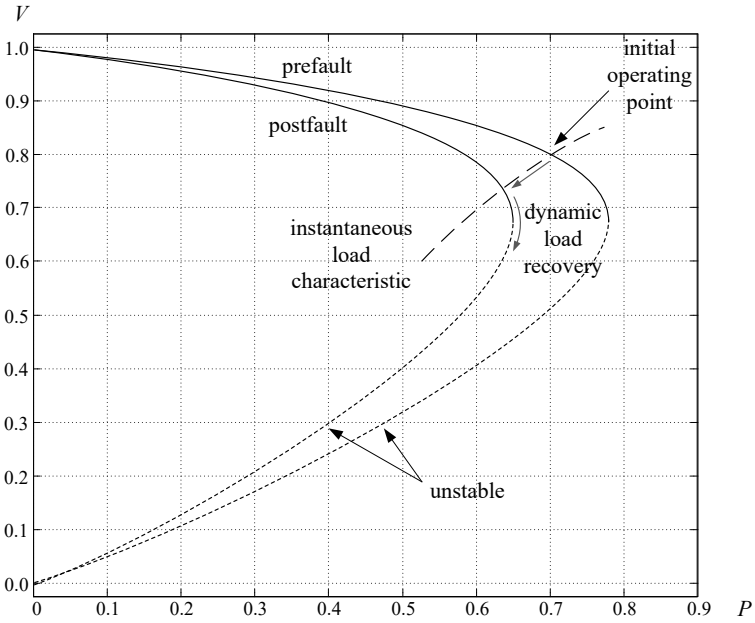


Fig. 2.17. PV curves and dynamic voltage collapse [81].

systems normally operate in the upper part of the curve, where an increase in the active power transfer can be achieved by decreasing its voltage. Nevertheless, there is a maximum power that can be transmitted and if it is reached both an increase and a decrease in voltage will result in a decrease in the power transfer. Moreover, the shape of the curve is strongly dependent on the line impedance, which limits the maximum power that can be transferred, as happens in Fig. 2.17 for the pre- and post-fault curves.

Therefore, a voltage collapse can be induced by a progressive increase of the active power demand until it exceeds the line capacity, but it can also be a consequence of the fact that one device reaches its operation limits, thus altering the shape of the curve describing the transmission characteristics. Furthermore, when a transmission line is operating close to its maximum loadability, a fault in the transmission line, which will modify this curve, can render the maximum power transfer smaller than the power to be transmitted after the fault, or the subsequent load recovery can take the system beyond its new maximum loadability point, as depicted in Fig. 2.17.

The analysis requires adequate models of the elements that influence voltage stability. This implies modeling loads, conventional and power-electronics-based generators, tap-changing transformers, capacitor banks, Flexible Alternating Current Transmission Systems (FACTS), secondary frequency controllers, and protections.

### 2.3.3 Dynamic analyses

Power system stability studies employ different kinds of analysis depending on the phenomena under study. In fact, the stability can be assessed through static analyses that consider only algebraic equations, like continuation power flows employed in classical voltage stability in order to determine the voltage vs active power curves of the system; or dynamic analyses that take into account the differential equations that describe the dynamics of the system.

Among the dynamic analyses, it is possible to find conventional techniques like Laplace-domain and frequency-domain analyses. These techniques are usually applied to simple systems; for instance, they are usually applied to tuning the controller of one generator, or to study long-term frequency stability, considering secondary frequency control and load following issues [29, pp. 595–609]. However, due to the size and complexity of real power systems, the commonest techniques when the stability of the whole system is studied are based on modal analysis and time-domain simulation.

#### 2.3.3.1 Modal analysis

Modal analysis is usually employed to determine how stable a power system operating in a particular state is in front of small disturbances. A disturbance is considered small when a linearized version of the equations describing the behavior of the power system can be employed to analyze its effects [29, pp. 699–825]. In that case, the power system state-space equations can be written as:

$$\begin{aligned} \dot{x} &= Ax + Bu \\ y &= Cx + Du \end{aligned} \tag{2.20}$$

Where $x$ is the state vector, $u$ is the input vector, $y$ is the output vector, and matrices $A$, $B$, $C$, and $D$ describe the dynamics of the system around a particular operating point. In particular, the stability of the system depends on the eigenvalues of matrix $A$, which are complex numbers in general. The imaginary part determines whether an eigenvalue gives rise to an oscillatory mode, and the frequency of the corresponding oscillations; whereas the real part determines whether the mode is stable or not, and how fast it fades away or develops. Namely, only eigenvalues with a negative real part result in stable dynamics, and the closer their real part is to zero, the longer its dynamics affect the state of the system. In the case of oscillatory modes, the ratio between the real part and the absolute value of the eigenvalue also defines the damping of the resulting oscillations.

Furthermore, modal analysis provides information about the state variables, i.e., the power system elements, that are involved in each mode, and the input variables, i.e., the control actions, that can affect each mode. This employs the eigenvectors of matrix $A$, which for each eigenvalue $\lambda_i$ are defined as:

$$\text{Right eigenvector:} \quad A\phi_i = \lambda_i \phi_i \tag{2.21}$$

$$\text{Left eigenvector:} \quad \psi_i A = \lambda_i \psi_i \tag{2.22}$$

In order to avoid the possible disparity of the orders of magnitude of different eigenvectors, they can be normalized and grouped in matrices $\Phi$ and $\Psi$. In those conditions, right eigenvectors show how state variables vary when their corresponding mode is excited. Thus, the $k$-th element of the right eigenvector $\phi_i$, $\phi_{ki}$, measures the degree of activity of the state variable $x_k$ when the $i$-th mode is excited. On the other hand, left eigenvectors express the linear combination of state variables that form the corresponding mode, so the $k$-th element of the left eigenvector $\psi_i$, $\psi_{ik}$, is the relative weight of the state variable $x_k$ in the $i$-th mode. Furthermore, the net participation of the state variable $x_k$ in the $i$-th mode can be obtained as the product $\psi_{ik}\phi_{ki}$, which is usually referred to as *participation factor* of state $k$ in mode $i$.

Due to these properties of eigenvectors, it is possible to determine whether a particular mode is controllable or observable. Namely, the elements of the $i$-th row of matrix $\Phi^{-1}B$ measure the effect of each input on the $i$-th mode, i.e., its control-

lability. On the other hand, the elements of the $i$-th column of matrix $C\Phi$ represent the weight of the $i$-th mode on each output, i.e., its observability. This information can be employed in the design of controllers that aim at correcting the behavior of certain modes.

#### 2.3.3.2 Time-domain analysis

Time-domain analysis is based on integrating the equations that describe the system in order to simulate its response to different events. The integration can take into account the full nonlinear behavior of the system, and thus be used to analyze large disturbances. Thus, simulations allow studying whether the system can withstand severe events like a significant loss of generation or consumption, a short-circuit fault, or the disconnection of one or more lines. Furthermore, given the detailed information about the evolution of the system that simulations provide, they can be very useful to identify the mechanisms that lead to instability. And, although they cannot be used to calculate how far the system is from instability directly, this can be assessed through an iterative process where the severity of the event is modified depending on whether it leads to a stable or an unstable situation, until the critical condition is found. For instance, this can be employed to determine the critical clearing time for the protections of a generator.

In order to perform an analysis of this type, it is necessary to model the power system as a set of differential and algebraic equations that describe its behavior and can be integrated by a solver. The equations to be considered depend on the focus of the analysis, which usually leads to two types of models: ElectroMagnetic Transient (EMT) models and transient stability models. In both cases, the equations are usually handled by a power system analysis tool that allows easily introducing the model data and visualizing the results of the simulation.

EMT programs focus on the electromagnetic interactions that take place in a power system immediately after a large disturbance takes place. These interactions involve energy exchanges between capacitors and inductors, the actuation of system protections, sudden changes in the impedance or the topology of the system due to faults or resulting from the operation of protections, or the effects of external events like lightning. EMT models are multi-phase and include dynamics with short

time constants. The resulting detail and range of time in which the interactions of interest take place require short integration steps that, in turn, are able to capture the behavior of the system at very high frequencies. Thus, EMT analysis allows studying also grid imbalances, harmonics, peak voltages and currents, and the exact moment when protections are activated.

On the other hand, transient stability models focus on the electromechanical interactions that occur in a power system, i.e., the interactions between voltage and current, and generator power input and speed. They do not usually reach the same degree of detail as EMT models, and consider a single-phase representation of the power system unless an imbalanced system is studied. Furthermore, they do not work with instantaneous voltage and current values, but Root Mean Square (RMS) values are used instead. The dynamics of interests are those of synchronous machines and different controllers, like voltage regulators, governors, power system stabilizers, power converter controllers, load controllers, or transformer tap changers; the dynamics of the generation resources, power conversion systems, or loads may be included depending on the time horizon of the study.

These models reproduce how the elements in the power system exchange active and reactive power, and how the speed of the synchronous machines is affected by this; thus, they allow studying angle and frequency stability. Furthermore, they employ longer integration steps, in the order of milliseconds, that capture what happens for the fundamental frequency and below, like power oscillations; in this way, the size of the analyzed power system and the simulated time can be extended with respect to EMT analysis, enabling the study of the evolution of power system with hundreds or even thousands of buses for many seconds or even a few minutes. This time horizon can be further increased in order to calculate the long-term response of the system; this may require, however, using simpler models, for instance, linearizing some equations and considering that the fastest dynamics are instantaneous.

## 2.4 Modeling of renewable power plants employing power electronics

In the study of stability, it is necessary to employ adequate models that capture the phenomena under study. In the case of classical power system elements, like synchronous machines, transformers, shunt devices, or loads, and even in the case of typical FACTS, the models required for stability studies have been widely addressed in the literature [29,76]. However, when renewable energy sources employing power electronics are concerned, the availability of models is constrained by the quick evolution of the technology and the multiple configurations in which the devices may appear.

### 2.4.1 Modeling of power converters

Given the fast response of power electronics devices, and some of their associated controllers, the model of a dc-ac power converter as those used for wind and solar generation can vary depending on the goal of the analysis. On the one hand, the hardware model can have different degrees of detail. It can include each individual component of the power conversion system, i.e., dc capacitor, power switches, grid-connection filter and transformer, and protections, considering the losses of all devices, and employing a complete three-phase representation. For EMT analysis, this may be a useful approach, or it can be simplified slightly, neglecting the losses of some components, and assuming that transistors behave as ideal switches with certain blanking time to avoid short circuits. However, this model can be further simplified considering part of the hardware as a voltage or a current source, behind the filter or at the point of connection, depending on the controllers and nature of the analysis. Furthermore, a single-phase equivalent model can be used. In transient stability studies, it is common to represent converters as current injections, or even as active and reactive power injections.

On the other hand, certain control systems may admit different representations. This is especially visible when the converter is controlled through a hierarchical structure, where lower levels can be considered very fast for a type of analysis and higher levels may be very slow for another kind of study. Namely, the modula-

tion can be modeled in full detail, including exactly the same equations that are programmed in the device, and sending the resulting signals to the hardware, as is typical in EMT analyses, for instance, to study the harmonic content of the generated signals; alternatively, an average model may replace it with a short delay, and consider the aggregation of the converter power switches and the modulation as a voltage source connected behind the grid-connection filter and following the modulation voltage reference with this short delay.

The current controller, or voltage controller, may also be considered in full detail, with its transform to the $\alpha\beta$ or the $dq$ frame, and generation of three-phase signals, as would be done for EMT analysis; or it can be aggregated with the modulation, the power switches, and the grid-connection filter, as a current source that follows its reference with a delay that reproduces the settling time of the original current loop. This latter approach can be applied both to three-phase and single-phase models. In the case of single-phase models, the real and imaginary parts of currents and voltage can be easily linked to $dq$, and thus also $\alpha\beta$, components. In most transient stability studies, whose integration step is of several milliseconds, and which do not aim at capturing dynamics at frequencies higher than the fundamental grid frequency, this degree of detail is enough. In fact, some models may focus on the active and reactive power the exchange with the grid [76, pp. 400–403].

The modeling of controllers above this one, for which there may be more diversity, will follow a similar approach: detailed for EMT studies, including the use of three-phase measurements and the generation of three-phase references, and simpler for transient stability, keeping the dynamics but employing RMS values of voltages, currents, and power injections. However, high-level controllers like those involved in frequency and voltage regulation, especially those that correspond to secondary control, may be neglected in an EMT study if they are deemed sufficiently slow to have any influence on the period of time that is analyzed, or if the variables they regulate are assumed to be fixed by a stronger system.

Ancillary controllers, like synchronization systems or dc voltage controllers, may play an important role for the current controller, the modulation, or the correct operation of the hardware. Therefore, their models must be as detailed as the models of the main controllers that depend on them. Otherwise, it would not be possible to

obtain significant results about the specific performance of the current controller, the modulation, or the hardware. When this degree of detail is not necessary, ancillary systems may be replaced by simplified equivalents that introduce the corresponding time constant.

With respect to the resource, similar guidelines can be given. A slow-varying resource, for instance, can be considered a constant power source in short-term analyses, whereas the variations of a fast-varying resource can be considered instantaneous in analyses that take into account slow dynamics. However, the adequate model will depend on the nature of the resource and the type of analysis. In the case of wind, the resource model may take into account the wind speed, the turbine rotor speed, and the turbine blade angle in order to determine the power actually extracted from the incoming wind. Similarly, in the case of PV, the power may be calculated as the product of the dc voltage and current, where the current is a function of the voltage, the solar irradiance, and the temperature; in many cases, a simple two-diode model [82] is enough to capture how the PV resource conditions affect the stability of a power system. Different examples of resource models, considering PV and wind, but also storage devices, are presented in [76, pp. 403–408, 435–456].

### 2.4.2 Modeling of distributed power plants

Conventional power plants consist usually of a small number of synchronous generators with a large power handling capability, which are electrically close and are connected to the grid at a common point. However, renewable power plants based on wind turbines or solar PV have a totally different topology. The main reason for this is the fact that the energy density of the resource they employ is low and distributed over wide areas, and it is not technically feasible or economically viable to concentrate it in a single point of conversion. Therefore, many wind turbines or PV converters are deployed to harness the power that can be generated in those areas, each of them with a power rating normally limited to one or two megawatts. In the case of transmission-system-scale power plants, whose power rating can range from 50 MW to 100 MW and beyond, the number of power converters involved can reach the hundreds. Furthermore, the internal network that connects each of these devices with the grid covers long distances, and the impedance of the cables and lines cannot

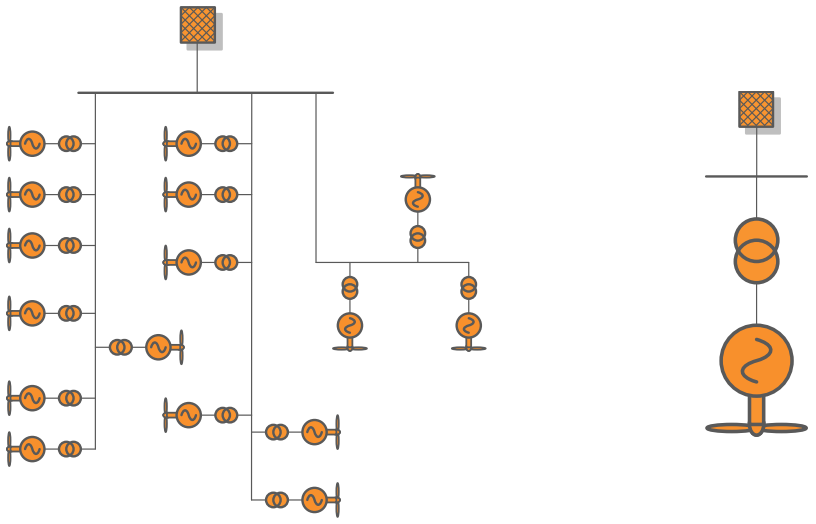

(a) Original model. (b) Equivalent model.

Fig. 2.18. Wind farm equivalent model.

be neglected. Therefore, it is not possible to assume that all the power converters are connected at the same point and their voltage is the same.

Power plant models may consider this complexity in full detail, including the internal network impedance and the model of each power converter. However, this degree of detail is not necessary in many cases when the stability of the power system, and the aggregate impact of the plant on the system, but not the internal state of the plant, are studied. Moreover, the amount of data to introduce and results to analyze, and the time taken by numerical methods employed to determine the stability of the power system or to simulate its evolution, grow with the degree of detail of the model. Therefore, it is interesting to reduce the complexity of the model, as in Fig. 2.18, in such a way that it retains the necessary information to reproduce the aggregate behavior of the plant, but speeding up calculation processes, and facilitating the preparation of the model and the analysis of the results.

In fact, this approach is sometimes taken with conventional power plants employing synchronous generators. Several machines with common characteristics, which can be considered coherent, are grouped and represented by an aggregate equivalent [83]. In the case of distributed power plants using renewable energy, this

aggregation is not as direct. This is due to the already mentioned effect of the internal network, which introduces certain impedance between the point of connection of the plant and the generating units, and to the nature of the resource, which may produce different amounts of power for each power converter. In any case, it is still possible to determine equivalent models that reproduce the desired dynamics with enough accuracy, and the literature provides several works in this sense.

A wind power plant equivalent model for EMT analysis is presented in [84]. The model is divided in two parts. The first one is a frequency-dependent equivalent model of the plant passive components in the frequency range 0–50 kHz, which is obtained from a frequency scan. The second part is a dynamic equivalent model of the plant control and the aggregated low-frequency dynamics of the generating units, considering a single power conversion system with the total power rating. The complete model considers both parts are connected in parallel at the point of connection of the plant.

A different approach is to focus on slower dynamics, as those of interest for transient stability analysis, and consider a scaled-up wind generator model plus an equivalent network impedance. The differences among models usually reside in the type of wind generator employed, and how the equivalent impedance is calculated. In [85], wind turbines are classified in groups depending on the technology they employ and also on their operating point, which may vary substantially and affects the response of the generating unit; whereas the equivalent model of the network is obtained from the reduction of a static model. [86, 87] present equivalent models of wind power plants employing doubly-fed induction generators, and [88] considers permanent-magnet synchronous generators.

Furthermore, [87,88] define different aggregation levels in order to allow certain flexibility when wind turbines operate in different conditions, whereas the equivalent network considers only the impedance of the transformers, which is equal for all the units. An example of a single-machine, multi-turbine model would be given by Fig. 2.19.

Institutions like the National Renewable Energy Laboratory and the Western Electricity Coordinating Council have worked in the development of equivalent models and published their own guidelines [89–91], which have been employed

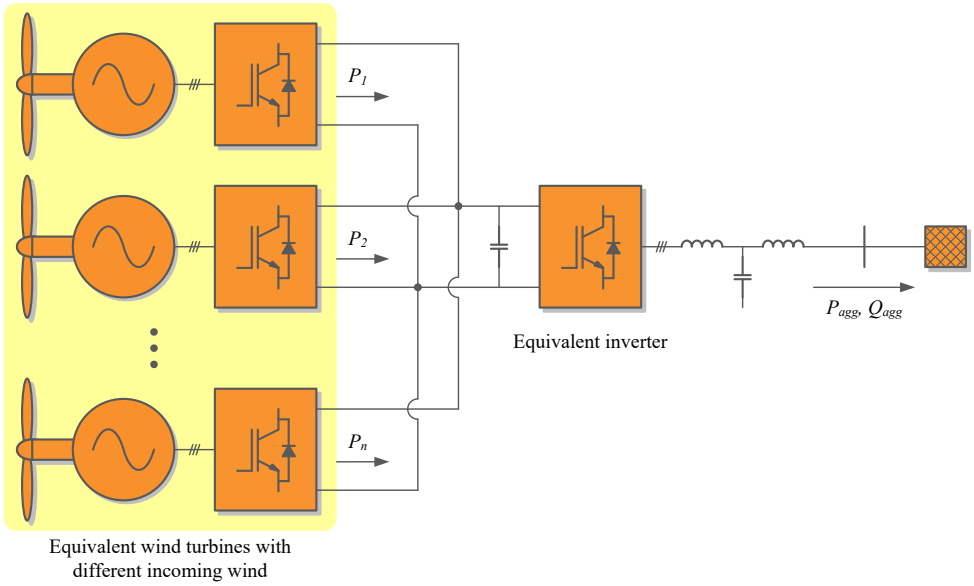


Fig. 2.19. Wind farm equivalent model considering multiple equivalent wind turbines with different incoming wind and a common inverter.

by some of these works. Other approaches include calibration and validation with measurements [92,93], sensitivity [94], perturbation theory [95,96], and probabilistic clustering [97]. In [98], different aggregation methods are compared against a detailed model; namely, a single-machine equivalent, a cluster representation of the plant, an intermediate compound aggregation level, and a probabilistic clustering model are considered.

In the case of PV plants, equivalent models usually focus on the steady-state behavior of the power plant and the calculation of losses. For instance, a method to determine the equivalent model of a PV plant taking into account active and reactive power losses is presented in [99], where it is conceived as a tool for plant design. Nevertheless, it is possible to find initial works that address dynamic models, like [100], where both the internal network and the converter controllers are taken into account. And, as in the case of wind, the Western Electricity Coordinating Council has developed a series of guidelines for PV plant dynamic modeling [101], where they also discuss the assumptions of equivalent models.

## 2.5 Impact of renewable power plants

The production of electricity from renewable energy sources has many benefits for power systems. First, it makes the generation mix more sustainable, thus diluting the threaten that the depletion of fossil fuel reserves poses on energy systems. Secondly, most of the renewable sources employed for electricity generation are clean, with zero emissions during operation. Thirdly, their marginal generation cost is low, so once the investment is recovered, they are sources of very economic electricity. Fourthly, sources like wind and solar energy are widespread, and allow bringing generation closer to consumption, thus reducing transmission losses. Lastly, they allow countries with limited nuclear or fossil fuel resources to have their domestic sources and to reduce their dependence on third countries.

Nevertheless, they also have an impact that may be negative for power systems, especially when the penetration of renewable sources reaches significant values. This impact is caused by two main factors: the characteristics of the source, and the power conversion technology. Renewable resources like wind and solar energy are not available when requested, but depend on weather conditions or the time of the day. Furthermore, this dependence on weather conditions, and the inability to store their energy efficiently as in water reservoirs, make them intermittent sources, subject to variability. Besides, their energy density is low and spread over vast extensions of land, thus requiring the deployment of a large number of energy conversion systems, perhaps connected to parts of the electricity grid that were not designed for hosting generation. On the other hand, wind turbines and solar PV systems are connected to the power system through power converters instead of synchronous generators, which are the technology employed by conventional power plants and have traditionally defined how power systems are designed and controlled. One of the main concerns of system operators is the resulting loss of inertia, which makes the system more prone to larger frequency excursions.

Therefore, it is necessary to analyze the impact that these sources have on power systems, and to study the controllers involved in the conversion of energy from these sources and the coordination of different generating units, in order to mitigate any adverse effect and fully utilize their strengths. This is even more important in the

case of wind and solar PV, which are expected to reach important penetration levels in the near future [102]. This has led many researchers to explore how these sources affect power systems, and a wide range of research works address the impact of these sources from different points of view.

Many authors have focused on the effects of these sources on the design and operation of power systems. For instance, the consequences of high penetration levels of wind generation on different aspects of the design and operation of power systems, like load following and frequency regulation, voltage regulation, technical characteristics of thermal plants, or the response of wind generators during contingencies, are explored in [103]. And power system planning is addressed in [104], taking into account the optimal location of wind power plants for a good power system performance.

Other authors pay attention to the impact of variable sources on the power system generation and demand balance. This is the case of [105], which studies necessary changes in the energy dispatch to accommodate large amounts of PV; [106], where wind power curtailment is proposed as a solution in certain situations; or [107], which reviews several methods to reduce fluctuations in the active power generated by PV plants.

Distribution systems have also been a matter of interest for researchers as distributed energy resources proliferate. This interest has normally focused on voltage profiles, which are altered with active power injections, power flow reversal, and the possibility of unintended islanding when the local generation matches the consumption. However, other topics have also been addressed. This is the case of the interaction of distribution system equipment like tap-changing transformers or capacitor banks with distributed PV systems [108], or how these systems may affect the power quality with the injection of harmonics [109].

Taking into account the scope of this thesis, other works that focus on power system stability are more interesting. For example, the low-voltage ride-through capability of PV systems, and their short-term effects on voltage stability are addressed in [110]. Other papers study the transient stability of a test power system with an important penetration of wind or PV. [111] analyzes the rotor angle stability of a power system with a large penetration of doubly-fed induction generator wind

turbines, whereas [112] analyzes the transient stability of a system with an important amount of PV generation, also comparing the performance of the system depending on the LVRT capability of the PV system. With respect to small-signal stability and system oscillations, [113] studies a system with high wind penetration rates, and the analysis is sometimes extended to the identification of subsynchronous resonance in the presence of series-compensated lines [114]; whereas the transient stability of a system with PV is studied in [115], and oscillatory phenomena are identified.

Furthermore, system operators are usually concerned about the maximum instantaneous penetration of renewable generators that the power system can integrate without harming its stability, taking into account the reduction of the total system inertia and regulation capability. The impact of wind penetration on frequency regulation is analyzed in [116], whereas the effects of high penetrations of both wind and PV in the frequency response of a power system are addressed by [117].

Controllers that coordinate the response of conventional and alternative generators have been proposed in order to overcome the issues originating from such high penetration scenarios [118]. With similar objectives, the use of fast-responding storage systems is presented in [119], where the storage system injects or absorbs active power, opposing to the frequency variations, as a synchronous machine would naturally do due to its inertia.

Another approach is to control the power electronics systems interfacing renewable generators in such a way that they emulate the inertial response of a synchronous generator. The impact of wind turbines employing such technique on a transmission system is analyzed in [42]. Further steps would include considering virtual synchronous machines like those described in Section 2.2. However, the analyses that can be found about the impact of these controllers are restricted to small microgrids or a single unit connected to the distribution grid, and do not address the impact on transmission systems.

Taking into account the type of plants and systems studied, it is possible to define two main types of works in the literature. In many cases, the analyses focus on theoretical power plants and test power systems. For instance, [111] and [112] study the transient stability of a 9-bus system, depicted in Fig. 2.20, under the presence of wind and PV sources, respectively. In other papers, the impact of renewables

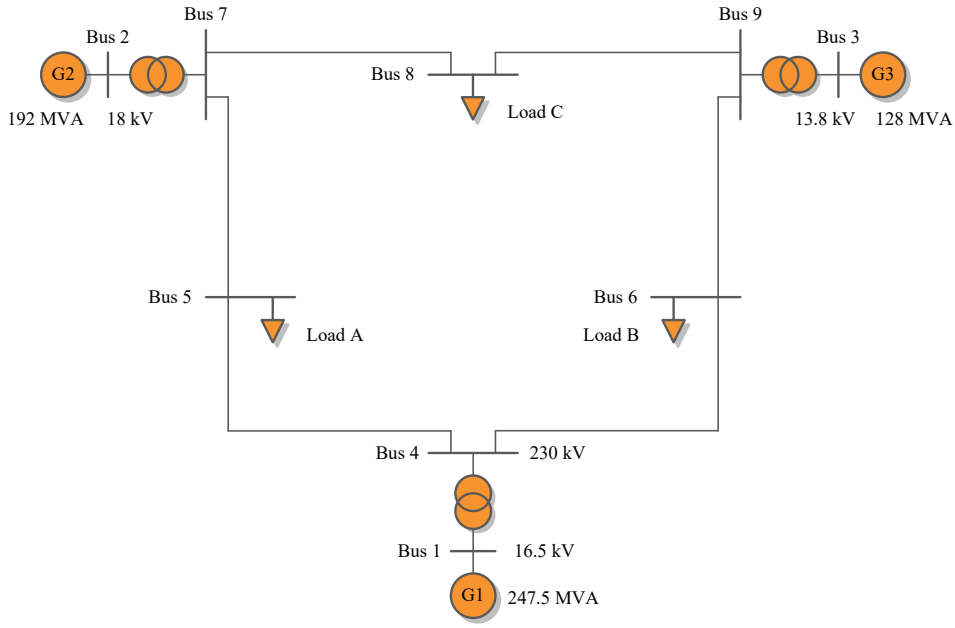


Fig. 2.20. 9-bus test system analyzed in [111, 112].

on the operations and economics of real systems is considered. This is the case of [106], with wind curtailment in Spain; [120], which analyzes reactive power reserves in Denmark; [121], where load-following, regulation, and associated markets in California are discussed; or [122], considering generation imbalances in Finland. Additionally, the stability of real systems has also been studied. [123] focuses on the impact of renewable generation on the inertia of the European interconnected system, whereas [124] addresses the western interconnection in North America and the impact of PV on its small-disturbance and transient stability. Weaker systems, usually corresponding to islands, have also been studied, considering the possible instability problems that may arise under the presence of wind generators [119, 125, 126]. The schematic diagram of one such system is shown in Fig. 2.21.

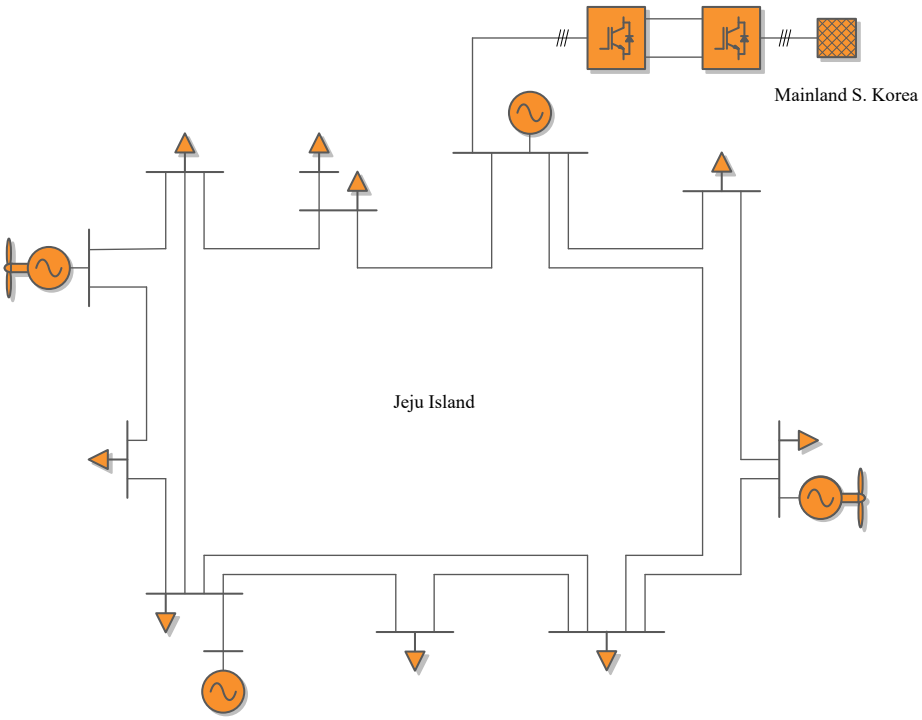


Fig. 2.21. Jeju island power system analyzed in [125].

Chapter
3.

# Classification of virtually rotating controllers for power converters

*This chapter presents a classification of power converter controllers based on droop and virtual synchronous machines. After analyzing their structure, the main features and the performance of these controllers are compared in theoretical discussions and time-domain simulations.*

The evolution of power systems, with increasing numbers of renewable sources using power electronics interfaces, has led to the development of a wide range of power converter controllers that aim at achieving a harmonious interaction between these generating units and the power grid. Among them, those with the objective of reproducing certain features of synchronous machines, like their contribution to frequency regulation, their inertial response, or their ability to energize a grid, which are summarized in Section 2.2, are of special interest.

Despite sharing common objectives, it is possible to identify differences in their design that have a translation into their performance and their impact on power systems. In the following, a common general structure is defined, and the design and capabilities of several kinds of grid-friendly power converter controllers are compared, taking into account how they embed the functions defined in this structure. Furthermore, their response to different grid events is studied through simulations

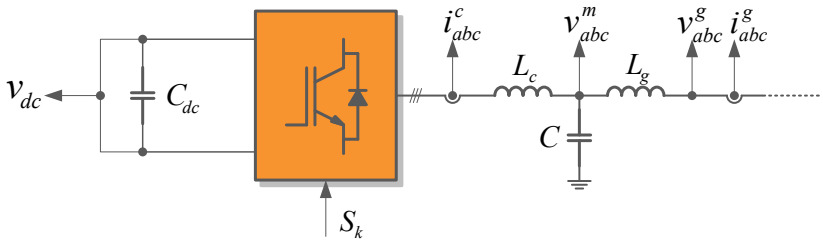


Fig. 3.1. Power converter connected to the grid through an LCL filter.

and analyzed.

## 3.1 General description of advanced power converter control structures

The power converter controllers studied here usually rely on conventional low-level current/voltage controllers, like those described in [21]. The objective of these low-level controllers is to generate the switching signals $S_k$ employed by the converter in order to synthesize a reference voltage, or to inject a reference current, such that the desired active and reactive power injection takes place. As shown in Fig. 3.1, where the diagram of a typical power converter connected to the grid through a harmonic filter is depicted, the voltage or current to be controlled may be chosen among several options, depending on the filter topology and the connection requirements. In addition to the signal that is fed back to the controller, other measurements can be considered in order to calculate the active and reactive power exchanged with the grid, and the dc voltage is also monitored to ensure a correct performance of the power conversion system. The following discussion will not dwell on the points where measurements are taken since it is focused on the higher-level converter controllers.

The advanced power converter controllers discussed in this chapter present a variety of control structures, but these structures follow certain patterns that can be considered common to all of these controllers. First, it is possible to identify a controller core, which includes the functions that give the power converter its advanced characteristics, and thus introduces the main differences among this kind of

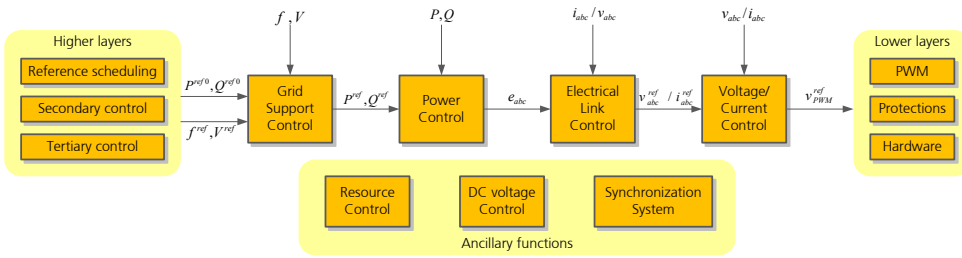


Fig. 3.2. General control structure of advanced power converter controllers.

controller. In addition to this core, other control functions are necessary to make the converter work safely, to manage the services provided for the power grid according to the system operator requirements, and to support the correct operation of the controller core. A general control structure of power converters with advanced functionalities can be seen in Fig. 3.2.

As shown in Fig. 3.2, the converter frequency, voltage, and power references are set by higher-level controllers, which comprise a power plant or system operator dispatcher that schedules the references, and secondary and even tertiary controllers performing frequency and voltage regulation at a wide grid scope. In general, the rate of execution of these functions is slow from the point of view of the converter control, with time constants in the range of minutes, and they can be performed manually by a plant operator. Therefore, their outputs can be considered constant when the controller core is analyzed.

At the opposite end of the control hierarchy, the low-level control of the power converter ensures that the conversion system behaves as dictated by the controller core. This usually involves a PWM algorithm that generates the switching signals required to obtain, in average through a switching period, the voltage requested by the converter controller, plus sensors, signal processing devices, and the equipment that protects the converter hardware from damage. In the analysis of the power converter controller, functions like the PWM, which work in a range below milliseconds, can be considered to have an instantaneous response.

The core of the controller defines the main characteristics of the power converter response and the dynamics of its interaction with the grid. In Fig. 3.2, different blocks are identified. The first one, receiving references from higher-level con-

trollers, performs functions related to the control of the grid, like primary frequency and voltage regulation, which takes place in the range of several seconds. The obtained active and reactive power, or alternatively voltage, references are processed by a power controller that generates a three-phase voltage signal. This voltage is a virtual version of the electromotive force of a synchronous generator, and the power controller defines the electromechanical characteristic of the virtual machine, with a time constant of some tenths of a second or a few seconds. The output of the power controller is optionally processed by an electrical link controller that generates the voltage or current references to be followed by the converter. Finally, the voltage and/or current controller ensures that these references are properly tracked by the converter, generating the adequate output for the low-level controllers, with a response range that can vary between a few milliseconds and a few grid cycles, depending on the controller structure. The functions performed by the blocks forming the controller core, and the different implementations employed by advanced power converter controllers are defined in the following paragraphs.

Running in parallel with the main control functions, some structures incorporate ancillary functions, such as a synchronization system providing frequency and angle measurements that may be used by the controller core blocks, or a dc voltage controller that maintains the dc-side voltage within a safe range that allows the correct operation of both the converter and the primary source of power. The dc voltage controller output may act on the converter active power reference or other variables of the controller in order to fulfill its control objectives. Therefore, despite these functions are not included in the controller core, it is necessary to analyze the impact they may have on the complete control structure. Additionally, a resource controller, whose characteristics are strongly dependent on the nature of the primary resource, is usually employed to achieve a power production objective taking into account the availability of the resource.

It is worth noting that conventional power converter controllers, composed of the blocks described in Section 2.1.2, may respond to the same higher-level controller references, and use the same low-level control and ancillary functions as the advanced power converter controllers whose control structure is represented in Fig. 3.2. In fact, the main differences reside in the core of the controller. Namely,

a conventional controller is formed by a power reference processor that generates the current reference to be injected by the converter. This current reference may be obtained algebraically from the active and reactive power reference and the voltage measurement, operating in open loop, or through a PI controller that takes into account the power error [7, pp. 221–225]. Optionally, primary regulation and low-voltage ride-through modules can be appended to the conventional controller.

### 3.1.1 Voltage and current controllers

The lowest control level in the controller core generates a PWM reference such that the power converter behaves as dictated by the upstream control blocks, which may constitute an advanced controller or a conventional one. The objective of this controller is to track the voltage or current reference as fast as possible, without introducing any additional dynamics. However, its speed of response limits the performance of the whole power conversion system, and depends greatly on its structure, which can take four main approaches:

#### 3.1.1.1 By-pass

The voltage reference is directly sent to the PWM algorithm. Therefore, the controller works in open loop, which has several drawbacks like the possible steady-state error and the lack of control on current and voltage.

#### 3.1.1.2 Voltage control

A voltage measurement is fed back and compared with the reference to obtain an error signal, which is cancelled by the controller. Operating in closed loop, the controller is able to correct errors due to losses and other steady-state effects, and compensate voltage variations. However, this type of control may result in hunting phenomena as a consequence of its interaction with the grid and the controllers of other devices, and it does not have any control over the injected current. The combination of a controlled voltage and an uncontrolled current may result in damage or unintended disconnection of the converter during faults.

#### 3.1.1.3 Current control

In this case, the output of the electrical link control block must be a current reference, and the controller feeds back a measurement of the current being injected by the converter, so it is possible to close the loop. The response of this type of controller lies in the range of a few milliseconds up to a grid cycle, depending on the converter rated power and switching frequency. With this structure, the converter interacts in a more natural way with the grid as a current source, avoiding hunting phenomena, and simple current limitation strategies can be implemented to avoid overcurrent problems. In fact, this is the commonest control strategy in commercial converters.

#### 3.1.1.4 Voltage and current control

This solution aims at controlling the converter voltage without losing control of the injected current, so it can be properly limited to prevent overcurrent issues. It is based on the sequential connection of a voltage controller, which generates a current reference, and a current controller, which generates the final PWM reference. Its speed of response is thus constrained by the speed of the current controller and a requisite on the voltage controller speed, which should be five to ten times as slow in order to avoid the coupling of the dynamics of both controllers. Therefore, its total time of response can be of several grid cycles, which may introduce an undesired delay in the complete control structure. In addition, as any other voltage controller, it may be subject to hunting phenomena.

Voltage and current controllers are usually implemented in the synchronous $dq$ frame through PI controllers, or in the stationary $\alpha\beta$ frame using proportional-resonant controllers. Alternative approaches can also be applied, like hysteresis control, which allows removing the PWM block, but introduces a variable switching frequency.

### 3.1.2 Electrical link controller

The electrical link controller determines how the virtual electromotive force interacts with the grid, and, in some controllers, it allows transforming a voltage refer-

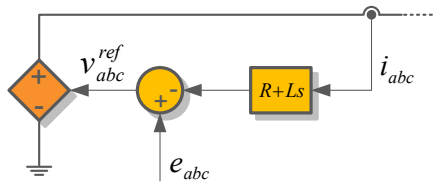


(a) Virtual impedance with derivative term.

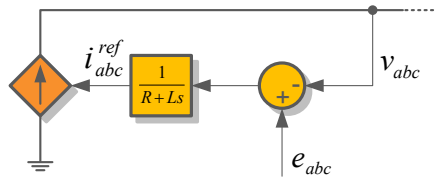


(b) Virtual admittance with low-pass filter.

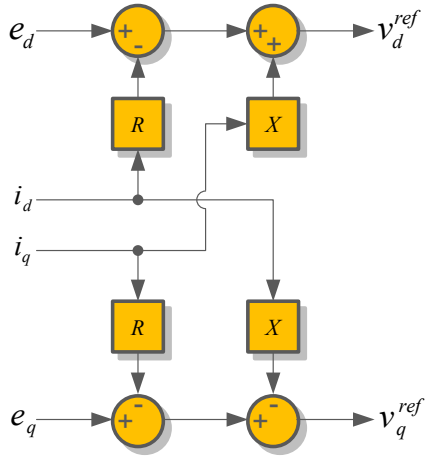


(c) Algebraic virtual impedance in [63].

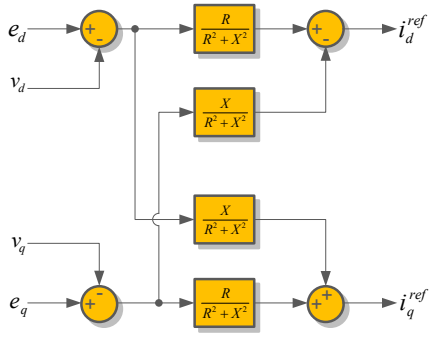


(d) Algebraic virtual admittance in [70].

Fig. 3.3. Comparison of virtual impedance and virtual admittance implementations.

ence into a current reference, so a current controller can be directly applied. It is possible to define the following types of electrical link controllers:

#### 3.1.2.1 Virtual impedance

The block considers a virtual impedance formed by a resistor and an inductor connected in series between the electromotive force and the point of connection of the converter. As shown in Fig. 3.3a, the measured current is used to calculate the voltage drop through the virtual impedance, which is subtracted from the electromotive force to determine the converter voltage reference. The inductance introduces a derivative in the control system.

#### 3.1.2.2 Virtual admittance

The underlying idea is the same as in the case of the impedance, but the virtual admittance follows a different approach. Namely, it considers the difference between the virtual electromotive force and the converter voltage measurement as the voltage drop through the virtual admittance, which is then used to calculate the induced current taking into account the resistance and inductance value, following the scheme in Fig. 3.3b. In this case, the virtual admittance acts as a low-pass filter on the voltage error.

#### 3.1.2.3 Algebraic versions

In an effort to avoid the dynamics introduced by the virtual impedance and admittance, especially those related to the derivative term in the impedance case, algebraic versions have also been considered. These alternative approaches, respectively shown in Fig. 3.3c and 3.3d, produce very similar results to their differential counterparts in steady state, but may introduce differences when the frequency deviates (although it may be taken into account in the calculation of $X$) or during transients.

### 3.1.3 Power controller

The power controller controls the active and reactive power injected by the power converter, generating the virtual electromotive force, and giving advanced power converter controllers their main dynamics. The magnitude of the electromotive force is modified taking into account the output of the reactive power controller. Alternatively, this magnitude can be the output of a controller regulating the voltage at the point of connection of the converter. On the other hand, the angle of the virtual voltage source is used to control the active power injection. In fact, the active power controller defines a virtual rotor speed, which is subsequently integrated to determine the angle. This loop defines the electromechanical characteristics of the power conversion system, and its ability to work in synchronism with the grid. Different types of active power controllers can be identified:

#### 3.1.3.1 Droop control

A proportional controller is applied to the active power error to generate the virtual speed. It allows power converters to participate in primary frequency regulation.

#### 3.1.3.2 Swing control

The controller consists of a first-order low-pass filter that reproduces the swing equation of a synchronous machine with damping:

$$2H\frac{df}{dt} = \frac{P_{in} - P_{out}}{f} - D\Delta f, \tag{3.1}$$

where $f$ is the speed of the machine, $H$ is its inertia constant, $D$ is its damping coefficient, and $P_{in}$, $P_{out}$ are the input and output power, with all variables given in per unit. Taking into account that $f$ takes values close to 1 p.u., its effect on the denominator is usually neglected.

#### 3.1.3.3 Other controllers

Different control structures, with a general transfer function $C(s)$, can be applied to the control of active power. Some examples can be the PI controller in (3.2), where the integral term defines the inertia of the machine, and the proportional term defines its damping; or the generalized controller in (3.3), which allows defining the inertia, damping and steady-state droop of the machine [127]; but more complex structures can be defined.

$$C(s) = \frac{1}{2H}\left(\frac{1}{s} + \tau_z\right) \tag{3.2}$$

$$C(s) = \frac{\tau_z s + 1}{2Hs + K_f} \tag{3.3}$$

### 3.1.4 Grid-support controller

The grid-support controller modifies the active and reactive power references sent by higher-level controllers taking into account local measurements, in order to participate in primary regulation. The following structures can be employed:

#### 3.1.4.1 Proportional action

A proportional controller determines a steady-state droop, usually applied when more than one unit control the same variable; i.e., the system frequency or the voltage of a single bus.

#### 3.1.4.2 Integral action

This type of controller cancels the steady-state error, but it may lead to stability problems when more than one generating unit try to control the same variable in this way.

#### 3.1.4.3 Derivative action

Neglecting the damping term in (3.1), it is possible to identify the inertia of a synchronous machine with a derivative response to frequency variations. Therefore, a derivative controller reproducing (3.4), or a simplified version utilizing the fact that $f$ is close to 1 p.u., can be used to reproduce the inertial response of the machine.

$$P^{ref} = P^{ref0} - 2Hf\frac{df}{dt} \tag{3.4}$$

Obviously, these actions can be combined depending on the control objective. For instance, a proportional-integral controller could cancel the steady-state error while keeping a good dynamic response, or a proportional-derivative controller would reproduce the steady-state droop and inertia of a synchronous generator.

## 3.2 Overview of advanced power converter controllers

This section reviews several advanced power converter controllers, which have been presented or widely used in recent years, and are representative of different implementations using the previously discussed structure. These controllers have usually been classified as droop controllers or virtual synchronous machines. The former aim at reproducing a given steady-state droop characteristic, which allows them to participate in primary regulation or load sharing; whereas the objective of the latter

is not only to perform a steady-state droop but to emulate several aspects of synchronous machines, including their inertia and operation in synchronism with the grid. Nonetheless, it is worth noting that, depending on the particular implementation of a droop controller, it may be able to generate also an inertial response, as proven in [20].

### 3.2.1 Classical droop

The basic structure of this controller is that of a conventional power converter controller, with current references generated by a power reference processor, plus a grid support controller that gives the power conversion system its droop characteristic through a proportional action on the frequency deviation. In this way, the active power-frequency droop is implemented like in the case of conventional synchronous generators [29]. However, due to the widespread use of the converter droop controller discussed next, this classical approach to the droop has been named sometimes *inverse* or *reverse* droop [26, 128]. Analogously, the control of voltage and reactive power can be based on modifying the reactive power as a result of voltage deviations, but it could also employ a more general voltage or reactive power controller.

Following this approach, a grid-feeding converter with controllable active and reactive power can become a grid-supporting converter [21], with external droops determining its power references, as shown in Fig. 3.4, where $S_k$ corresponds to the switching signals received by the converter in Fig. 3.1.

### 3.2.2 Converter droop controller

This controller, commonly employed with power converters contributing to the control of weak grids, considers a model based on a voltage source, which could be conceived as a virtual electromotive force, and thus can be described through the structure depicted in Fig. 3.2. In this case, the grid support controller does not alter the active and reactive power references, but the droop characteristics are embedded in the power controller. Thus, the frequency of the voltage source is determined from the given droop characteristics, taking into account the active power error. Similarly, its magnitude is defined by the reactive power deviation. Although some

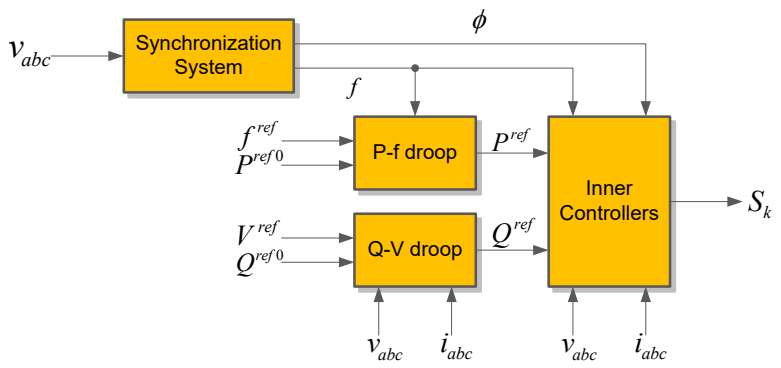


Fig. 3.4. Conventional converter controller with active power-frequency and reactive power-voltage droops through its power references.

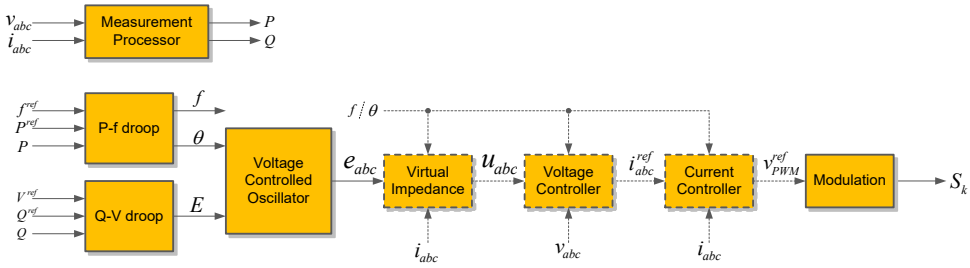


Fig. 3.5. Converter droop controller defining a voltage source whose voltage is generated by the converter, being controlled by cascaded voltage and current controllers, or directly applied to the modulation.

authors have proposed variations of this structure that take into account the grid impedance and its influence on the relation between the power flows and the voltage magnitude and angle, the study here will focus on the conventional structure, which has more similarities with virtual synchronous machines.

With respect to the associated voltage or current controllers, the resulting voltage can be directly used as a reference for a modulation algorithm, or controlled with cascaded voltage and current controllers, and an electrical link control block may be included in the form of a virtual impedance [21]. The overall control structure would be like in Fig. 3.5, where dashed lines indicate optional blocks. Alternatively, an electrical link controller based on a virtual admittance and a current controller could also be employed.

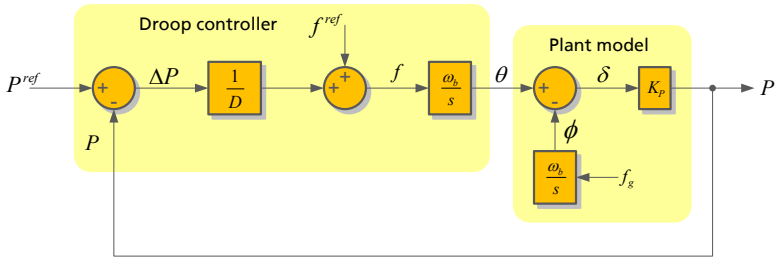


Fig. 3.6. Small-signal model of the active power loop resulting from a converter droop controller defining a voltage source.

The resulting active power loop is shown in Fig. 3.6. The plant model depicted in this figure represents the interaction of the converter with the grid, assuming the converter reproduces the model of the electromotive force $E\angle\theta$ behind an impedance, and considering an equivalent model of the grid where it is seen as another voltage source $V\angle\phi$ behind an equivalent impedance, such that the total impedance is dominated by a reactance $X$. In that case, the active power interaction is given by

$$P = \frac{EV}{X}\sin\delta, \tag{3.5}$$

where $\delta = \theta - \phi$ is the angle difference between the voltage sources. This expression can be linearized around an initial operating point where active power variations are proportional to the angle difference variations:

$$\Delta P = K_P \Delta\delta = \frac{\partial P}{\partial \delta}(\delta_0)\Delta\delta = \frac{EV}{X}\cos\delta_0\Delta\delta \tag{3.6}$$

The diagram depicted in Fig. 3.6 results in a first-order closed-loop transfer function. However, the equivalence with the virtual synchronous machine reported in [20] requires the active power measurement used in the feedback loop to be filtered through a first-order low-pass filter, whose time constant introduces an inertial effect while the order of the closed-loop transfer function becomes two.

The literature about this controller is extensive, and some examples can be [22], which is one of the first proposals and employs flux control, or [23–26], which discuss the controller and its implementation in detail. Additionally, it is worth

mentioning other controllers, which are not usually classified as droop controllers but give rise to equivalent dynamics. This is the case of the Power-Synchronization Control presented in 2010 [27, 28]. Its active power loop, which generates the voltage source angle directly from an integrator that cancels the active power error, can be divided in two blocks; one is simply a gain that generates a frequency value, whereas the other one integrates this frequency to calculate the angle, as given by:

$$\frac{\Delta\theta}{\Delta P}(s) = \frac{k_p}{s} = \frac{1}{D}\frac{\omega_b}{s} = \frac{\Delta f}{\Delta P}(s)\frac{\Delta\theta}{\Delta f}(s) \tag{3.7}$$

### 3.2.3 Inertia emulation

A controller with a conventional structure plus a grid support controller with a derivative action can be considered a first example of virtual synchronous machine. Through this derivative action, the converter can emulate the inertial response of a synchronous machine following (3.4). Nevertheless, this kind of controller does not reproduce other features of synchronous generators, like their natural ability to operate in sychronism and to form a grid.

The active power reference variation defined in (3.4) can be modified to include the effect of the damping of the virtually rotating machine, which is usually considered proportional to its speed deviation, or a droop to participate in frequency regulation with other generators, which results in an active power variation proportional to the frequency error. Therefore, these two effects can be represented as a proportional gain multiplying the frequency error, and the final reference would be given by a proportional-derivative action:

$$P^{ref} = P^{ref0} - 2Hf\frac{df}{dt} - K_f\Delta f, \tag{3.8}$$

where $\Delta f = f - f_0$ for a constant $f_0$, normally equal to the rated frequency.

In the generation of the modified reference, the factor $f$ multiplying the derivative term can be neglected, taking into account that $f$ is close to 1 p.u. Moreover, in order to decouple the effects of damping, which is usually a transient effect, and frequency regulation, for which a contribution must be maintained as long as there is a deviation, it is possible to include complementary high-pass and low-pass filters

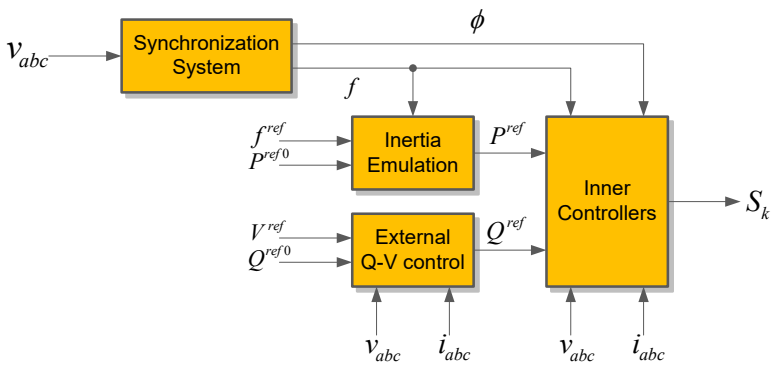


Fig. 3.7. Conventional converter controller emulating inertia through its active power reference.

of the frequency error, whose output is respectively employed by the damping and droop terms.

Additionally, the controller can also include a block to regulate voltage or reactive power, for instance through a proportional droop, generating the reactive power reference for the lower-level controllers of the power converter. The resulting diagram is then given by Fig. 3.7. It is worth noting that the classical droop controller described in Section 3.2.1 can be considered a particular case of this controller for $H = 0\,\mathrm{s}$.

The inertia emulation approach is the basis for the *virtual synchronous generator* proposed within the VSYNC project in 2008 [31], usually applied to energy storage systems [32], and also used by other authors to support isolated systems with renewables [39, 40], or directly to control a renewable generator [129]. In [130], a central VSG is considered for each frequency control area, and the resulting additional active power contribution is shared among the storage systems in that control area. Similar controllers have been proposed by other authors, like in [131], and some have had a commercial application for wind generators [43]. In [132], a more complex model obtaining a virtual frequency and angle is considered; the angle is used to calculate the corresponding active power to be injected by the converter, and is then used as a reference.

### 3.2.4 Full-order virtual synchronous machines

Despite reacting to frequency variations similarly to synchronous generators, the controllers based on inertia emulation do not share other characteristics of synchronous machines that are beneficial for the power system and define its natural characteristics to a great extent. Namely, they do not work in synchronism with the grid intrinsically, but they require an additional synchronization system, and the converters would have to switch from one control mode to another if they are required to work as either a grid-supporting generator or a grid-forming generator.

These issues are overcome by more detailed proposals that consider more aspects of synchronous generators than only their inertial response. The first proposals of virtual synchronous machines, in fact, embed a complete synchronous machine model, as in the case of the virtual synchronous machine presented in 2006 [133] and known as *VISMA* [46,47]. This controller is based on a synchronous machine model that receives virtual mechanical torque and excitation voltage inputs and includes the swing equation and flux linkage equations of the electrical machine, considering the stator, excitation and damper windings. These equations, using the speed and angle resulting from the virtual mechanical interactions, determine the current that the machine would generate depending on the grid voltage. This current is then employed as the current reference for the power converter, which is tracked by a hysteresis current controller in this particular case. Additionally, the input torque and excitation voltage may be given respectively by frequency and voltage regulators, resulting in the complete diagram in Fig. 3.8.

The use of this model allows the controller to eliminate the additional synchronization system and to generate a set of three-phase currents even when the converter is the only generator in an electrical island. However, it is rather complex, requiring the definition of multiple parameters and larger computation times, and inherits other characteristics of synchronous machines which may be undesired, like a weak damping or a relatively slow response to changes in the excitation.

Taking this into account, many authors, including those presenting the VISMA, have opted for simpler models that retain the main features of synchronous generators, considering a model where their electromotive force is represented as a voltage source behind an impedance. The magnitude of this voltage source is then given by

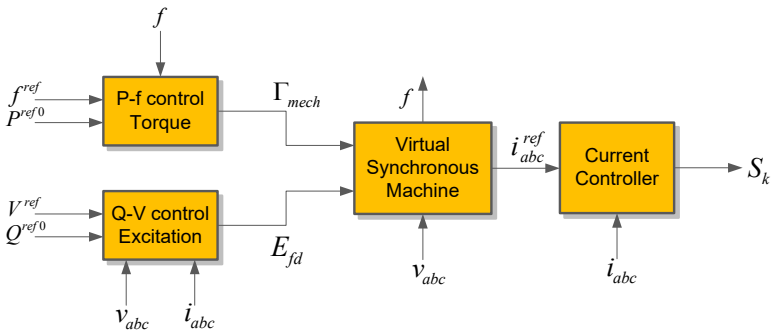


Fig. 3.8. Converter controller based on a full-order virtual synchronous machine model.

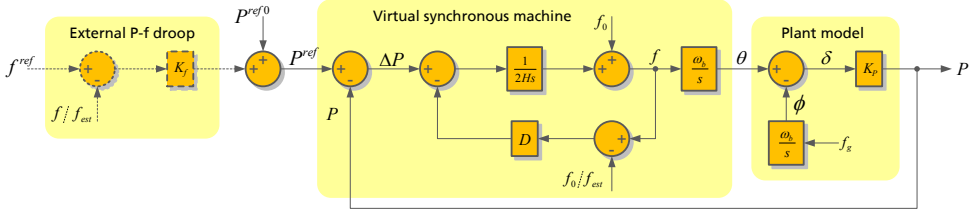


Fig. 3.9. Small-signal model of the active power loop resulting from a virtual synchronous machine based on a voltage source.

a voltage or reactive power controller, whereas its angle is defined by the machine swing equation. Nevertheless, the way in which the converter is controlled to reproduce this voltage source has resulted in different proposals, which are explained in the following.

In any case, regardless of the implementation approach, the way in which these controllers interact with the grid is determined by a common set of equations. In particular, the dynamics of active power and frequency, which are those related to the inertial response of the generator, can be summarized by the control loop in Fig. 3.9. Within the virtual synchronous machine model, the swing equation determines the virtual speed of the machine $f$, taking into account the active power balance (assuming the speed is around 1 p.u.) and the effective damping. The voltage source angle $\theta$ is directly calculated through the integration of the machine speed.

In some proposals, the $D$ coefficient performs also the function of a steady-state droop, whereas in others, an external loop is added for frequency regulation

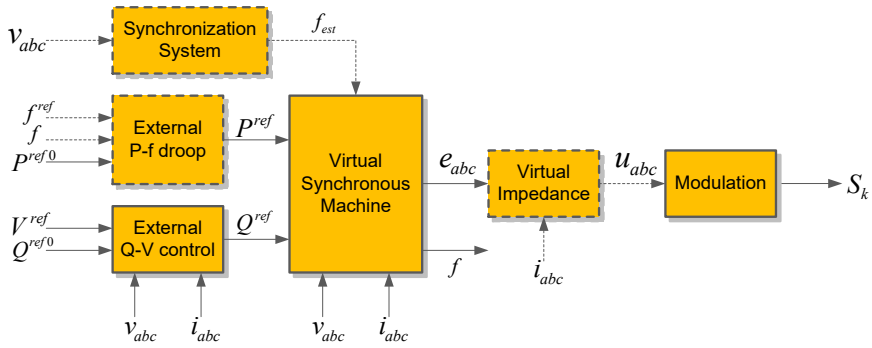


Fig. 3.10. Converter controller based on a virtual synchronous machine represented by its electromotive force and an optional virtual impedance, where the resulting voltage is directly used by the modulation.

purposes. Similarly, certain controllers use an estimation of the grid frequency by an additional synchronization system, $f_{est}$ in order to calculate the damping power, or to determine the contribution to frequency regulation.

### 3.2.5 VSM with direct modulation

The simplest solution to reproduce the virtual machine electromotive force $E\angle\theta$ is to use the associated three-phase voltage provided by the power controller as the reference for the modulation block, without considering an electrical link controller, nor voltage or current controllers. In such a case, the source impedance is determined by the grid-connection filter. This approach normally includes a voltage or reactive power controller that determines the voltage magnitude $E$ within the power controller, and some authors have considered also a grid support block formed by a governor, a synchronization system, or an electrical link controller based on a virtual impedance. A general diagram observing the main possible configurations is given in Fig. 3.10. As commented next, several controllers commonly found in the literature follow this approach.

The *synchronverter* presented in 2008 [58], and extended in further works [57, 59,60], considers the swing equation and a simple reactive power controller, without employing any of the optional blocks represented by dashed outlines in Fig. 3.10. In particular, these control blocks use active and reactive power measurements cal-

culated from the measured current and the virtual electromotive force. Since no additional governor is considered, the $D$ term in the active power loop is designed to provide the desired steady-state droop, which may result in a relatively low damping of the transient response. The issue of low damping is dealt with in [134], using communications between two converters to increase the effective damping. Another drawback of this controller, common to other controllers based on direct modulation, is the lack of direct control of the injected currents. This is identified in [135], where an auxiliary loop is activated when an overcurrent is detected. The additional loop calculates the current that would be injected taking into account the grid voltage and the filter impedance, and limits the obtained value before using it as the reference of a current controller. Additional current controllers are also considered in [136], however, their objective is to control the injection of harmonics.

Another controller based on the direct modulation solution is the *virtual synchronous generator* presented in [52] in 2011. In this case, an external governor is considered, so the term $D$ in the virtual synchronous machine is reserved for damping purposes. In fact, the frequency deviation that causes the damping is calculated with respect to the frequency estimation $f_{est}$ provided by an additional synchronization system. In this way, the steady-state injection of active power due to the internal loop does not depend on the grid frequency. On the other hand, the active power-frequency droop block uses the virtual machine speed $f$. This control system is completed with a reactive power controller in [53]. Other works by the same authors present different variations of the controller, for instance, the use of a variable moment of inertia depending on the machine speed and acceleration is considered in [137], or a modified swing equation that takes into account the reactive power is introduced in [56] to attenuate oscillations. As in the previous case, overcurrents may be a concern, and additional blocks are added to the controller in [138] to limit the active power reference and adapt the synthesized voltage depending on the grid conditions.

References [139–141] present a family of controllers based on calculating the signals defining the voltage source and applying directly a modulation algorithm. In [139], an additional droop/damping branch that takes into account the virtual machine angle is included, and in [140], the active power balance is analogously

affected by the dc link voltage. The controller in [141] presents a more complex structure with cross terms between the $P$-$\theta$ and $Q$-$E$ branches.

Finally, the virtual impedance block with a direct modulation approach is considered in [71]. Although it does not provide full control of the current being injected by the power converter, the use of the virtual impedance allows limiting this current indirectly. Furthermore, it allows modifying the total impedance in the connection of the virtual electromotive source, thus modifying the dynamics of its interaction with the grid. In the implementation in [71], the voltage drop in the virtual impedance is calculated only for the fundamental-frequency, positive-sequence component of the current, and uses derivative terms.

### 3.2.6 VSM with voltage and current controllers

A different option to emulate the behavior of the voltage source modeling the virtual machine, with the objective of controlling the current injected by the converter, is given in [62] in 2013. The controller presented in this paper uses the three-phase voltage determined by the virtual synchronous machine as a reference for a voltage controller, which in turn determines a current reference. This current reference can easily be limited and fed to a current controller that calculates the reference to be followed by the modulation. The voltage and current controllers are defined in the synchronous $dq$ frame defined by the virtual machine angle. The control structure is complemented with a virtual impedance block in [63], so the functional structure may be represented by the diagram in Fig. 3.11. In this case, the virtual impedance does not require the calculation of time derivatives, since it is applied algebraically, utilizing the fact that the time derivative of a sinusoidal signal is in quadrature with the original signal in the $dq$ frame, like in Fig. 3.3c.

The virtual synchronous machine model in [62, 63] includes a damping branch where the frequency deviation is calculated with respect to a frequency estimation $f_{est}$ given by an additional synchronization system, and considers an external droop block for frequency regulation, which uses the virtual machine speed $f$. Further developments of this controller include its extension to a single-phase conversion system [65], and the design of a synchronization controller to be used before the converter is connected to a working grid [64].

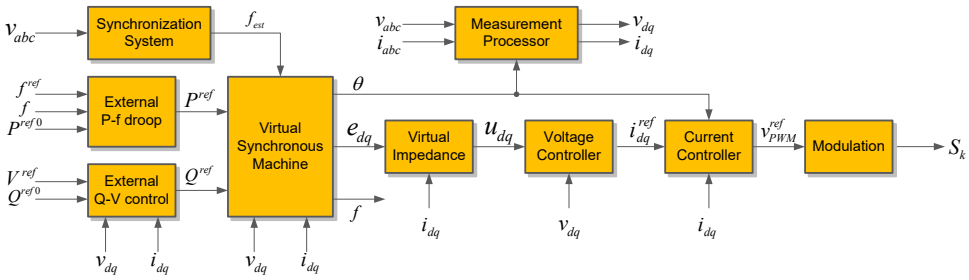


Fig. 3.11. Converter controller based on a virtual synchronous machine represented by its electromotive force and a virtual impedance, where the resulting voltage is controlled by cascaded voltage and current controllers.

Other authors have also proposed solutions in this way. For instance, the controller in [139], considering droop/damping as a function of both the virtual machine speed and its angle, is presented in a more general design that accounts for optional cascaded voltage and current controllers in [142]. Another alternative, for which the damping is obtained proportionally to the frequency deviation with respect to a constant value, is studied in [143]. Finally, it is worth noting that converter droop controllers like those in Section 3.2.2 can be considered a particular case of this type of VSM, with $H = 0$ s.

### 3.2.7 VSM with virtual admittance

The third main group of virtual synchronous machines that consider a simplified model with a virtual electromotive force consists of those controllers that generate a current reference to be tracked by a current controller. This is achieved through a virtual admittance block that calculates the current that would flow through the virtual admittance taking into account the voltage of the virtual electromotive force and the voltage at the point of connection of the converter. The complete control structure would then be like the one shown in Fig. 3.12.

Despite an admittance and an impedance can be electrically equivalent as long as they have a finite, nonzero value, the use of one component model or the other has an important effect on the control system. The main impact is related to the use of time derivatives of the current measurements in the impedance-based imple-

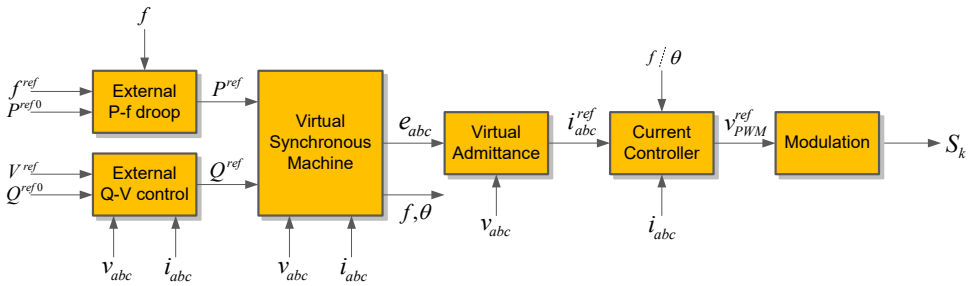


Fig. 3.12. Converter controller based on a virtual synchronous machine represented by its electromotive force and a virtual admittance, where the resulting current is the reference of a current controller.

mentation approach of Fig. 3.3a. This is particularly important when the nature of the waves generated by power converters, due to the high-frequency switching, is taken into account. In order to avoid problems of noise amplification or instability, the derivative term in the virtual impedance should probably consider some additional filtering elements, which would affect the overall dynamics. This is avoided by adopting the virtual admittance approach of Fig. 3.3b, which in fact is naturally filtering any noise in the voltage measurement. Alternatively, the use of derivative terms can be avoided if the voltage drop through the impedance is calculated algebraically, utilizing the relations between quadrature signals in the stationary $\alpha\beta$ frame or the synchronous $dq$ frame, like in Fig. 3.3c. Although not necessary to avoid these problems affecting the control, a similar technique can be applied in the case of the admittance, as shown in Fig. 3.3d. In both cases, the reactance $X = \omega L$ can be calculated taking into account the instantaneous value of the frequency given by the virtual machine or a synchronization system.

The choice between the impedance or admittance implementation approach also affects the control and limitation of the converter current. With a virtual impedance, it is possible to limit the current generated or absorbed by the converter indirectly, setting a large impedance value. Alternatively, cascaded voltage and current controllers can be used, as in Section 3.2.6. On the other hand, with a virtual admittance, the current reference is directly available, and can be limited in case it exceeds the converter limits. Furthermore, the current-source character of the power conversion system does not reduce its capability to form a grid, since the virtual admittance is

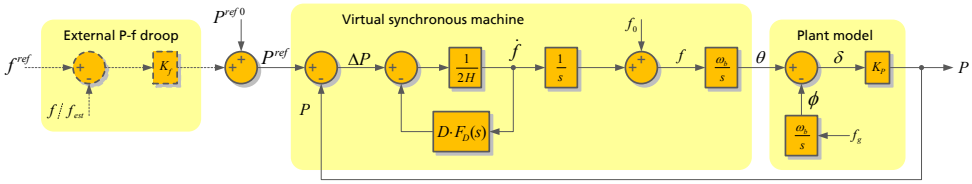


Fig. 3.13. Small-signal model of the active power loop resulting from a virtual synchronous machine implemented as a voltage source and a virtual admittance, where the damping is a function of the machine acceleration.

acting as a voltage controller in practice. Additionally, using a virtual impedance or a virtual admittance may provide different options for the synchronization of the converter prior to its connection to the grid, or to control the harmonics injected by the power conversion system, as discussed in Section 3.3.

Among the proposals taking the virtual admittance approach, it is possible to cite a simplified version of VISMA, presented in 2011 [49], and compared with the direct modulation alternative in [51]. In both cases, a generalization of the swing equation is considered, and the damping torque is calculated as a function of the virtual machine acceleration through transfer function $F_D(s)$, which modifies slightly the active power loop, as shown in Fig. 3.13. The usual loop can be obtained from this one if $F_D(s)$ consists only of an integrator.

Another controller utilizing a virtual admittance is the *synchronous power controller* presented in Spanish in [66] in 2011, and described in English in [67, 68]. This controller considers an internal damping branch applied to the frequency deviation measured with respect to a constant value $f_0$, and an outer droop branch that adjusts the contribution to frequency regulation [144]. In this way, it is possible to obtain a sufficiently damped response and the expected steady-state droop. The current controller may be defined in the stationary $\alpha\beta$ frame, employing the virtual frequency of the machine [145], or in the synchronous $dq$ frame, using the virtual machine angle [146]. Additionally, [66] considers the use of parallel current controllers and different admittance values for each harmonic or sequence. Other implementations of the SPC have also been proposed; for instance, the effect of the swing equation is replaced in [127] by a more general active power controller that allows fixing the inertia, damping, and steady-state droop without an external branch,

and a dc voltage controller based on the equivalence between the virtual rotor kinetic energy and the dc link capacitor electrostatic energy is proposed in [147].

Finally, an alternative application of the virtual admittance concept is presented in [70], where the low-pass filter is replaced by the algebraic structure in Fig. 3.3d.

## 3.3 Comparison

The power converter controllers discussed in the previous sections present several common characteristics, since they are all designed with the objective of reproducing certain aspects of synchronous machines. In particular, their active power loops, which determine the inertial and frequency regulation contribution of the power conversion system, share a common structure and differ in some details. Similarly, all the controllers offer a great flexibility in the selection of parameters like the inertia or the damping, which is not available for conventional synchronous machines, and even for the machine impedance in the cases with a virtual impedance or admittance. In this way, it is theoretically possible to apply the same parameter optimization algorithms to most of the studied controllers.

In this section, the main differences between the controllers are discussed, focusing on the design details that affect the implementation of the whole power converter control system, or constrain the response of the power conversion system.

### 3.3.1 Synchronization system

Opposite to synchronous machines, power converters usually require an additional synchronization system to operate adequately in a grid-connected mode. This synchronization system is usually based on a PLL that provides an estimation of the grid frequency and angle, or, less frequently, on an FLL, which produces only a frequency signal but has usually a faster and more stable response than a PLL. Under adverse grid conditions, these systems may negatively impact the behavior of the power conversion system, with phase jumps, or bad definitions of the frequency and angle for very low voltages. Therefore, for power converters emulating the behavior of synchronous generators, it would be interesting to utilize the natural ability of synchronous machines to operate in synchronism with the grid, and reduce their

dependence on an additional synchronization system, at least for the lower layers of the control system whose dynamics could be affected by transient variations or by the filters applied as a countermeasure.

During normal operation, the converter droop controller (Section 3.2.2) and the controllers referred to as VSMs (Sections 3.2.4 to 3.2.7) are able to generate a voltage or current reference without using an additional synchronization system, and, when needed, they provide a frequency and angle estimation that can be used by the inner controllers to track the corresponding reference. There are two cases, however, that deserve especial attention: the VSG with direct modulation in [52], and the VSM with cascaded voltage and current controllers in [62]. These two proposals use the frequency estimation provided by a PLL to calculate the damping torque of the virtual synchronous machine. The external synchronization system should not lead to severe problems in the control system, since the instantaneous value is not necessary and the estimation can be properly filtered. This is also the case of the controllers that consider an external active power-frequency droop block for active power regulation, which can use a slowly-varying frequency estimation instead of the virtual machine frequency. On the other hand, the controllers performing a classical droop or emulating inertia, based on conventional controllers, as in Sections 3.2.1 and 3.2.3, do not generate their own frequency or angle signals, and require a synchronization system for their inner controllers. Moreover, the emulation of inertia based on calculating the time derivative of the measured frequency, requires a relatively fast and smooth estimation of the frequency to be able to provide an adequate inertial response without ripple.

Additionally, the power converter, or the synchronous machine, must be properly synchronized before the generating system is connected to the grid in order to avoid a voltage mismatch that results in large currents. Synchronous generators usually rely on synchronization systems for this purpose. In the case of the studied controllers, different designs provide alternative ways to perform the connection to the grid. On the one hand, the controllers based on conventional inner controllers, like those in Sections 3.2.1 and 3.2.3, rely on the synchronization system that they use during normal operation. On the other hand, the controllers in Sections 3.2.2 and 3.2.4 to 3.2.7, which are not necessarily equipped with such a system, require

a different connection procedure, normally consisting in synchronizing the internal voltage with the grid voltage at the point of connection of the converter. This can be done with an additional controller that modifies the frequency reference signal taking into account the grid frequency and angle, and makes the voltage magnitude equal to the measured value, as is done in [64].

EDIT Add reference to paper with Weiyi about presynchronization when accepted.

Alternatively, those controllers considering a virtual admittance, like the simplified VISMA or the SPC, can activate the controller, measuring the grid voltage, and use the reference current as a virtual measurement for calculating virtual values of the exchanged active and reactive power, which are fed back to the controller and allow the natural synchronization of the system as in normal operation. In fact, the use of a temporary virtual admittance to synchronize a synchronverter before connecting it to the grid, is the alleged contribution of [60].

Another possible procedure when a virtual admittance is considered is to set it to a sufficiently low value, and to connect the converter without a prior synchronization of the internal voltage source. A sufficiently low value of admittance results in a small current injection, regardless of the voltage drop between the virtual electromotive force and the grid voltage. Once the converter is connected to the grid through this high impedance path, the admittance value can be steadily increased to its normal operation value, while the virtual electromotive force gets synchronized with the grid.

It must be noted that these procedures cannot be employed if a virtual impedance is used. In the first case, the grid voltage is not fed back to the controller, and the current measurement is zero because the circuit is open, so the controller does not have information about the grid state. In the second case, the virtual impedance would only limit the current indirectly, after measuring it, which can result in an initial current spike that trips the conversion system.

### 3.3.2 Response to grid events

The response of a synchronous machine to grid events, especially to frequency deviations, oscillations, or faults, defines the dynamics of power systems and how they

are operated to a great extent. Virtual synchronous machines are thus expected to behave similarly, allowing a harmonious integration of power conversion systems in conventional power systems.

#### 3.3.2.1 Damping

A simple analysis of the dynamics of synchronous machines based on a swing equation with no damping shows that their active power response is marginally stable. To avoid the associated problems, synchronous machines are usually equipped with damper windings, but their effectiveness is limited because there is a tradeoff between damping and losses. In the case of a virtual synchronous machine, damping can be introduced without incurring in losses. However, each of the studied controllers has particularities that result in different damping values. For instance, in the case of the synchronverter, the lack of an external loop forces the damping coefficient $D$ to be calculated as a function of the desired steady-state droop, which normally results in a very low damping ratio for the closed loop. Other virtual synchronous machines, like the VSG with direct modulation or the VSM with cascaded voltage and current controllers, determine the damping with respect to the actual grid voltage and have a separate external droop for frequency regulation purposes. This allows decoupling the steady-state and the transient response, so large damping coefficients may be defined without altering the steady-state characteristic of the machine, but may lose effectiveness when dealing with oscillations that involve more than one machine. In the case of the simplified VISMA or the SPC, for which the damping is calculated with respect to a constant frequency value, the external droop must compensate the resulting inherent steady-state droop.

#### 3.3.2.2 Speed of response

The speed of the response, which shows the inertial effect introduced by the controllers, can be assessed through the study of the active power loop transfer function for each of the main controllers studied in previous sections. To compare only the effects of the outer loops responsible for the virtual synchronous machine, the dynamics of the inner loops are considered to be ideal in the following analysis.

Taking into account the similarities of the active power loops, it is possible to define a general transfer function. Nevertheless, this transfer function will depend on the effectively operating control blocks in each design, and the measurements being used. To this respect, it is worth taking into account that the external active power-frequency droop may use a frequency measurement estimated from the grid frequency $f_g$ through

$$F_f(s) = \frac{\Delta f_{droop}}{\Delta f_g}(s), \tag{3.9}$$

or from the machine speed $f$ through

$$G_f(s) = \frac{\Delta f_{droop}}{\Delta f}(s). \tag{3.10}$$

Depending on the signal being used, one of these transfer functions is zero, and the other one has a steady-state gain equal to one. As a particular case, the transfer function is exactly one when the signal is directly used or the dynamics of the measurement processing can be neglected. Similarly, the damping term can be calculated with respect to an estimation of the grid frequency $f_g$ through

$$H_f(s) = \frac{\Delta f_{damp}}{\Delta f_g}(s) \tag{3.11}$$

with $H_f(0) = 1$, or simply with respect to a constant $f_0$, which can be represented by $H_f(s) = 0$.

With this, it is possible to derive general expressions for the active power response of the converter under variations of the modified active power reference $P_{r1}$ or the grid frequency $f_g$. In fact, the response to grid frequency variations can be obtained as the product of the transfer function linking $P$ and $P_{r1}$ and an auxiliary function $G_{Pf}(s)$ such that:

$$\frac{\Delta P}{\Delta f_g}(s) = G_{Pf}(s)\frac{\Delta P}{\Delta P_{r1}}(s) \tag{3.12}$$

In the case of the controllers using a conventional structure as in Sections 3.2.1

and 3.2.3:

$$\frac{\Delta P}{\Delta P_{r1}}(s) = 1 \tag{3.13}$$

$$G_{Pf}(s) = -(2Hs + K_f)F_f(s), \tag{3.14}$$

where $H$ is different from 0 if there is inertia emulation.

On the other hand, for the controllers based on a virtual voltage source as in Sections 3.2.2 and 3.2.4 to 3.2.7:

$$\frac{\Delta P}{\Delta P_{r1}}(s) = \frac{\frac{K_P \omega_b}{2H}}{s^2 + \frac{D\left(1 - H_f(s)\right) + K_f G_f(s)}{2H} s + \frac{K_P \omega_b}{2H}} \tag{3.15}$$

$$G_{Pf}(s) = -\left[2Hs + D\left(1 - H_f(s)\right) + K_f\left(F_f(s) + G_f(s)\right)\right] \tag{3.16}$$

The transfer functions of the main controllers are summarized in Table 3.1, where $F_D'$ is the steady-state gain of $F_D(s)\,s$, used in the simplified VISMA.

The analysis of the transfer functions allows identifying different effects. First, the inclusion of the swing equation in the controller introduces certain dynamics in the controller. Actually, its order increases by two with the inertia, and only by one when the converter droop is considered. As could be expected, larger inertia values cause slower responses. This does not occur when the emulation is done through the active power reference. Second, the inertial effect appears as a derivative term acting on frequency variations, which adds to the proportional effect of the droop. In this case, the response of the machine grows proportionally to the inertia. Third, the damping and external droop branches are intertwined: the droop modifies the response damping if it is based on the machine speed ($G_f(s) \neq 0$), and the damping coefficient affects the steady-state droop when the speed deviation is calculated with respect to a constant value ($H_f(s) = 0$).

Additionally, the response of the virtual synchronous machines depends on the total grid impedance. Controllers using a virtual impedance or admittance have another degree of freedom to define how they interact with the grid.

The time-domain response of these controllers to different events has been studied through simulation with PSCAD®. The studied system consists of a 100 kW

Table 3.1. Characteristic transfer functions of virtually rotating controllers.

| Controller | Defined by | $\frac{\Delta P}{\Delta P_{r1}}(s)$ | $G_{Pf}(s)$ | $\frac{\Delta P}{\Delta f_g}(0)$ |
|---|---|---|---|---|
| Classical droop | $\frac{\Delta P}{\Delta P_{r1}}(s) = 1, H = 0$ | $1$ | $-K_f F_f(s)$ | $-K_f$ |
| Converter droop | $f_0$ for damping $H = 0, K_f = 0$ | $\frac{K_P \omega_b}{Ds + K_P \omega_b}$ | $-D$ | $-D$ |
| Inertia emulation | $\frac{\Delta P}{\Delta P_{r1}}(s) = 1, H \neq 0$ | $1$ | $-(2Hs + K_f)F_f(s)$ | $-K_f$ |
| Synchronverter | $f_0$ for damping, $K_f = 0$ | $\frac{\frac{K_P \omega_b}{2H}}{s^2 + \frac{D}{2H}s + \frac{K_P \omega_b}{2H}}$ | $-(2Hs + D)$ | $-D$ |
| VSG direct PWM Cascaded V&I | $f_{est}$ for damping $f$ for droop, $G_f(s) = 1$ | $\frac{\frac{K_P \omega_b}{2H}}{s^2 + \frac{D\left(1 - H_f(s)\right) + K_f}{2H}s + \frac{K_P \omega_b}{2H}}$ | $-\left[2Hs + D\left(1 - H_f(s)\right) + K_f\right]$ | $-K_f$ |
| VISMA | Damping on $\dot{f}$ $f_{est}$ for droop | $\frac{\frac{K_P \omega_b}{2H}}{s^2 + \frac{D}{2H}F_D(s)s^2 + \frac{K_P \omega_b}{2H}}$ | $-\left(2Hs + DF_D(s)\,s + K_f F_f(s)\right)$ | $-(DF'_D + K_f)$ |
| SPC | $f_0$ for damping $f$ for droop | $\frac{\frac{K_P \omega_b}{2H}}{s^2 + \frac{D + K_f G_f(s)}{2H}s + \frac{K_P \omega_b}{2H}}$ | $-\left(2Hs + D + K_f G_f(s)\right)$ | $-(D + K_f)$ |

Table 3.2. Virtually rotating controller parameters for simulation.

| Parameter | Symbol | Value |
|---|---|---|
| Base power | $S_b$ | 100 kVA |
| Base voltage | $V_b$ | 400 V |
| Base frequency | $f_b$ | 50 Hz |
| Inertia constant | $H$ | 5 s |
| Resistance | $R$ | 0.1 p.u. |
| Reactance | $X$ | 0.3 p.u. |
| Damping ratio (SPC) | $\zeta$ | 0.95 |
| Damping coefficient (VSM with V&I controllers) | $k_D$ | 400 p.u. |
| Reactive power controller proportional gain | $k_{pQ}$ | 0.5 p.u. |
| Reactive power controller integral gain | $k_{iQ}$ | 0.25 $s^{-1}$ |
| Frequency regulation constant | $1/R_f$ | 20 p.u. |
| Voltage regulation constant | $1/R_V$ | 0 |

converter, with a maximum transient current corresponding to 125 kVA at 400 V, fed by a dc voltage source, and connected to an ideal 400 V, 50 Hz grid with a 1 MVA short-circuit power and a 0.1 resistance-to-reactance ratio.

The converter control system allows comparing the different studied grid-friendly controllers. Namely, it considers classical droop (Section 3.2.1), conventional droop (Section 3.2.2), inertia emulation (Section 3.2.3), VSM with direct modulation (Section 3.2.5) with and without virtual impedance, VSM with voltage and current controllers (Section 3.2.6), and VSM with virtual admittance (Section 3.2.7) using the SPC. Their dynamics are defined by the parameters in Table 3.2; it is worth noting that some parameters apply only to certain controllers.

The active power response of the converter, employing different controllers, is

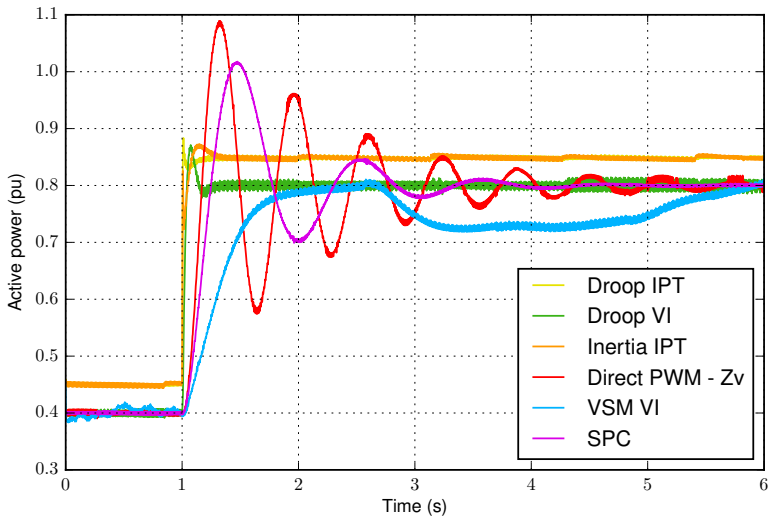


Fig. 3.14. Power converter active power response to a step in the active power reference.

shown in Fig. 3.14. The converter is initially injecting 0.4 p.u. active power and 0.6 p.u. reactive power, and the active power reference is increased to 0.8 p.u. at $t = 1$ s.

In general, the converter exhibits a fast response regardless of the employed controller, but the transient response is significantly affected by the controller. On the one hand, both types of controllers based on droop, and the inertia emulation controller reach a steady state in approximately 200 ms. On the other hand, the three other controllers, which embed the swing equation in the converter control system, have an oscillating response that takes longer to achieve a steady state. In fact, there are significant differences among them. The VSM with direct modulation, due to the contribution to damping only through frequency regulation, shows a very weakly damped response; whereas the SPC presents smaller oscillations that fade out faster, and the VSM with voltage and current controllers has a slow evolution, similar to a first-order system, but suffers a low frequency oscillation that delays it steady state until 5 s after the event. In addition to the dynamic behavior, it is worth mentioning that the controllers adding droop or inertia to conventional controllers, which are based on open loop control of active and reactive power, have an appreciable steady-state error both before and after the reference step.

Taking into account that these controllers aim at improving the power system performance when there are large generation and demand imbalances that affect the frequency stability of the system, it is also interesting to study the response of the converter when there is a grid frequency variation. The results of one such study are presented in Fig. 3.15. Once again, the converter is initially injecting 0.4 p.u. active power and 0.6 p.u. reactive power, an the event consists on a grid frequency ramp of -1 Hz/s, starting at $t = 1$ s and finishing at $t = 1.5$ s.

As shown in Fig. 3.15a, all the controllers respond to this event by increasing the output of the power converter. However, two types of response can be clearly identified. The controllers not including a swing equation, i.e., those described in Section 3.2.1 to 3.2.3, increase their power almost linearly, proportionally to the frequency deviation as defined by their droop response. In the case of the controller emulating inertia, it is possible to see a slightly stronger contribution than in the case of the droop controllers, but limited compared with the response of the remaining controllers. Indeed, the natural embodiment of inertia through the swing equation causes the other three controllers to respond in a much more appreciable way at the beginning of the transient. Furthermore, the total contribution is given not only by the emulated inertia constant, but also by the damping introduced by the controller. Thus, the VSM with direct modulation contributes about one half as much as the other two controllers. Furthermore, the VSM with direct modulation and the SPC exhibit a more oscillating response than the VSM with voltage and current controllers. Once again, it is possible to see a steady state error for those controllers acting on active and reactive power in open loop.

The virtual speed calculated by those controllers that consider one is shown in Fig. 3.15b. It is possible to see that the controllers emulating inertia oppose to changes more firmly than the controller based on droop and, when the frequency ramp finishes, present some oscillations. When analyzing both graphs in Fig. 3.15 together, it is interesting to see how the VSM with voltage and current controllers provides a large injection of active power during the ramp but does not suffer oscillations once the frequency is stabilized again, which is not the behavior of the other two VSMs. This is due to the way in which the damping is calculated. In the case with voltage and current controllers, the frequency deviation is calculated with

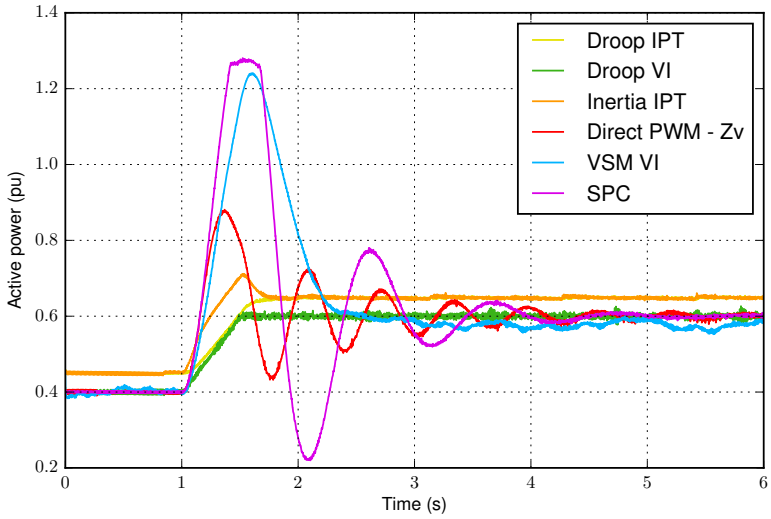


(a) Active power.

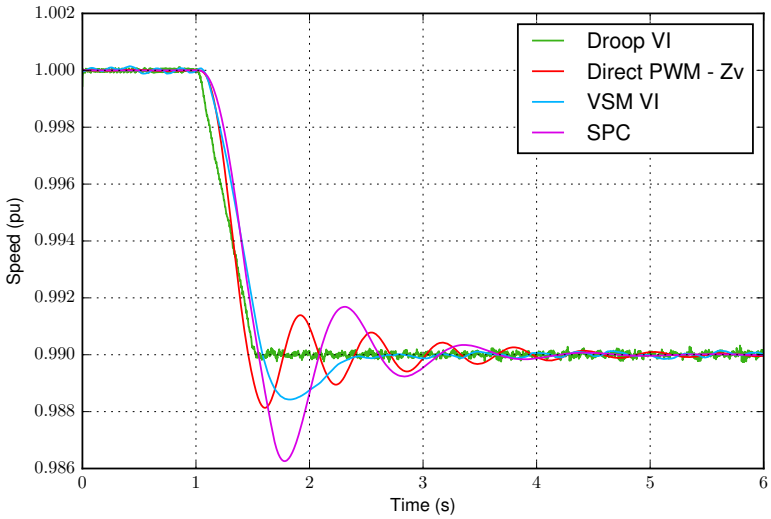


(b) Virtual rotor speed.

Fig. 3.15. Power converter response to a grid frequency ramp.

respect to the frequency of the grid, detected by a PLL, so the effect of the damping term fades away as the virtual speed converges to the grid frequency value. In the other two cases, the deviation is calculated with respect to the rated frequency, which results in larger damping torque values and relative variations; this affects

the virtual machine to a greater extent, and this more aggressive action brings a response with more oscillations. Furthermore, the SPC damping is larger than for the VSM with direct modulation, which results in larger amplitude oscillations at the beginning of the transient, and a faster reduction of this amplitude.

#### 3.3.2.3 Behavior during faults

The controllers based on an electromotive force source will have a response similar to synchronous machines, supporting the grid voltage, increasing their current injection, and accelerating as a result of the active power balance, and will present a similar oscillating behavior after the fault is cleared, depending on their damping. Nevertheless, it must be noted that power converters based on power electronics cannot reach the same short-circuit current levels as conventional electromechanical synchronous machines and thus the injected current must be limited before an unintended trip occurs. As in the previous case, the converters using a virtual impedance or admittance have an additional design parameter to constrain the current values during a fault. On the other hand, virtual synchronous machines can avoid some of the problems that affect their conventional counterparts, and their speed can be limited, since it is not linked to any physical magnitude.

The solutions that emulate the response of conventional generators only through their power reference rely on their inner controllers and must incorporate conventional low-voltage ride-through schemes.

The response of the 100 kW converter to grid faults has also been studied in simulation, and Fig. 3.16 and 3.17 show the results obtained when this converter suffers a voltage sag. In this event, the converter is initially injecting 0.4 p.u. active power and 0.6 p.u. reactive power, and the voltage is initially 1 p.u. At $t = 1$ s, it starts decreasing, reaching a minimum value equal to 0.2 p.u. in 60 ms; it remains at this level for 140 ms; and finally it recovers in 100 ms, so that the voltage is back at its rated value at $t = 1.3$ s.

The active and reactive power injected by the converter are shown in Fig. 3.16. During the sag, the active power output of the converter, which can be seen in Fig. 3.16a, is constrained by the low voltage, and all the controllers reduce this magnitude. After the voltage recovery, however, there are important differences

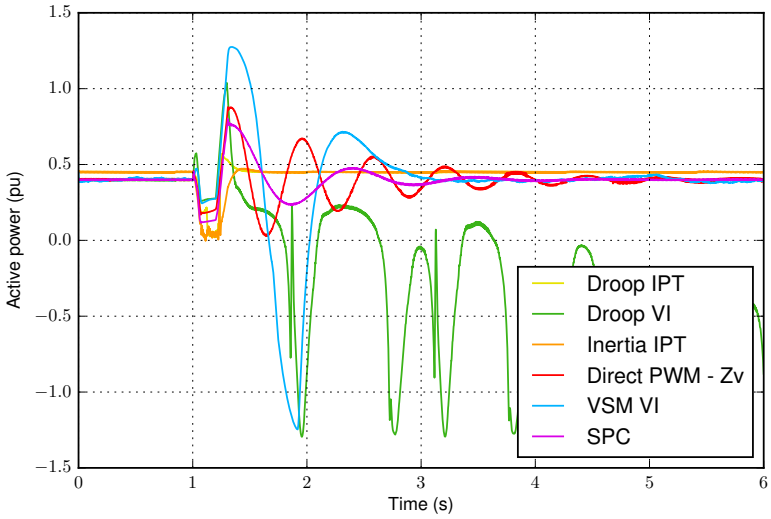


(a) Active power.

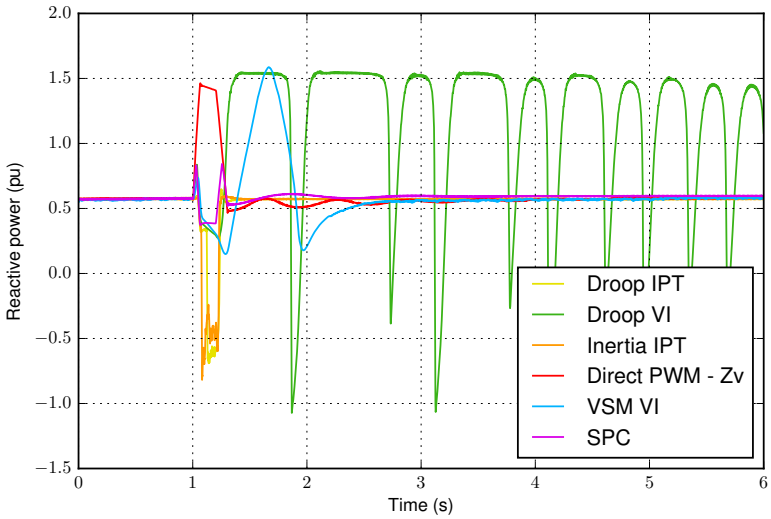


(b) Reactive power.

Fig. 3.16. Power converter response to a grid voltage sag.

among controllers. The classical droop and inertia emulation controllers, based on conventional control loops, reach back their initial operation point soon and without oscillations; whereas the other controllers exhibit an oscillating behavior, as a synchronous machine would. The SPC presents a moderate overshoot and very well

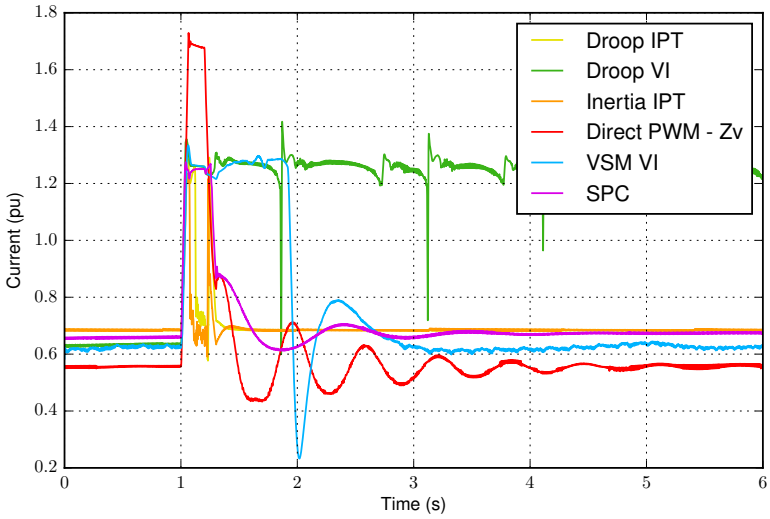


Fig. 3.17. Power converter current during a grid voltage sag.

damped oscillations, and the VSM with direct modulation has a slightly larger overshoot and longer oscillations. The remaining controllers, which employ cascaded voltage and current controllers, give rise to larger overshoot and oscillation amplitude. In fact, the VSM with voltage and current controllers reacts to the voltage recovery by injecting the maximum allowed power, then suffers a large swing that results in absorbing the maximum allowed power, and finally goes back to the initial active power injection with better damping. In the case of the droop controller, the severity of the swing results in a loss of synchronism, and a pulsating active power injection that should be avoided through the disconnection of the converter.

The reactive power injected by the converter is shown in Fig. 3.16b. In this case, the controllers behave differently, not only after the voltage recovery, but also during the sag. The classical droop and inertia emulation controllers absorb reactive power when the voltage is low, which further pushes the voltage down, thus having a detrimental effect on the system performance. On the other hand, the VSM with direct modulation injects a large amount of reactive power, which might require extremely large currents and be harmful for the converter. The other controllers reduce their reactive power injection slightly with respect to the pre-fault level, and the SPC is able to maintain it almost constant. After the recovery, the VSM with

voltage and current controllers does a large reactive power injection when the active power magnitude is low, exploiting its full power capability; whereas the droop controller injects a large amount of reactive power in a pulsating way due to the loss of synchronism.

Finally, Fig. 3.17 presents the evolution of the magnitude of the current injected by the converter with each controller. During the sag, the controllers based on conventional control systems maintain their current injection around its initial value, does not contributing to support the grid voltage; whereas the other controllers inject large amounts of current. Indeed, the droop controller, the VSM with voltage and current controllers, and the SPC inject the maximum current that the converter can withstand during transients, around 1.25 p.u., because the current magnitude is limited by the control system. However, the VSM with direct modulation, which lacks a current limitation, induces a current injection of more than 1.6 p.u. during the sag, which cannot be withstood by the converter and would activate overcurrent protections. After the sag, the SPC smoothly recovers the initial current injection level, with well damped oscillations; whereas the VSM with voltage and current controllers remains at the maximum current magnitude for almost 1 s, and then suddenly recovers the initial value with a large swing and a relatively well damped oscillation. The VSM with direct modulation recovers its initial value with significant oscillations, and the droop controller current remains at a high level even after synchronism is lost.

### 3.3.3 Ability to maintain a grid

The ability of these controllers to form a grid, or to keep it in stable operation after its disconnection from a larger system, also depends on whether they employ a voltage source model or not. In this way, the controllers described in Sections 3.2.2 and 3.2.4 to 3.2.7 are theoretically able to energize their own system, since they are able to fix a given voltage. This is not the case, however, of the controllers described in Sections 3.2.1 and 3.2.3, which require an external voltage source to operate, because they are basically grid-feeding converters with additional grid-support functionalities.

### 3.3.4 Current limitation

A power converter controller must take into account the limited capability of the power electronics switches to handle large currents. Although, in a properly designed power conversion system, overcurrent protections would open the circuit before the converter suffers any damage, it is usually required that the converter remains connected for a minimal period of time. To avoid an undesired trip, the converter controller must limit the injected current so that it does not exceed the permissible values. This can be effectively done with a fast current controller, and properly saturating the current reference, which can be applied to most of the studied controllers. The exceptions are found among those that consider a voltage source whose three-phase signals are directly used as the reference of a modulation algorithm, discussed in Section 3.2.5. Namely, it affects the controllers proposed in [52, 57, 139], and, for some of them, these issues have already been identified in [135, 138].

### 3.3.5 Active power limitation and dc bus control

Coordinating the active power injected by the converter and generated by the primary source connected to the dc bus is critical in practical applications. Despite the performance of the studied controllers is only demonstrated for a power conversion system connected to a dc voltage source or a storage system in most of the papers presenting them, it is possible to analyze how the design of each controller could affect the control of the actual amount of active power being injected or the dc bus voltage.

The controllers emulating inertia or a droop response through the active power reference of the converter are limited only by the speed of the inner controllers and the final active power reference can be limited or affected by the dc voltage controller directly, so it is possible to assume that the active power injection can be controlled instantaneously. This changes for the other controllers, which introduce additional dynamics. In the case of the converter droop control in Section 3.2.2, the dynamics are those of a first-order system and it is possible to determine a bound for the active power variations given the frequency deviation.

However, the controllers that model a virtual synchronous machine in Sections 3.2.4 to 3.2.7 have more complex dynamics, with a possibly oscillatory second-order response, plus the derivative effect due to the inertia. Thus, the transient power injection depends on the parameter choice and the magnitude of the grid event. One approach to limit this injection is to determine a value of $H$ that ensures that the active power remains within the allowed limits for any admissible frequency deviation. Alternatively, the selection of $H$ can follow different criteria that take into account the stability of the system, but a fast dc voltage controller should override the orders of the virtual synchronous machine when the dc voltage is out of its safe range.

The steady-state active power injection, which can depend on the frequency deviation, or may be limited by variations in the primary source, is easier to control, but still not straightforward in all cases. It can be directly limited when the machine response effect is achieved through the active power reference, or when the damping is calculated with respect to the grid frequency as in the VSG with direct modulation or the main VSM with cascaded voltage and current controllers. In the other cases, the damping generates an intrinsic droop that must be taken into account, for which it is necessary to feed back the value of the frequency. The generalized SPC presented in [127] includes an interesting particular case where the active power error is processed by a proportional-integral controller determining the emulated inertia and damping, while an external droop can perform the steady-state contribution to frequency regulation. In this way, the resulting active power reference can be limited to effectively limit the steady-state injection of active power without an additional feedback branch.

### 3.3.6 Distortion and imbalances

One of the objectives of the controller of a power conversion system may be to control the generation of distorted or unbalanced voltages or currents. In some applications, it may be required that the converter injects purely sinusoidal currents into the grid, whereas in other cases it might be interesting to inject certain harmonics to mitigate the impact of local loads on the power quality of a wider grid, participating as an active filter. However, this aspect has not been studied deeply

when different models of virtual synchronous machines have been proposed.

In the case of the controllers analyzed in Sections 3.2.1 and 3.2.3, the performance of the power conversion system regarding distortion and imbalances depends on the inner controllers employed. This is not the case of the other controllers studied, whose model is a voltage source. Without auxiliary controllers, the injected current will simply be the result of the interaction of the electromotive force of the virtual synchronous generator with the grid voltage, affected by the connection impedance. In [136], a virtual synchronous machine controller based on direct modulation is enhanced with additional proportional-resonant current controllers tuned for different frequencies that ensure the corresponding current injection is zero. In some cases, the virtual impedance has been designed to reject harmonic currents, reproducing the effect of a large inductor. However, these solutions are not flexible, and they do not allow the operation of the converter as an active filter that injects harmonic currents for local nonlinear loads. The virtual admittance approach, together with selective filtering of the grid voltage, is exploited in [66] to allow different types of interaction for different harmonics and sequences, using separate admittances and current controllers for each frequency of interest. Theoretically, a similar idea could be applied with virtual impedances, but it would not be as effective to totally cancel the injection of a particular harmonic, since that would require the use of large impedance values, which could be an issue for the controller, instead of a zero admittance.

The main characteristics of each controller regarding the aspects compared in this section are summarized in Table 3.3.

Table 3.3. Virtually rotating controllers implementation details.

| Controller | Additional PLL | Fault ride-through | Grid-forming | Current limitation | Power limitation |
|---|---|---|---|---|---|
| Classical droop (3.2.1) | Required | Depends on inner controllers | No | Yes | Instantaneous |
| Converter droop (3.2.2) | Not used | Constrained by limited current | Yes | Yes | Steady-state with $f$ feedback |
| Inertia emulation (3.2.3) | Required | Depends on inner controllers | No | Yes | Instantaneous |
| Synchronverter (3.2.5) | Not used | Depends on current protections | Yes | No | Steady-state with $f$ feedback |
| VSG direct PWM (3.2.5) | Used for damping | Depends on current protections | Yes | No | Steady-state |
| Cascaded V&I (3.2.6) | Used for damping | Constrained by limited current | Yes | Yes | Steady-state |
| Admittance (3.2.7) | Not required | Constrained by limited current | Yes | Yes | Steady-state with $f$ feedback |

Chapter
4.

# Models of photovoltaic power plants using synchronous power controllers

*The power plant models used in the analyses carried out in this thesis are presented in this chapter. The detailed model of an actual PV plant is developed, and a method to obtain equivalent models of different groups of converters using the SPC is derived. Finally, different equivalent models are obtained and compared with the original model in terms of both accuracy and computation effort. This chapter extends and improves the work in the MSc thesis* D. Remon, "Model of a distributed PV plant for power system stability analysis," University of Seville, 2015*, considering the model of the resource and dc side, and new versions of the controllers. It includes the work presented in* D. Remon, A. M. Cantarellas, and P. Rodriguez, "Equivalent model of large-scale synchronous photovoltaic power plants," *IEEE Transactions on Industry Applications*, vol. 52, no. 6, pp. 5029–5040, Nov.–Dec. 2016.

## 4.1 Reference PV plant

The PV plant model employed in the analyses carried out in this thesis is based on an actual 100 MW photovoltaic power plant connected to the power system of

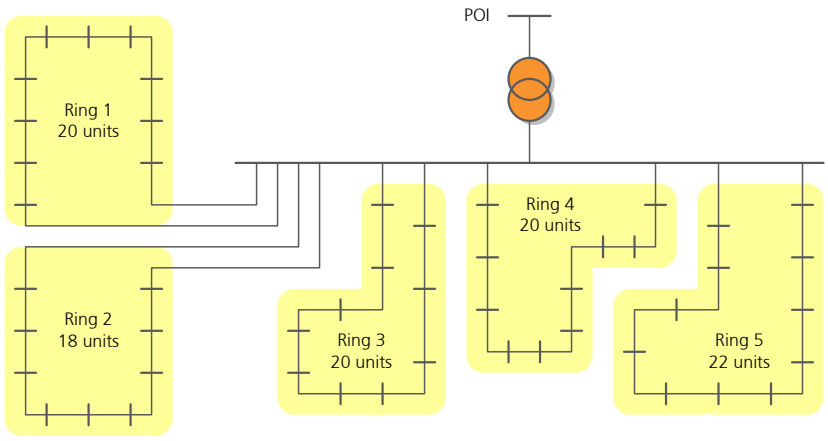


Fig. 4.1. Simplified diagram of the PV power plant.

northern Chile (*Sistema Interconectado del Norte Grande*, SING).

The PV power plant is connected to a 50 Hz, 220 kV grid. It is formed by 100 power conversion units whose rated voltage and power are, respectively, 365 V and 1 MW. These converters are connected to the power system through an internal 33 kV network and a 33/220 kV, 110 MVA transformer. The connection of the power converters to the internal network is done through 50 three-winding transformers that allow the connection of two power converters to two equal 365 V, 1.15 MVA terminals.

As shown in Fig. 4.1, the internal network is formed by 5 rings, each of them connecting approximately 20 conversion units. The cable distance between transformers is approximately 300 m, and rings 1 and 2, which are located further from the plant substation, are connected through additional 1700 m overhead lines.

The plant is controlled in two levels defined by a central plant controller and 100 station controllers, each of them controlling one power converter independently from the others. The behavior of each of these control levels is assumed to be as follows.

The central plant controller sends a global active power reference to all the station controllers, which react to this reference taking into account their own participation coefficient. This plant controller is also in charge of regulating the voltage at

the Point Of Interconnection (POI) of the plant. This is achieved through a global reactive power reference sent to all the station controllers, also shared by means of different participation coefficients. In addition to the active and reactive power signals, the plant controller sends the value of the frequency measured at the point of interconnection to all the station controllers.

On the other hand, each station controller determines the dynamics of its associated power converter. The plant model will consider that the power converters will be able to respond both to a conventional PV converter controller and to the SPC discussed in Sections 2.2.2 and 3.2.7, allowing the plant operator to choose between them depending on the desired power plant performance.

The following sections present the model developed taking into account the characteristics of this PV plant, and including a more general control structure and additional types of primary power sources. The objective of the model is to carry out power flow, dynamic, and transient stability analyses, under the assumption of balanced power systems. Therefore, it is implemented in *DIgSILENT PowerFactory*® (DSPF) by means of a single-phase equivalent of the PV plant useful for both modal analysis and RMS simulation.

## 4.2 PV plant static model

The definition of the PV plant static model is straightforward in DSPF. The elements forming the PV plant can be introduced and connected graphically, describing the single-line diagram of the plant; afterwards, it is necessary to define their characteristics, which can be done through a type definition which can be used by multiple elements. The following steps allow defining the electrical model of the PV plant.

First, 160 terminal elements are created, and their voltage is defined. They correspond to the point of connection of the PV plant, at 220 kV; the common Medium Voltage (MV) bus, at 33 kV; 50 other MV buses forming the different PV rings, with 8 additional MV buses at the endpoints of the four overhead lines connecting rings 1 and 2 to the common MV bus; and 100 power converter buses, with a rated voltage of 365 V.

Secondly, line and cable elements forming the MV network, i.e., the rings and

Table 4.1. PV plant conductor data.

| Conductor | $R'$ (Ω/km) | $X'$ (Ω/km) | $C'$ ($\mu$F/km) |
|---|---|---|---|
| 95 mm$^2$ | 0.4096 | 0.1913 | 0.153 |
| 120 mm$^2$ | 0.3238 | 0.1854 | 0.165 |
| 150 mm$^2$ | 0.2637 | 0.1797 | 0.178 |
| 185 mm$^2$ | 0.2099 | 0.1747 | 0.191 |
| 240 mm$^2$ | 0.1600 | 0.1681 | 0.209 |
| 300 mm$^2$ | 0.1280 | 0.1630 | 0.226 |
| 400 mm$^2$ | 0.1009 | 0.1561 | 0.252 |
| 500 mm$^2$ | 0.0774 | 0.1511 | 0.274 |
| Overhead line | 0.2087 | 0.2940 | 0.018 |

Table 4.2. PV plant transformer data.

| Parameter | Plant transformer | Converter transformer |
|---|---|---|
| High voltage | 220 kV | 33 kV |
| Low voltage | 33 kV | 365 V |
| Rated power | 110 MVA | 1.15 MVA |
| Short-circuit impedance | 12.5% | 6.2% |
| Copper losses | 0.3% | 0.8% |

their connection to the common MV bus, are connected, each one linking a pair of 33 kV terminals. The definition of each element requires setting its length and choosing a line type that defines its impedance. The types employed are summarized in Table 4.1.

Thirdly, a two-winding transformer is defined to connect the plant POI and the common MV bus, and 50 three-winding transformers are created, connecting each intermediate bus within a ring with two 365 V terminals. Their characteristics are introduced through the transformer type, following the data summarized in Table 4.2.

Fourthly, 100 static generator elements, which correspond to power converters,

are created and connected, each one to a different 365 V terminal. A rated power of 1 MW and power factor of 1 are defined, so DSPF employs an internal apparent power base of 1 MVA. The actual active and reactive power operational limits are defined in the load flow tab of the element definition.

Lastly, it is necessary to define the initial operating point of the plant. In this case, this supposes setting the active power initially injected by each static generator, and creating a steady-state voltage controller that defines which voltage is controlled and how much each converter participates.

## 4.3 PV plant dynamic model

The dynamic model of the PV plant considers both the devices forming the power plant and the different controllers ensuring a correct operation of each device and the whole power plant, focusing on the interactions that affect power system stability in a range of 10 s to 1 min. Furthermore, it assumes that magnetic saturation effects of inductors and transformers are negligible, so the internal network is formed by passive elements represented by constant impedances; whereas the power converter dynamics are fast enough to model these devices as current sources whose current follows the given reference, only modified by a first-order lag representing the time delay introduced by the current control loop. Therefore, the main modeling requirements concern the power converter controllers, other controllers in the plant, and the power converter dc side and primary resource dynamics.

The PV plant control structure considers a more general configuration with three layers, including an additional level between the plant and station controllers. The top layer is the central plant controller that handles active and reactive power references, and controls the voltage at the POI. The middle layer is formed by cluster controllers, each one in charge of a group of different power converters. For this PV plant, five clusters are defined, each one corresponding to one of the rings forming the MV internal plant network. Lastly, the bottom layer consists of the individual power converter control system defining the dynamics of each generating unit.

### 4.3.1 Plant level

The plant controller ensures that the plant follows a given active power reference, and regulates the voltage at its POI. Alternatively, the reactive power injected by the power plant can be controlled instead of the voltage. For this purpose, this controller measures the voltage and the active and reactive power injected by the PV plant at the POI, and sends active and reactive power reference signals to the control layers below. Additionally, it sends frequency and voltage references for local regulation, and parameters that define the response of the power converters in the power plant that are common to all the generating units in the plant.

In DSPF, the plant controller is described by a composite model employing several common models, and interacting with subordinated composite models. Each composite model is described by a frame, where the interaction between different blocks are indicated; whereas each common model is defined by a block definition that includes a set of differential and algebraic equations reproducing the dynamics of the modeled element.

#### 4.3.1.1 Control frame

The control frame describing the relations among blocks in the plant control level is depicted in Fig. 4.2. It contains two main blocks, “References” and “Parameters”, 25 subsystem blocks, and ancillary blocks to obtain the voltage, active power, and reactive power measurements. The frame is defined in such a way that the plant controller can receive references and parameters from a higher control layer, and it sends references and parameters to its subsystems, using a compatible format for both connections. This feature allows employing the same frame for different control levels; in particular, the plant and the cluster level.

Furthermore, in order to enable the use of this frame both at the plant and the cluster level, it allows calculating the total active and reactive power at a given point when it flows through one or two elements like a line or a transformer, and a sufficient number of subsystems is considered for both applications. In case more current measurements or subsystems should be considered, the frame could easily be updated.

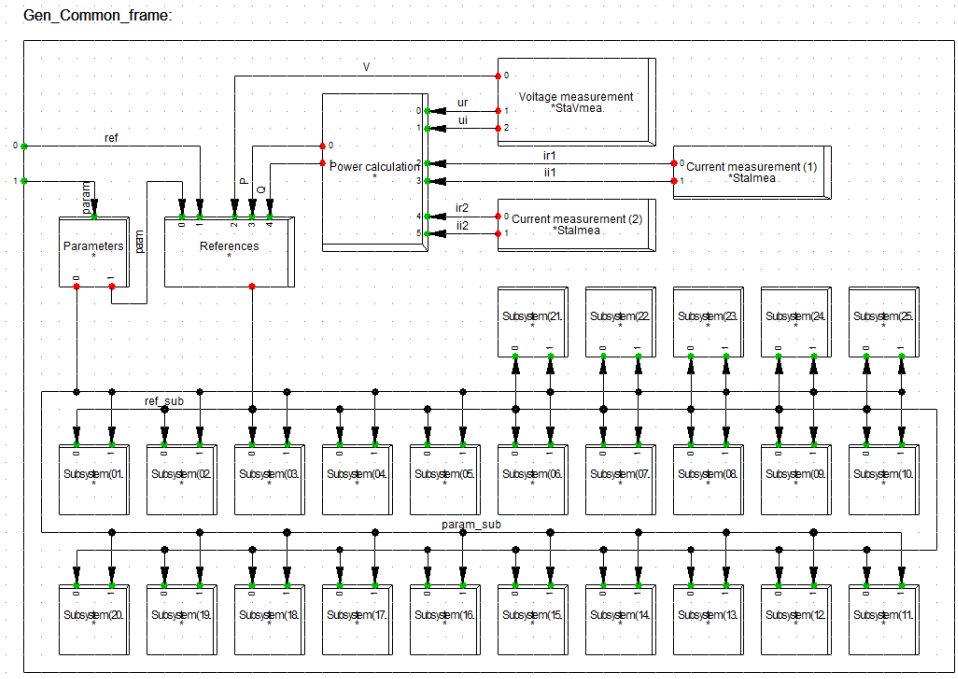


Fig. 4.2. Plant and cluster level control frame.

At the plant control level, the voltage is measured at the POI, and only one current measurement is employed, monitoring the current flowing through the high-voltage side of the plant transformer. With respect to the subsystems, they correspond to the cluster level, and thus only five blocks are used.

#### 4.3.1.2 References

The reference block sends active and reactive power reference signals, and frequency and voltage references for local regulation to subsystems. The model assumes that the plant controller sends a common signal to all the subsystems downstream, and each of them reacts accordingly. For compatibility between the plant and the cluster levels, an analogous set of signals can be received from an upstream layer, or introduced in the common model as DSPF parameters.

Therefore, the block receives three different groups of signals:

- A set of references from an upstream layer, consisting of active power, reactive power, frequency reference for regulation, voltage reference for regulation.

- Voltage, active power, and reactive power measurements.

- Parameters set by the parameter block, including the base voltage and apparent power, the active and reactive power limits, and gains and time constants of controllers.

On the other hand, it produces four output signals: active power, reactive power, frequency, and voltage reference, matching the format of the group of signals received from upstream layers. And it considers five DSPF parameters, which also correspond to the references optionally received from higher control levels, with an additional parameter setting the plant voltage reference.

Internally, the block employs the per-unit system corresponding to the plant control level. However, the input and output signals that carry power magnitudes are converted to MVA, so each controller can easily employ its own power base.

In general, in this block, the output signals are generated in different ways depending on whether references are received from a higher control layer or not. For instance, the active power reference signal sent downstream is given by:

$$P^{ref} = \begin{cases} P^{ref}_{input} & \text{if } P^{ref}_{input} \text{ is active} \\ P^{ref}_{param} & \text{otherwise} \end{cases}$$

That is to say, if an active power reference is received, it is directly transmitted; when no signals are received from a higher control layer, the corresponding DSPF parameter is used instead. The latter is the case of the plant level, whereas the former corresponds to the cluster level. The frequency and voltage references for local regulation are handled in the same way as the active power reference. However, in the case of the reactive power reference, the output is calculated in a different way when no reference is received, i.e., at the plant level. Thus, it is possible to define

the output reactive power reference signal as:

$$Q^{ref} = \begin{cases} Q^{ref}_{input} & \text{if } Q^{ref}_{input} \text{ is active} \\ Q^{ref}_{control} & \text{otherwise} \end{cases}$$

Here, $Q^{ref}_{control}$ requires a more complex calculation process, optionally involving the POI voltage and its reference set as a DSPF parameter. First, the voltage error is calculated:

$$\Delta V = \begin{cases} V^{ref}_{param} - V & \text{if } V^{ref}_{param} \text{ is active} \\ 0 & \text{otherwise} \end{cases}$$

This error is optionally filtered:

$$\frac{d\Delta V_{filt}}{dt} = \frac{\Delta V - \Delta V_{filt}}{T_V}$$

And then it is used to determine a proportional control action so different power plants can contribute to the control of the voltage at the same point. This modifies the plant reactive power reference set as a DSPF parameter (note that $\Delta V_{filt} = 0$ when voltage control is disabled):

$$Q^{ref}_{plant} = Q^{ref}_{param} + \frac{\Delta V_{filt}}{R_V} \in \left[Q^{min}_{plant}, Q^{max}_{plant}\right]$$

The resulting value is the reactive power to be injected by the plant at the POI, and takes into account the PV plant capability at this point. The correct tracking of this reference is enforced by a PI controller, which generates a common reactive power reference signal indicating power converters to adapt their injection, and is limited taken into account the capability of the power converters at their point of connection:

$$\Delta Q = Q^{ref}_{plant} - Q$$

$$Q^{ref}_{control} = k_p \Delta Q + k_i \int \Delta Q \in \left[Q^{min}, Q^{max}\right]$$

The calculation of the initial state of the system for simulations or modal analysis requires special attention in DSPF. It uses the results of the system power flow,

but each dynamic model must also be initialized, giving values to its input and output signals, and its state variables.

For this block, the initial state is calculated taking into account that errors are initially zero, assuming the analysis starts from a steady state. When references are received from higher control layers, they are transmitted unmodified. Otherwise, the output active and reactive power reference signals are also made equal to zero, so they represent variations with respect to the initial operating point, and the frequency and voltage regulation references are initialized considering the corresponding DSPF parameters.

In the latter case, the initial values of the DSPF parameters setting the plant active power, reactive power, and voltage references are ignored, and each of them is taken into account only once it changes during a simulation. Before this happens, the plant active power reference (variation) is equal to zero, whereas the plant reactive power and voltage references are made equal to the values measured in the initial conditions. The value of each of these parameters is only taken into account once it is modified during the simulation.

#### 4.3.1.3 Power calculation

The power calculation block generates the active and reactive power measurements employed by the reference block. It is based on a simple definition that considers a voltage measurement and one or two current measurements, and determines the apparent power as the product of the voltage and total current phasors.

Current measurements in DSPF have a given sign depending on whether the branch where the measurement is taken corresponds to a generator, or a load or passive element. Therefore, this block includes a DSPF parameter for each current measurement in order to adapt the sign of the measurement to the application.

At the plant level, the voltage measurement monitors the voltage of the bus where the PV plant is connected, and only one current measurement is used. This current measurement is located at the same bus, connected to the high-voltage side of the PV plant transformer. The measurement sign is corrected so the calculated active and reactive power are positive when the plant injects them into the grid.

#### 4.3.1.4 Parameters

The parameter block provides values to the reference block connected at the same control level, and generates the parameter signals to be sent downstream and employed by power converters.

The parameters for the reference block are set only through DSPF parameters of the parameter block, and include the base voltage and apparent power, the active and reactive power limits, and gains and time constants of controllers. On the other hand, the parameters that are sent downstream can be received or also set as DSPF parameters. In order to handle them correctly, flag values are used. If the received signal is equal to the flag, the DSPF parameter is used instead; otherwise, the received signal is directly transmitted.

The parameters sent downstream are of different kinds:

- Converter characteristics, including base and rated voltage and power.
- Frequency and voltage regulation, with droop slopes, deadbands, and filter time constants.
- Active and reactive power controller data, including gains and limits.
- Dc side characteristics and dc voltage controller parameters.
- Resource data, like rated power, irradiance, temperature, storage capacity, or initial state of charge among others. Each resource will process only those that are relevant.

At the plant level, the parameters employed by the plant reference block are defined, like a base power of 100 MVA. Additionally, most parameters of stations, which are common to all of them, are defined at this level. This include the converter characteristics, their participation in frequency and voltage, and the control and resource parameters that are equal for all of them. When different control parameters, types of resource, or resource conditions are considered, the corresponding parameters are given flag values and set by lower control layers.

### 4.3.2 Cluster level

The cluster level transmits the references set by the plant level, and allows setting different parameters for its associated group of converters. Thus, it receives active and reactive power references, frequency and voltage references for regulation, and converter parameters set at the plant level, and sends these references and converter parameters, which may include additional data, to the converters that belong in that cluster.

In DSPF, the cluster control level is also described by a composite model employing different common models. The design of the PV plant model discussed here allows using the same frame as in the plant level, shown in Fig. 4.2, and also the same block definitions. However, the behavior of the blocks is adapted to the cluster level.

First, the reference block barely transmits the received signals to the converter level, without modifying them. Nonetheless, it receives voltage and power measurements taken at the cluster level, which can be used for monitoring purposes. In case clusters were allowed to behave independently, with respect to active or reactive power control, a flag value could be set at the plant level, and each cluster reference block could assume the same role as the plant controller.

Secondly, the power calculation block employs the voltage measured at the MV common bus, where the transformer MV side, and all five PV rings are connected. In this case, each cluster employs two current measurements, located at this common bus, but each one monitoring one of the lines that connect the ring to this common bus. The power calculation block adapts their sign and sums both signals to obtain the total current and, thus, the total active and reactive power reaching the common MV bus.

Lastly, the parameter block defines the cluster reference block parameters, which are not relevant when the cluster follows the plant references, but also the converter parameters that are specific for that particular cluster. For instance, different clusters may take different responsibility in frequency regulation, inertia emulation, or reactive power control, or they might be composed of converters employing different resources, as would be the case if storage were included in the plant.

### 4.3.3 Converter level

The converter level processes the references and parameters received from higher levels in order to determine the current reference of a power converter. For this purpose, it also takes into account measurements of the ac grid, and the state of the converter dc side and its associated resource. The dynamic model developed in DSPF integrates the model of the power converter, and its connection to the grid, in this level. Namely, the power converter is represented by a current source, whose current follows the calculated reference modified by a first-order lag representing the delay of the current loop.

Once again, each converter controller is represented by a composite model involving different common models. The control frame describing the converter level composite model, and thus the interactions among blocks in this level, differs from the one used at the plant and cluster levels, and is shown in Fig. 4.3. In this case, several blocks are defined. The reference and parameter blocks receive the signals set by the plant and cluster levels, process these signals, and provide them for the central block, called "SPC", which corresponds to the converter controller and current loop model. This block also interacts with the resource, whose characteristics are described by parameters set by the parameter block, exchanging the active power measurement and a control signal to correct the state of the dc side. And it generates the signals that a DSPF "Static generator" device reads to reproduce the current source modeling the converter.

In addition to these blocks, several measurements are considered. A voltage measurement provides the voltage phasor at the point of connection of the converter, and the frequency of the bus that determines the angle reference for the phasors employed by DSPF. Two optional measurements for regulation are provided, one of them is a voltage magnitude, and the other one is the frequency detected by a PLL. These two measurements can be taken at the converter point of connection or at a different point, like the common MV bus, or the plant POI, and then transmitted to the converter control level; furthermore, they can be replaced by other signals generated by the converter controller itself, like the virtual frequency generated by the SPC. Lastly, a current measurement is included to provide the converter controller with the initial current measurement and allow its initialization.

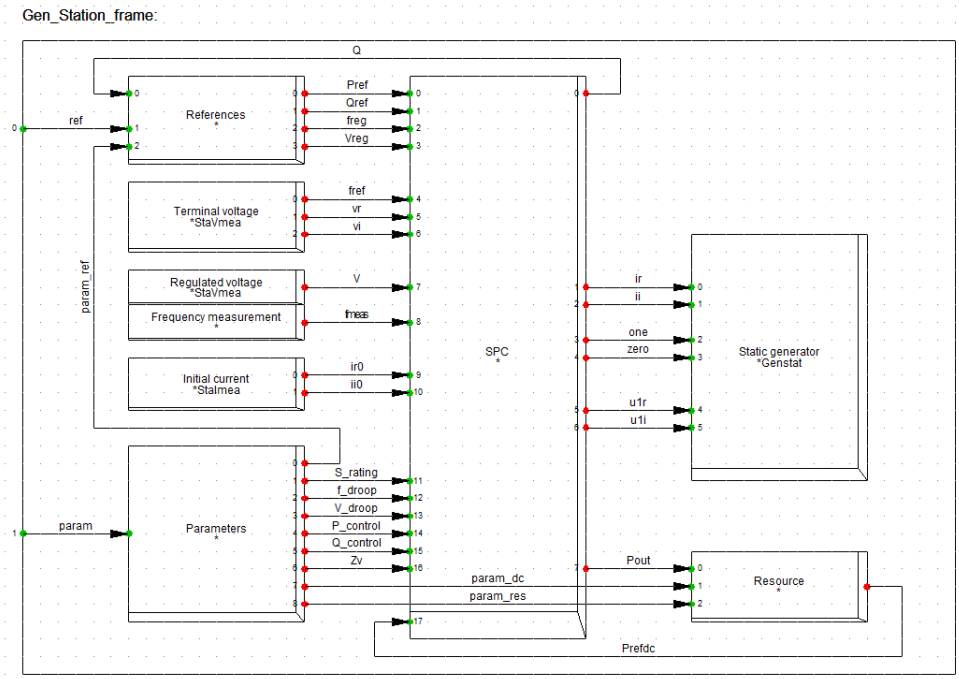


Fig. 4.3. Converter level control frame.

The need for this additional measurement is due to the particular configuration of the initialization process, which does not allow obtaining this measurement from the static generator. In fact, an additional connection between the converter controller and the reference block is included to allow a correct initialization of the reactive power reference for certain configurations of the reactive power reference generation system.

#### 4.3.3.1 References

At the converter level, the reference block updates the converter active and reactive power reference taking into account the signals received, and transmits the frequency and voltage reference employed for regulation. The power references are received in MVA, and converted to p.u., so all the blocks in this level use a local per-unit system.

The reference block receives parameters indicating the participation of the as-

sociated converter in the active and reactive power control of the PV plant. Additionally, it may receive additional parameters if more complex control strategies are defined.

The active and reactive power references generated by this block are given by:

$$P^{ref} = P^{ref0} + c_P P^{ref}_{input}$$

$$Q^{ref} = Q^{ref0} + c_Q Q^{ref}_{input}$$

$P^{ref0}$ and $Q^{ref0}$ are the active and reactive power injected by the power converter in the initial operating point, which are provided by the converter controller; whereas $P^{ref}_{input}$ and $Q^{ref}_{input}$ are the reference variations received from higher levels. The coefficients $c_P$ and $c_Q$ indicate the participation of this converter in the plant active and reactive power control. They can be set as parameters or, when a flag value is set, calculated taking into account its participation in the initial plant conditions.

#### 4.3.3.2 Synchronous power controller

The SPC block in the converter frame corresponds to the power converter controller. Given the fact that the main purpose of the analysis is to study the behavior of PV plants using the synchronous power controller, the frame is designed to embed the SPC, but other types of controllers can be connected to the same frame.

The objective of this block is to generate the signals used by the DSPF static generator. This element requires a current signal in the *dq* frame, and the cosine and sine of the angle that relates this frame with the phasor reference. Alternatively, the real and imaginary part of the current phasor can be directly provided, setting the cosine and sine equal to one and zero, respectively. Furthermore, DSPF may introduce the static generator directly as a current source, or as a voltage source, which may be interesting from a numerical point of view. Two additional signals, corresponding to the real and imaginary part of the voltage phasor are thus also considered, so it is possible to choose between both models.

The synchronous power controller block definition can be divided in different sections, corresponding to frequency and voltage regulation, active and reactive power control, the virtual admittance, or the converter model. These are explained

in the following.

Frequency regulation is performed following a droop curve. The first step is to calculate the frequency deviation:

$$\Delta f = f^{ref} - f$$

The resulting error signal can be optionally filtered to avoid interactions between the droop response and the inertial response of the synchronous power controller which may reduce its damping:

$$\frac{d\Delta f_{filt}}{dt} = \frac{\Delta f - \Delta f_{filt}}{T_f}$$

With the resulting signal, a modified active power reference is determined, modifying the active power reference received from the reference block, $P_{input}^{ref}$ internally, in an amount proportional to the frequency deviation. The droop response may consider a deadband, and an asymmetric response to overfrequencies and underfrequencies, both in terms of deadband and droop slope. In this way, PV converters are able to operate at their maximum power point and participate in regulation only when active power reductions are required. The modified active power reference would be given by:

$$P^{ref} = \begin{cases} P_{input}^{ref} + \frac{\Delta f_{filt} - \delta_f^{up}}{R_f^{up}} & \text{if } \Delta f_{filt} > \delta_f^{up} \\ P_{input}^{ref} + \frac{\Delta f_{filt} + \delta_f^{down}}{R_f^{down}} & \text{if } \Delta f_{filt} < -\delta_f^{down} \\ P_{input}^{ref} & \text{otherwise} \end{cases} \tag{4.1}$$

Taking into account the fact that the steady-state gain of the active power loop introduces an intrinsic droop when the equilibrium frequency is not equal to its rated value, the droop coefficients $R_f^{up}$ and $R_f^{down}$ should be modified to achieve the desired droop response. This is done through

$$\frac{1}{R_f^{mod}} = \frac{1}{R_f} - \frac{1}{k},$$

where $k$ is the active power controller gain.

Voltage regulation is carried out analogously, modifying the reactive power reference with the voltage error. In the case of voltage, since the reactive power controller performs an integral action, no correction of the droop coefficient is considered.

After applying the droop, the active power reference is limited, taking into account the power conversion system capabilities in steady state. In the case of a PV converter, this means considering, not only the converter ratings, but also the maximum power point of the PV system in the actual conditions, and its inability to absorb power. Limiting the reference is straightforward for the rated frequency, and must take into account the active power controller gain when there is a frequency deviation because the steady-state active power injection for a given steady-state frequency deviation would be

$$P_{ss} = P^{ref} + \frac{1}{k}\Delta f_{ss}$$

Finally, the reference is modified by adding the control signal sent by the resource and dc voltage controller $P_{dc}^{ref}$, which adapts the amount of power exchanged by the converter and the grid in order to keep the dc voltage within its desired range. However, the inertia introduced by the SPC may render the active power loop too slow to control the dc voltage correctly. Therefore, this additional control signal is also fed forward as an angle variation that immediately modifies the injected active power. For that purpose, the signal is processed by a high-pass filter that removes the contribution of the feed-forward branch in steady state:

$$\Delta P_{filt} = P_{dc}^{ref} - P_{filt}$$

$$\frac{dP_{filt}}{dt} = \omega_{ff}\,\Delta P_{filt}$$

And the corresponding angle variation is calculated through an approximation of the relation between generated power and phase-angle difference, taking into

account the virtual reactance introduced by the SPC:

$$\theta_{ff} = X\,\Delta P_{filt}$$

In the original implementation of the SPC, the active power controller takes the form of a first-order low-pass filter, defined by the cut-off frequency and gain:

$$\omega_c = 2\zeta\sqrt{\frac{\omega_g}{2HX}}$$

$$k = \frac{1}{2H\,\omega_c}$$

where $H$ is the inertia constant, $X$ is the virtual reactance, $\zeta$ is the desired damping coefficient, and $\omega_g$ is the base grid frequency in rad/s.

The active power error is calculated as $\Delta P = P^{ref} - P$, and may also include additional signals to limit the angle lead or lag of the controller with respect to the grid. The resulting signal is filtered to obtain the frequency increment with respect to the initial value, which is then added to obtain the absolute frequency:

$$\frac{df_{inc}}{dt} = \omega_c\,(k\,\Delta P - f_{inc}) \in \left[f_{inc}^{min}, f_{inc}^{max}\right] \tag{4.2}$$

$$f = f_0 + f_{inc}$$

This value can be converted to rad/s using the base grid frequency, and integrated to obtain the absolute angle of the virtual machine. The corresponding phasor phase-angle used in the RMS simulation is calculated taking into account the frequency of the reference bus:

$$\frac{d\theta}{dt} = \omega_g\,(f - f_{syst})$$

On the other hand, the reactive power controller applies a proportional-integral action to the reactive power error $\Delta Q = Q^{ref} - Q$ to obtain the magnitude of the electromotive force:

$$E = k_p\,\Delta Q + k_i \int \Delta Q \in \left[E^{min}, E^{max}\right]$$

The resulting magnitude and angle define a voltage phasor. The electrical model embedded by the SPC considers that this voltage is applied behind a virtual admittance that is connected to the grid at the point of connection of the converter. Therefore, the current reference is obtained as:

$$\underline{I}^{ref} = \frac{E\left(\cos\left(\theta+\theta_{ff}\right)+j\sin\left(\theta+\theta_{ff}\right)\right)-\underline{V}}{R+jfX}$$

where $R$ is the virtual resistance, and the reactance at the actual frequency is given by the product of this frequency and the virtual reactance at the rated frequency.

This reference is then saturated, taking into account the maximum transient current capability of the converter. The saturation modifies the current reference magnitude, thus not giving priority to active nor reactive power:

$$\underline{I}^{ref}_{sat} = \begin{cases} \underline{I}^{ref}\frac{I^{max}}{I^{ref}} & \text{if } I^{ref} > I^{max} \\ \underline{I}^{ref} & \text{otherwise} \end{cases}$$

And the components of the saturated reference $\underline{I}^{ref}_{sat} = i_r^{ref} + j\,i_i^{ref}$ are filtered to emulate the effect of the converter current loop:

$$\frac{di_r^{conv}}{dt} = \frac{i_r^{ref} - i_r^{conv}}{T_{conv}}$$

$$\frac{di_i^{conv}}{dt} = \frac{i_i^{ref} - i_i^{conv}}{T_{conv}}$$

The resulting converter current components $\underline{I}^{conv} = i_r^{conv} + j\,i_i^{conv}$ are thus sent to the DSPF static generator. Additionally, in case the static generator is chosen to work as a voltage source behind an impedance $R_s + jX_s$, the voltage that results in the desired current injection is given by:

$$\underline{U}_s = \underline{V} + (R_s + X_s)\underline{I}^{conv}$$

Besides the equations describing the dynamics of the model, the block definition monitors the grid voltage and generates a warning signal when it is below certain threshold, and processes tripping signals due to overcurrents, or dc voltage excur-

sions out of its safe operation range.

The initialization of the block takes a bottom-up approach. The initial current measurement determines the initial current value, and the voltage drop through the virtual admittance, which is then used to calculate the electromotive force magnitude and angle. Furthermore, the active and reactive power measurements are used to determine the initial references, assuming that the error of the controllers is initially zero.

**Synchronous power controller with PI active power controller**

The alternative implementation of the SPC considering a PI controller in the active power loop has also been developed in DSPF. The block definition is very similar to the original one, with only a few changes that are explained here.

First, the active power controller is modified to include the PI controller. However, this only requires defining a new parameter $\omega_z$ instead of the low-pass filter gain and cut-off frequency, and replacing the equation defining the frequency increment, (4.2), with a new one:

$$\omega_z = \frac{1}{2\zeta}\sqrt{\frac{\omega_g}{2HX}}$$

$$f_{inc} = \frac{1}{2H}\left(\frac{\Delta P}{\omega_z} + \int \Delta P\right) \in \left[f_{inc}^{min}, f_{inc}^{max}\right]$$

Secondly, as a direct consequence of the utilization of a PI controller, the active power injected by the converter in steady state follows its reference regardless of the frequency deviation. Therefore, the frequency droop coefficient and the active power reference saturation do not require any corrections related to the active power loop gain.

Lastly, the PI controller introduces a zero that results in a larger overshoot of the response to an active power reference step. This zero can be canceled with a filter applied to the active power reference input $P_{input}^{ref}$, which would then be replaced by $P_{filt}^{ref}$ in (4.1):

$$\frac{dP_{filt}^{ref}}{dt} = \omega_z\left(P_{input}^{ref} - P_{filt}^{ref}\right)$$

#### 4.3.3.3 Conventional controller

In order to compare the performance of the PV plant using the SPC with the results that would be obtained with a conventional power converter controller, an additional block definition is considered, where the converter control is based on voltage oriented control in open loop.

The main differences with respect to the SPC affect the active and reactive power controllers, which are replaced by a simple calculation of the reference current:

$$\underline{I}^{ref} = \text{conj}\left(\frac{P + jQ}{\underline{V}}\right)$$

Furthermore, since this loop introduces no additional delay, the dc voltage control signal is applied only to the active power reference and does not require a feedforward branch.

Other sections of the block definition, like the frequency and voltage droop, and the current saturation and converter model, are not modified. Regarding the frequency droop it is worth noting that the conventional controller does not require any modification of the droop slope, nor any active power reference filter; likewise, the active power saturation does not have to take into account any steady-state deviation induced by the active power controller.

#### 4.3.3.4 Parameters

The parameter block processes the information received from higher control levels, and the values set as DSPF parameters for each converter parameter block. As in the case of the plant and cluster levels, those parameters that are received from upstream are directly used; otherwise, if a flag value is received, the DSPF parameters are applied.

The converter parameters can be classified in several groups. One group defines the behavior of the converter reference block; other groups define different aspects of the converter controller, like its operating limits, the frequency and voltage droops, the active and reactive power controller, or the virtual admittance; and two other groups describe the converter dc side and its control, and the resource.

### 4.3.4 Resource models

The resource model introduces the dynamics of the converter dc side and its power source. In the case of the PV plant, this is the PV system connected to each converter. However, in order to have a sufficiently general plant model, simple models of storage systems like a supercapacitor or a battery have also been developed.

In DSPF, the resource block receives the active power injected by the converter as an input, includes the converter dc side model, and, taking into account the dc voltage, determines the active power produced by the resource. The following sections describe the different resource models that have been considered.

#### 4.3.4.1 Photovoltaic system

The converters are operated in such a way that they work in the stable part of the PV characteristics, i.e., in the voltage range between the maximum power point voltage and the open-circuit voltage. The model assumes that the PV system is correctly protected with diodes that prevent active power being absorbed by the PV modules.

Taking into account both the PV characteristics and the converter operation range, a valid dc voltage range is defined. Within its boundaries, the power converter is allowed to inject the active power determined by the controller that determines its interaction with the ac grid. However, if the voltage reaches one of the limits, a PI controller is activated, and its output is sent to the converter controller as a dc voltage control signal.

In addition to the signals exchanged with the converter controller, this resource block receives signals from the parameter block. One group of parameters defines the dc side capacitor, voltage limits, and controller gains; whereas the other group determines the PV curve taking into account the solar irradiance and the temperature. Furthermore, a DSPF parameter is used to introduce the converter losses.

The dc voltage controller observes the dc voltage deviation with respect to the maximum and minimum allowed voltage. Respectively, they correspond to the active power margin with respect to its lower and upper bounds. The resulting error signals,

$$e_{Pl} = v_{dc} - v_{dc}^{max} \tag{4.3}$$

$$e_{Pu} = v_{dc} - v_{dc}^{min}, \tag{4.4}$$

are processed by independent PI controllers, which are limited so that they generate a control signal only when the voltage is outside the desired range:

$$\Delta P_l = k_{pl}\, e_{Pl} + k_{il} \int e_{Pl} \in [0, S_{lim}]$$

$$\Delta P_u = k_{pu}\, e_{Pu} + k_{iu} \int e_{Pu} \in [-S_{lim}, 0]$$

The total control signal is obtained as the sum of both PI output signals, which cannot be different from zero simultaneously:

$$P_{dc}^{ref} = \Delta P_l + \Delta P_u$$

The model of the physical dc link of each converter considers the power balance affecting its capacitor voltage. In this power balance, the converter losses can be taken into account, modifying the amount of power drawn from the capacitor:

$$\frac{dv_{dc}}{dt} = \frac{P_{in} - \frac{P_{out}}{1-\varepsilon_{loss}}}{C\, v_{dc}}$$

Besides the dc voltage limits for control, two operational limits are considered. If the dc voltage reaches any of them, a trip signal is activated.

Finally, the PV model is described by an approximation of the two-diode model proposed in [82], which allows a direct computation of the current injected by the PV system, avoiding iterations during each integration step:

$$P_{in} = v_{dc} \left[ I_{sc}\, G - A_T \left( e^{B_T v_{dc}} - 1 \right) (w_I\, G + 1 - w_I) \right],$$

where $I_{sc}$ is the PV system short-circuit current for the rated irradiance, $A_T$ and $B_T$ are temperature-dependent coefficients, and $w_I$ is a weighting factor used to correct the open-circuit voltage given by the approximated PV curve. In addition, the effect of a diode blocking reverse currents is considered, so $P_{in}$ is constrained to be $P_{in} \geq 0$.

The initialization of the model considers the controller states are zero, and determines the dc voltage as a function of the injected active power, taking into account

the PV characteristics.

**Photovoltaic system with maximum power point tracking**

The dc voltage controller can be adapted to track the maximum power point of the PV system. The necessary changes affect the way in which the dc voltage error is calculated in (4.4), i.e., in undervoltage conditions. Thus, the lower dc voltage limit $v_{dc}^{min}$ is replaced by the maximum power point voltage $v_{MPP}$:

$$e_{Pu} = v_{dc} - v_{MPP}$$

The maximum power point voltage is updated whenever the resulting error is negative, and the variation of the objective voltage is positive or negative depending on the relation between active power and dc voltage variations:

$$x_{MPP} = \begin{cases} 1 & e_{Pu} < 0 \\ 0 & \text{otherwise} \end{cases}$$

$$s_{MPP} = \begin{cases} 1 & \left(P_{in} - P_{in}^{prev}\right)\left(v_{dc} - v_{dc}^{prev}\right) > 0 \\ -1 & \text{otherwise} \end{cases}$$

The update of the voltage reference uses an update rate $\Delta v_{MPP}$, which can be fixed or adaptive, and takes into account other constraints that may also limit the dc voltage:

$$v_{MPP} = \max\left(v_{MPP}^{prev} + x_{MPP}\, s_{MPP}\, \Delta v_{MPP}, v_{dc}^{min}\right)$$

It is worth noting that a zero update rate determines a constant lower dc voltage limit, which corresponds to the previous control implementation.

#### 4.3.4.2 Supercapacitor

Another type of resource whose model has been considered is a supercapacitor. Its model considers it is a large capacitor connected to the converter dc link in series with a dc resistance, which represents losses in the supercapacitor and the cables.

Table 4.3. Supercapacitor current and dc voltage control actions.

| Event | Low $i$ | High $i$ |
|---|---|---|
| Low $v_{dc}$ | - | Decrease $P^{ref}$ |
| High $v_{dc}$ | Increase $P^{ref}$ | - |

The dc link model is the same as in the case of the PV system, and the dc voltage control has the same structure as in that case, but also limits the current injected to, or extracted from, the supercapacitor.

In order to coordinate both control objectives, the relation between the current extracted from the supercapacitor and the dc link voltage must be analyzed. For this purpose, it is worth taking into account that a large current will be extracted from the supercapacitor only when the dc link voltage is too low, assuming that the large capacitance prevents significant voltage variations in the supercapacitor. Analogously, a large current will be injected into the supercapacitor only if the dc link voltage is too high. In each case, a modification of the active power exchanged between the power converter and the grid mitigates the contingency. The actions to be taken in each case are summarized in Table 4.3, where the current is considered positive if it is extracted from the supercapacitor.

Using this, the dc voltage error signals defined in (4.3) and (4.4) are modified to perform the current control action. The current limits, and the weight of the current in the control signal can be set differently in each direction:

$$e_{Pl} = \max\left(v_{dc} - v_{dc}^{max}, w_{ic}\left(-i_c^{max} - i\right)\right)$$

$$e_{Pu} = \max\left(v_{dc} - v_{dc}^{min}, w_{id}\left(i_d^{max} - i\right)\right)$$

On the other hand, the supercapacitor model considers the supercapacitor and dc link voltages, and the resistance connecting both points in order to calculate the current extracted from the supercapacitor:

$$i = \frac{v_s - v_{dc}}{R_{dc}}$$

With this current, the supercapacitor voltage is updated, and the power reaching the dc link is calculated:

$$\frac{dv_s}{dt} = -\frac{i}{C_s}$$
$$P_{in} = v_{dc}\, i$$

The initialization considers an initial State Of Charge (SOC) of the supercapacitor, and its corresponding voltage. With this voltage and the initial active power injection, the dc link voltage is calculated.

#### 4.3.4.3 Battery

The last type of resource considered is a Battery Energy Storage System (BESS). The model employed is a simple one that assumes that the battery is working in a linear range where the voltage varies proportionally to the state of charge of the battery, and the electrical model of the battery is that of a real voltage source.

In this case, the control of the dc voltage must take into account the battery SOC, and keep it within the linear operation limits. Once again, due to the fact that the battery voltage depends on the SOC, this variable is also related to the dc link voltage and the current extracted from the battery. For instance, a low value of the battery SOC will result in a low battery voltage; in that case, a high dc link voltage would charge the battery and both problems would be naturally mitigated, whereas a low dc link voltage could further discharge the battery and would require a decrease of the power converter active power reference. The possible situations and actions to take are summarized in Table 4.4

This can be used to further modify equations (4.3) and (4.4) and take into account the battery SOC in the control of the dc voltage, with independent weighting coefficients:

$$e_{Pl} = \max\left(v_{dc} - v_{dc}^{max}, w_{ic}\left(-i_c^{max} - i\right), w_{SOCc}\left(SOC - SOC^{max}\right)\right)$$

$$e_{Pu} = \max\left(v_{dc} - v_{dc}^{min}, w_{id}\left(i_d^{max} - i\right), w_{SOCd}\left(SOC - SOC^{min}\right)\right)$$

The battery model itself considers the dependence of the battery voltage with

Table 4.4. Battery state of charge, current and dc voltage control actions.

| Event | Low $SOC$ | High $SOC$ |
|---|---|---|
| Low $v_{dc}$ | Decrease $P^{ref}$ | - |
| High $v_{dc}$ | - | Increase $P^{ref}$ |

| Event | Low $SOC$ | High $SOC$ |
|---|---|---|
| Low $i$ | - | Increase $P^{ref}$ |
| High $i$ | Decrease $P^{ref}$ | - |

the SOC:

$$v_s = v_0 + k_v SOC$$

and determines the current extracted from the battery taking into account the voltage of the battery and the dc link, and the total dc resistance including the internal battery resistance and the cables:

$$i = \frac{v_s - v_{dc}}{R_{dc}}$$

The state of charge of the battery is updated taking into account the power exchanged by the battery voltage source, which already takes into account the internal losses represented by the internal battery resistance:

$$\frac{dSOC}{dt} = -\frac{v_s\, i}{C_s}$$

And the power fed to the dc link is calculated as in the previous cases:

$$P_{in} = v_{dc}\, i$$

Once again, the initialization considers the SOC of the battery, and its corresponding voltage, which is used to determine the initial dc link voltage taking into account the active power injected by the power converter.

**Battery with soft saturation**

An alternative battery control strategy considers variable current limits as the battery SOC approaches its limits. This is done through a further modification of (4.3) and (4.4):

$$e_{Pl} = \max\left(v_{dc} - v_{dc}^{max}, w_{ic}\left(i_c^{lim} - i\right), w_{SOCc}\left(SOC - SOC^{max}\right)\right)$$

$$e_{Pu} = \max\left(v_{dc} - v_{dc}^{min}, w_{id}\left(i_d^{lim} - i\right), w_{SOCd}\left(SOC - SOC^{min}\right)\right),$$

where the current limits are modified linearly when the SOC is close to its limits:

$$i_c^{lim} = \begin{cases} -i_c^{max} & SOC \leq SOC^{max} - \delta_{SOC}^{max} \\ \frac{SOC - SOC^{max}}{\delta_{SOC}^{max}} i_c^{max} & SOC^{max} - \delta_{SOC}^{max} < SOC < SOC^{max} \\ 0 & SOC \geq SOC^{max} \end{cases}$$

$$i_d^{lim} = \begin{cases} i_d^{max} & SOC \geq SOC^{min} + \delta_{SOC}^{min} \\ \frac{SOC - SOC^{min}}{\delta_{SOC}^{min}} i_d^{max} & SOC^{min} < SOC < SOC^{min} + \delta_{SOC}^{min} \\ 0 & SOC \leq SOC^{min} \end{cases}$$

## 4.4 Equivalent PV plant static model

As discussed in Section 2.4.2, when analyzing large power systems with PV plants like this, it is interesting to employ an equivalent plant model with reduced complexity but enough accuracy for the analysis. Taking this into account, a method to aggregate several power converters employing the SPC has been studied, and different equivalent models of the PV plant have been developed and compared. Namely, four models, with different degrees of detail, are considered. The first one is the complete model of the plant just described, whereas the other three aggregate some converters at the cluster and even at the plant level. These models, depicted schematically in Fig. 4.1 and Fig. 4.4, are the following:

1. 100×1 model (Fig. 4.1): Original model of the plant, including all the converters.

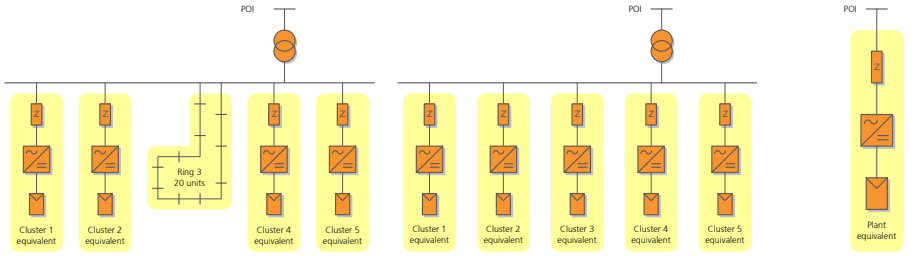


(a) $4\times20+20\times1$ model. (b) $5\times20$ model. (c) $1\times100$ model.

Fig. 4.4. Simplified representation of the equivalent power plant models.

2. $4\times20+20\times1$ model (Fig. 4.4a): Rings 1, 2, 4, and 5 are each of them represented by their cluster equivalent, consisting of one equivalent converter. Ring 3 is modeled in its original form. This model allows reducing the number of equations without losing all the information about the individual behavior of each station.

3. $5\times20$ model (Fig. 4.4b): Each ring is represented by its cluster equivalent. A further reduction in the number of equations is achieved, keeping track of the power injected by each cluster.

4. $1\times100$ model (Fig. 4.4c): The power plant is modeled by a single equivalent converter, and its equivalent impedance also includes the plant transformer.

In these models, each cluster or plant equivalent is controlled by one equivalent converter controller whose parameters are calculated in such a way that the equivalent model reproduces the aggregate response of the groups of converters considered. In addition to the models of the controllers of converters or equivalent converters, each of these power plant models contains the model of the central controller generating the active and reactive power reference signals, and also the cluster controllers of clusters that are not represented by an equivalent converter.

The remaining of the chapter presents the method employed to determine the equivalent model of a group of power converters controlled by the SPC, and the validation of the equivalent models of the studied PV plant. In particular, this section addresses the calculation of the equivalent static model of a group of converters,

which basically consists on determining the impedance behind which the equivalent converter is connected.

Unlike more complex methods as those discussed in Section 2.4.2, the equivalent impedance calculation method presented here exploits the fact that the conductors inside each ring of the PV plant are relatively short, and their impedance is significantly smaller than the MV/LV transformer impedance. Thus, a simplified calculation method can be applied without incurring in appreciable errors.

The first step is to define the correct per unit systems that allow an easy translation from the original model to the equivalent one, and expressing the impedance of all cables and transformers in the corresponding per unit system.

The studied PV plant involves three different voltage levels. Namely, it is connected to the grid at 220 kV, its internal network operates at 33 kV, and the converters employ 365 V. These rated values are considered the base voltage for each of these parts of the plant. The equivalent model takes the value corresponding to the level where it is connected. The base power considered at the converter level is 1 MVA, and for a group of converters it will be the sum of the individual values. For instance, cluster 1 will employ a base power of 20 MVA, and the PV plant will use 100 MVA, which is also a typical base value for power system analysis.

When comparing the data in Tables 4.1 and 4.2 in a common per unit system, it is possible to observe that the shunt impedance of the cables is very large with respect to the cable and transformer impedance, so it can be neglected. Furthermore, the impedance of the cables, considering the total distance involved, is two orders of magnitude smaller than the transformer impedance. Thus, a first approximation may neglect the effect introduced by the cables, and consider all the converters being aggregated as if they were voltage sources, with a series impedance corresponding to their transformers, connected in parallel, like in Fig. 4.5.

The Thévenin equivalent of a group of n real voltage sources connected in parallel, as those depicted in Fig. 4.5, is straightforward:

$$\underline{U}_{th} = \frac{\sum_{k=1}^{n} \frac{\underline{U}_k}{\underline{Z}_k}}{\sum_{k=1}^{n} \frac{1}{\underline{Z}_k}} \tag{4.5}$$

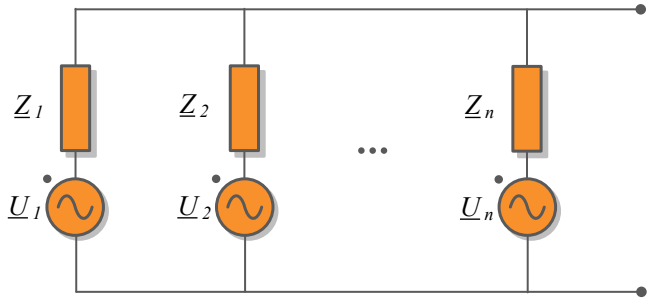


Fig. 4.5. Simplified representation of MV ring with power converters as real voltage sources.

$$\underline{Z}_{th} = \frac{1}{\sum_{k=1}^{n} \frac{1}{\underline{Z}_k}} \tag{4.6}$$

Equation (4.6) expresses the fact that the Thévenin impedance is the parallel of all the source impedances. Taking into account that they correspond to the converter transformers, which have the same impedance, the equivalent impedance is equal to the impedance of one transformer divided by the number of power converters being aggregated.

The approximate equivalent impedance of a cluster can thus be obtained as the sum of this Thévenin impedance and the parallel of the impedance of the conductors connecting the endpoints of the ring to the substation. In case one wants to take into account the effect of the cables forming the rings, especially in order to account for the conduction losses, it is possible to include it in approximate way, taking into account the current circulating through each cable in the ring. Namely, the impedance of each conductor, multiplied by a factor that takes into account the ratio of the current circulating through that conductor to the total current of the group of converters in nominal conditions, can be added to the equivalent impedance.

Finally, the plant equivalent impedance is calculated taking into account that all clusters are connected in parallel, and adding the series impedance corresponding to the plant transformer. The results obtained for each cluster of the studied PV plant, and for the whole plant, are given in Table 4.5 in the plant per-unit system.

Table 4.5. Equivalent plant model. Equivalent impedance of each group of converters, in per unit for a 100 MVA power.

| Group | Devices | Impedance (p.u.) |
|---|---|---|
| Cluster 1 | 20 | $0.0615 + 0.3040\,j$ |
| Cluster 2 | 18 | $0.0613 + 0.3251\,j$ |
| Cluster 3 | 20 | $0.0423 + 0.2763\,j$ |
| Cluster 4 | 20 | $0.0437 + 0.2785\,j$ |
| Cluster 5 | 22 | $0.0388 + 0.2539\,j$ |
| Plant | 100 | $0.0128 + 0.1707\,j$ |

## 4.5 Equivalent PV plant dynamic model

The derivation of a dynamic equivalent model requires taking into account the behavior of the converters, determined by their controllers. Therefore, each equivalent converter will be controlled by an SPC, and it is necessary to determine the values of its defining parameters. Namely, the equivalent inertia, damping, virtual impedance, reactive power controller gains, and droop slopes must be calculated. In order to obtain an accurate model, it is necessary that the converters being aggregated have the same virtual impedance resistance-to-reactance ratio and a coherent active and reactive power response.

Like in the case of the static model, it is convenient to express all variables and parameters in per unit, both for the original and the equivalent model. For the original model, a converter base voltage of 365 V and base power of 1 MVA are employed. For the equivalent model, the rated voltage at the point of connection and the sum of the base powers of all the converters being aggregated are used.

### 4.5.1 Mechanical equivalent

The first equivalent parameter to be determined is the SPC inertia. This is done by taking into account that the total kinetic energy of the virtual rotors must be the

same for the original model and its equivalent:

$$E_\omega = \frac{1}{2} J_{eq} \omega_g^2 = \sum_k \frac{1}{2} J_k \omega_g^2, \tag{4.7}$$

where $J_{eq}$ is the equivalent moment of inertia and $J_k$ is the moment of inertia of station $k$ in SI units, and $\omega_g$ is the rated angular speed in rad/s, corresponding to the grid rated frequency. This means that the equivalent moment of inertia is equal to the sum of the moments of inertia of all the stations. In per unit:

$$H_{eq} S_{eq} = \sum_k H_k S_k \Rightarrow H_{eq} = \frac{\sum_k H_k S_k}{S_{eq}}, \tag{4.8}$$

i.e., the equivalent inertia constant is the weighted average for all the stations.

Now, if the objective of the dynamic equivalent is to reproduce the aggregate dynamics of the converters, its constituting swing equation

$$2H\omega \frac{d\omega}{dt} = P_{in} - P_{out} - D\Delta\omega, \tag{4.9}$$

should correspond to the addition of the swing equations describing the dynamics of each converter. Assuming $\omega \approx 1$ and comparing each side of the equation:

$$2H_{eq} \frac{d\omega_{eq}}{dt} S_{eq} = \sum_k 2H_k \frac{d\omega_k}{dt} S_k \tag{4.10}$$

$$(\Delta P_{tot} - D_{eq} \Delta\omega_{eq}) S_{eq} = \sum_k (\Delta P_k - D_k \Delta\omega_k) S_k \tag{4.11}$$

Thus, the equivalent frequency is obtained from (4.10):

$$\omega_{eq} = \frac{\sum_k H_k \omega_k S_k}{H_{eq} S_{eq}}, \tag{4.12}$$

which is again a weighted average with the total inertia of each station. The frequency deviation $\Delta\omega$ has an analogous expression because of the definition of $H_{eq}$ in (4.8).

Additionally, it is worth noting that the power balance of both models must be the same and therefore:

$$\Delta P_{tot}\, S_{eq} = \sum_k \Delta P_k\, S_k, \tag{4.13}$$

so (4.11) can be reduced to the terms related to the damping and the frequency deviation. And substituting the equivalent frequency in the left hand side:

$$D_{eq}\,\Delta\omega_{eq}\,S_{eq} = D_{eq}\frac{\sum_k H_k \Delta\omega_k S_k}{H_{eq}} = \sum_k \frac{D_{eq}}{H_{eq}} H_k \Delta\omega_k S_k \tag{4.14}$$

Whereas rewriting the right-hand side:

$$\sum_k D_k \Delta\omega_k S_k = \sum_k \frac{D_k}{H_k} H_k \Delta\omega_k S_k \tag{4.15}$$

Therefore, if there are no constraints on the values of the different $\omega_k$, the equality would require:

$$\frac{D_{eq}}{H_{eq}} = \frac{D_k}{H_k} \quad \forall k \tag{4.16}$$

This is possible if all the stations have the same $D/H$ ratio, and determines the value of the equivalent damping parameter. Otherwise, an approximate value of $D_{eq}$ can be calculated introducing certain error.

### 4.5.2 Electrical equivalent

The objective of the equivalent model is to reproduce the active and reactive power response of the power plant, so the control loops determining these responses must be analyzed.

In the case of active power, it is necessary to model the injection resulting from the voltage source magnitude and angle, the terminal voltage, and the virtual impedance. Neglecting the effect of the resistance, and denoting the angle lead of the voltage source with respect to the terminal voltage by $\delta$, the injected active power is:

$$P = \frac{EV}{X}\sin(\delta) \tag{4.17}$$

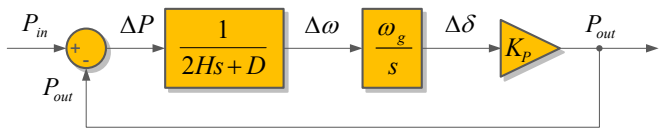


Fig. 4.6. Active power closed loop with the synchronous power controller.

For small angle variations, this injection would vary according to:

$$\Delta P = K_P \Delta\delta = \frac{\partial P}{\partial \delta}\Delta\delta = \frac{EV}{X}\cos(\delta)\Delta\delta, \tag{4.18}$$

where $E, V$ are normally around its rated value of 1 p.u. and $cos(\delta)$ is also close to unity because $\delta$ is small.

This relation can be introduced in the closed loop of Fig. 4.6, from which it is easy to obtain the closed-loop transfer function for the active power of an SPC converter:

$$\frac{\Delta P_{out}}{\Delta P_{in}}(s) = \frac{\frac{K_P\omega_g}{2H}}{s^2 + \frac{D}{2H}s + \frac{K_P\omega_g}{2H}} \tag{4.19}$$

If a single equivalent controller must reproduce the aggregate effect of several units with this transfer function, it is necessary that their active power responses are coherent in terms of (4.19), i.e., that they define the same poles.

This requires $D/H$ and $K_P/H$ to be the same for all the stations. The first one is already expressed by (4.16), whereas the second one introduces new constraints. Assuming the voltages are around 1 p.u. and their phase-difference is small, the second one can be expressed as:

$$X_{eq} H_{eq} = X_k H_k \quad \forall k, \tag{4.20}$$

Therefore, if the product $XH$ is the same for all the stations, the equivalent reactance is the result of dividing that product by the equivalent inertia. And once the equivalent reactance is defined, the equivalent resistance is obtained using the same resistance-to-reactance ratio of all the converters that are aggregated. Like in the case of the equivalent damping, an approximate value can be used if the product $XH$ or the resistance-to-reactance ratio are not exactly the same for all the stations.

With a similar analysis of the reactive power loop, taking into account the fact that the expression of the reactive power when the resistance is neglected is

$$Q = \frac{EV}{X}\cos(\delta) - \frac{V^2}{X} \Rightarrow \Delta Q = \frac{V}{X}\cos(\delta)\,\Delta E, \tag{4.21}$$

both gains of the PI controller in charge of reactive power must keep a common proportionality factor with respect to the virtual reactance, so the responses are coherent and a single equivalent controller can reproduce the same aggregate response. In that case, the gains of the PI controller in the equivalent model are calculated from the equivalent reactance, keeping the same proportionality factor. And otherwise, if that condition does not hold, an approximate value can be used.

### 4.5.3 Equivalent droop

The droop response of the equivalent model, using the frequency measurement at the point of interconnection, is given by

$$\Delta P_{droop,tot} S_{eq} = \frac{1}{R_{f,eq}}(f_{ref} - f)\,S_{eq} \tag{4.22}$$

And it should match the aggregate response to frequency variations of the original group of converters:

$$\sum_k \Delta P_{droop,k} S_k = \sum_k \frac{1}{R_{f,k}}(f_{ref} - f)\,S_k \tag{4.23}$$

Therefore, the droop slope is obtained as a weighted average depending on the rated power of each unit:

$$\frac{1}{R_{f,eq}} = \frac{\sum_k \frac{1}{R_{f,k}} S_k}{S_{eq}} \tag{4.24}$$

The equivalent voltage droop slope, which is disabled in the particular case under study, would be obtained in an analogous way.

### 4.5.4 Resource equivalent

Finally, it is necessary to obtain an equivalent representation of the dc bus and the photovoltaic system connected to it in order to model the impact that the resource behavior could have on the grid.

For this type of analysis, considering an RMS model of the ac components, the dc bus is modeled simply by a capacitor. In order to calculate the equivalent capacitance, the electrostatic energy stored by the capacitor in the equivalent model and by all the capacitors of the original converters is equated:

$$E_C = \frac{1}{2} C_{eq} V_{dc,r}^2 = \sum_k \frac{1}{2} C_k V_{dc,r}^2 \tag{4.25}$$

This equation is very similar to (4.7), used to determine the equivalent inertia. Analogously, the per unit equivalent capacitance is the weighted average of the capacitance of each converter taking into account its rated power.

The photovoltaic system, introduced through a two-diode model, is reproduced in the same way by the dynamic equivalent model. A single irradiance value is determined for the equivalent model as a weighted average considering the irradiance and rated power of each converter, whereas the dc voltage evolves as determined by the resulting PV curve and the active power exchanged with the grid through the equivalent converter. Similarly, supercapacitor and battery equivalents can be defined using weighted averages of the parameters describing the original resources.

### 4.5.5 Discussion

As mentioned, the proposed method relies on hypotheses like a common virtual impedance resistance-to-reactance ratio and coherent active and reactive power responses for all the converters being aggregated. When these conditions are not met, depending on the degree of the deviations, approximate values can be used to determine some parameters like the equivalent damping or reactance. Nevertheless, under certain conditions the error resulting from these approximations may not be admissible. In that case, different subgroups of converters working in similar conditions can be defined, determining one equivalent converter for each subgroup.

Similarly, the derivation of the equivalent droop response assumes that frequency and voltage are measured at the point of interconnection and are common for all the stations. If this is not true in a different application, where several measurements are considered, the equivalent droop response can be obtained as the sum of several terms, each one taking into account the contribution of one subgroup of converters using the same measurement, or an average value can be used.

Finally, given the characteristics of the curve describing the power generated by a photovoltaic system, it may be necessary to consider converters working in different conditions of radiation, temperature or active power reference separately. However, if their ac side response is similar, it is enough with modeling several dc buses, each of them contributing to generate the active power requested by the converter with a certain weight, and considering its own radiation, temperature or operating point, as is done in [87] for wind.

## 4.6 Equivalent model validation

In this section, the effectiveness of the equivalent model of the PV power plant is studied through simulation. In the tests presented here, the power plant is connected to a very simple grid model that allows measuring the accuracy of the equivalent model of the power plant in isolation, as well as the time taken to solve the equations describing only the dynamics of the plant, without the interference of additional elements.

The grid is modeled as a real voltage source of 220 kV with a short-circuit current of 5 kA and a resistance-to-reactance ratio of 0.1, which approximately correspond to the characteristics of the northern Chile grid at the point of interconnection of the actual PV power plant. Furthermore, the control of the plant assumes that the converter controller employs a measurement of the frequency at the POI, whereas the voltage control is managed exclusively at the plant level and the converter droop is disabled.

### 4.6.1 Test scenarios

The accuracy of the equivalent models is tested under five scenarios with different references and SPC parameters, following the information respectively summarized in Table 4.6 and Table 4.7. The scenarios are defined in the following way:

1. Scenario 1: All the stations have an initial active power reference of 0.6 and share the parameters corresponding to the plant in Table 4.7.

2. Scenario 2: The stations in each cluster have an initial active power reference equal to the average of that cluster in Table 4.6 and all the stations share the parameters corresponding to the plant in Table 4.7.

3. Scenario 3: Each station has the initial active power reference listed in Table 4.6 and all the stations share the parameters corresponding to the plant in Table 4.7.

4. Scenario 4: All the stations have an initial active power reference of 0.6 and the stations in each cluster use the parameters corresponding to that cluster in Table 4.7.

5. Scenario 5: All the stations have an initial active power reference of 0.6 and the stations in clusters 1, 2, 4, and 5 use the parameters corresponding to that cluster in Table 4.7, whereas stations 1 to 10 and stations 11 to 20 in cluster 3 respectively use the parameters corresponding to cluster 3a and cluster 3b in Table 4.7.

The remaining SPC parameters are defined as a function of those of Table 4.7: The damping coefficient is such that the damping ratio of the active power response described by (4.19) is 0.7; the resistance-to-reactance ratio is $1/3$; and the proportional and integral gains of the reactive power controller are respectively obtained by multiplying the virtual reactance by $1/30$ and $4/3$. In these scenarios, the solar radiation is considered to be 1000 W/m$^2$ for all the PV systems feeding the converters. At the plant level, the proportional gain applied to the voltage error is $1/40$, whereas the proportional and integral gains of the plant reactive power controller are respectively $5/3$

and 5. It must be noted that the active power references are shared proportionally to the initial reference, so stations with a larger initial reference will do a greater contribution to any plant active power reference change.

### 4.6.2 Model accuracy

The accuracy of the model is tested for four different events. The first two involve plant reference variations; namely, an active power reference step, and a voltage reference step. The last two correspond to grid events such as a frequency ramp and a voltage sag.

#### 4.6.2.1 Active power response

The active power response of the power plant is compared for all four models under scenarios 1 through 5. The event consists in a plant active power reference step from 0.6 p.u. to 0.8 p.u. at $t = 1$ s.

As a response to this change in the active power reference, the PV plant modifies its current injection, which also has an effect on the grid voltage at the POI. The evolution of this voltage and the current injected by the plant can be seen in Fig. 4.7, where the voltage at the POI is the phasor angle reference that defines the real ($I_r$) and imaginary ($I_i$) parts of the current phasor. The main effect of the active power reference change is an increase in the real part of the current, accompanied by transient variations of the voltage and the imaginary part of the current of reduced magnitude, and the results obtained are very similar for the four proposed models.

In addition, Fig. 4.8 shows the evolution of the active power injected by the PV plant under scenario 1 for the four models. In this figure, it is possible to see that the response follows the trajectory defined by the SPC through (4.19) for all the models, and there are slight differences among them. Corresponding results are obtained for the dc voltage of the power converters in the plant; this is represented in Fig. 4.9, considering the weighted average of each converter in the cases where the plant model consists of more than one converter.

In fact, the small differences are not due only to the homogeneous conditions of operation under scenario 1. Table 4.8 summarizes the information about the maximum absolute error incurred by each aggregated model with respect to the

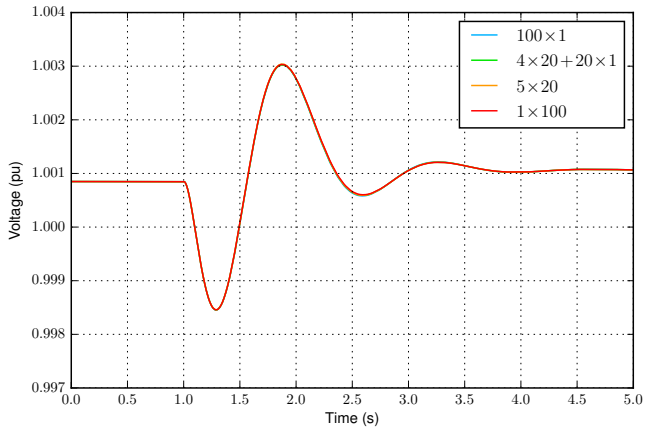


(a) Voltage.

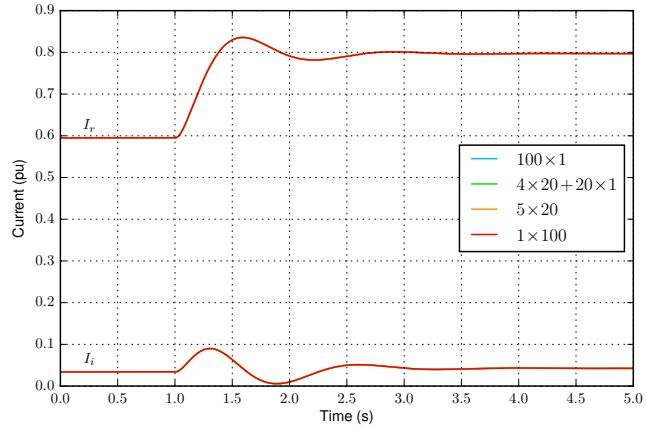


(b) Current.

Fig. 4.7. Power plant voltage and current response to an active power reference step for different models in scenario 1.

original 100×1 model and shows a maximum error around $7 \cdot 10^{-3}$ among all the models and scenarios. The largest errors correspond to the two least detailed models and the scenarios where the references or the parameters are less homogeneous, but are in any case acceptable.

The maximum absolute errors occur approximately between $t = 1.5\,\text{s}$ and $t = 1.9\,\text{s}$ in all cases, which corresponds to the maximum of the response and the subsequent decrease in the active power injection. Fig. 4.10 allows a graphical compar-

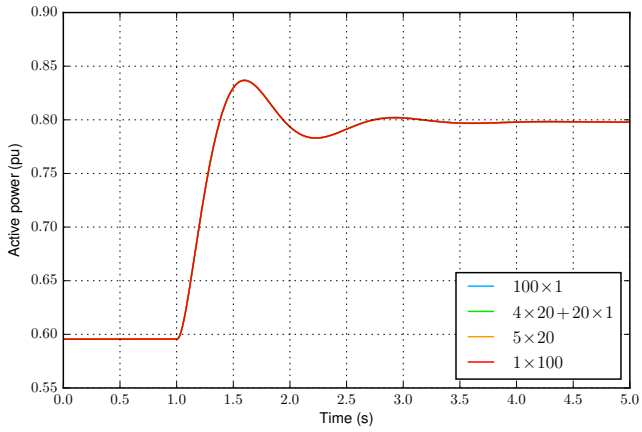


Fig. 4.8. Active power injected by the power plant after an active power reference step for different models in scenario 1.

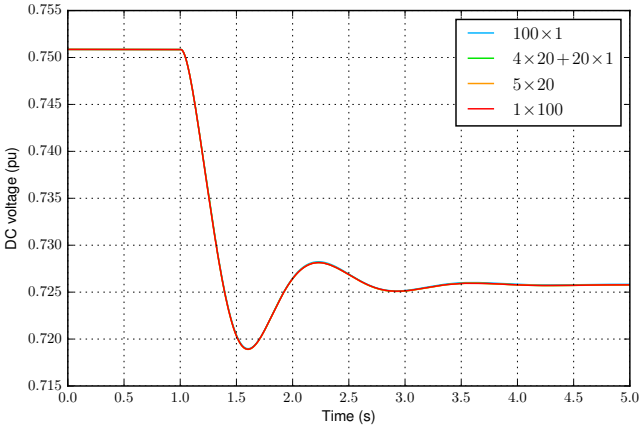


Fig. 4.9. Average dc voltage of the power plant converters after an active power reference step for different models in scenario 1.

ison of the errors during this period for scenarios 2-5. In Fig. 4.10b it is possible to see that the aggregated models overestimate the active power injection because they are not able to capture the saturation of stations whose initial reference is over 0.75 p.u., which results in a final reference over 1 p.u. after the step. This can be seen in greater detail in Fig. 4.11, where the active power injected by cluster 3 for different models (20 MVA base) and by converters 1 and 13 of this cluster (1 MVA base), and their dc voltage, are shown. In this figure, it is possible to see convert-

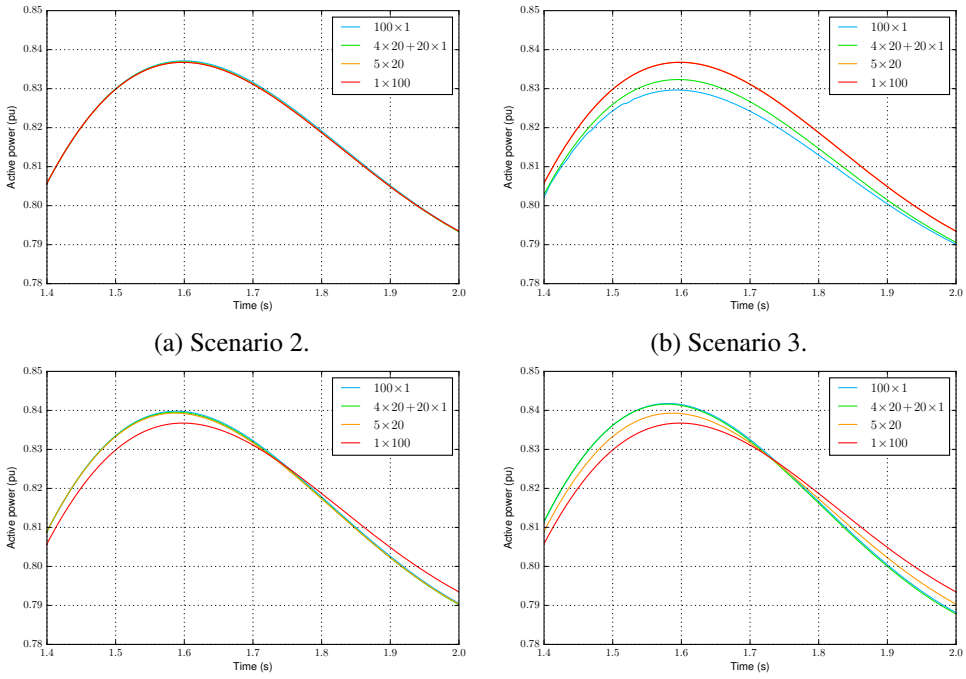


(a) Scenario 2.

(b) Scenario 3.

(c) Scenario 4.

(d) Scenario 5.

Fig. 4.10. Detail of the active power injected by the PV power plant after an active power reference step for different models in different scenarios.

ers 1 and 13 reach the lower dc voltage limit, set to 0.64 p.u., for an active power injection slightly over 1 p.u., around their maximum power point. Furthermore, the fast reaction of the dc voltage controller has a sudden effect on the active power injection that is still appreciable in the cluster response of the most detailed models.

#### 4.6.2.2 Reactive power response

The reactive power response of the different models is also compared for all five scenarios. In this case, the plant voltage reference is modified from 1 p.u. to 1.01 p.u. at $t = 1$ s. For scenario 1, this causes a voltage variation, which is induced by a change in the imaginary part of the current injected by the plant, as shown in Fig. 4.12. Since the voltage controller is proportional, there is a steady-state error, but the response is practically the same for all the models. The reactive power behaves similarly, as

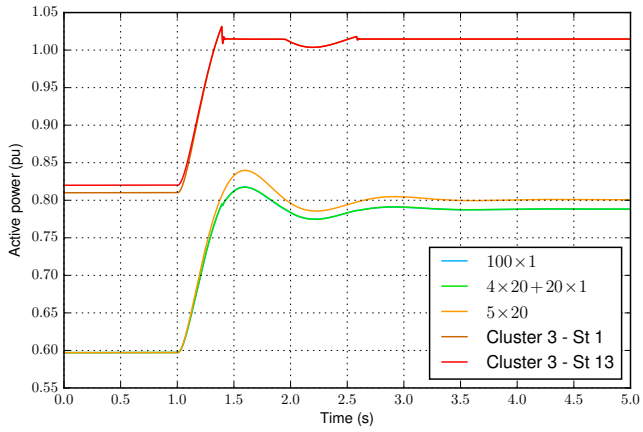


(a) Active power.

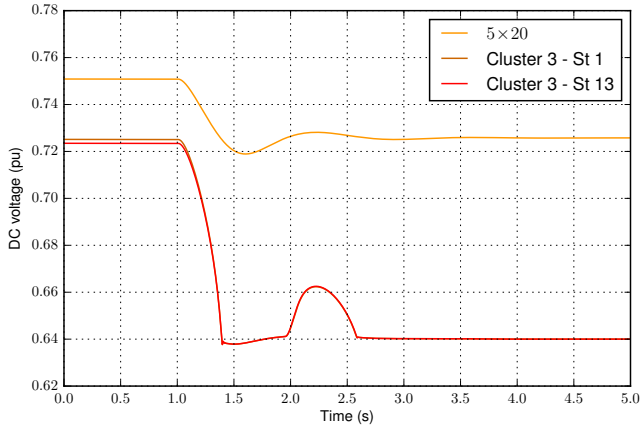


(b) DC voltage.

Fig. 4.11. Response of cluster 3 and selected units to an active power reference step for different models in scenario 1.

shown in Fig. 4.13, and the errors among models are very limited.

The maximum absolute reactive power error incurred by each model with respect to the 100×1 reference model is given in Table 4.9 for all scenarios. In this case, the largest error is below $2.5 \cdot 10^{-3}$, and the largest discrepancies appear again when models 5×20 and 1×100 are employed in scenarios 3, 4, and 5, with less homogeneous conditions. Now, the maximum errors take place between $t = 1.3\,\mathrm{s}$ and $t = 1.6\,\mathrm{s}$, immediately before the maximum reactive power injection and the

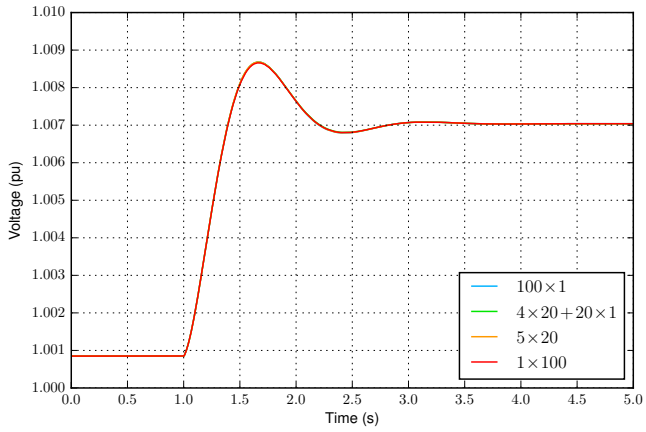


(a) Voltage.

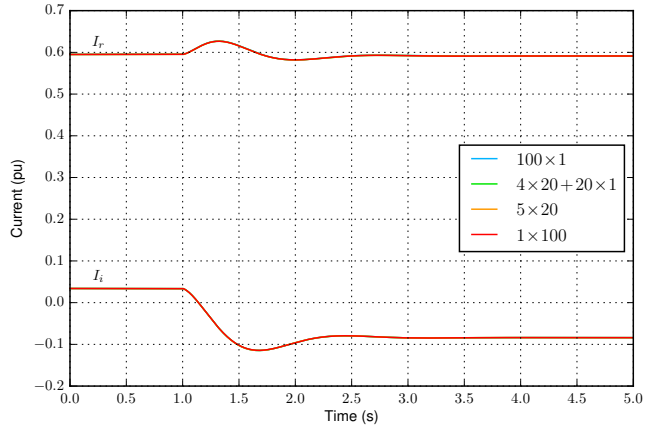


(b) Current.

Fig. 4.12. Power plant voltage and current response to a voltage reference step for different models in scenario 1.

different results for scenarios 2-5 can be seen graphically in Fig. 4.14.

#### 4.6.2.3 Response to a grid frequency ramp

The response of the power plant to grid frequency variations is compared for all four models under scenarios 1 through 5. The event consists in a grid frequency ramp from 1 p.u. to 0.99 p.u., starting at $t = 1$ s and ending at $t = 3$ s.

As in the case of the active power reference step, the PV plant response affects

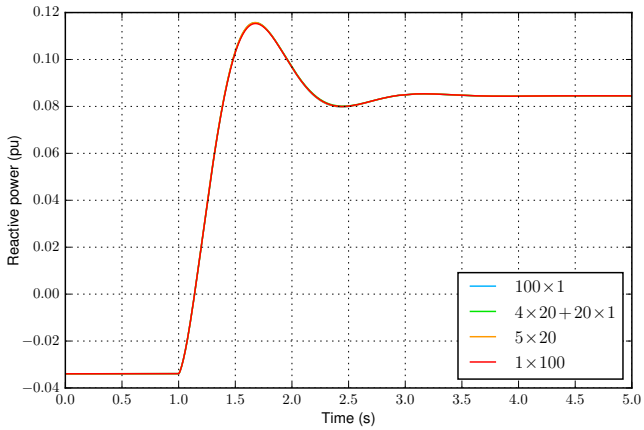


Fig. 4.13. Reactive power injected by the power plant after a voltage reference step for different models in scenario 1.

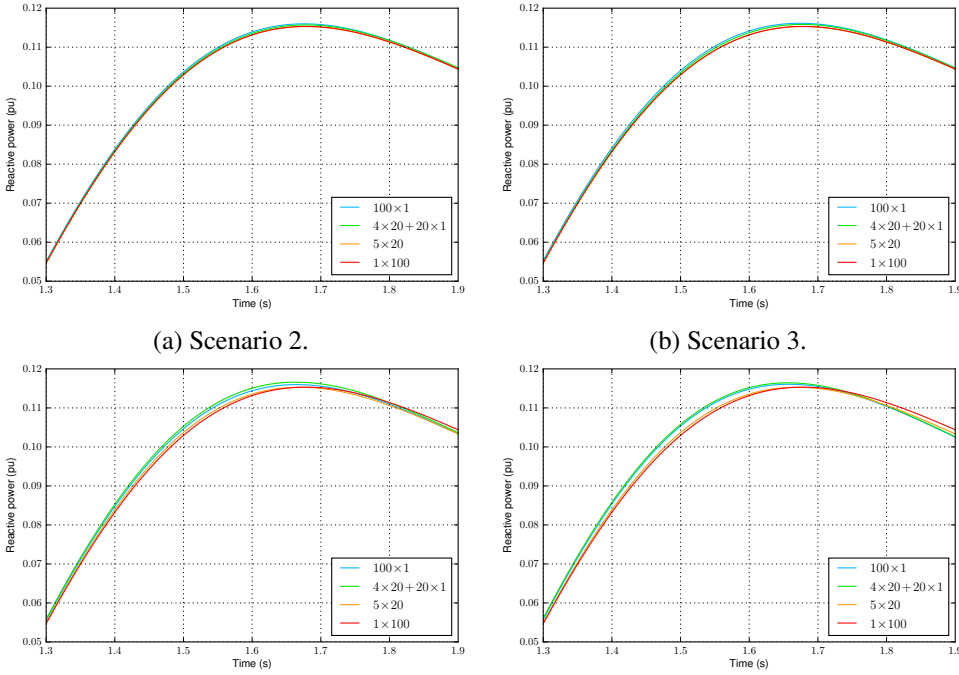


(a) Scenario 2.

(b) Scenario 3.

(c) Scenario 4.

(d) Scenario 5.

Fig. 4.14. Detail of the reactive power injected by the PV power plant after a voltage reference step for different models in different scenarios.

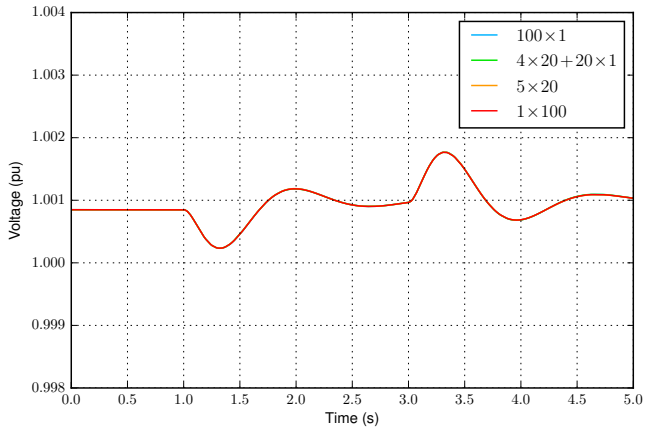


(a) Voltage.

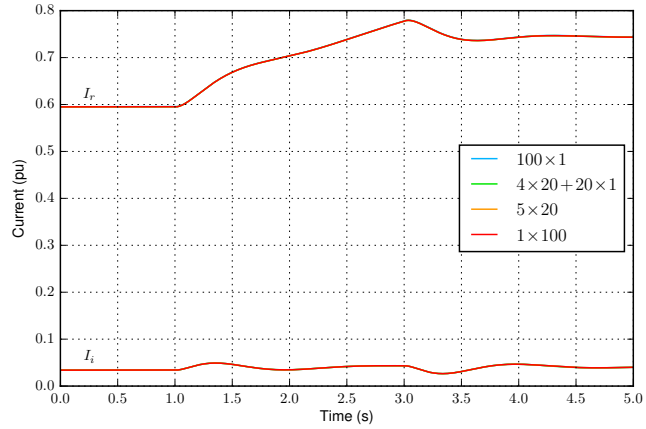


(b) Current.

Fig. 4.15. Power plant voltage and current response to a grid frequency ramp for different models in scenario 1.

the voltage at the POI. In this case, as shown in Fig. 4.15a, the amplitude of the voltage variations is below 0.1%, and the main variations occur at the start and the end of the frequency ramp.

Regarding the injected current, depicted in 4.15b, the real part of the current phasor increases, following the frequency ramp, since the plant response consists mainly of an active power variation, and the imaginary part remains approximately at the same level, with transient variations in both components which agree with

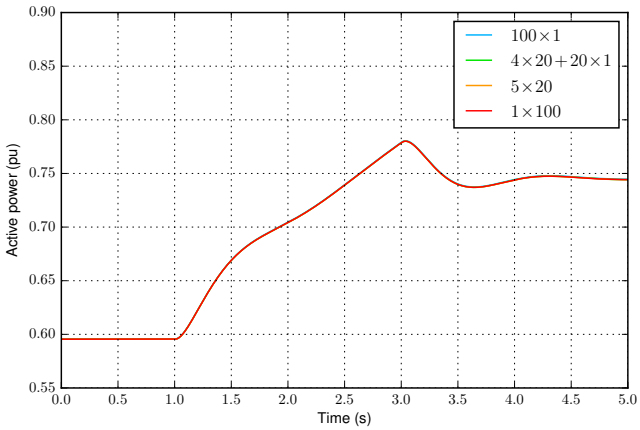


Fig. 4.16. Active power injected by the power plant after a grid frequency ramp for different models in scenario 1.

the inertial response of the SPC. Once again, the results are very similar for all the models when scenario 1 is considered.

Furthermore, Fig. 4.16 shows the evolution of the active power injected by the PV plant as a response to this disturbance, under scenario 1. The inertial response is added to the droop response, accelerating the response and contributing an extra active power injection that counters the grid frequency variation. When the ramp ends, the active power decreases to reach the steady-state value defined by the droop response. The corresponding dc voltage evolution, with a ramp decrease safely over the maximum power point voltage, is shown in Fig. 4.17, again considering the weighted average of each converter in the cases where the plant model consists of more than one converter.

The absolute error in the active power injection during this transient incurred by each model with respect to the original $100\times1$ model is summarized in Table 4.10. The errors are smaller than in the case of the active power reference step, and their maximum is below $1.3\cdot10^{-3}$. The largest errors correspond again to the two least detailed models, but only the use of different parameters seems to have a slight influence.

The maximum absolute errors, which can be compared in Fig. 4.18, occur approximately between $t = 2.7$ s and $t = 3.7$ s in all cases, which corresponds to the

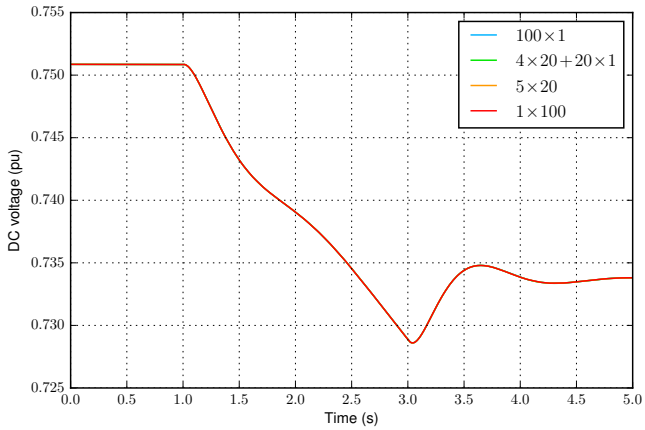


Fig. 4.17. Average dc voltage of the power plant converters after a grid frequency ramp for different models in scenario 1.

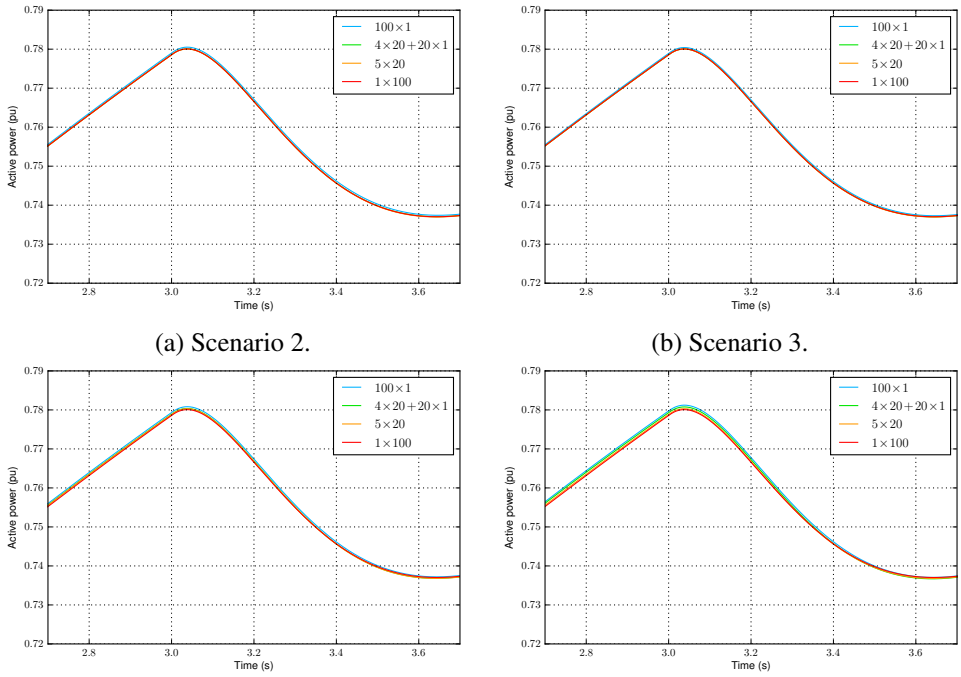


(a) Scenario 2.

(b) Scenario 3.

(c) Scenario 4.

(d) Scenario 5.

Fig. 4.18. Detail of the active power injected by the PV power plant after a grid frequency ramp for different models in different scenarios.

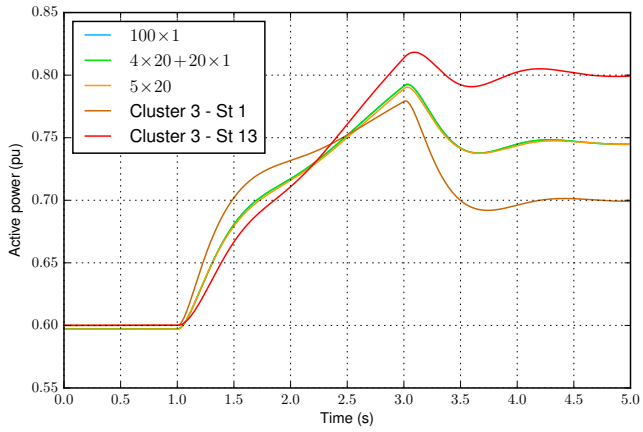


(a) Active power.

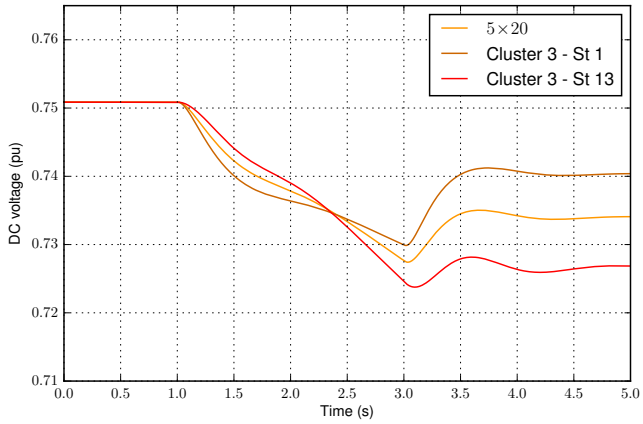


(b) DC voltage.

Fig. 4.19. Response of cluster 3 and selected units to a grid frequency ramp for different models in scenario 1.

end of the frequency ramp. In this case, the main errors take place under scenario 5, shown in Fig. 4.18b, and the aggregated models slightly underestimate the amplitude of the oscillations. This is due to the lack of detail about the different parameters employed by different converters, which give rise to different dynamics for each of them, as shown in Fig. 4.19 for cluster 3 (20 MVA base) and converters 1 and 13 of this cluster (1 MVA base). Nonetheless, the errors incurred by the aggregated models are negligible in all the scenarios.

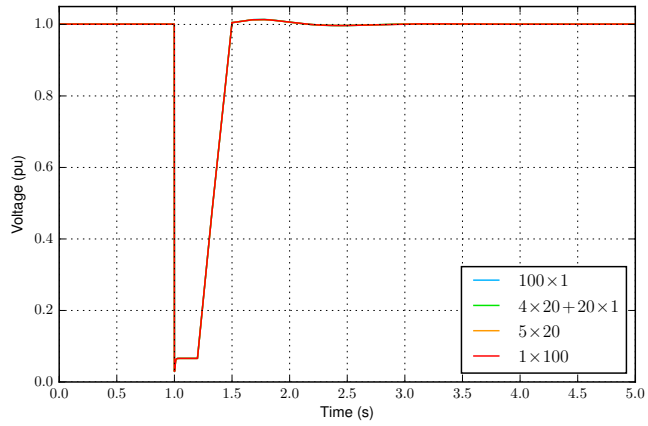


(a) Voltage.

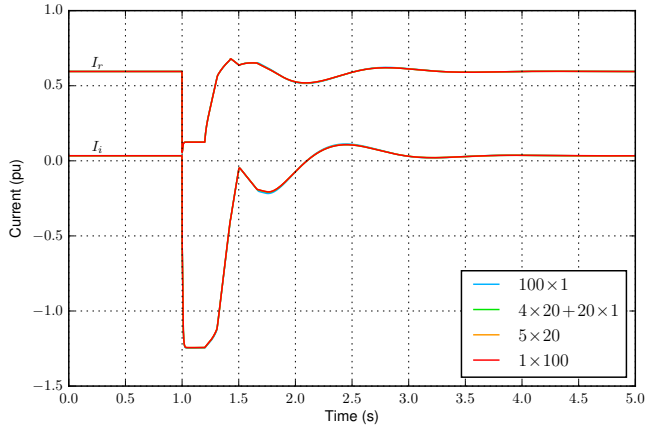


(b) Current.

Fig. 4.20. Power plant voltage and current response to a grid voltage sag for different models in scenario 1.

#### 4.6.2.4 Response to a grid voltage sag

Finally, the PV plant response to a fault is studied. The event is a grid voltage sag; in the simulation, it is induced by the voltage source representing the grid, whose voltage decreases from 1 p.u. to 0 p.u. at $t = 1$ s, remains at 0 p.u. for 0.2 s, and recovers linearly its original value in 0.3 s.

The large disturbance at the POI can be seen in Fig. 4.20 for scenario 1. The voltage at the POI drops suddenly, and is slightly greater than 0 for the first 0.2 s;

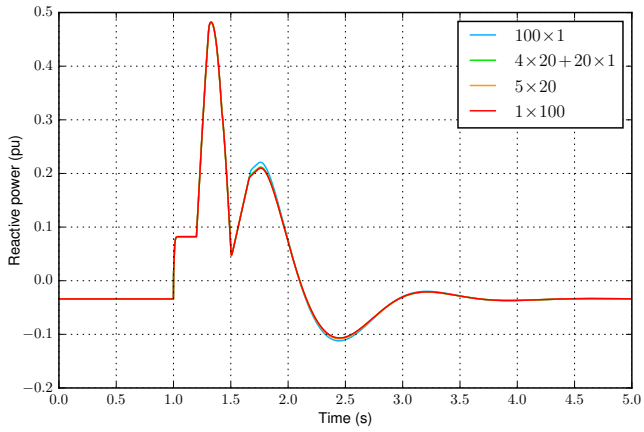


Fig. 4.21. Reactive power injected by the power plant after a grid voltage sag for different models in scenario 1.

afterwards, it recovers linearly, and slightly oscillates around 1 p.u. when the grid voltage reaches this value. This has a corresponding response by the PV plant current. Its real part decreases, proportionally to the voltage, and its imaginary part increases until it reaches the maximum value the converters are allowed to inject during a transient. When the voltage starts to recover, both current components tend linearly to their original value, but the grid voltage trend variation when it reaches 1 p.u causes some oscillations. These oscillations, which are nonetheless well damped, match the expected behavior of a rotating machine.

On the other hand, despite the large current magnitude during the first part of the sag, the reactive power injected by the plant is limited by the low voltage, as shown in Fig. 4.21. Once the voltage starts to recover, the reactive power injection is able to increase, until it reaches a maximum, since the voltage recovery reduces the need for reactive power. When the voltage is back at 1 p.u., the oscillations seen in the current are translated also into reactive power. In general, the errors among models are very limited, but there is a visible difference in the peaks of the reactive power oscillations following the end of the sag, where model 100 $\times$ 1 gives slightly different results than the aggregated models.

The maximum absolute error incurred by each model with respect to the 100$\times$ 1 reference model, when the reactive power of the PV plant is concerned, is given in

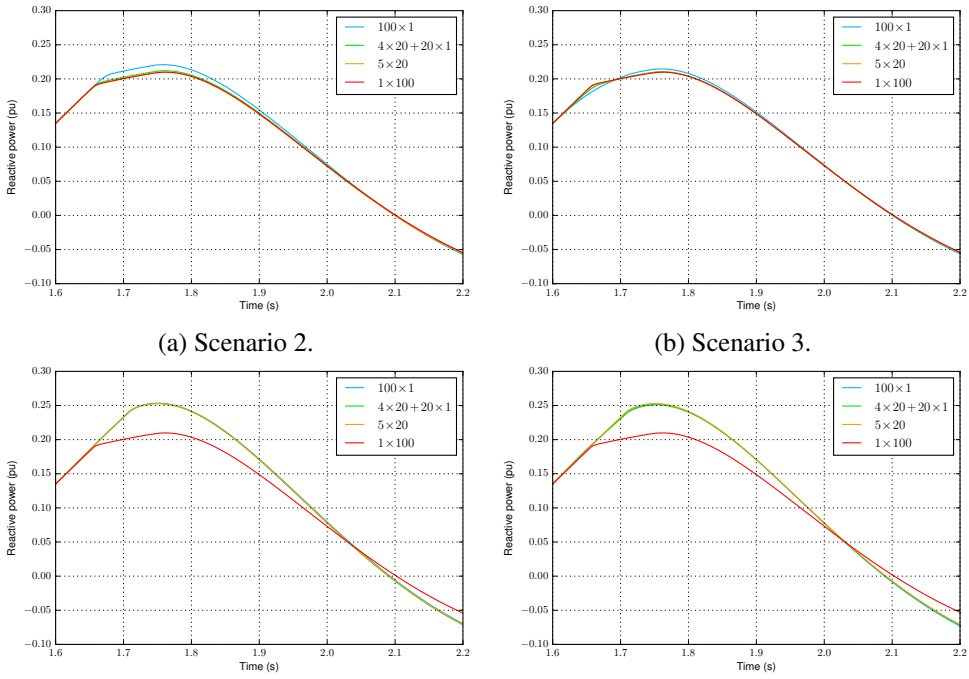


(a) Scenario 2.

(b) Scenario 3.

(c) Scenario 4.

(d) Scenario 5.

Fig. 4.22. Detail of the reactive power injected by the PV power plant after a grid voltage sag for different models in different scenarios.

Table 4.11 for all scenarios. In this case, errors are in most cases around 1%, which would be acceptable, but there are three values that are significantly above this figure. These correspond to the scenarios where different parameters are employed, and affect the simplest two models, especially the $1 \times 100$ model. Therefore, these two models are not the best option for analyses considering voltage sags if the parameters describing the behavior of the converters in the plant vary among devices. Otherwise, if all the converters in the plant employ similar parameters, these two models can still be of great value, giving rise to acceptable errors. The differences among models, in the period between $t = 1.6$ s and $t = 2.2$ s where the largest errors take place, can be seen in Fig. 4.22 for scenarios 2 to 5.

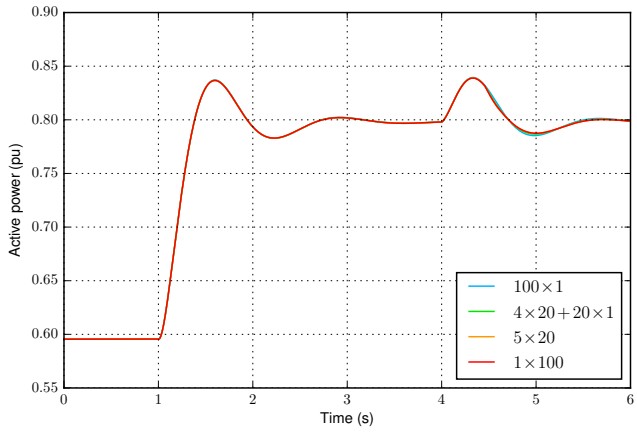


(a) Active power.

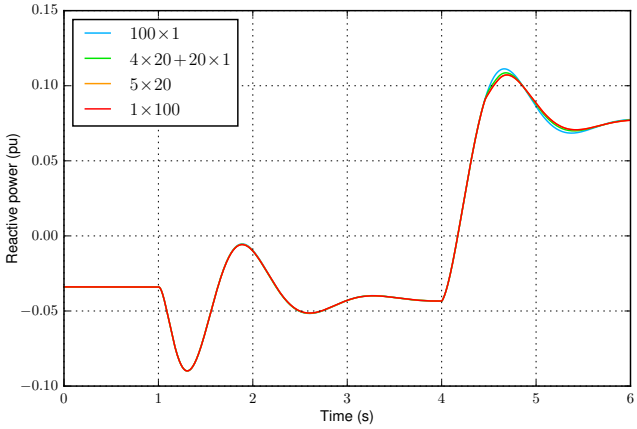


(b) Reactive power.

Fig. 4.23. Response of the power plant to an active power reference step followed by a voltage reference step in the tests executed to measure the computation time of different models.

### 4.6.3 Computation time

The ability of the equivalent model to reduce the computation time is analyzed by measuring the time employed by each model to simulate a 6 s period where two events are included. The first one is an active power reference step at $t = 1$ s, and the second is a voltage reference step at $t = 4$ s. The response of the plant during this simulation is shown in Fig. 4.23.

In order to obtain an accurate measurement of the time needed to initialize the model and run the simulation, these processes are run from a Python script that measures the time before and after each process up to a precision of microseconds. For each model, ten measurements are taken in the same CPU and RAM loading conditions, and their average is calculated. The results are summarized in Table 4.12.

Table 4.12 shows an important reduction of the total simulation time with the reduction in the number of stations. Namely, the $4\times20+20\times1$ model is able to reduce the computation time of model $100\times1$ to less than one half, with the $5\times20$ model reducing it further below one tenth of its original value. The reduction of time achieved with the fully aggregated model is around a factor of 27. Despite the total time is mainly due to the simulation, the time taken by the initialization process also has an interesting behavior, with a significant decrease from the original $100\times1$ model to the $4\times20+20\times1$ model that is not so evident for further reductions in the size of the model.

The fact that both the initialization and simulation times are reduced when the complexity of the model decreases, but not in the same proportion as the number of stations of each model, can be explained by the presence of additional elements, like the central controller, and how the simulation is handled by the software, with processes that are independent of the complexity of the model, such as writing messages to the output window.

Taking into account the results presented in this section, an equivalent model proves to be a very useful tool to reduce the simulation time without incurring in significant errors. Moreover, the results show that, in case of having different groups of converters working in different conditions, a model considering several groups, like the $5\times20$ model, can be a good tradeoff solution for accuracy and time reduction. Taking that into account, the detailed models considering the behavior of individual units can be used for analyses with the main objective of studying the internal dynamics of the plant, applying the aggregated models to the analysis of the interaction between the plant and the power system.

Table 4.6. Equivalent plant model validation. Station active power references, in megawatts.

| Station | Cluster 1 | Cluster 2 | Cluster 3 | Cluster 4 | Cluster 5 |
|---|---|---|---|---|---|
| 1 | 0.64 | 0.72 | 0.81 | 0.53 | 0.64 |
| 2 | 0.54 | 0.64 | 0.78 | 0.77 | 0.49 |
| 3 | 0.57 | 0.50 | 0.52 | 0.39 | 0.38 |
| 4 | 0.73 | 0.67 | 0.63 | 0.77 | 0.45 |
| 5 | 0.67 | 0.70 | 0.41 | 0.63 | 0.69 |
| 6 | 0.74 | 0.61 | 0.52 | 0.58 | 0.59 |
| 7 | 0.64 | 0.61 | 0.69 | 0.72 | 0.50 |
| 8 | 0.48 | 0.68 | 0.37 | 0.44 | 0.71 |
| 9 | 0.74 | 0.60 | 0.56 | 0.23 | 0.48 |
| 10 | 0.65 | 0.66 | 0.71 | 0.58 | 0.73 |
| 11 | 0.57 | 0.59 | 0.68 | 0.62 | 0.51 |
| 12 | 0.21 | 0.41 | 0.56 | 0.72 | 0.56 |
| 13 | 0.33 | 0.45 | 0.39 | 0.66 | 0.71 |
| 14 | 0.66 | 0.62 | 0.54 | 0.65 | 0.28 |
| 15 | 0.68 | 0.67 | 0.80 | 0.74 | 0.64 |
| 16 | 0.62 | 0.55 | 0.41 | 0.63 | 0.61 |
| 17 | 0.52 | 0.61 | 0.64 | 0.75 | 0.73 |
| 18 | 0.56 | 0.69 | 0.82 | 0.66 | 0.50 |
| 19 | 0.56 | | 0.45 | 0.62 | 0.67 |
| 20 | 0.49 | | 0.71 | 0.75 | 0.72 |
| 21 | | | | | 0.73 |
| 22 | | | | | 0.66 |
| Total | 11.60 | 10.98 | 12.00 | 12.44 | 12.98 |
| Average | 0.580 | 0.610 | 0.600 | 0.622 | 0.59 |

Table 4.7. Equivalent plant model validation. Controller parameters of each group of devices.

| Group | $H$ (s) | $X$ (p.u.) | $1/R_f$ (p.u.) |
|---|---|---|---|
| Cluster 1 | 5 | 0.3000 | 20 |
| Cluster 2 | 2.5 | 0.6000 | 10 |
| Cluster 3a | 8 | 0.1875 | 10 |
| Cluster 3b | 2 | 0.7500 | 20 |
| Cluster 3 | 5 | 0.3000 | 15 |
| Cluster 4 | 5 | 0.3000 | 10 |
| Cluster 5 | 2.5 | 0.6000 | 20 |
| Plant | 4 | 0.3750 | 15.2 |

Table 4.8. Maximum active power error for an active power reference step, in per unit, with respect to model $100\times1$.

| Scenario | $4\times20+20\times1$ | $5\times20$ | $1\times100$ |
|---|---|---|---|
| 1 | $3.705\cdot10^{-4}$ | $4.090\cdot10^{-4}$ | $4.465\cdot10^{-4}$ |
| 2 | $3.614\cdot10^{-4}$ | $4.285\cdot10^{-4}$ | $5.199\cdot10^{-4}$ |
| 3 | $2.732\cdot10^{-3}$ | $7.278\cdot10^{-3}$ | $7.208\cdot10^{-3}$ |
| 4 | $3.640\cdot10^{-4}$ | $5.971\cdot10^{-4}$ | $3.666\cdot10^{-3}$ |
| 5 | $4.441\cdot10^{-4}$ | $2.875\cdot10^{-3}$ | $6.328\cdot10^{-3}$ |

Table 4.9. Maximum reactive power error for a voltage reference step, in per unit, with respect to model $100\times1$.

| Scenario | $4\times20+20\times1$ | $5\times20$ | $1\times100$ |
|---|---|---|---|
| 1 | $4.328\cdot10^{-4}$ | $2.863\cdot10^{-4}$ | $4.436\cdot10^{-4}$ |
| 2 | $5.237\cdot10^{-4}$ | $7.497\cdot10^{-4}$ | $7.644\cdot10^{-4}$ |
| 3 | $5.840\cdot10^{-4}$ | $1.084\cdot10^{-3}$ | $1.079\cdot10^{-3}$ |
| 4 | $6.629\cdot10^{-4}$ | $9.735\cdot10^{-4}$ | $1.720\cdot10^{-3}$ |
| 5 | $4.381\cdot10^{-4}$ | $1.680\cdot10^{-3}$ | $2.435\cdot10^{-3}$ |

Table 4.10. Maximum active power error for a grid frequency ramp, in per unit, with respect to model 100×1.

| Scenario | 4×20 + 20×1 | 5×20 | 1×100 |
|---|---|---|---|
| 1 | $5.201 \cdot 10^{-4}$ | $5.851 \cdot 10^{-4}$ | $5.379 \cdot 10^{-4}$ |
| 2 | $5.273 \cdot 10^{-4}$ | $6.133 \cdot 10^{-4}$ | $5.586 \cdot 10^{-4}$ |
| 3 | $4.287 \cdot 10^{-4}$ | $4.953 \cdot 10^{-4}$ | $4.426 \cdot 10^{-4}$ |
| 4 | $5.312 \cdot 10^{-4}$ | $6.122 \cdot 10^{-4}$ | $8.220 \cdot 10^{-4}$ |
| 5 | $5.345 \cdot 10^{-4}$ | $1.005 \cdot 10^{-3}$ | $1.259 \cdot 10^{-3}$ |

Table 4.11. Maximum reactive power error for a grid voltage sag, in per unit, with respect to model 100×1.

| Scenario | 4×20 + 20×1 | 5×20 | 1×100 |
|---|---|---|---|
| 1 | $9.306 \cdot 10^{-3}$ | $1.144 \cdot 10^{-2}$ | $1.133 \cdot 10^{-2}$ |
| 2 | $9.316 \cdot 10^{-3}$ | $1.146 \cdot 10^{-2}$ | $1.143 \cdot 10^{-2}$ |
| 3 | $5.160 \cdot 10^{-3}$ | $7.995 \cdot 10^{-3}$ | $8.997 \cdot 10^{-3}$ |
| 4 | $1.835 \cdot 10^{-3}$ | $1.907 \cdot 10^{-3}$ | $4.756 \cdot 10^{-2}$ |
| 5 | $2.379 \cdot 10^{-3}$ | $2.309 \cdot 10^{-2}$ | $6.595 \cdot 10^{-2}$ |

Table 4.12. Average computation time with different models, in seconds.

| Model | Initialization | Simulation | Total |
|---|---|---|---|
| 100×1 | 1.648 | 83.384 | 85.032 |
| 4×20 + 20×1 | 0.483 | 36.344 | 36.827 |
| 5×20 | 0.232 | 6.780 | 7.012 |
| 1×100 | 0.173 | 3.013 | 3.186 |

Chapter
5.

# Analysis of the 12-bus system under increasing PV penetration scenarios

*The impact of PV power plants with synchronous power controllers on a 12-bus test power system is analyzed in this chapter. Different PV penetration scenarios are defined, considering a base case without PV, a low penetration case with a 10% share of this type of generators, a case with a 30% penetration level, and a prospective scenario where have of the load is supplied by photovoltaic plants. The analysis addresses both the small-signal effects on the response of the power system, and the impact on the frequency stability when large generators or loads are disconnected. The work presented here is based on the paper* D. Remon, A. M. Cantarellas, J. M. Mauricio, P. Rodriguez, "Power system stability analysis under increasing penetration of photovoltaic power plants with synchronous power controllers," *IET Renewable Power Generation*, vol. 11, no. 6, pp. 733–741, May 2017.

## 5.1 PV power plant model

The PV power plants considered in this study are formed by 100 power conversion units of 1.1 MVA each, and are modeled following Chapter 4. In particular, the

equivalent $1 \times 100$ model is employed. Taking into account the power and current ratings of the original power plant converters, the equivalent aggregated converter at the plant level has a steady-state apparent power limit of 110 MVA, and a transient current limit corresponding to 125 MVA at the rated voltage. This equivalent converter inherits the control of the original power plant converters, based on the SPC, and a central plant controller handles the references and measurements at the POI of the power plant.

### 5.1.1 Converter controller and model

Both the SPC and the conventional controller described in Sections 4.3.3.2 and 4.3.3.3 are used in this analysis. However, since the analysis focuses on short-term phenomena that do not involve radiation variations, the dynamics of the PV arrays and dc link are not considered in the model [148]. Instead, an active power reference limiter is included to avoid unrealistic active power injections for a PV system.

### 5.1.2 Power plant controller

The central plant controller generates the active and reactive power references to be followed by the equivalent converter and measures the frequency and voltage at the POI. The frequency measurement is obtained from a conventional PLL [149] connected at the POI, and filtered to remove high-frequency oscillations that are not of interest for primary frequency regulation.

In the tests presented here, the active power reference is kept constant and equal to 100 MW, whereas the frequency measurement is sent to the equivalent converter controller to be used only by the frequency droop controller. On the other hand, the voltage is controlled at the plant level through a proportional controller, and the converter voltage droop is disabled.

## 5.2 Test power system and scenarios

The analysis of the impact of these PV plants is carried out on a 12-bus test power system [150]. The system is adapted following [151], where typical generator, exciter, and governor models are selected to define a benchmark for renewable energy

Table 5.1. Power system stabilizer parameters.

| Parameter | Symbol | Value |
|---|---|---|
| Stabilizer gain | $K$ | 2 p.u. |
| Washout time constant | $T$ | 10 s |
| Lead-lag zero time constant | $T_1$ | 0.8895 s |
| Lead-lag pole time constant | $T_2$ | 0.03 s |
| Output limit | $H_{lim}$ | 0.2 p.u. |

integration. This is a 230 kV, 60 Hz grid, where the generating units and their control systems are characterized by inertia constants in the range 3.2 s – 4.8 s, high-transient-gain excitation systems performing a proportional control of the voltage at the generator terminals, and a common frequency droop slope of 5%; whereas the dynamic model of the loads is a constant impedance model. In addition, the control systems of generators 3 and 4 are completed with Power System Stabilizers (PSS) using a simple model [29], defined by the parameters given in Table 5.1.

To analyze the impact of the PV plants depending on the total share of solar generation in the power system, four different solar scenarios are defined by gradually increasing the load and the number of PV plants connected to the system:

1. 0% PV scenario: Base case with four conventional generators and a total demand of 1450 MW.

2. 10% PV scenario: Both generation and demand increase by 200 MW with the connection of PV plants 1 and 2 at bus 5.

3. 30% PV scenario: The demand remains the same as in the 10% scenario but the share of PV increases another 400 MW after the connection of PV plant 3 at bus 5, PV plant 4 at bus 3 and PV plants 5 and 6 at bus 4.

4. 50% PV scenario: The demand increases by 200 MW and PV plants 7, 8 and 9 are installed at buses 3, 7 and 6, respectively.

The resulting single-line diagram of the 12-bus system, indicating the location of the PV plants, is shown in Fig. 5.1. These four scenarios are defined taking into account

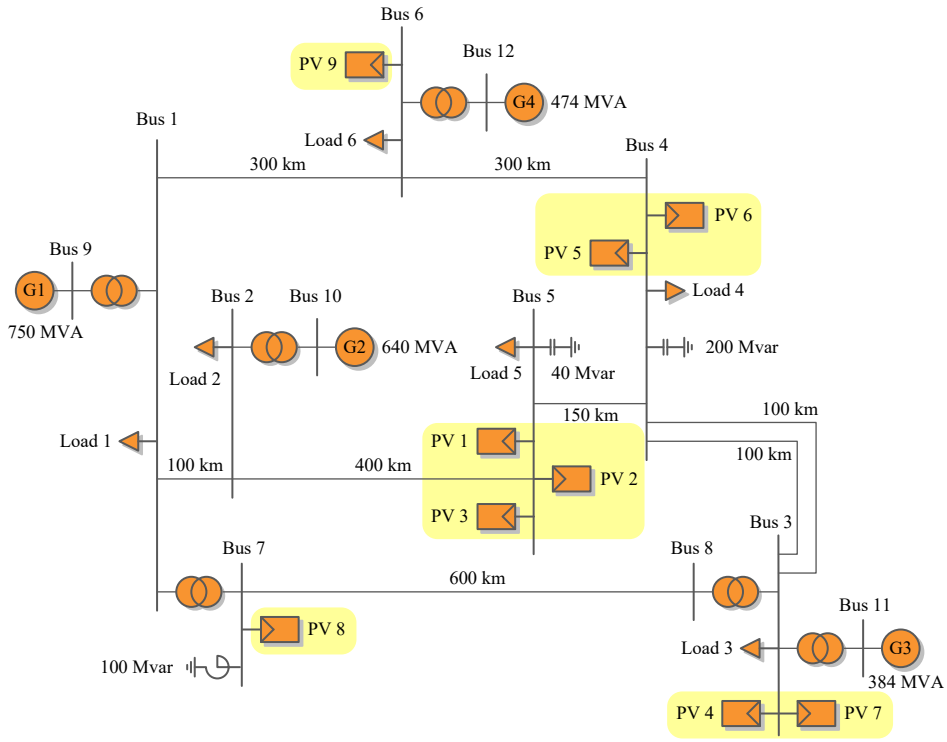


Fig. 5.1. 12-bus system diagram showing the location of the PV power plants.

the evolution of power systems, with increasing renewable penetration, and can be considered respectively as a traditional power system totally based on conventional generators (case 1), a currently realistic case of PV penetration in some power systems (case 2), a prospective case in the near future with a 30% PV penetration level during certain hours of the day (case 3), and a futuristic scenario beyond the usual renewable penetration limits (case 4).

In all the scenarios, generator 1 compensates the active power mismatch due to the losses in the system and the synchronous generators control the voltage at their terminals, i.e., at buses 9 to 12. The PV plants, on the other hand, control the voltage at their POI, sharing the reactive power reference evenly when several plants are connected at the same bus. The operating points of generators and loads that define the initial state of the system are summarized in Table 5.2, employing a base power of 100 MVA.

Table 5.2. Operation scenario definition for different PV penetration levels, in per unit.

| Element | Variable | 0% | 10% | 30% | 50% |
|---|---|---|---|---|---|
| G1 | P | 4.77 | 4.47 | 1.72 | 3.32 |
| | V | 1.00 | 1.00 | 1.00 | 1.00 |
| G2 | P | 4.00 | 4.10 | 3.57 | 2.55 |
| | V | 1.01 | 1.01 | 1.01 | 1.01 |
| G3 | P | 2.70 | 2.77 | 2.41 | 1.72 |
| | V | 1.01 | 1.01 | 1.01 | 1.01 |
| G4 | P | 3.30 | 3.38 | 2.95 | 2.11 |
| | V | 1.01 | 1.01 | 1.01 | 1.01 |
| Load 1 | P | 3.00 | 3.41 | 3.41 | 3.83 |
| | Q | 1.86 | 2.12 | 2.12 | 2.37 |
| Load 2 | P | 2.50 | 2.84 | 2.84 | 3.19 |
| | Q | 1.21 | 1.38 | 1.38 | 1.54 |
| Load 3 | P | 3.50 | 3.98 | 3.98 | 4.47 |
| | Q | 1.15 | 1.31 | 1.31 | 1.47 |
| Load 4 | P | 3.00 | 3.41 | 3.41 | 3.83 |
| | Q | 1.86 | 2.12 | 2.12 | 2.37 |
| Load 5 | P | 1.00 | 1.14 | 1.14 | 1.28 |
| | Q | 0.48 | 0.55 | 0.55 | 0.61 |
| Load 6 | P | 1.50 | 1.71 | 1.71 | 1.91 |
| | Q | 0.49 | 0.56 | 0.56 | 0.63 |

For each of the scenarios including PV, two different cases are considered in order to assess the real impact of power plants using synchronous power controllers. In the first case, the PV plants are controlled following a conventional strategy that includes controlling the voltage at the POI and contributing to frequency regulation through the frequency droop, but the converter controller is based on vector oriented control using the IPT. In the RMS model, this means that the current reference is obtained from the division of the reference apparent power and the terminal

voltage phasors. The second case considers the PV plant model with the SPC. For simplicity, the parameters that define the behavior of the PV plants are given equal values for all the plants and scenarios. The main parameters are an inertia constant $H = 5$ s, counteracting the loss of inertia due to the connection of renewables with a slightly higher inertia constant than the synchronous machines in the system; an active power closed-loop damping ratio $\zeta = 0.7$, which provides additional damping for the power system response; a virtual reactance $X = 0.3$ p.u., allowing a close interaction between the SPC and the grid; and a frequency droop slope of 5%, so the PV plants contribute to frequency regulation in the same proportion as the synchronous generators.

## 5.3 Small-signal analysis

The amount and location of the PV plants connected to the power system and the type of controller employed by these plants have an impact on the modes that describe the system dynamics, and could affect the damping of the oscillations that occur in the system.

### 5.3.1 Base case

The results of the analysis show that three modes can be identified as critical, with a damping ratio between 5% and 10% for most of the scenarios defined in Section 5.2; whereas the other modes have damping ratios over 20% and can be considered well damped. The eigenvalue plot in Fig. 5.2 and the data summarized in Table 5.3 allow studying the evolution of the critical modes under these scenarios. In general, increasing the number of PV plants in the system, and therefore the total frequency and voltage regulation capability, is beneficial for the system and results in a larger damping of the critical modes.

Furthermore, the least damped mode, referred to as mode 1 in Table 5.3, shows a special sensibility to the type of PV controller. This mode corresponds to the inter-area oscillations between generators 1 and 3, as can be concluded from Fig. 5.2b, which shows the contribution of each synchronous generator to this mode. Taking into account the participating machines, it is reasonable that PV plants connected at

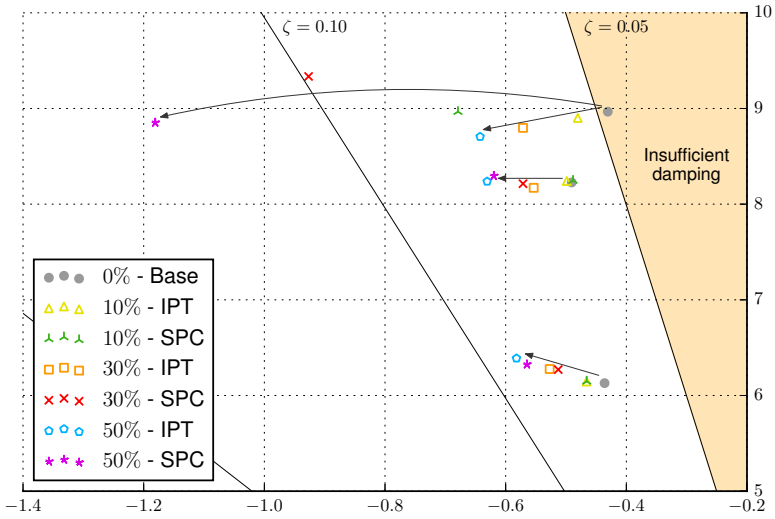


(a) Eigenvalue plot for different scenarios.

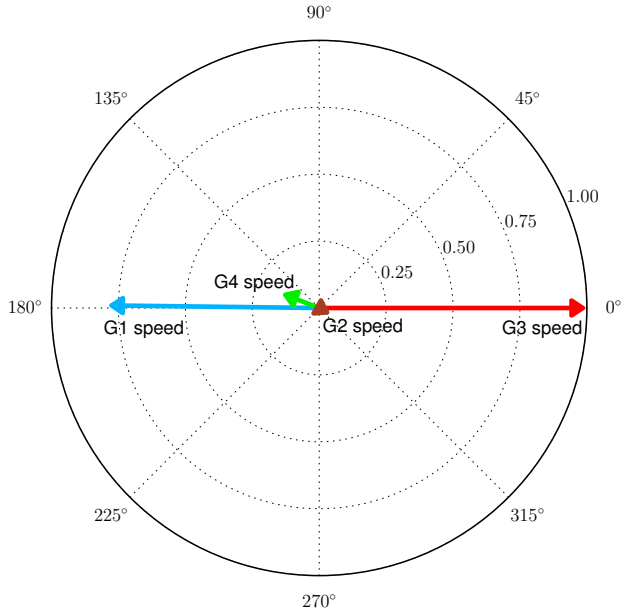


(b) Controllability of mode 1 in the 0% PV scenario.

Fig. 5.2. 12-bus system critical eigenvalues.

Table 5.3. 12-bus system critical eigenvalues and damping ratio for different scenarios.

| Scenario | Mode 1 | Mode 2 | Mode 3 |
|---|---|---|---|
| 0% | $-0.4307 \pm 8.9666j$<br>4.80% | $-0.4905 \pm 8.2269j$<br>5.95% | $-0.4360 \pm 6.1293j$<br>7.10% |
| 10% - IPT | $-0.4805 \pm 8.9011j$<br>5.39% | $-0.4988 \pm 8.2419j$<br>6.04% | $-0.4659 \pm 6.1460j$<br>7.56% |
| 10% - SPC | $-0.6791 \pm 8.9665j$<br>7.55% | $-0.4884 \pm 8.2466j$<br>5.91% | $-0.4657 \pm 6.1481j$<br>7.55% |
| 30% - IPT | $-0.5713 \pm 8.7976j$<br>6.48% | $-0.5536 \pm 8.1709j$<br>6.76% | $-0.5271 \pm 6.2766j$<br>8.37% |
| 30% - SPC | $-0.9268 \pm 9.3348j$<br>9.88% | $-0.5714 \pm 8.2136j$<br>6.94% | $-0.5130 \pm 6.2707j$<br>8.15% |
| 50% - IPT | $-0.6424 \pm 8.7054j$<br>7.36% | $-0.6307 \pm 8.2373j$<br>7.63% | $-0.5821 \pm 6.3885j$<br>9.07% |
| 50% - SPC | $-1.1809 \pm 8.8526j$<br>13.22% | $-0.6197 \pm 8.2964j$<br>7.45% | $-0.5648 \pm 6.3252j$<br>8.89% |

buses 3, 4, and 5, which are near generator 3, have an important impact on this mode. In particular, its damping ratio improves significantly when the SPC is employed, reaching values of 9.88% and 13.22% for the 30% and 50% penetration scenarios, respectively; whereas it remains close to 7% when the IPT controller is used. On the other hand, the controller does not have an important effect on the other two critical modes.

Considering the least damped mode for each penetration level from Table 5.3, it can be concluded that the SPC makes possible to increase the minimum damping ratio of the modes in the system. This is mainly due to its effect on mode 1, that does not require an equivalent reduction of the damping of the other critical modes.

The impact on the system modes can also be seen in its time-domain response to a small disturbance. In this case, Fig. 5.3 shows the response of the system to a step

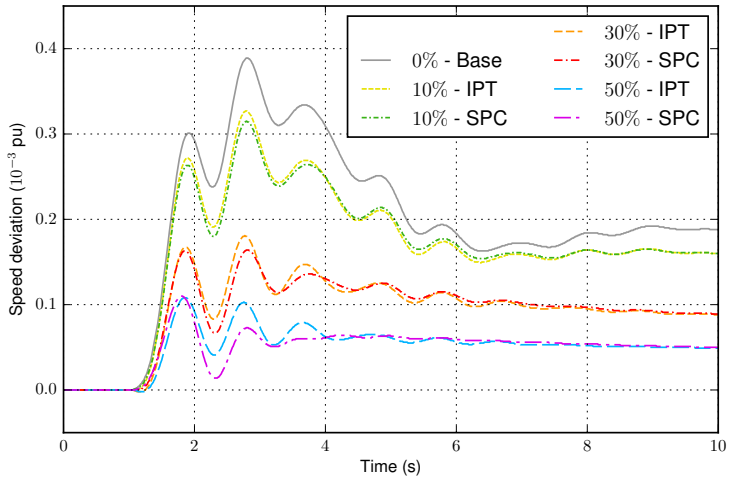


(a) Generator 2 speed deviation.

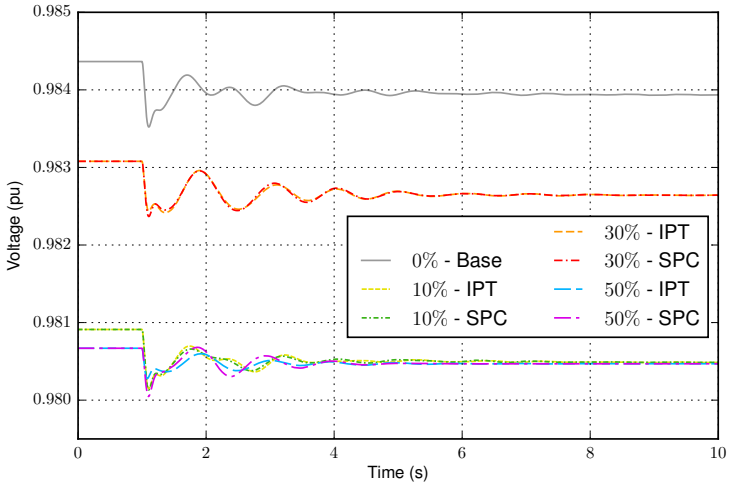


(b) Bus 1 voltage.

Fig. 5.3. 12-bus system response to a step in the voltage reference of generator 4.

variation in the voltage reference of generator 4, which is reduced from 1.01 p.u. to 1.00 p.u. at t = 1 s.

The system frequency is represented in Fig. 5.3a by the speed deviation of generator 2, which is one of the largest generators in the 12-bus system, and is connected at a central bus considering other generators and loads, as shown in Fig. 5.1.

When the voltage reference of generator 4 is decreased, the consumption in neighboring buses, which depends on the voltage, automatically decreases. This results in an excess of generation, which increases the system frequency. Due to the action of the primary frequency controllers, the average frequency is stabilized around a new value after 7 s. It is worth noting that the speed deviation is in all cases below $0.2 \cdot 10^{-3}$ p.u., which justifies the study in small-signal terms and allows focusing on the oscillatory behavior due to the excitation of different power system modes.

This makes possible to observe some differences among scenarios. First, both the maximum deviation and the settling time of the response decrease as the PV penetration increases, which agrees with the results shown about the eigenvalues of the system in Table 5.3. Regarding the type of controller, the responses are very similar for both controllers in the 10% PV scenario, whereas the SPC achieves a slight damping improvement with respect to the IPT controller for a 30% penetration level, and a more appreciable beneficial effect in the 50% case.

In Fig. 5.3b, the voltage magnitude at bus 1, which is closer to the origin of the disturbance, is shown to have a similar behavior under all scenarios, with oscillations during the first three seconds after the reference change, but within a close range around the initial value. The slight voltage variation in steady state, below $0.5 \cdot 10^{-3}$ p.u. in all the scenarios, is due to the fact that the voltage is not directly controlled at bus 1, but at generator 1 terminals, and the voltage reference variation at generator 4 affects the neighboring buses.

On the other hand, Fig. 5.4 shows the active power contribution of PV plant 1, connected at bus 5. Responding to the frequency increase, the active power injected by PV plant 1 decreases. The final active power variation is proportional to the frequency deviation and decreases when the penetration rises regardless of the type of controller. However, during the first seconds after the reference change, there are important differences depending on the PV plant controller. With the SPC, the PV plant absorbs part of the active power oscillations that the synchronous generators suffer during this event and contributes to damping them, more effectively as the number of PV plants increases.

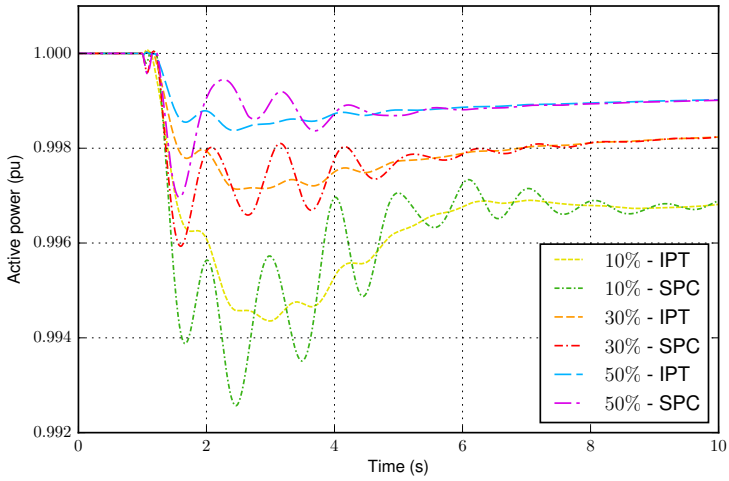


Fig. 5.4. PV plant 1 active power response to a step in the voltage reference of generator 4.

### 5.3.2 Contingencies

Large changes in the system, like the disconnection of a large generator or load, or an important line, modify the system eigenvalues, and thus its natural response to any disturbances taking place after this large disturbance. In this section, the effect of three large disturbances on the eigenvalues of the system, calculated after it reaches a new steady state, is analyzed for the different scenarios considered in this chapter.

#### 5.3.2.1 Disconnection of a generator

The eigenvalues of the 12-bus system after generator 4 is suddenly disconnected and the system reaches a new steady state are plotted in Fig. 5.5. Comparing this plot with Fig. 5.2a, the main difference is due to mode 3, which is not present in this case. This is due to the fact that generator 4 has a great participation in it, so, when it is disconnected, the mode associated to the oscillations involving this machine disappears.

Regarding the other two critical modes, similar conclusions as in the base case can be drawn. Namely, increasing the PV penetration improves the damping of the power system, and the SPC also contributes to this effect. Furthermore, in this case,

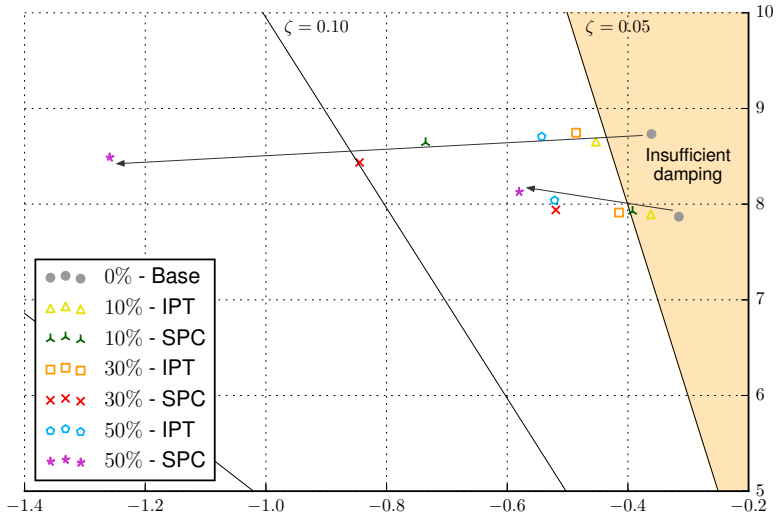


Fig. 5.5. 12-bus system eigenvalue plot after the disconnection of generator 4.

the beneficial effect of the SPC is evident, not only on mode 1, but also on mode two, whose damping is significantly increased in all three scenarios when the SPC is used, thus countering the weakness of the system because of the loss of an important generator.

#### 5.3.2.2 Disconnection of a load

The opposite contingency, the disconnection of a load, is considered here. In particular, Fig. 5.6 shows the eigenvalues of the system after the disconnection of load 4. As in the base case, there are three critical modes, whose damping improves as PV penetration grows, and the controller affects mainly mode 1.

Nevertheless, in this case the SPC is not able to improve the damping of mode 1 when the PV penetration is 10%. In the 30% and 50% penetration scenarios, the effect of the SPC is to significantly increase the damping of this mode, making it greater than 10%. Additionally, the damping of mode 3 practically doubles and reaches 20% in the 50% scenario. Therefore, the SPC proves to be an effective measure to improve the power system damping for high penetrations of PV in the system.

Furthermore, the flexibility of the SPC parameters allows correcting the unde-

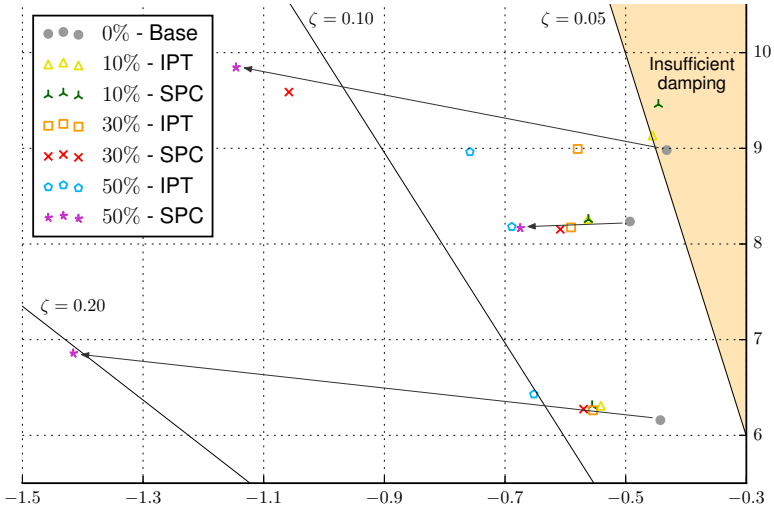


Fig. 5.6. 12-bus system eigenvalue plot after the disconnection of load 4.

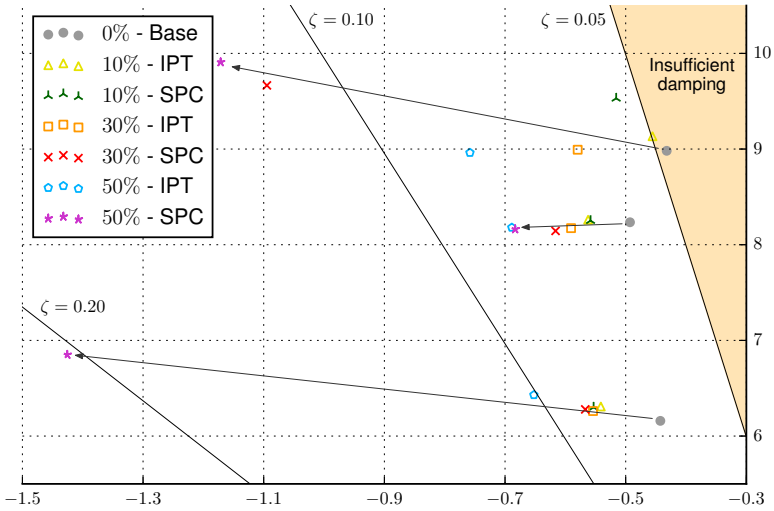


Fig. 5.7. 12-bus system eigenvalue plot after the disconnection of load 4 for an alternative tuning.

sired trend observed in the 10% scenario by considering a different tuning. For instance, it is possible to modify the inertia constant of plants PV1 and PV2, which are connected to the system in the 10% scenario, and whose controllers can have an

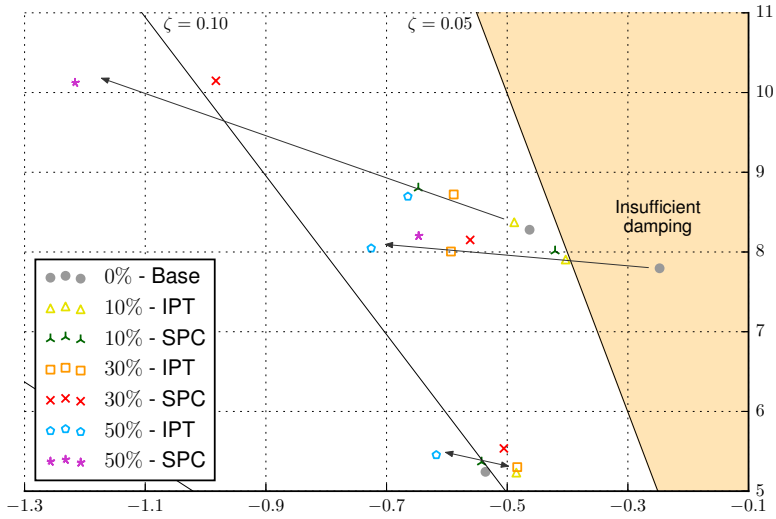


Fig. 5.8. 12-bus system eigenvalue plot after an event on line 4-6.

influence on the power system modes for that scenario. Fig. 5.7 shows the eigenvalue plot obtained when the inertia constant of these two plants is set equal to 2 s, keeping all other parameters at their original value. This change is enough to improve the damping of mode 1 for all scenarios, and achieve a better performance with the SPC than with the conventional controller. The damping of the other critical modes also increases slightly.

#### 5.3.2.3 Event on a line

Finally, the consequences of an event on line 4-6, consisting of a short-circuit fault and the disconnection of the line, are shown in Fig. 5.8. As usual, the damping of modes 1 and 2 increases as the PV penetration grows, and the SPC achieves significantly greater improvements in the damping of mode 1. In the case of mode 2, which is the least damped when this contingency is considered, the SPC achieves better damping than the IPT controller in the 10% scenario, but it is not able to match the results of the conventional controller for this mode for the scenarios with higher penetration. Nonetheless, both the damping of the least damped mode, and the sum of damping ratios of the critical modes in the 30% and 50% PV penetration scenarios are better when the SPC is employed, because of the relatively weak effect

of the conventional controller on mode 1.

Mode 3, which is well damped for this contingency under all the scenarios considered, exhibits an unusual behavior, with its damping decreasing for scenarios considering 10% and 30% PV penetration, increasing for the 50% scenario when the IPT controller is employed, and not appearing for this last scenario when the PV plants use the SPC. To this respect, it is worth noting that the 50% scenario involves connecting a PV plant at bus 6, one of the endpoints of the line suffering the contingency.

## 5.4 Frequency stability analysis

This analysis will focus on the first few seconds after a large disturbance that alters the active power balance in the system, like the disconnection of a generator or a load, and will not address long-term effects. Therefore, the dynamics of interest are those of machines and their primary regulators, and a secondary controller that would modify the active power references of the generators in order to ensure that the frequency returns back to its nominal value is not considered.

### 5.4.1 Disconnection of a generator

The first event studied in this analysis is the disconnection of generator 4 at $t = 1\,\mathrm{s}$. Depending on the scenario, this machine generates between 11% and 22% of the total active power in the 12-bus system and its disconnection causes a severe imbalance in the system before it reaches a new steady state, as can be seen in Figs. 5.9 and 5.10.

The speed of generator 2, which is used as a measurement of the system frequency, is shown in Fig. 5.9a. For a low penetration level of 10%, the presence of PV results in a deeper frequency fall than in the original case, and the speed of the response is approximately the same. However, in the 30% scenarios, although the maximum deviation is similar to the previous cases, the recovery is faster and the response is better damped. Finally, for a 50% penetration, the frequency deviation and the amplitude of the oscillations are reduced significantly as compared to the previous cases. As obtained from the eigenvalue analysis, the use of the SPC results

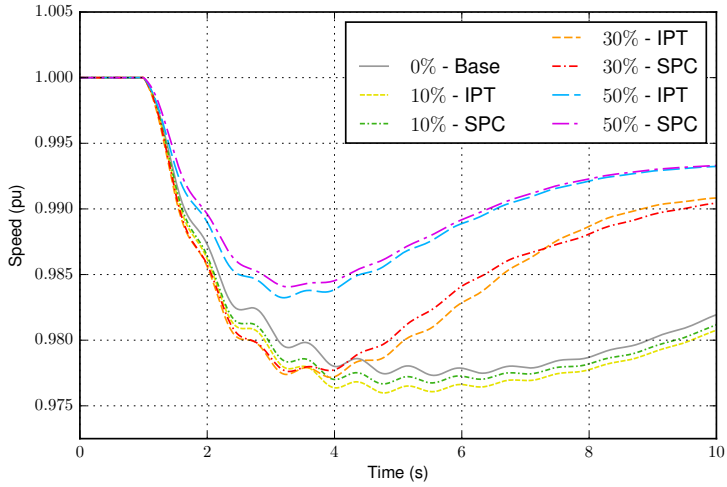


(a) Generator 2 speed.

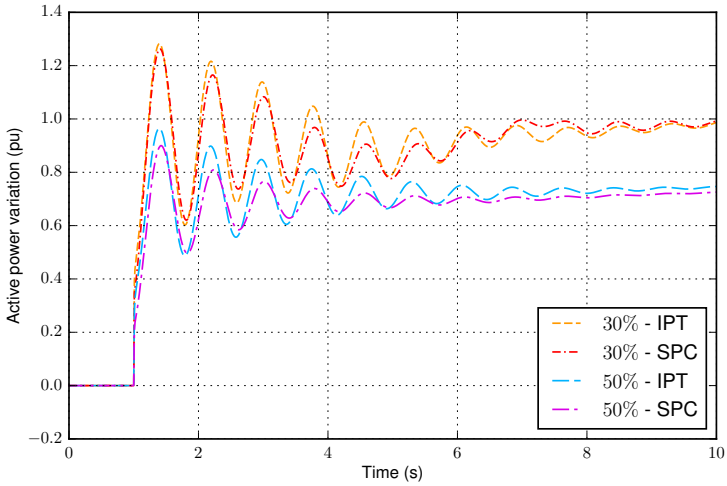


(b) Generator 2 active power variation.

Fig. 5.9. 12-bus system response to the disconnection of generator 4.

in a better damping of the response for the 30% and 50% scenarios and, in the last case, also reduces the maximum frequency deviation.

All the generating units connected to the system react to this event to a greater or lesser extent. Fig. 5.9b shows the active power response of generator 2 for the 30% and 50% penetration cases. For these scenarios, the effect of the SPC on the

damping of the oscillations is clearly beneficial and the stress of the synchronous machines is reduced. In this particular case, the amplitude of the oscillations in the active power generated by generator 2 after its first swing decreases by 0.05 p.u. to 0.10 p.u. when the SPC is employed, achieving relative amplitude reductions over 30% in the 50% penetration scenario.

On the other hand, Fig. 5.10a allows comparing the response of PV plant 1 in the different scenarios with PV. In all cases, the PV injection is around 1 p.u., but its behavior depends on the type of controller used. With the controller based on IPT, the plant output power is almost constant before and after the event. However, when the SPC is employed, it naturally oscillates to counteract the frequency oscillations in the system. The amplitude and duration of the oscillations is larger when there are fewer PV plants connected to the system, as also happens in the case of the frequency.

These oscillations, which overload the PV plant, have a reduced amplitude and the maximum overload is around 2% for a few tenths of a second in the worst case. A power converter can safely withstand such an overload and the necessary active power can be extracted from the PV system as long as it is operating with a narrow reserve margin, or from a small, short-term storage device.

The energy extracted from the PV equivalent converter after the disconnection of generator 4, expressed in time units considering the system base power, is shown in Fig. 5.10b for the scenarios where the SPC is employed. The energy variation depends on the system inertia and the parameters defining the SPC, and, for this severe event, the total amount of energy delivered by the plant is below 10 ms. As in the case of the oscillations, the amplitude of the energy variation decreases as the number of PV plants connected to the system increases. Taking into account the little amount of energy involved, the necessary storage can be integrated in each converter through a proper design of its dc bus capacitance.

Therefore, there is a tradeoff where oversizing the power plant PV field or the dc capacitance of the power converters results in an appreciable reduction of the torque oscillations suffered by the synchronous machines in the system, which contributes to reduce their mechanical and electrical wear.

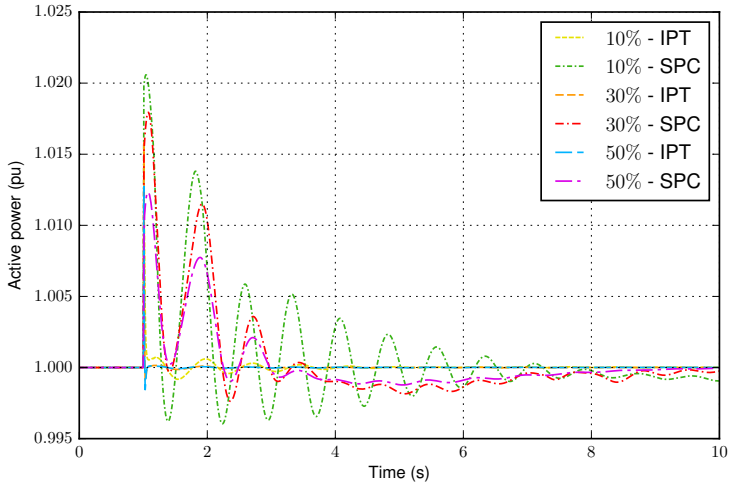


(a) Active power.

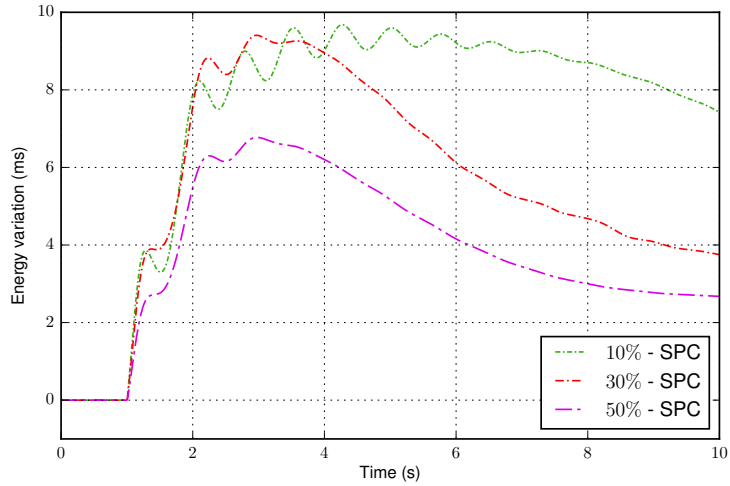


(b) Energy variation.

Fig. 5.10. PV plant 1 response to the disconnection of generator 4.

### 5.4.2 Disconnection of a load

The opposite event, i.e., the disconnection of a large load, is also considered in the analysis. In this case, load 4, connected at bus 4, is disconnected at $t = 1$ s. Opposite to generators, each load approximately represents the same share of the total demand under all the scenarios–around 21% for load 4–and the relative severity of the dis-

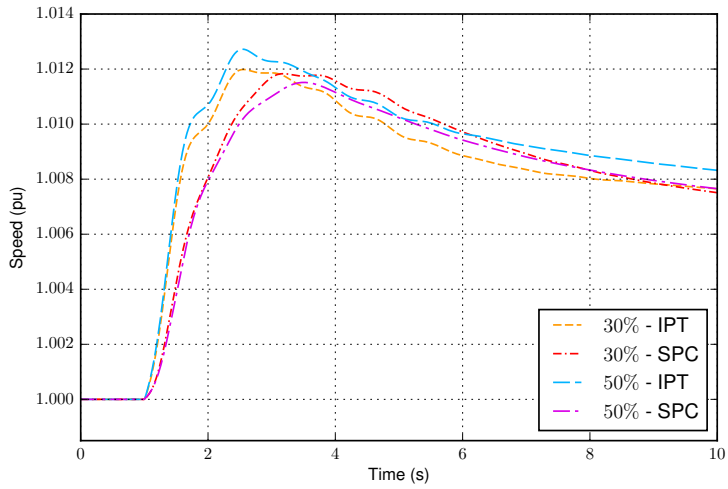


(a) Generator 2 speed.

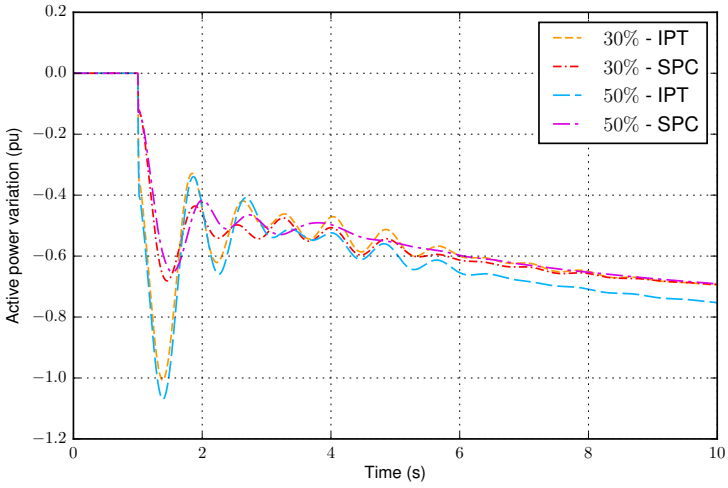


(b) Generator 2 active power variation.

Fig. 5.11. 12-bus system response to the disconnection of load 4.

connection is similar for all the PV penetration levels. Therefore, in order to allow a better comparison of the responses depending on the type of PV controller employed, the following discussion focuses only on the results obtained for the highest PV penetration levels. Taking this into account, Fig. 5.11 shows the response of the system to this disturbance for the 30% and 50% PV penetration scenarios.

The frequency of the system, which is represented by the speed of generator 2 in Fig. 5.11a, exhibits relevant differences between both types of controllers. First, when the PV plants use the SPC, the frequency varies more slowly, due to the addition of their virtual inertia to the physical inertia of the synchronous generators. This reduces the response slope and delays the moment when it reaches its maximum deviation for approximately 1 s for both scenarios. Moreover, the response is more damped when the SPC is employed and, under the 50% scenario, the maximum speed deviation is visibly reduced, around 10%, without compromising the speed of the recovery.

Furthermore, the type of PV controller used by the PV plants also affects the response of the synchronous generators in the system, which suffer a more moderate reduction of their active power injection when the controller is virtually synchronous than when it is based on IPT, as shown in Fig. 5.11b for generator 2. In this figure, it is possible to observe how the initial active power variation of the synchronous machine is reduced to less than one half and the absolute value of its maximum active power variation decreases by approximately 0.4 p.u. when the PV plants employ the SPC. In fact, the beneficial effects are not limited to the period immediately following the disturbance, but the subsequent oscillations are also better damped, with amplitude reductions around 60%.

Both the system frequency and the response of other generating units show that the relative impact of the controller is larger in the case of the load disconnection than in the case of the generator disconnection, and this can be explained through Fig. 5.12, where the active power response of PV plant 1 is shown. In this case, the plant can reduce its output as set by the SPC and it is not constrained by any active power limitation. Therefore, the disconnection of the load automatically causes a large reduction of the active power injected by the power plant, around 0.25 p.u., when the SPC is used. This response makes a significant difference in the initial frequency slope with respect to the IPT controller, that only modifies the output of the PV plant proportionally to the frequency deviation, which results in a slower response and a faster acceleration of the system. It is worth mentioning that the active power reduction determined by both controllers can be achieved due to the fast dynamics of PV systems. Furthermore, this response is naturally stable when

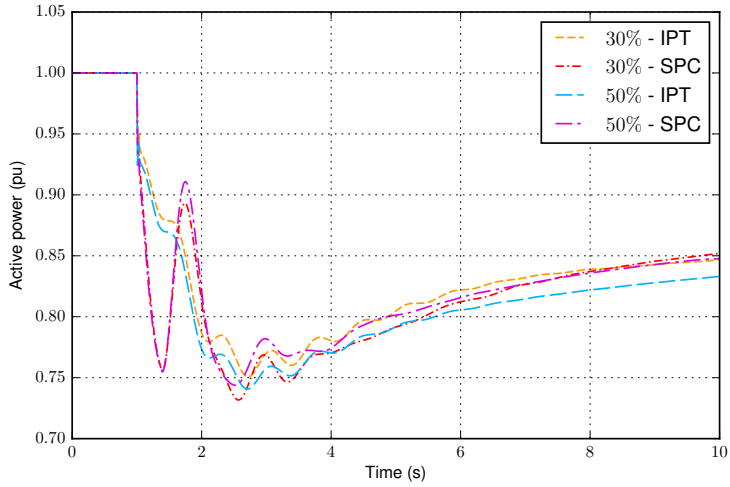


Fig. 5.12. PV plant 1 active power response to the disconnection of load 4.

the PV plant converters operate in the region of the PV characteristics where the dc voltage is greater or equal than the maximum power point voltage, since any reduction of the output active power results in a dc voltage increase, which reduces the PV power production, leading to a new equilibrium point.

Chapter
6.

# Analysis of the power system of northern Chile

*This chapter studies the impact of a PV plant with synchronous power controllers in a real power system. In this case, the PV plant model considers the full model of the converter dc side and PV system. A preliminary analysis considering two PV penetration levels and the extended PV plant model is carried out in the 12-bus system. This is followed by a more detailed stability analysis of the power system of northern Chile, where the influence of the PV plant parameters on the power system eigenvalues and the power system time-domain response are studied. The work presented here includes the results in the paper* D. Remon, C. A. Cañizares, P. Rodriguez, "Impact of 100-MW-scale PV plants with synchronous power controllers on power system stability in northern Chile," accepted for publication in *IET Generation, Transmission & Distribution*, May 2017.

## 6.1 PV power plant model

As in Chapter 5, the PV power plant considered in this study employs the model described in Chapter 4. Nonetheless, there are some changes that affect how the PV plant is modeled and how it operates with respect to the previous analysis.

On the one hand, the dynamics of the dc side and the PV system, as well as the dc voltage controller, are taken into account here. Thus, the complete model, including the resource explained in Section 4.3.4.1, is employed. For this analysis, the solar irradiance and the temperature are considered constant, because their dynamics are significantly slower than those of the magnitudes of interest. Thus, the maximum power point tracking algorithm is not enabled, and the dc voltage controller uses constant upper and lower voltage bounds.

On the other hand, the initial operating point of the power plant is such that it has a 10% active power reserve margin, so it can contribute to frequency control. With respect to the central plant controller, it is worth noting that it operates as in Chapter 5, i.e., a common active power reference signal is sent to all the converters in the plant, and the voltage at the POI is controlled through another common reactive power reference signal sent to all these devices; whereas the frequency control is done locally, but based on the frequency estimated at the POI.

## 6.2 12-bus test system results

A preliminary analysis is carried out in the 12-bus test system in order to compare the results obtained in a realistic power system with those obtained in a test power system that may be more prone to instability, considering in both cases the same PV power plant model, i.e., taking into the dynamics of the dc side and the PV system.

The base 12-bus system is the same as in Section 5.2, including the adaption for renewable integration studies done in [151], and the power system stabilizers defined for generators 3 and 4 in Table 5.1. However, the number of PV plants and scenarios is simplified with respect to the analysis described in Chapter 5.

Namely, two PV penetration scenarios are considered. In both cases, the total demand and the active power references of generators 2, 3, and 4 are given in Table 6.1. As shown in Fig. 6.1, two PV plants are connected at buses 4 and 5, regulating the voltage at these buses to 1 p.u. in both scenarios. The scenarios are defined by the power rating of the PV plants and generator 1 as follows:

- 10% PV penetration: The rated power of the PV plants is 100 MW, and they operate with a 10% reserve. Generator 1 balances generation and demand and

Table 6.1. Initial operating point parameters for 12-bus system.

| Element | P (p.u.) | Q (p.u.) | V (p.u.) |
|---|---|---|---|
| G1 | Slack | - | 1.00 |
| G2 | 4.00 | - | 1.01 |
| G3 | 2.70 | - | 1.01 |
| G4 | 3.30 | - | 1.01 |
| Load 1 | 3.41 | 2.12 | - |
| Load 2 | 2.84 | 1.38 | - |
| Load 3 | 3.98 | 1.31 | - |
| Load 4 | 3.41 | 2.12 | - |
| Load 5 | 1.14 | 0.55 | - |
| Load 6 | 1.71 | 0.56 | - |

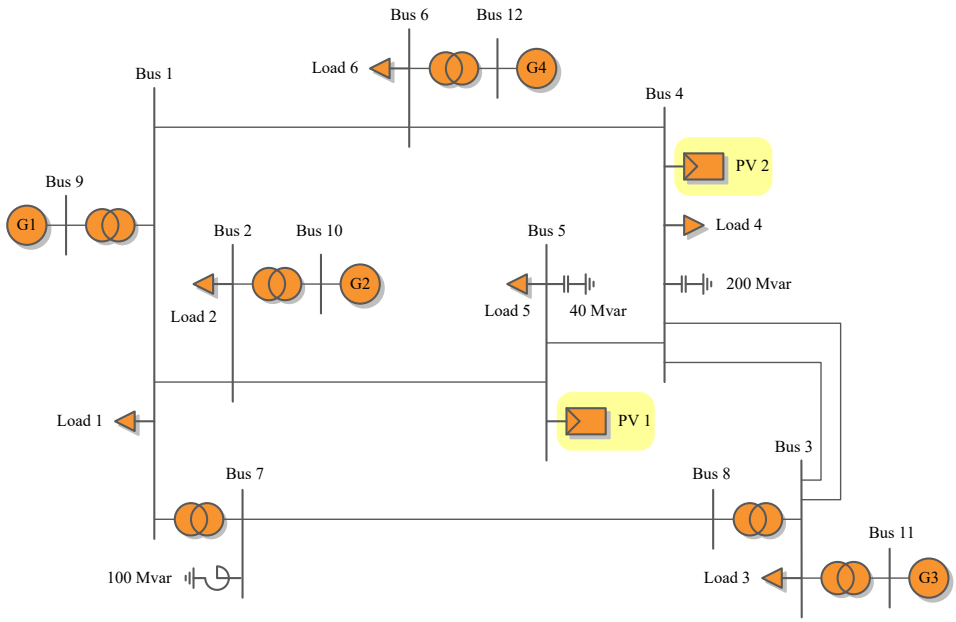


Fig. 6.1. 12-bus system diagram showing the location of the PV power plants.

is the equivalent of six units as defined in [151].

- 30% PV penetration: The rated power of the PV plants is 300 MW, and they operate with a 10% reserve. Generator 1 balances generation and demand, with a reduced power injection, and only two of its six units are connected to the system, reducing its total inertia.

In both scenarios, the PV plants contribute to frequency regulation with a frequency droop defined by a 5% slope, like the other generators in the system, whereas the voltage control is performed only by the central plant controller with the voltage droop at the converter level disabled. Given that only short-term studies are performed, no secondary frequency regulation scheme is taken into account. Additionally, two study cases are considered within each scenario depending on whether the PV plant controller is based on IPT or uses the SPC. In case of using the SPC, the PV plant behavior is defined by a 5 s inertia constant, which is similar to the inertia of the synchronous machines in the system, and a value of the damping coefficient $D$ that ensures a 0.7 damping ratio in the active power loop of the SPC.

The impact of the PV plants on this system, depending on the type of controller, is studied here by means of the response of the system to two different disturbances, as explained next.

### 6.2.1 Line contingency

This event is a short circuit at the midpoint of line 4-5, which starts at $t = 1$ s, and the corresponding line trip at $t = 1.05$ s as the protections are activated. As a result of the event, the power system is weakened. with the system eigenvalues getting closer to a 5% damping. Figure 6.2 shows the location of the critical eigenvalues in the complex plane, corresponding to the least three damped oscillatory modes. In all cases, all the modes have a damping ratio over 5% and thus can be considered sufficiently damped.

Additionally, some differences can be seen in Fig. 6.2 depending on the amount of PV and the type of controller employed, and the corresponding numerical values are given in Table 6.2. In general, the use of the SPC results in a significantly better damping of the critical modes than the IPT controller for both penetration scenarios,

Table 6.2. 12-bus system critical eigenvalues and damping ratio after the disconnection of line 4-5 for different scenarios.

| Scenario | Mode 1 | Mode 2 | Mode 3 |
|---|---|---|---|
| 10% - IPT | $-0.5455 \pm 8.6190\,j$<br>6.32% | $-0.5878 \pm 7.9653\,j$<br>7.36% | $-0.3810 \pm 5.8578\,j$<br>6.49% |
| 10% - SPC | $-0.5873 \pm 8.1977\,j$<br>7.15% | $-0.8296 \pm 9.1724\,j$<br>9.01% | $-0.7064 \pm 5.7498\,j$<br>12.19% |
| 30% - IPT | $-0.7702 \pm 10.5845\,j$<br>7.26% | $-0.7250 \pm 8.1750\,j$<br>8.83% | $-0.4061 \pm 5.8901\,j$<br>6.88% |
| 30% - SPC | $-0.8813 \pm 10.8013\,j$<br>8.13% | $-0.8388 \pm 9.0672\,j$<br>9.21% | $-0.7194 \pm 6.2435\,j$<br>11.45% |

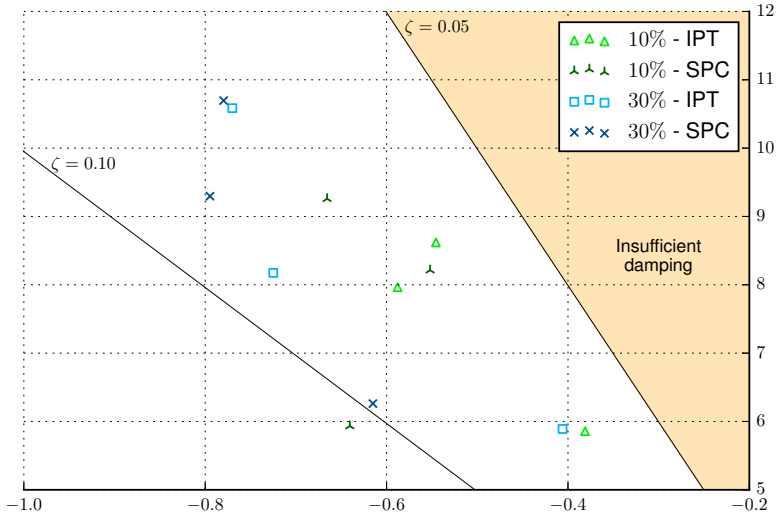


Fig. 6.2. 12-bus system eigenvalue plot after a short circuit on line 4-5 and its trip for different scenarios.

with some modes reaching damping ratios around 10%. In addition, it is possible to see further damping improvements as the PV penetration grows, benefiting from the fact that generation is more distributed throughout the system.

The time-domain response of the system to the disturbance is shown in Figs. 6.3

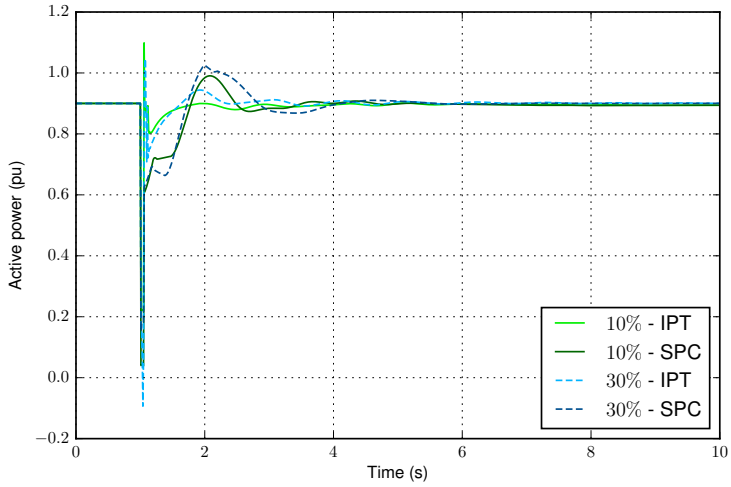


Fig. 6.3. Plant PV 1 active power response to a short circuit on line 4-5 and its trip for different scenarios, in a plant-per-unit system.

and 6.4. The differences in the plant response when both types of controllers are compared are evident in Fig. 6.3. Thus, with the IPT controller, the plant suffers large and fast oscillations during the short circuit and immediately after it is cleared. After approximately 0.5 s, the active power injection basically goes back to its pre-fault level with small oscillations. On the other hand, with the SPC, the immediate response is more stable than in the IPT case, and the active power injection oscillates like in a synchronous machine as a result of the inertia emulation.

Figure 6.4a shows the evolution of the system frequency during and after the disturbance, represented by the speed of generator 2. In this case, the PV penetration level determines the main trend, with a rise in the 10% penetration case, and a drop in the 30% case. As expected from the eigenvalue analysis, the SPC contributes to damping the oscillations in the system for both penetration levels, which results in a more stable frequency evolution. As shown in Fig. 6.4b, this is translated into the active power generated by this machine, which presents significantly larger oscillations when the conventional controller is used. Moreover, the amplitude and stabilization time of these oscillations increases with the PV penetration.

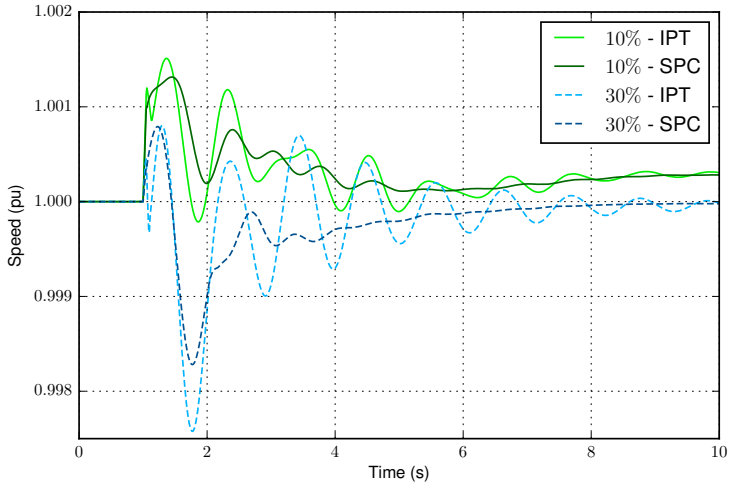


(a) Generator 2 speed.

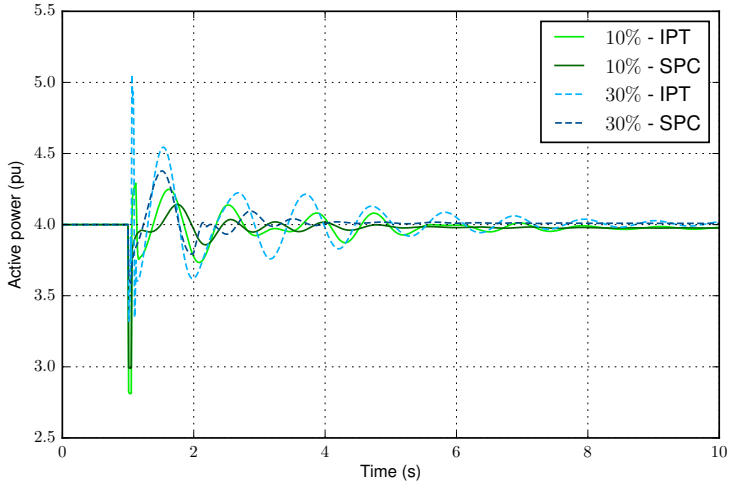


(b) Generator 2 active power.

Fig. 6.4. 12-bus system response to a short circuit on line 4-5 and its trip for different scenarios.

### 6.2.2 Generator contingency

In this case, the disturbance is the disconnection of one of the three units that form the generator 4 plant at $t = 1$ s, which causes a sudden generation-demand imbalance in the system, and reduces the total inertia and regulation capability. The effects of

Table 6.3. 12-bus system critical eigenvalues and damping ratio after the disconnection of one unit at the generator 4 plant for different scenarios.

| Scenario | Mode 1 | Mode 2 | Mode 3 |
|---|---|---|---|
| 10% - IPT | $-0.5467 \pm 8.2609\,j$<br>6.60% | $-0.5935 \pm 8.8854\,j$<br>6.67% | $-0.6345 \pm 6.5868\,j$<br>9.59% |
| 10% - SPC | $-0.5133 \pm 8.2642\,j$<br>6.20% | $-0.6099 \pm 9.5857\,j$<br>6.35% | $-0.7549 \pm 6.6137\,j$<br>11.34% |
| 30% - IPT | $-0.7720 \pm 10.6541\,j$<br>7.23% | $-0.7711 \pm 8.6780\,j$<br>8.85% | $-0.6612 \pm 6.7316\,j$<br>9.78% |
| 30% - SPC | $-0.7711 \pm 10.8033\,j$<br>7.12% | $-0.8095 \pm 9.4320\,j$<br>8.55% | $-0.7658 \pm 6.7424\,j$<br>11.29% |

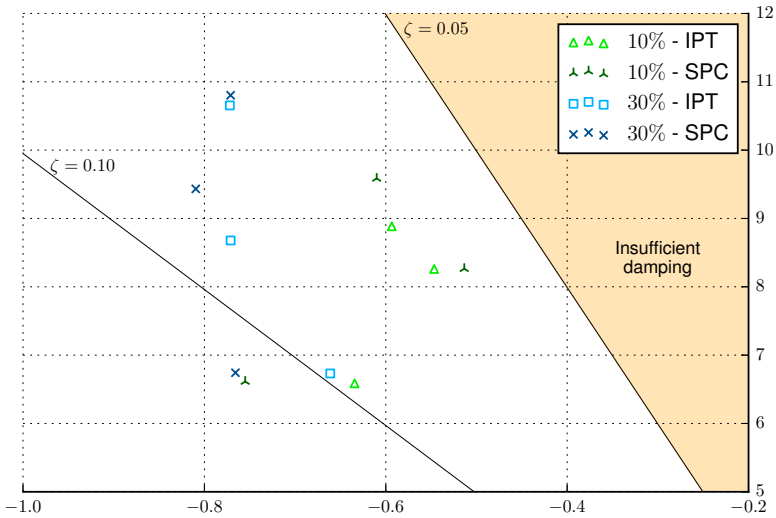


Fig. 6.5. 12-bus system eigenvalue plot after the disconnection of one unit at the generator 4 plant for different scenarios.

the event on the eigenvalues can be seen in Fig. 6.5 and Table 6.3 for all four study cases, where it can be observed that the damping ratio of the oscillatory modes is in all cases over 5%.

For this contingency, the SPC slightly reduces the damping of modes 1 and 2,

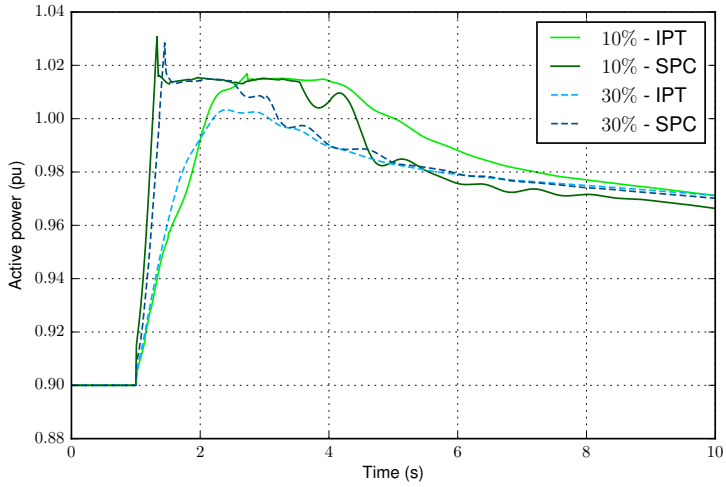


(a) Plant PV 1 active power in a plant-per-unit system.

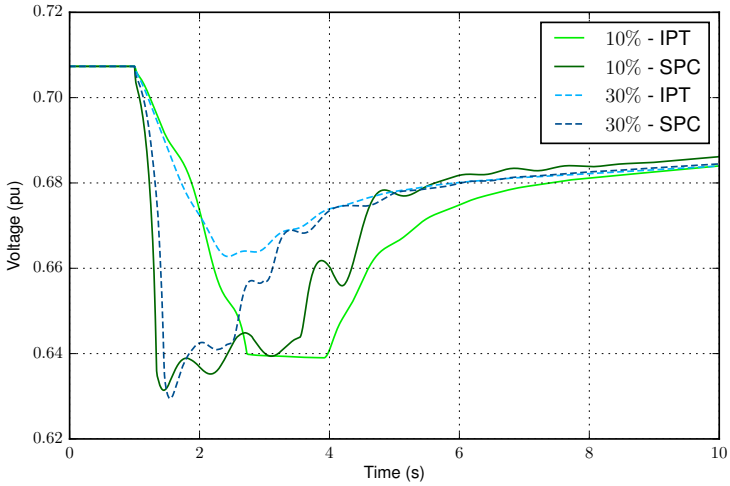


(b) Plant PV 1 equivalent converter dc voltage.

Fig. 6.6. PV plant 1 response to the disconnection of one unit at the generator 4 plant for different scenarios.

whose damping ratio is nonetheless over 6% in the worst case. On the other hand, it significantly increases the damping of mode 3, and thus the sum of the damping ratios of these three modes is greater for the SPC than for the conventional controller.

The response of the system is shown in Figs. 6.6 and 6.7. The active power injection of PV plant 1, which can be seen in Fig. 6.6a in a plant-per-unit system,

shows two appreciably different types of behavior depending on the employed controller. Namely, the initial response of the plant is improved by the effect of the inertia emulated by the SPC, since the active power injection increases faster than with the IPT controller, which only modifies the generated power as a result of the frequency droop. The fast reaction caused by the SPC results in an early saturation of the plant, which does not harm the stability of the system. In fact, the IPT controller also saturates the PV plant in the 10% case, but this saturation occurs appreciably later than in the case of the SPC, and it results in a delayed contribution from the plant.

The effects of the active power response on the dc voltage of the equivalent converter are shown in Fig. 6.6b. The faster reaction when the SPC is employed results in a faster decrease of the dc voltage, and the activation of the dc voltage controller when it reaches a value below 0.64 p.u. The moderate active power response of the plant in the 30% penetration case when the conventional controller is used is translated into a higher dc voltage level during this transient.

This effect of the controller on the oscillation damping can be seen in the active power generated by generator 2, shown in Fig. 6.7a. In this case, the impact of the controller is larger for the 30% scenario, where the utilization of the SPC by PV plants allows the amplitude of the active power oscillations of generator 2 to decrease by 27%.

Furthermore, the frequency is severely affected by the disturbance, as can be seen through the plot of the speed of generator 2 in Fig. 6.7b. Thus, the frequency drop is more significant for a 10% penetration level, and this causes the observed larger contribution of the PV plants. Comparing both controllers, the SPC yields a slight improvement on the maximum frequency deviation in the 10% penetration scenario. For the 30% scenario, this contribution is again more evident, limiting the frequency deviation during its first three swings, and reducing the maximum deviation by approximately 20%. This is accompanied by a slight improvement in the frequency oscillation damping.

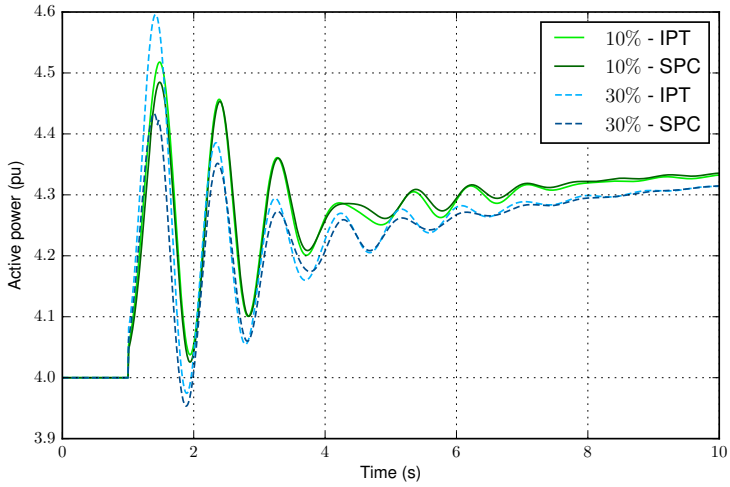


(a) Generator 2 active power.

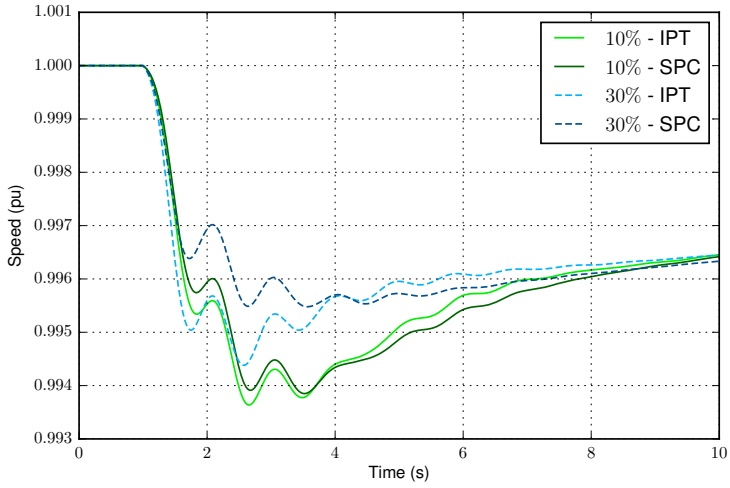


(b) Generator 2 speed.

Fig. 6.7. 12-bus system response to the disconnection of one unit at the generator 4 plant for different scenarios.

## 6.3 Power system of northern Chile

The power system of northern Chile is a 50 Hz system with an average demand around 2,000 MW [152]. Industrial loads associated with mining constitute the main part of this demand, with relatively small hourly variations. The generation mix is

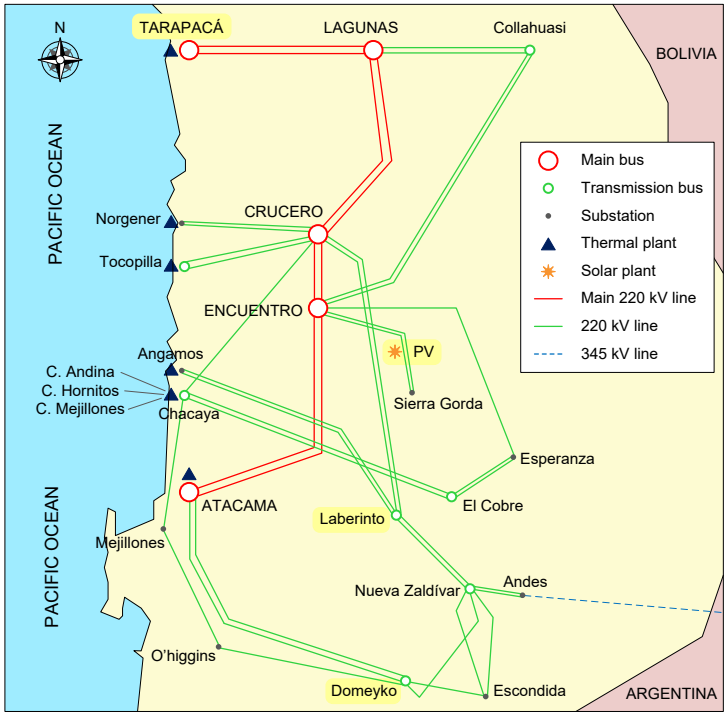


Fig. 6.8. Simplified diagram of the power system of northern Chile [153].

mainly coal, natural gas, and diesel, although a significant number of PV plants are being installed or are planned to be connected in the near future.

A schematic view of the central part of the system is illustrated in Fig. 6.8. The main trunk of the system stretches from Tarapacá to Atacama, containing large power plants connected electrically close to the Crucero bus. One of the studied PV plants is a 100 MW PV power plant currently being constructed, connected to one circuit of the Encuentro-Sierra Gorda line, as depicted in Fig. 6.8. This plant is designed to use power converters that can operate with the SPC option.

The study here takes into account the power system model published by the system operator [154]. A low demand operation scenario is considered, which corresponds to maximum existing PV power generation and no interconnection with Argentina. This operation scenario is modified to add the planned 100 MW PV plant at the same demand level, disconnecting a synchronous generator. Furthermore, in

order to evaluate the impact of PV plants with SPCs for an increased penetration level, the rated power of the planned PV plant is increased to 200 MW, and three more 200 MW PV plants are added to the system, summing up a total of 800 MW, and increasing the total demand accordingly. The additional PV plants are located at future solar PV sites; thus, one of these plants is connected at Parinacota bus north of Tarapacá, whereas the other two are connected at Domeyko and Laberinto buses.

In both scenarios, the solar radiation and temperature are such that the PV plants are able to generate a maximum of 1.015 p.u. active power at 0.64 p.u. dc voltage, and their open-circuit dc voltage is 0.79 p.u., considering a plant per-unit system. Additionally, the initial operating point of the PV plants considers a 10% active power reserve margin, so that they can contribute to frequency control and stability, and both IPT and SPC controllers are considered.

The active power generation for the main generators in the modified scenarios is slightly modified with respect to the June 2015 low demand data in [154], as shown in Table 6.4. In both 100 MW and 800 MW PV scenarios, it is assumed that the PV plant replaces unit U14 at Tocopilla, whereas unit U16, also at Tocopilla, increases its active power injection to 211 MW. On the other hand, the setpoint of unit U15 is modified in each scenario; in the 100 MW PV case, U15 operates at its technical minimum of 75 MW, and in the 800 MW PV case, it generates 130 MW, close to its maximum. The load increase that takes place in the 800 MW scenario is compensated by both the increase of power generated by U15 and the additional PV generation. It is worth noting that, although this high PV penetration scenario brings benefits to the power system economics and sustainability, the resulting dispatch causes a reduction of the ratio of power generated by conventional synchronous machines, and thus the total system inertia decreases.

Taking into account the characteristic of the generators connected to the power system of northern Chile, described in [154], the PV plants are assumed to contribute to frequency and voltage regulation with a 5% and 2.5% droop respectively, and the SPC considers an inertia constant of 5 s. Furthermore, a damping coefficient $D$ such that the damping ratio of the PV plant active power loop is 0.7, and a virtual reactance equal to 0.3 p.u. are chosen, so that the plant response is sufficiently damped, closely interacting with the grid.

Table 6.4. Active power injections (p.u.) of the main generators in northern Chile for different penetration scenarios.

| Generator | No PV | 100 MW PV | 800 MW PV |
|---|---|---|---|
| ANG1 | 2.05 | 2.27 | 2.23 |
| ANG2 | 2.63 | 2.63 | 2.63 |
| U16 | 1.70 | 2.11 | 2.11 |
| CTH | 1.58 | 1.58 | 1.58 |
| CTM2 | 1.54 | 1.54 | 1.54 |
| CTM1 | 1.49 | 1.49 | 1.49 |
| CTTAR | 1.40 | 1.40 | 1.40 |
| NTO1 | 1.35 | 1.35 | 1.35 |
| NTO2 | 1.35 | 1.35 | 1.35 |
| CTA | 1.30 | 1.30 | 1.30 |
| U14 | 1.22 | - | - |
| U15 | 1.16 | 0.75 | 1.30 |
| TG1A | 0.95 | 0.95 | 0.95 |
| TV1C | 0.60 | 0.60 | 0.60 |
| PV1 | - | 0.90 | 1.80 |
| PV2 | - | - | 1.80 |
| PV3 | - | - | 1.80 |
| PV4 | - | - | 1.80 |

## 6.4 Power system of northern Chile results

The impact of these PV plants on the system is analyzed in this section. First, the sensitivity of the eigenvalues of the system to the PV plant parameters in the 100 MW scenario is studied. Afterwards, the stability of the system for three types of disturbances is discussed for different penetration levels and converter controllers.

### 6.4.1 Eigenvalue sensitivity

The influence of certain PV plant parameters on the eigenvalues of the power system of northern Chile is analyzed here. The study considers only the actual case where a 100 MW PV plant is connected to the Encuentro-Sierra Gorda line. The impact of each parameter is assessed taking into account how the eigenvalues vary for different values of that parameter, while the other parameters keep the values given at the end of Section 6.3.

One of the main parameters describing the response of a converter controlled by the SPC is its inertia constant. The influence of this parameter on the eigenvalues of the power system can be seen in Fig. 6.9. For the inertia constant values considered, the weakest three modes are practically unaffected. A fourth mode, whose eigenvalue is around $-0.8 \pm 6j$ (mode 4), shows a special sensitivity to the type of controller, with the SPC reducing its damping, which is in any case well over 10%. Furthermore, the real part of this eigenvalue has an interesting behavior with respect to the inertia constant, and results in better damping for very low or very high values of this parameter, and a minimum when the default value of 5 s is considered. The reverse trend can be seen in the eigenvalue around $-1.14 \pm 4.5j$ (mode 7), for which 5 s–10 s lead to a clear maximum, and, more slightly, for the eigenvalues around $-0.97 \pm 6.7j$ (mode 5) and $-1.15 \pm 7j$ (mode 6). Nonetheless, it can be concluded that the impact of the SPC inertia constant is small, and all modes have damping ratios over 10%.

The impact of the other parameter describing the electromechanical response of the SPC, its active power closed-loop damping ratio, is visible in Fig. 6.10. Once again, the damping of all modes is safely over 10%, and the same four modes are affected. Mode 4 sees its damping reduced again when the SPC is employed, but now it shows a clear trend with increasing damping as the SPC damping ratio increases, and so does mode 6. On the other hand, the damping of mode 5 decreases when the SPC damping ratio increases. Finally, like in the case of the inertia constant, mode 7 has a maximum of damping for intermediate values of this parameter.

Fig. 6.11 shows the eigenvalues obtained for different values of the SPC admittance. In this case, the resistance-to-reactance ratio is equal to $1/3$ for all the cases, and the reactance takes the values indicated in the legend of the plot. Like in pre-

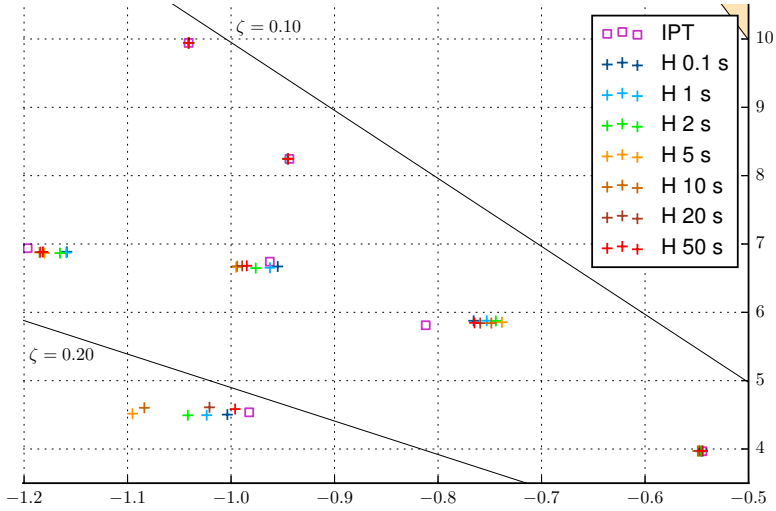


Fig. 6.9. Eigenvalue plot of the power system of northern Chile for different values of the SPC inertia constant.

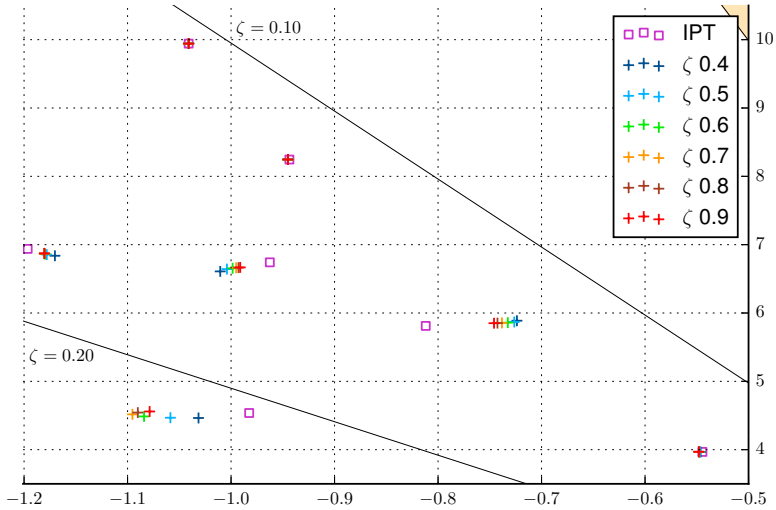


Fig. 6.10. Eigenvalue plot of the power system of northern Chile for different values of the SPC damping ratio.

vious cases, the effect of the PV plant is very limited on the three critical modes, but the other four modes visible in the plot have an interesting behavior. Mode 4 initially reduces its damping as the impedance increases, reaching a minimum for

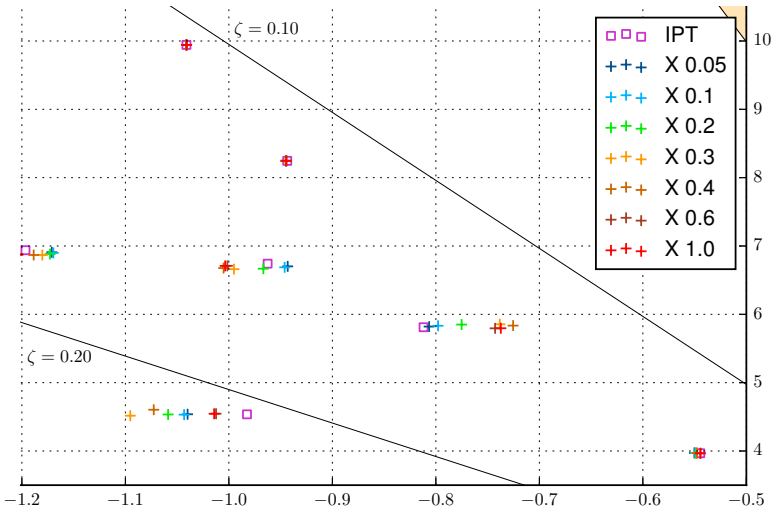


Fig. 6.11. Eigenvalue plot of the power system of northern Chile for different values of the SPC virtual admittance.

$X = 0.4$, then it increases slightly for $X = 0.6$, and finally it decreases again for $X = 1.0$. Modes 5 and 6 have clear trends of growing damping as the impedance increases; whereas mode 7, like in the previous cases, has maximum damping for an intermediate value of the parameter.

Finally, the impact of a PV plant parameter that is not directly related to the SPC is considered. Namely, the PV plant voltage controller gain, inverse of the voltage droop slope, is given different values for both the conventional controller and the SPC, obtaining the eigenvalue plot of Fig 6.12. As in the case of the SPC parameters studied previously, the three critical modes are not affected by the PV plant, but the other four modes are. Mode 4 exhibits a steady trend of increasing damping as the gain of the voltage controller increases when the IPT controller is employed. With the SPC, it has similar values for moderate controller gains, with less damping than in the case of the IPT controller, but its damping improves significantly when the gain is high. Mode 5, on the other hand, shows very similar results in most cases, with high gains reducing its damping. However, the highest gain, combined with the SPC, gives rise to a significant reduction of the damping of this eigenvalue. Something similar happens with mode 6, and even with mode 7 if the conventional

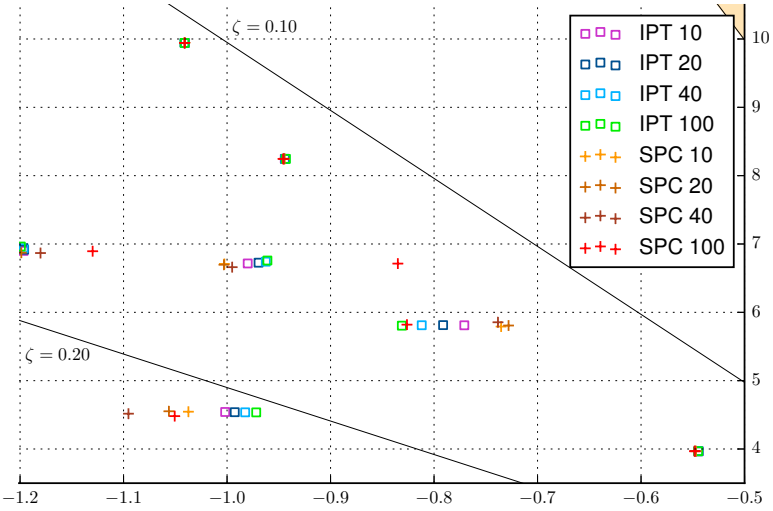


Fig. 6.12. Eigenvalue plot of the power system of northern Chile for different values of the PV plant voltage control gain.

controller is considered. When the SPC is used, there is again a maximum value of damping for intermediate values of the studied parameter.

In general, the damping of the system is acceptable, with all modes over 10%, and the PV plant parameters have a limited impact on the system. This reduced influence is due to the small relative size of the PV plant respect to the whole power system, and the well-damped nature of the system without PV.

### 6.4.2 Line contingency

The event is a short circuit on circuit 2 of the Crucero-Encuentro line, that starts at $t = 1$ s, and is cleared when the affected circuit is tripped at $t = 1.06$ s.

The power system is well damped even when this line is tripped after the short circuit, and the damping ratio of all the eigenvalues is still over 10%, as can be seen in Fig. 6.13. In the 100 MW scenario, the modes seem to be just slightly affected by the type of control of the PV plants, whereas in the 800 MW scenario, more differences can be observed, with the SPC reducing the damping of mode 5, which is nonetheless greater than 10%.

The response of the PV plants to this event is determined by the type of con-

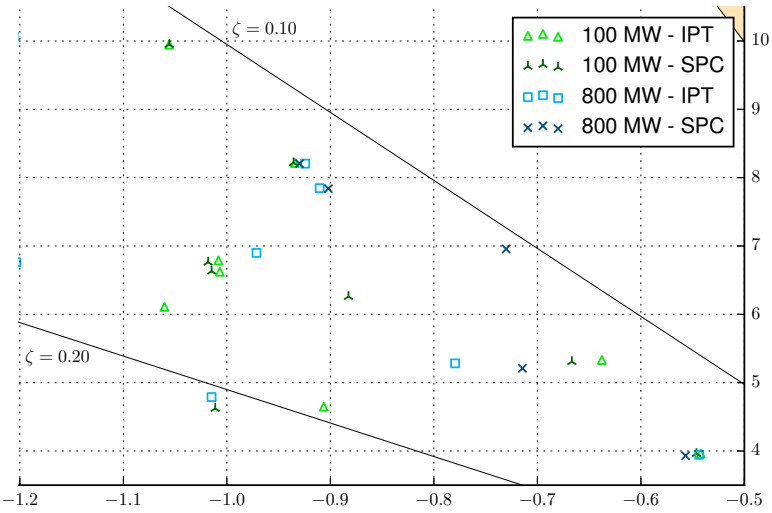


Fig. 6.13. Eigenvalue plot of the power system of northern Chile after a contingency on circuit 2 of the Crucero-Encuentro line for different scenarios.

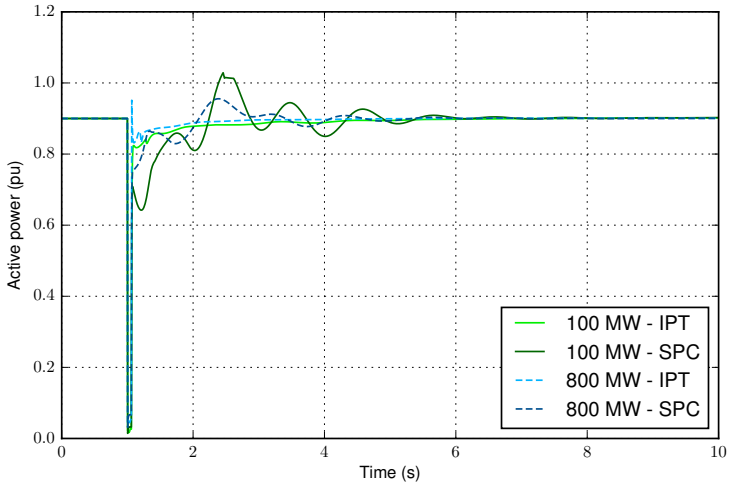


Fig. 6.14. Plant PV1 active power response to a contingency on circuit 2 of the Crucero-Encuentro line for different scenarios, in a plant-per-unit system.

troller, as shown in Fig. 6.14, where the active powers generated by the studied PV plant are depicted in a plant-per-unit system. For the IPT controller, there is a short active power spike when the line is tripped, followed by a steady recovery of the pre-

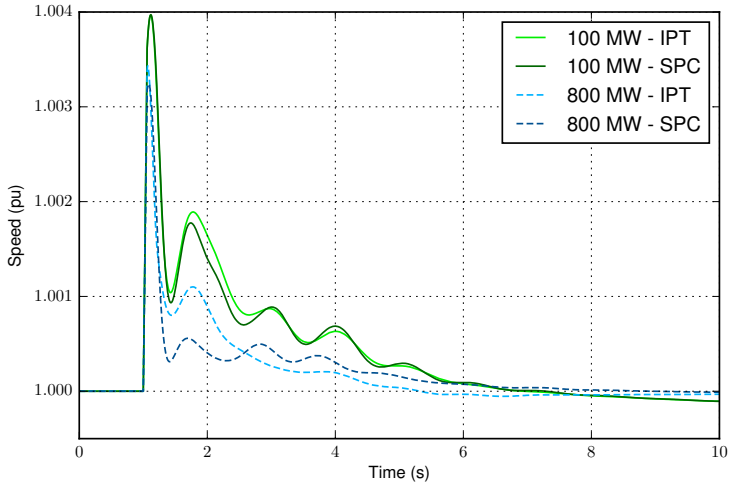


(a) Generator ANG2 speed.

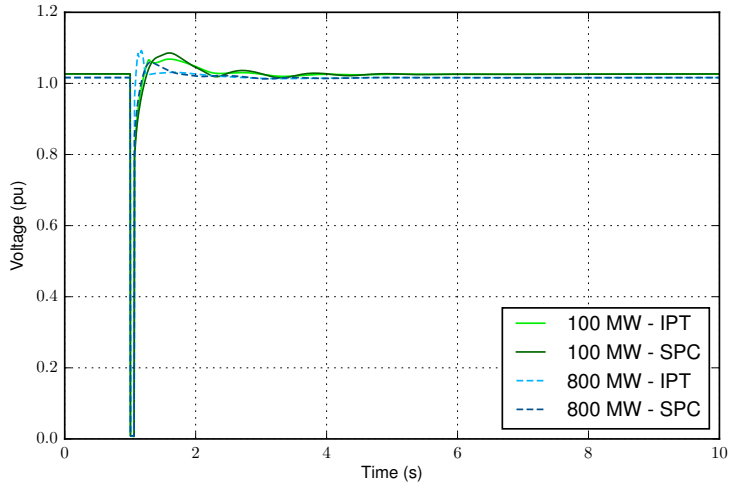


(b) Crucero bus voltage.

Fig. 6.15. Response of the power system of northern Chile to a contingency on circuit 2 of the Crucero-Encuentro line for different scenarios.

fault level in 1 s. With the SPC, the plant exhibits the expected oscillatory behavior of a synchronous machine, with the oscillations fading away in approximately 5 s.

Nevertheless, the general response of the system in terms of frequency and voltage is not especially affected by the type of controller, as shown in Fig. 6.15. Thus, the impact of the line trip on the frequency of the system and the speed of syn-

chronous machines can be seen in Fig. 6.15a, where the speed of generator ANG2 at the Angamos plant is shown. In this figure, the frequency evolution is affected by the PV penetration level and slightly by the selected controller; the impact of the 100 MW plant is limited, with the controller type having practically no effect on the system, but for the 800 MW case, the controllers have a visible influence, especially during the first 2 s after the event, with the SPC limiting the acceleration of the system. The effect on the voltage of the system is reduced in all cases, as shown in Fig. 6.15b for the Crucero bus.

### 6.4.3 Generator contingency

This event consists on the disconnection of generator U15 at $t = 1$ s. This machine is connected at the Tocopilla plant and its active power reference is adapted for each scenario in such a way that it represents approximately 4% of the total generation in both cases; hence, the severity of the disturbance is similar regardless of the considered PV penetration level.

The active power imbalance in the system does not affect its eigenvalues significantly, and the damping ratio of all modes is around 10% or above. Nevertheless, this disturbance has some effects on the response of the generating units in the system as shown in Figs. 6.16 and 6.17.

Fig. 6.16a depicts the active power response of the studied PV plant, on a plant-per-unit system, showing that the plant response depends fundamentally on the type of controller. When the SPC is employed, the response is initially faster due to the emulated inertia, and during the following 5 to 7 seconds, it has an oscillatory behavior superimposed on the droop response to the frequency variation, as in the case of a synchronous machine. With the IPT controller, a steadier active power increase is seen, due to the droop response. Therefore, the inertia emulated by the SPC enables the PV plant to respond faster to the frequency event.

The PV plant active power response is related to the dc voltage of the equivalent converter, as can be seen in Fig. 6.16b. As a result of the additional injection of active power, the dc capacitors discharge, and the voltage decreases. Furthermore, since the PV plant is operating in the stable region of the PV characteristics, this decrease of voltage results in a PV power increase, which rapidly balances the extra

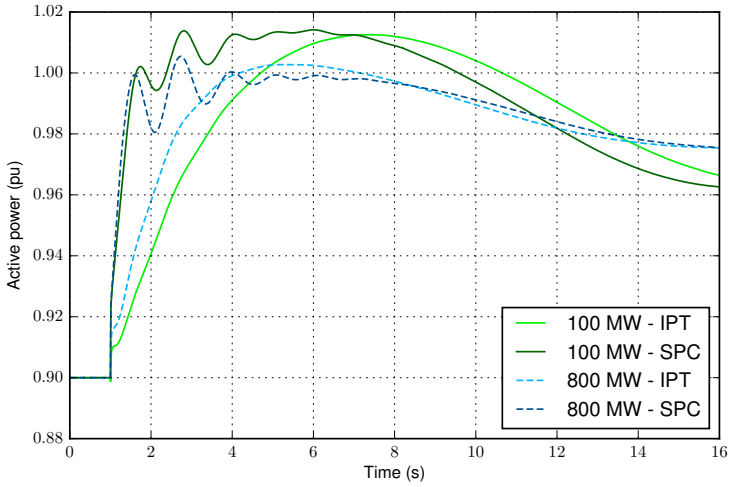


(a) Active power in a plant-per-unit system.

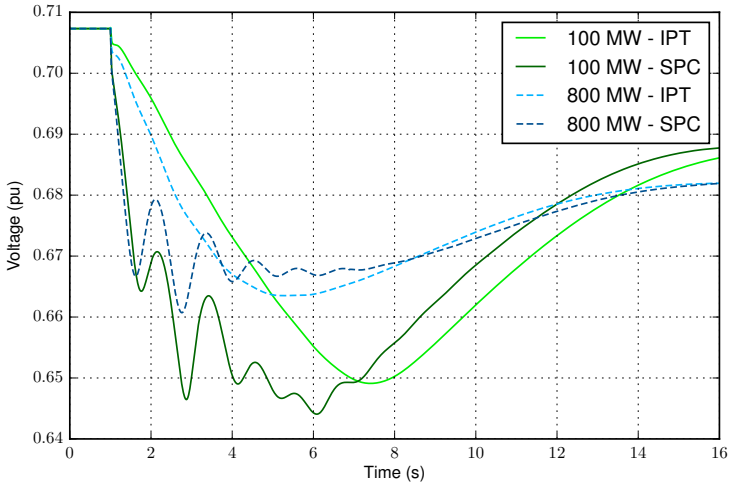


(b) Equivalent converter dc voltage.

Fig. 6.16. Response of plant PV1 to the disconnection of generator U15 for different scenarios.

power injected into the grid and maintains the active power balance. Comparing the different scenarios, it is possible to see how, at the beginning of the transient, the faster response of the SPC results in a faster dc voltage drop, i.e., a faster energy release to compensate the frequency deviation, which is analogous to the inertial response of synchronous machines. In any case, the dc voltage remains over the

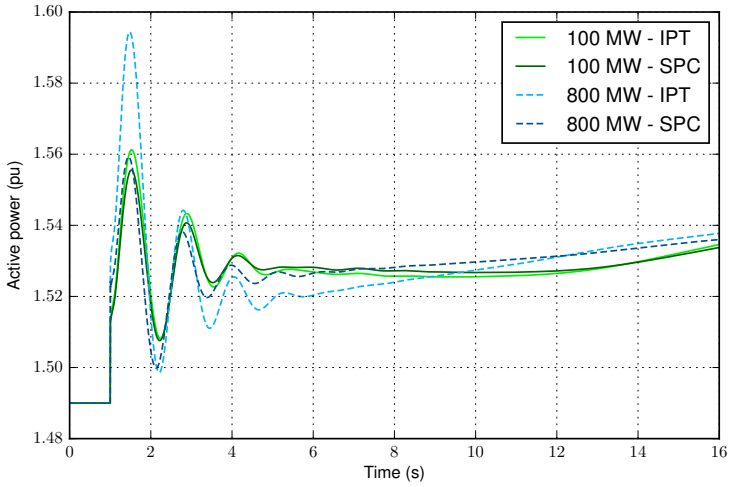


(a) Generator CTM1 active power.

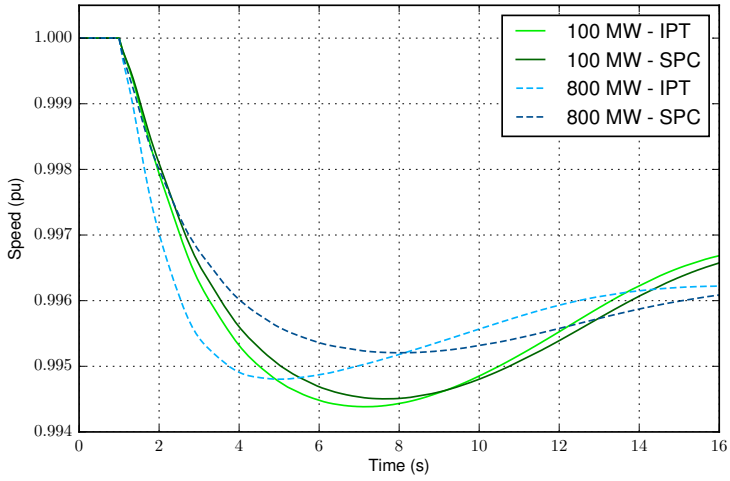


(b) Generator ANG2 speed.

Fig. 6.17. Response of the power system of northern Chile to the disconnection of generator U15 for different scenarios.

maximum power point voltage throughout the transient for all the scenarios, so the plant operates safely within the stable region of the PV curve.

The fast active power response of the PV plants when the SPC is employed has some beneficial effects for the power system, as shown in Fig. 6.17. In particular, it alleviates the effort of the synchronous machines in the system, like unit CTM1

at the Mejillones plant, whose active power injection is shown in Fig. 6.17a. In the 100 MW scenario, the use of the SPC by the PV plant contributes to a slight reduction of CTM1 active power oscillations with respect to the IPT controller. However, this contribution is more evident in the 800 MW scenario, since the SPC keeps the oscillations in the same range as for the 100 MW scenario, but the IPT results in appreciably larger oscillations, especially during the first swing of the machine.

Additionally, the SPC response has an influence on the system frequency, as can be inferred from the speed of generator ANG2 shown in Fig. 6.17b. The system frequency is affected differently in each scenario, and the differences due to the controller type are more evident as the PV penetration increases. In the 100 MW scenario, the influence of the PV plant controller on the system response is limited by the small relative size of the plant compared with the whole system, but the response induced by the SPC makes possible a slight reduction of the frequency slope and its maximum deviation. On the other hand, in the 800 MW scenario, there are more visible effects; thus, the SPC contributes to a significant reduction in the rate of change of the frequency, which eventually results in a reduced maximum frequency deviation of 8%, taking place 3 s later than in the case of the IPT controller. In this case, the voltage of the system is slightly affected, and exhibits slow dynamics related to the active power response of the system.

### 6.4.4 Load contingency

This third event is defined by the disconnection of several loads connected near the Crucero bus, which represent around 8% of total demand in all scenarios. Therefore, the active power balance is significantly affected, with the power system frequency increasing in this case, as expected. The response of the power system to this event, which takes place at $t = 1$ s, is shown in Figs. 6.18 and 6.19.

The active power response of plant PV1 for this event is shown in Fig. 6.18a, also on a plant-per-unit system. As in the case of the disconnection of the generator, the response is clearly dependent on the employed controller, and the SPC results in a faster reaction, with a sharp decrease of active power generation in order to compensate the loss of load. With the IPT controller, the active power reduction is slower, tracking the resulting frequency increase.

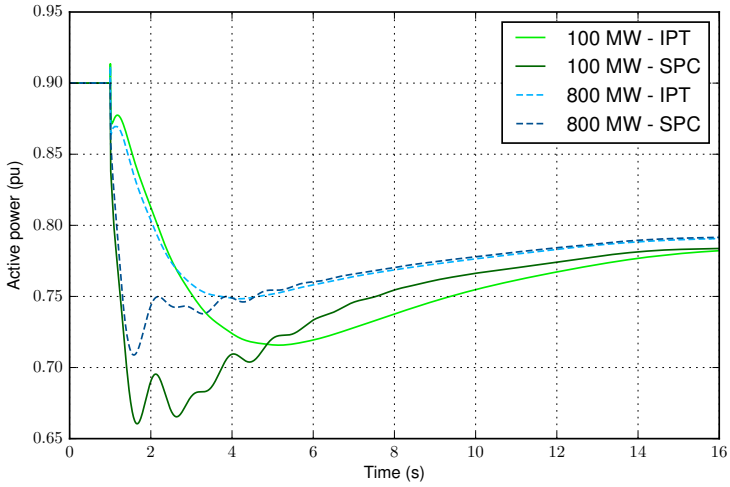


(a) Active power in a plant-per-unit system.

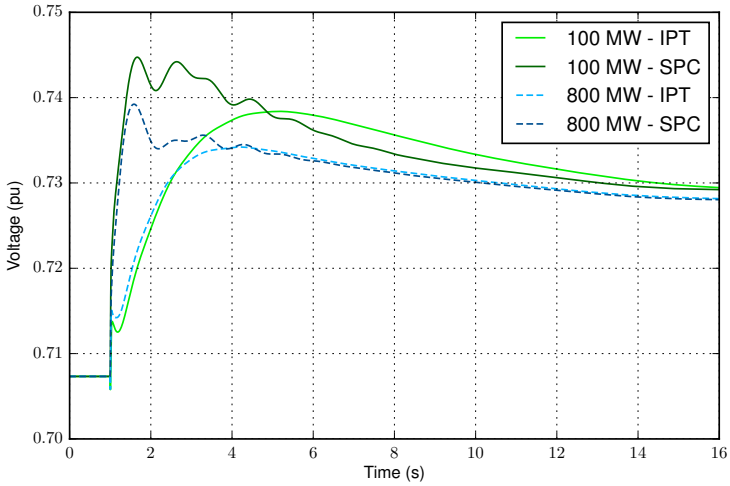


(b) Equivalent converter dc voltage.

Fig. 6.18. Response of plant PV1 to the disconnection of loads for different scenarios.

The effects of the event on the equivalent converter dc voltage can be seen in Fig. 6.18b. In this case, the active power reduction charges the dc capacitors, increasing their voltage and thus reducing the power generated by the PV system. With the SPC, the plant absorbs more power at the beginning of the transient, thus opposing the disturbance. In all scenarios, the dc voltage increase is moderate and

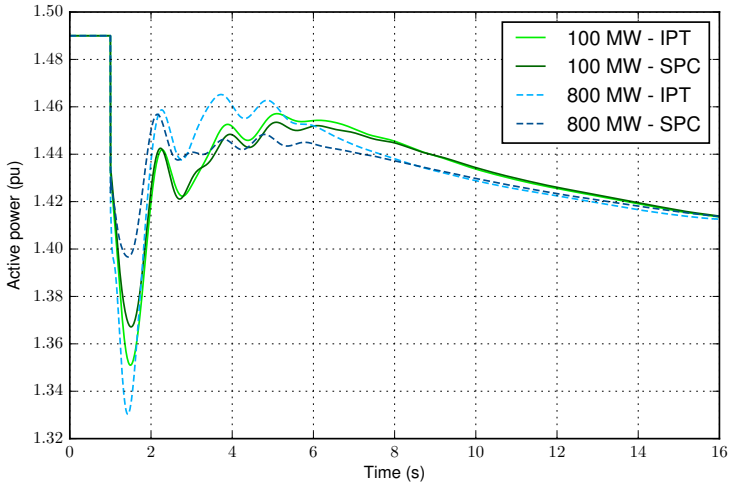


(a) Generator CTM1 active power.

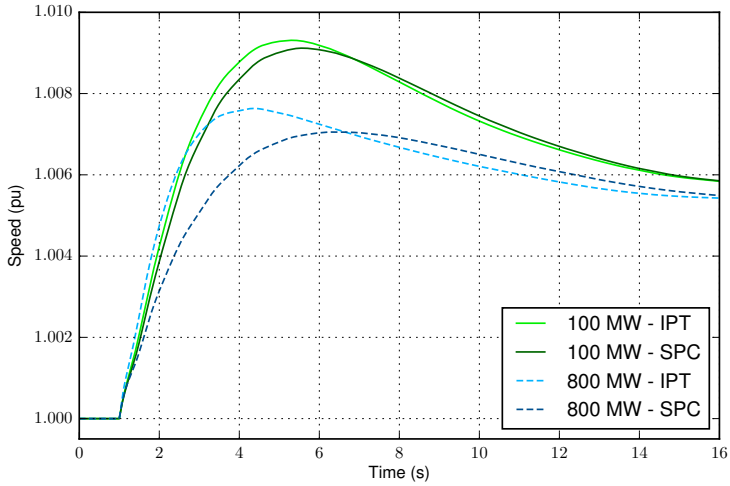


(b) Generator ANG2 speed.

Fig. 6.19. Response of the power system of northern Chile to the disconnection of loads for different scenarios.

the PV system continues operating in its stable region.

The SPC response also brings benefits for the power system when a load is disconnected. On the one hand, the effort of the synchronous machines is reduced once again, especially for the 800 MW scenario, as can be seen in Fig. 6.19a for unit CTM1, which presents a significant reduction of oscillations when the SPC

is employed. On the other hand, the additional inertia provided by the PV plants employing the SPC contributes decisively to limiting the rate of change of the frequency, and thus its maximum deviation, as shown in Fig. 6.19b. When the PV penetration increases, the effect on the maximum frequency deviation becomes evident, delaying the occurrence of the maximum for approximately 2 s, and reducing its value around 9%. With respect to the system voltage, the disconnection of the load causes a small voltage increase, once again with slow dynamics in accordance with the active power response of the system.

Chapter
7.

# Analysis of the impact of a hybrid SG-PV power plant on power systems

*Hybrid power plants combining synchronous generators and power electronics devices offer additional flexibility to integrate renewable energy sources in power system. In this chapter, the impact of a hybrid power plant consisting of a synchronous generator, PV, and a storage system is analyzed. First, the hybrid power plant model is discussed, and the ability of a small storage system to reproduce the response of a larger plant is studied. Afterwards, the stability of the 12-bus system is analyzed under the presence of a hybrid power plant that may adopt several configurations and use different power converter controllers. Finally, the impact of large renewable power plants on a simpler test power system, more prone to oscillatory instability, is analyzed considering hybrid and only-PV configurations with different penetration levels. This work has been partially presented in* D. Remon, A. M. Cantarellas, J. Martinez Garcia, J. M. Escaño, P. Rodriguez, "Hybrid solar plant with synchronous power controllers contribution to 12-bus system stability," accepted in *IEEE Energy Conversion Congress and Exposition (ECCE)*, Cincinnati, OH, 2017.

Solar energy is usually converted into electric power and injected into the grid through photovoltaic systems and power electronics interfaces, in a wide range of

power from residential applications to transmission-level power plants such as those considered in Chapters 4 to 6. Nevertheless, many installations also include certain amount of energy storage in order to avoid the adverse effects of the intermittency of the solar resource, usually employing batteries.

Furthermore, some transmission-level power stations combine different generation technologies in order to fully utilize a clean and economic power source while ensuring firm and reliable power generation. Possible combinations blend PV with solar thermal energy, which employs more conventional generating systems based on a steam turbine and a synchronous generator, and have the potential to store thermal energy for several hours; biomass, with a similar power conversion unit and greater flexibility in terms of fuel availability; or natural gas, through efficient combined cycles that allow the plant to easily adapt its production throughout the day. Therefore, it is also necessary to analyze the impact that these hybrid power plants have on power systems.

## 7.1 Hybrid power plant model

The hybrid power plants considered in the present analysis consider a thermal section employing a synchronous generator, PV, and a battery energy storage system. Different scenarios are considered, with different sections enabled and different converter controllers for the PV and storage systems. In all cases, the PV plant and the storage system share a common MV bus and step-up transformer; whereas the synchronous machine is connected to the grid at the same point, but through an independent transformer, together with its ancillary loads. The main characteristics of the models employed are explained next.

### 7.1.1 Synchronous generator

The conventional generation section of the hybrid power plant consists of a synchronous generator fed by a steam turbine, which may correspond to a solar thermal energy or biomass plant. The model considers a round-rotor synchronous machine with governor, exciter, and power system stabilizer. Furthermore, some scenarios take into account the consumption of the ancillary loads required to maintain the

plant in operation.

### 7.1.2 PV plant

The PV plant considers the full model presented in Chapter 4, including the dc side and PV system, through the equivalent $1\times100$ model. In this case, however, the plant transformer impedance is not integrated in the equivalent impedance. Instead, the plant transformer is kept in its original form, and the equivalent impedance represents the internal MV network and the converter transformers. The equivalent impedance and converter take into account that they are connected in MV.

### 7.1.3 Storage system

The battery energy storage system also considers the model in Chapter 4, and employs a single-converter equivalent where the equivalent battery has a rated power and capacity equal to the some of the individual values of all the units forming the storage system. Due to the short cable distances involved with respect to the case of PV, the equivalent impedance corresponds in practice to the converter transformer impedance. The equivalent impedance and converter take into account that they are connected in MV, at the PV plant common bus.

## 7.2 Plant inertia emulation with a BESS

The inclusion of a storage system allows increasing the flexibility of the power plant. In particular, the PV plant can be relieved of some or all of its frequency control duties. Thus, it can operate with no active power reserves, relying on the BESS when an active power increase is needed. In fact, the BESS could also respond when an active power reduction is necessary, absorbing active power and allowing the PV plant to continue operating close to its maximum power point.

Employing the same parameters in per unit as the PV plant, but considering its own per unit system, the response of the storage system would be similar to the PV plant response, but scaled down according to the storage system rating. This can be seen in Fig. 7.1, where the response of a 100 MW PV plant and a 7 MW BESS to

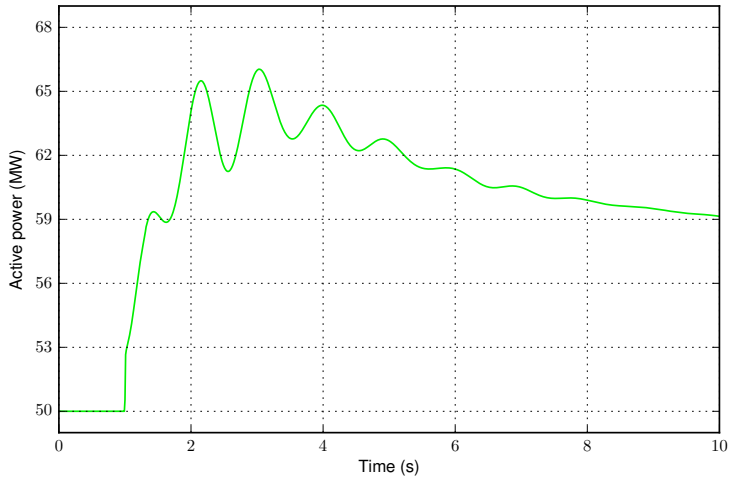


(a) 100 MW PV plant.

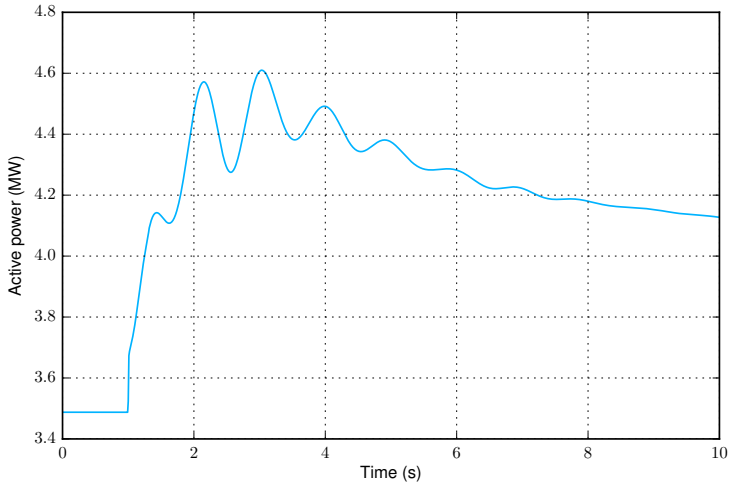


(b) 7 MW battery energy storage system.

Fig. 7.1. Active power response to a frequency decrease for different devices employing the SPC.

the same frequency event caused by the loss of generation in a test power system is shown.

Therefore, if the BESS is meant to reproduce the behavior of a larger unit, its parameters must be defined accordingly. Since these parameters depend on the type of converter controller being employed, their adaption to emulate the response of a

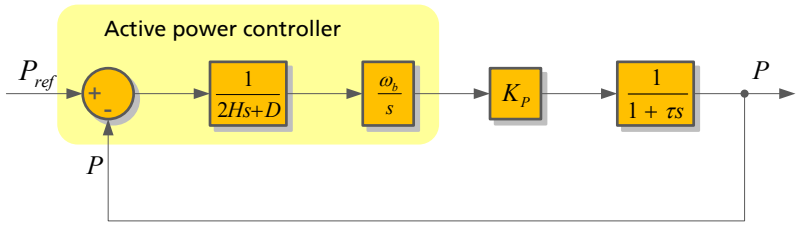


Fig. 7.2. Active power loop of the SPC with low-pass filter.

larger system will also be influenced by the type of converter controller employed. With a conventional controller, it may suffice with scaling up the active power reference affected by the frequency droop (analogously, the reactive power reference responding to voltage control). However, when the SPC is considered, it is necessary to take into account the inertia and other parameters defining the active power response.

### 7.2.1 SPC active power loop

The adaption of the BESS parameters when the SPC is employed requires studying the SPC active power loop in detail. In the following, this loop is analyzed for both SPC versions, modeled as in Section 4.3.3.2. This analysis considers that the grid frequency measurement employed for primary regulation is ideally estimated by an independent synchronization system, and evaluates the response to active power reference and grid frequency variations.

#### 7.2.1.1 SPC with low-pass filter

The resulting active power loop when the original SPC implementation is employed is shown in Fig. 7.2, where the dynamics of the current control loop are modeled simply as a first-order lag, as in the model described in Chapter 4, and $K_P$ is the coefficient linking angle and active power variations after linearizing around the initial operating point:

$$K_P = \frac{EV}{X}\cos\delta_0 \tag{7.1}$$

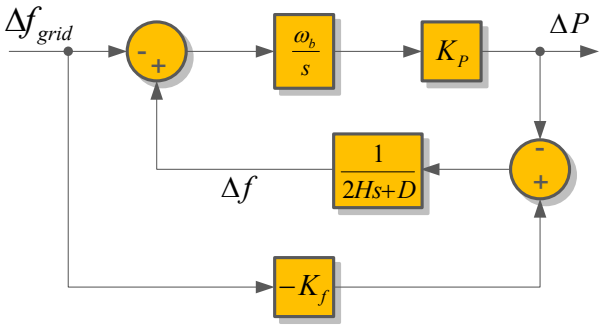


Fig. 7.3. Active power loop of the SPC with low-pass filter considering grid frequency disturbances.

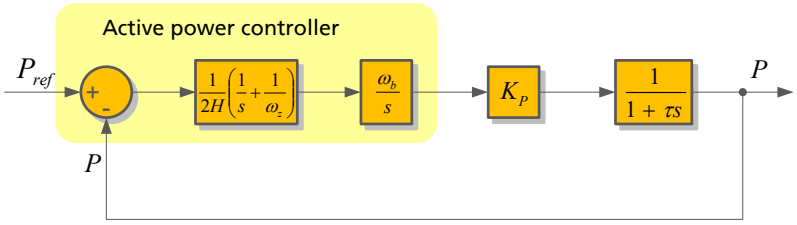


Fig. 7.4. Active power loop of the SPC with PI controller.

Neglecting the dynamics of the current loop, the closed-loop transfer function is then:

$$\frac{\Delta P}{\Delta P_{ref}}(s) = \frac{\frac{K_P \omega_b}{2H}}{s^2 + \frac{D}{2H}s + \frac{K_P \omega_b}{2H}} \tag{7.2}$$

On the other hand, the response to grid frequency variations, neglecting again the current loop dynamics and considering an ideal estimation of the grid frequency for the droop, is described by the loop in Fig. 7.3. In this case, the transfer function becomes:

$$\frac{\Delta P}{\Delta f_{grid}}(s) = -\frac{(2Hs + D + K_f)\frac{K_P \omega_b}{2H}}{s^2 + \frac{D}{2H}s + \frac{K_P \omega_b}{2H}} \tag{7.3}$$

#### 7.2.1.2 SPC with PI controller

The active power loop is slightly modified when the SPC version considering a PI controller is employed, as shown in Fig. 7.4. In this case, the closed-loop transfer

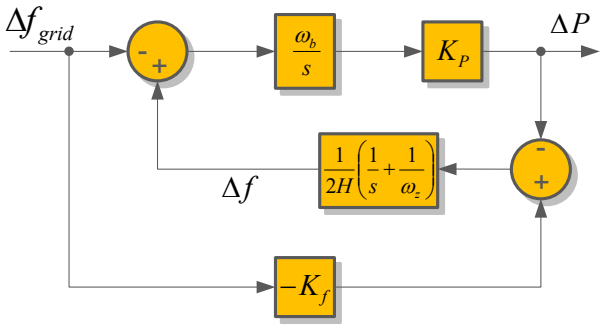


Fig. 7.5. Active power loop of the SPC with PI controller considering grid frequency disturbances.

function is:

$$\frac{\Delta P}{\Delta P_{ref}}(s) = \frac{\left(\frac{s}{\omega_z}+1\right)\frac{K_P\omega_b}{2H}}{s^2+\frac{K_P\omega_b}{2H\omega_z}s+\frac{K_P\omega_b}{2H}} \tag{7.4}$$

The response to grid frequency variations is described by the loop in Fig. 7.5 and the following transfer function:

$$\frac{\Delta P}{\Delta f_{grid}}(s) = -\frac{\left[(2H+K_f/\omega_z)\,s+K_f\right]\frac{K_P\omega_b}{2H}}{s^2+\frac{K_P\omega_b}{2H\omega_z}s+\frac{K_P\omega_b}{2H}} \tag{7.5}$$

### 7.2.2 Corresponding SPC parameters

In order to obtain the same response but scaled up to a greater power level, the adapted parameters should only affect the transfer functions (7.2)–(7.5) by introducing a multiplicative gain. Therefore, the denominator coefficients must remain unchanged, i.e., $\frac{K_P\omega_b}{2H}$, the ratio $\frac{D}{H}$, and the zero given by $\omega_z$ must keep their original values.

A first consequence of this is that the active power closed-loop transfer functions (7.2) and (7.4) with the adapted parameters would be identical to their counterparts with regular parameters. Thus, the active power reference would have to be multiplied by the corresponding gain before using it as an input for this loop.

Given the way in which the SPC reacts to frequency variations, a similar solution cannot be employed for the response to grid frequency variations. Thus, the

multiplicative factor must come from the terms multiplying $\frac{K_P \omega_b}{2H}$ in the numerator. That is to say, $H$, $D$, and $K_f$ have to be multiplied by the scaling-up factor. However, modifying the inertia constant $H$ requires a corresponding variation of $K_P$ in order to keep the same denominator. Theoretically, this variation can be introduced through the virtual reactance, affecting the total reactance $X$ that defines $K_P$.

Alternatively, the BESS can use the same parameters and per-unit system as the PV plant, but considering the current and power limits of the storage system. It is worth noting that this approach is sensitive to the total impedance, whose value changes among different per-unit systems, and may require further variations of the virtual reactance.

### 7.2.3 Performance of the plant inertia emulation with a BESS

Due to several factors, the BESS is not able to reproduce the response of the PV plant despite its parameters are defined to do so, as shown in Fig. 7.6, where the response of a 100 MW PV plant and a 7 MW BESS to a grid frequency event is compared. The PV plant initially injects 93 MW; whereas the BESS is initially not injecting nor absorbing any power, and two ways to emulate the response of the PV plant: the first one uses the same base power as the PV plant, and the second one adapts the values of the inertia constant and frequency droop slope.

The factors altering the performance of the PV response emulation by the BESS affect mainly the coefficient $K_P$, which is obtained from the linearization of the interaction between the SPC and the grid, and thus depends on the characteristics or the state of both elements.

#### 7.2.3.1 Total connection impedance

The factor having most influence on the different response of the BESS when it tries to emulate the complete response of the PV plant with the SPC is the different connection impedance. Despite the small differences due to the PV internal network cable impedance, the total connection impedance is similar for the PV plant equivalent and the BESS using the per-unit system corresponding to each section of the plant. Nevertheless, the BESS impedance is larger when it is written in the PV plant per-unit system, since the base impedance is inversely proportional to the base

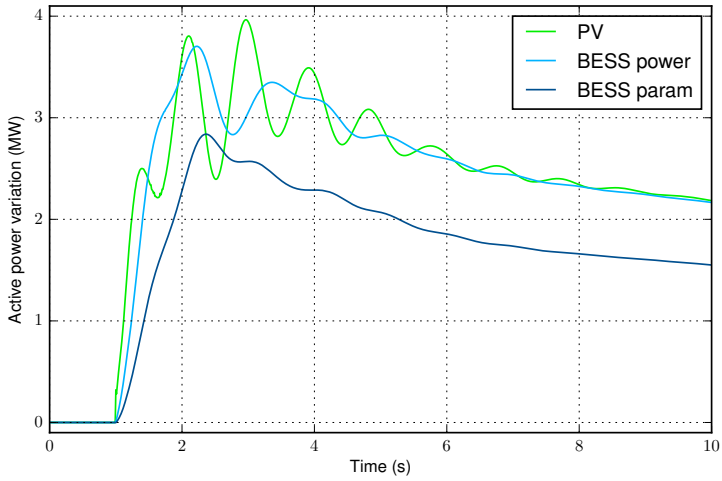


Fig. 7.6. Comparison of the active power response for PV and BESS emulating the response of a larger system.

power. Thus, $K_P$ is reduced, affecting the transfer function poles and slowing down the response.

The impact of the total connection impedance on the response to a grid frequency variation can be seen in Fig. 7.7. In this case, the PV and BESS are initially operating in the same conditions, with zero active power injection, and they do not control the plant voltage, so the only differences are due to their power ratings. Furthermore, the BESS uses the same parameters and base power as the PV. Nevertheless, the response of the BESS is substantially different from the PV plant response. This is avoided just by reducing the BESS equivalent impedance and making it equal to the PV plant impedance, which results in a response that matches the PV plant response almost perfectly (*BESS low Z*). However, this cannot be done in a practical application, since it would require oversizing the BESS transformer.

In order to overcome this issue, the virtual reactance should be reduced, or even made negative, in such a way that the total reactance, and thus also $K_P$, is unaltered. However, as seen in Fig. 7.7 (*BESS virtual Z*), the effectiveness of this solution is limited. This is due to the fact that the transfer function does not capture the full complexity of the model; namely, it neglects the influence of the voltage at the point of connection of the converter, which is affected by the actual connection

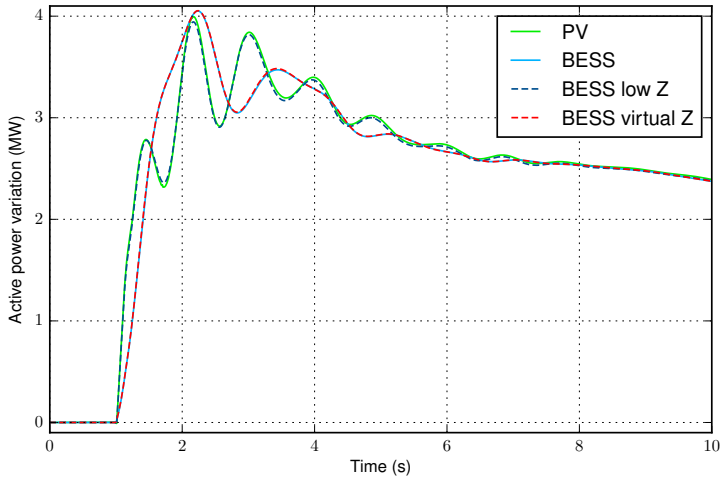


Fig. 7.7. Comparison of the active power response for PV and BESS with different impedance.

impedance.

#### 7.2.3.2 Initial operating point

Another factor influencing the response of the SPC is the initial operating point of the device. Normally, the plant sections whose response is being compared are operating in a different point when their response is required. The PV plant is operating close to its maximum power point, injecting a large amount of active power; whereas the BESS is neither injecting nor absorbing power, waiting for an event for which its contribution is needed.

The initial operating point also affects the coefficient $K_P$, since it determines the SPC internal voltage $E$ and angle relative to the grid $\delta_0$. Therefore, it also affects the active power response, even if the connection impedance is assumed to be equal. As an example, Fig 7.8 shows the active power response of the PV plant to the same grid frequency event, but considering two operating points. The first one is the regular operating point of the PV plant with an active power reserve for frequency control, whereas the other one considers that the PV plant is not injecting any active power, despite being able to do it, as the BESS would do. Additionally, the response of the BESS with a reduced impedance equal to the PV plant impedance is shown. In

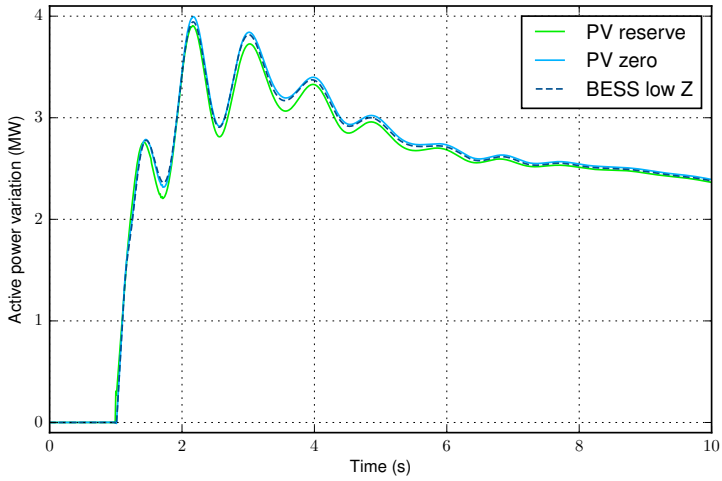


Fig. 7.8. Comparison of the active power response for PV and BESS with different initial operating points.

this figure, the response of the PV system and the BESS are almost identical when none of them injects power. However, if the PV plant is initially injecting 93 MW, its response is slightly different.

In practical applications, this situation cannot easily be avoided, since the PV plant and the BESS will have totally different initial operating points. Nevertheless, the differences in the performance are small and could be neglected.

#### 7.2.3.3 Plant voltage control

Similarly, the participation of the PV plant or the BESS in the plant voltage control may also influence the response of these systems and cause differences between them. The plant voltage controller affects the SPC internal voltage $E$, and thus $K_P$. The different responses obtained for the PV plant with an active power reserve for frequency control, but considering two cases in which it participates and does not participate in the control of the plant voltage, are shown in Fig. 7.9. Once again, there are differences between both responses, with larger oscillations in the case considering plant voltage control.

From this analysis, it is possible to conclude that the BESS has certain limi-

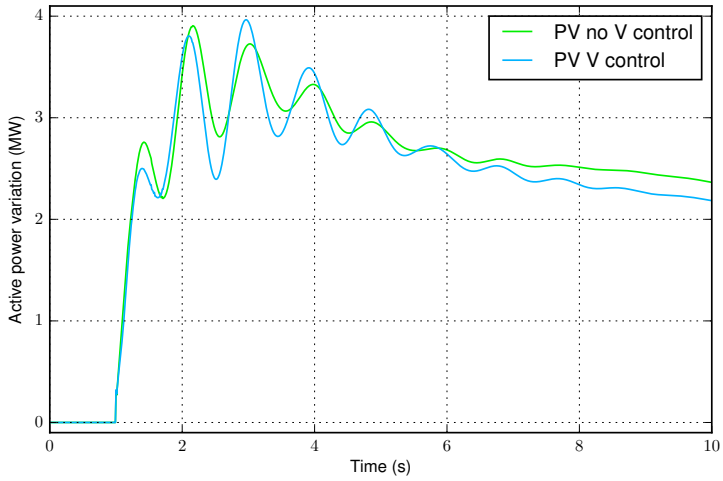


Fig. 7.9. Comparison of the active power response for PV with different plant voltage control options.

tations to reproduce the full response of the PV plant SPC, especially due to the differences in the connection impedance, which have a physical cause that cannot be overcome by modifications of the control. Therefore, the following studies will consider that the BESS performs the duties associated with the droop response of the PV plant when an active power increase is necessary, but it does not aim at emulating its inertial behavior; instead, the SPC BESS considers a regular inertia constant between 2 s and 10 s.

## 7.3 Impact on the 12-bus system

The impact of a hybrid plant consisting of a synchronous generator and PV, and supported by a BESS, is analyzed in the 12-bus test power system employed in previous chapters. Here, the system introduced in [150] is adapted taking into account [151], and no other additional controllers, such as the PSS employed in Chapters 5 and 6 are considered.

The assessment of the impact of the hybrid plant on this system considers a single location for this plant, taking into account that the weakest mode in the system involves generators 1 and 3, and the fact that bus 4 has the second lowest short circuit

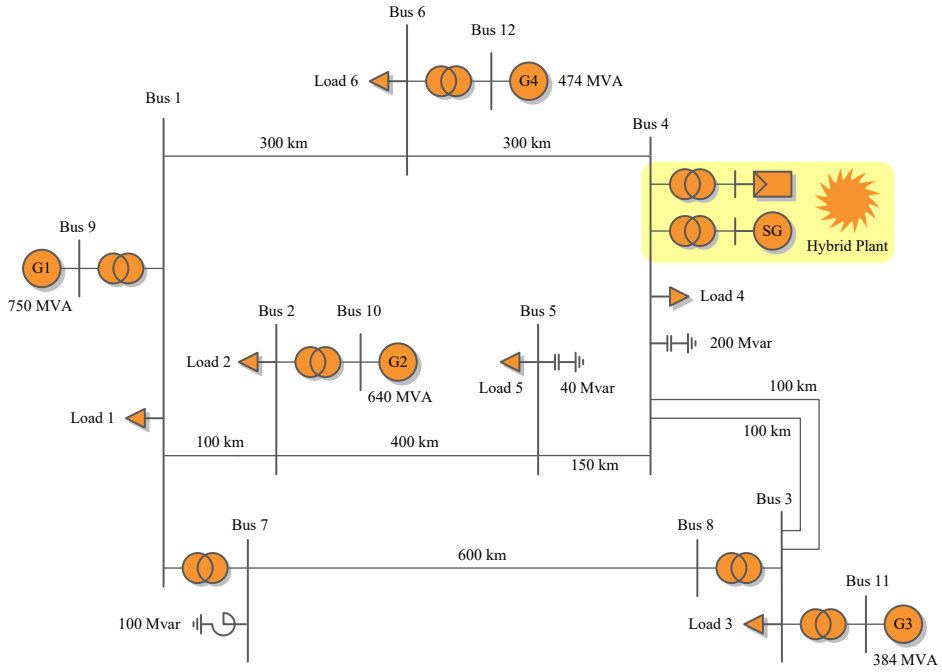


Fig. 7.10. 12-bus system diagram showing the location of the hybrid power plant.

power among the 12-bus system buses. The study comprises the modal analysis of the system and its response to events of different nature, such as load variations or voltage events, and compares the results obtained for a wide range of hybrid plant configurations and controllers.

### 7.3.1 Hybrid power plant scenarios

The analysis of the impact of a hybrid plant on the 12-bus test system considers a single plant connected to bus 4, as shown in Fig. 7.10. Several scenarios sharing a common operating point for the 12-bus system are defined. In these scenarios, the studied power plant injects 200 MW, whereas the remaining generators and the system loads follow Table 7.1, where a base power of 100 MVA is considered. The factors determining the different scenarios are the hybrid plant configuration and the power converter controllers employed.

One the one hand, five different configurations are considered:

Table 7.1. Initial operating point parameters for 12-bus system with a hybrid power plant.

| Element | P (p.u.) | Q (p.u.) | V (p.u.) |
|---|---|---|---|
| G1 | 4.66 | - | 1.00 |
| G2 | 4.00 | - | 1.01 |
| G3 | 2.70 | - | 1.01 |
| G4 | 3.30 | - | 1.01 |
| Load 1 | 3.41 | 2.12 | - |
| Load 2 | 2.84 | 1.38 | - |
| Load 3 | 3.98 | 1.31 | - |
| Load 4 | 3.41 | 2.12 | - |
| Load 5 | 1.14 | 0.55 | - |
| Load 6 | 1.71 | 0.56 | - |

1. Fully synchronous power plant: The power plant is formed by two equal *100 MW* synchronous generators, connected to bus 4 through independent transformers and each one feeding its ancillary loads.

2. Fully photovoltaic power plant: The power plant is formed by a *200 MW* PV generation system represented by a single-converter equivalent.

3. Hybrid power plant: The power plant is formed by one *100 MW* synchronous generator and one *100 MW* PV generation system.

4. Hybrid power plant with PV reserve: The power plant is formed by one *100 MW* synchronous generator and one *100 MW* PV generation system. The PV system injects only 93 MW into the grid, keeping a 7% reserve margin.

5. Hybrid power plant with energy storage: The power plant is formed by one *100 MW* synchronous generator, one *93 MW* PV generation system, and one *7 MW* battery energy storage system.

In the last two cases, generator 1 compensates the reduction in active power generation from the PV plant, injecting 474 MW.

Table 7.2. Code describing the hybrid power plant controllers.

| Code | $x$: SG | $y$: PV | $z$: BESS |
|---|---|---|---|
| 0 | Off | Off | Off |
| 1 | On | Constant | |
| 2 | | Droop | Droop |
| 3 | | SPC | SPC |
| 4 | | SPC, no droop | |
| $r$ | | | PV reserve |

On the other hand, three types of controllers are considered for PV converters. The simplest one considers a non-contributing open-loop vector oriented control with constant active and reactive power references. The second one also consists of an open-loop vector oriented control, but the PV plant controls the voltage at the MV side of the plant transformer, and contributes to frequency regulation. The third one considers the SPC with PI active power control, and the PV plant also controls the voltage at the MV side of the plant transformer. In the case of the BESS, the last two controllers, which enable the participation of the converters in the control of the grid, are also considered. When both the PV plant and the BESS participate in grid control, they share the duties of frequency regulation in such a way that the PV plant responds to overfrequency and the BESS mitigates underfrequency. Furthermore, a particular case where the PV plant is controlled by the SPC but does not contribute to frequency regulation through a droop, and the BESS uses the full SPC with bidirectional droop, is defined.

This wide range of scenarios allows analyzing the impact of different controllers and the performance of the plant when the BESS frees the PV plant from certain control tasks. In order to easily identify them, each scenario is given a code $xyz$, where $x$, $y$, and $z$ are defined according to Table 7.2. Specifically, a 0 means that the corresponding section of the plant is out of service, and letter $r$ is used to indicate that the BESS is not connected but the PV plant operates with a reserve margin (configuration 4).

Table 7.3. Main parameters of the hybrid plant synchronous generator in the 12-bus system.

| Parameter | Symbol | Value |
|---|---|---|
| Rated power | $S_r$ | 144 MVA |
| Rated voltage | $V_r$ | 15 kV |
| Power factor | $PF$ | 0.85 |
| Inertia constant | $H$ | 4.8 s |
| Droop slope | $R_f$ | 5% |
| Voltage controller proportional gain | $k_P^{AVR}$ | 12 p.u. |
| Voltage controller integral gain | $k_I^{AVR}$ | 6 $s^{-1}$ |

In the scenarios including the synchronous generator, its main parameters are the ones summarized in Table 7.3, and its initial active power generation is 112 MW, with 12 MW consumed by the ancillary loads and transformer, and injecting 100 MW at bus 4. In configuration 1, two equal synchronous generators are connected at bus 4 through independent transformers.

The main parameters of the PV plant are BESS are those of their controllers. The main ones, taking into account that some of them apply only for certain controllers, are given in Table 7.4. The power rating and initial active power injection of the PV plant depends on the hybrid plant configuration. Thus, for configuration 2 a base power of 200 MVA is used, for configurations 3 and 4 a base power of 100 MVA is employed, and for configuration 5 the base power is reduced to 93 MVA. The PV plant equivalent converter has a rated power of 1.06 p.u., and a maximum transient power of 1.3 p.u. Furthermore, its maximum power point is around 1.02 p.u., and, when no reserve is considered, it generates 1.013 p.u., which results in an injection of 1 p.u. at bus 4. In the case of the BESS, a base power of 7 MVA is employed, with the same converter ratings, and a capacity of 15 min is considered.

Table 7.4. Main parameters of the hybrid plant PV and BESS in the 12-bus system.

| Parameter | Symbol | Value |
|---|---|---|
| Inertia constant | $H$ | 7 s |
| Damping coefficient | $\zeta$ | 0.7 |
| Virtual resistance | $R$ | 0.1 p.u. |
| Virtual reactance | $X$ | 0.3 p.u. |
| Droop slope | $R_f$ | 5% |
| Voltage controller proportional gain | $k^V$ | 20 p.u. |
| Reactive power controller integral gain | $k_I^Q$ | 10 $s^{-1}$ |

## 7.3.2 Results

The analysis of the 12-bus system considering the different scenarios involving the hybrid power plant includes both modal analysis and time-domain simulation of important disturbances affecting the stability of the power system and the response of the studied plant.

### 7.3.2.1 Eigenvalue analysis

The tuning of the PV plant voltage controller and the SPC inertia constant has taken into account the damping of the critical modes of the power system for different values of these key parameters. The results obtained for the values finally selected can be seen in Fig. 7.11 for all the considered scenarios.

As expected, the hybrid plant has an important influence on the weakest mode of the system, which represents inter-area oscillations between generator 3 and generators 1 and 4. For configuration 1, considering two synchronous machines and no power electronics devices, this mode is poorly damped, with a damping ratio around 3%. However, if the synchronous machines are replaced by PV, as in configuration 2, the corresponding eigenvalue is significantly affected, moving to the surround-

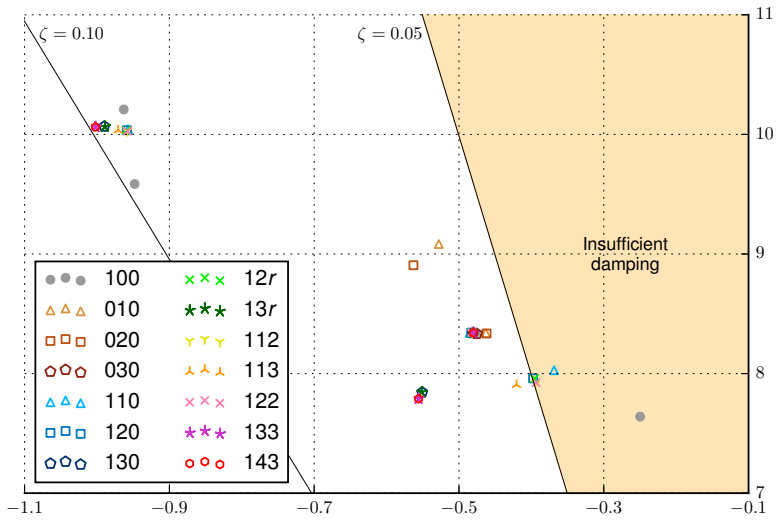


Fig. 7.11. 12-bus system eigenvalue plot considering different hybrid plant scenarios.

ings of $-0.55 \pm 9.0\,j$, and increasing the damping and frequency of the mode, when a controller fixing the output of the PV, or a controller contributing to frequency regulation is considered; when the plant employs the SPC, this mode does not appear among the weakest damped ones.

For actually hybrid configurations, like 3–5, different results are obtained depending on the converter controller. Thus, when neither the PV plant nor the BESS contribute to the control, as in scenario 110, the damping of the mode improves, but it is still below 5%. For the cases where the PV plant or the BESS provide a frequency droop response and voltage regulation (120, 12r, 112, 122), a further improvement is achieved, and the damping ratio of this mode is close to 5%. On the other hand, when the SPC is employed by the PV plant (130, 13r, 133, 143), great improvements of damping are seen, reaching values around 7%. Additionally, it is worth noting that, when the PV plant has a constant power injection and the BESS employs the SPC, the damping of this mode is only slightly better than the cases using the frequency droop.

The other critical modes are not so influenced by the hybrid plant configurations and controllers. Thus, a second mode with a damping ratio around 6% is very similar for all the scenarios considered, and a third one, whose damping approaches

10%, is similar for all the scenarios except without a synchronous machine. Finally, a fourth mode appears only in scenario 100, but its damping ratio is almost 10%.

#### 7.3.2.2 Load increase contingency

The study of the response of the hybrid plant and the whole test power system to an increase in the consumption allows assessing their ability to respond to frequency events that require increasing the active power output. In this case, a 34% increase of both the active and reactive power consumed by load 6, which generates an active power imbalance around 60 MW, is considered. The event starts at $t = 1$ s and the effect on the system frequency and the hybrid power plant active power is discussed next.

The response of the system and the hybrid plant is shown in Fig. 7.12 for configurations 1–3. Namely, the speed of generator 3, considered an indicator of the system frequency and the oscillations due to the critical mode, is depicted in Fig. 7.12a. Three main trends can be distinguished, one for each configuration, and the differences due to the controller employed by the PV plant are very limited. Basically, the amplitude of the frequency deviation increases as synchronous machines are replaced by PV.

The evolution of the frequency is the result of the different amounts of active power reserve available for the hybrid plant, which can be seen in further detail in Fig. 7.12b. The synchronous generator can be overloaded to a greater extent than the PV plant and, therefore, the hybrid plant does a larger contribution when there are two synchronous machines. When one of them is replaced by PV, this contribution is reduced to one half, corresponding to the synchronous generator that remains connected; whereas, in the case with no synchronous machines, the hybrid plant cannot increase its active power injection over its initial value, and the only appreciable response is the absorption of oscillations when the SPC is considered.

In this case, it is worth noting that the PV plant is able to ride through this frequency event despite having no active power reserve and not being able to contribute to a great extent. Anyway, the SPC allows the plant to contribute to the damping of the power system without compromising the stability of the power plant.

The results change when the PV plant operates with active power reserve, as

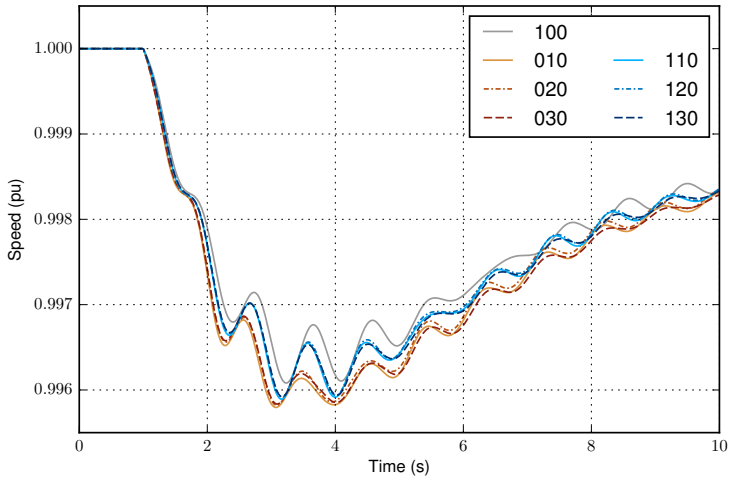


(a) Generator 3 speed.

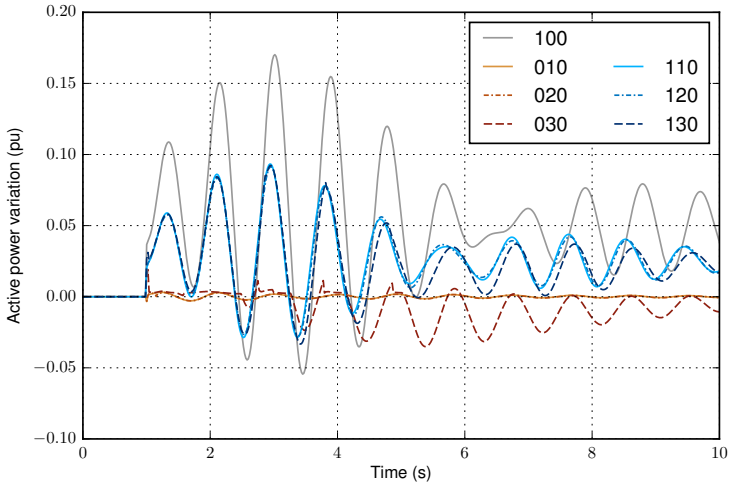


(b) Hybrid plant active power variation.

Fig. 7.12. 12-bus system response to a load increase for hybrid plant configurations 1–3.

seen in Fig. 7.13. In this case, the evolution of the power system frequency improves with respect to the scenarios without reserves, but also to the case with two synchronous machines. Furthermore, more differences are seen depending on the controller employed, and the SPC reduces the maximum deviation slightly. This is due to the response of the plant, which can now react to the event, as shown in

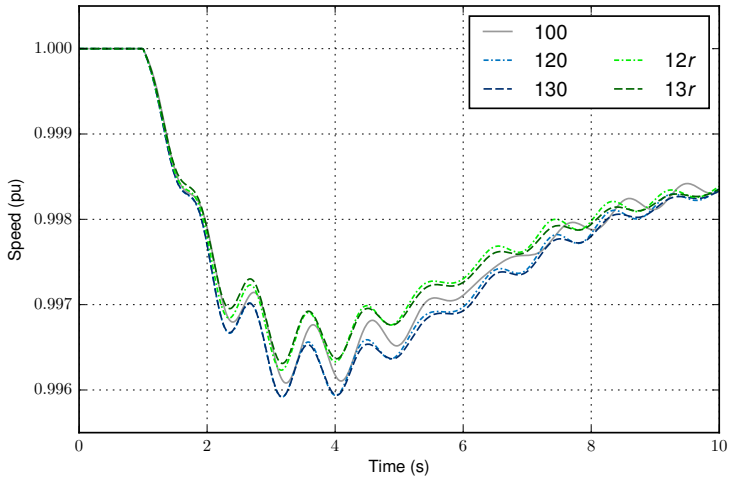


(a) Generator 3 speed.

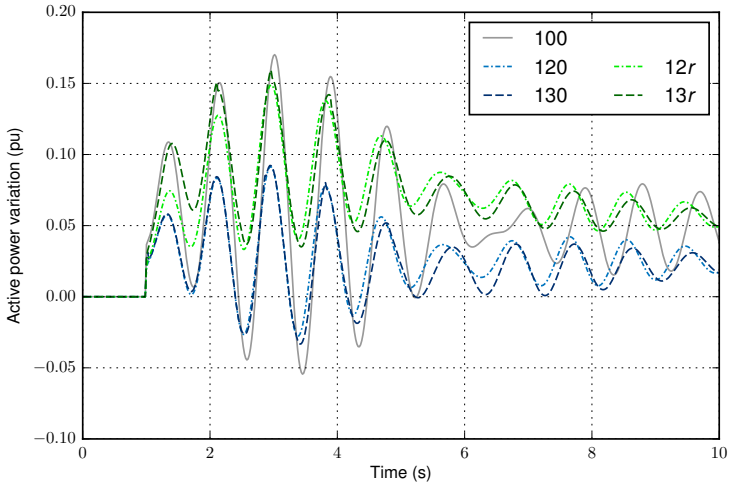


(b) Hybrid plant active power variation.

Fig. 7.13. 12-bus system response to a load increase considering PV active power reserve.

Fig. 7.13b. With droop, the response of the plant is similar to the case with synchronous generators after 2 s. However, at the beginning of the transient, it is not able to match the fast reaction of the synchronous machines. With the SPC and its additional inertia, the hybrid plant is able to reproduce the fast response of the synchronous machine, which allows reducing the maximum frequency deviation.

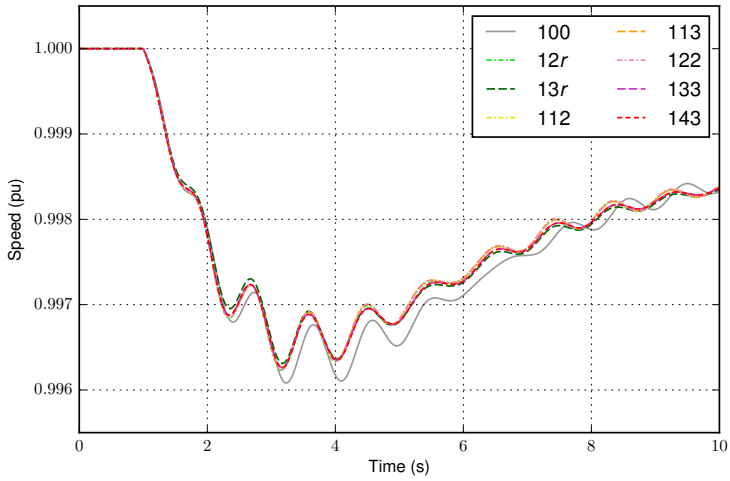


(a) Generator 3 speed.

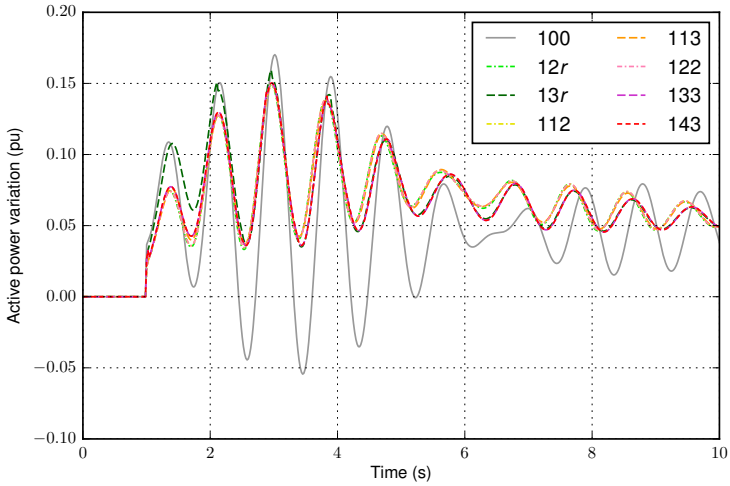


(b) Hybrid plant active power variation.

Fig. 7.14. 12-bus system response to a load increase considering the BESS.

Moreover, in both cases with PV considering reserve, the hybrid plant output is less oscillating than in configuration 1.

The response of the system, comparing the cases with PV reserve and BESS, is shown in Fig. 7.14. The response of the plant, and its effect on the system, is similar for all cases, with the only difference of the additional inertia provided by the PV

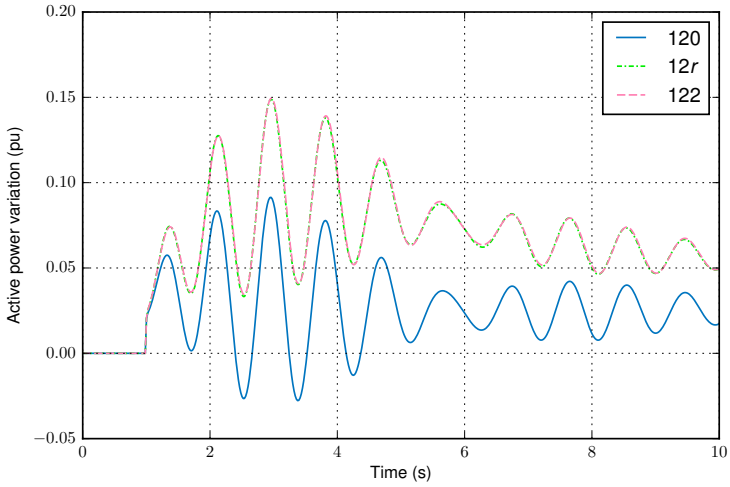


(a) Employing droop.

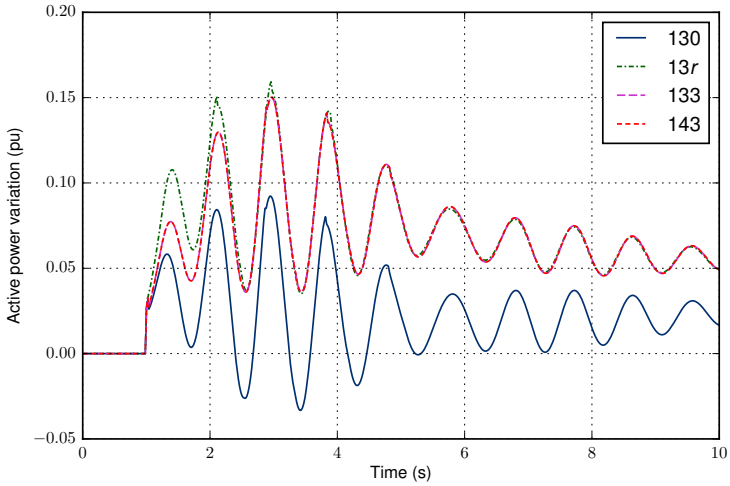


(b) Employing the SPC.

Fig. 7.15. Hybrid power plant active power variation after a load increase considering different controllers and configurations.

plant when it operates with reserve and employs the SPC.

Finally, a comparison of different configurations employing the same controllers is given in Fig. 7.15. In Fig. 7.15a, the cases considering a frequency droop are compared. The response of the hybrid plant is almost identical in scenarios 12$r$ and 122, where the PV plant and the BESS respectively contribute to the control

of the system; whereas it is reduced in scenario 120, where this contribution comes only from the synchronous generator. When the SPC is employed, as in Fig. 7.15b, there is again an important difference between scenario 130 and the other three scenarios. However, these give rise to different responses depending on whether the contribution is done by the PV plant or the BESS, due to the additional inertia emulated by the PV plant.

#### 7.3.2.3 Load decrease contingency

The opposite event is studied here. In this case, the plant must respond to a frequency rise by reducing its active power output, which can be done by the PV plant without active power reserve. In this case, a 60% reduction of load 6, occurring at $t = 1$ s, is considered, causing an imbalance of more than 100 MW.

The system response for hybrid plant configurations 1–3 is shown in Fig. 7.16. The system frequency represented by the speed of generator 3 in Fig. 7.16a shows that the worst cases are those that consider a non-reacting PV plant, 010 and 110. Otherwise, the maximum frequency deviation and the amplitude of the oscillations are reduced in a greater extent as the amount of PV increases. Furthermore, the use of the SPC contributes to reducing the frequency deviation and increasing the damping in the system.

The effects on the frequency agree with the hybrid plant response shown in Fig. 7.16b. The low contribution of the grid-feeding PV contrasts with the response when more participating controllers are used. Furthermore, the SPC enables a faster initial reaction of the plant that eventually results in a reduction of the maximum deviation. It is worth noting that the SPC gives the PV plant a more oscillating behavior in configuration 2, compared with the case with droop, but the oscillations are similar for both controllers when the actually hybrid configuration 3 is considered.

The independence from active power reserves can be checked in Fig. 7.17, which shows how the active power response of the PV plant, and thus the system frequency, is not affected by the availability of active power reserves. The response of the PV plant, in this case, is defined only but the type of controller employed, and it is not constrained by the active power handling capability of the PV plant. Therefore, no active power reserves nor BESS would be needed to respond to over-

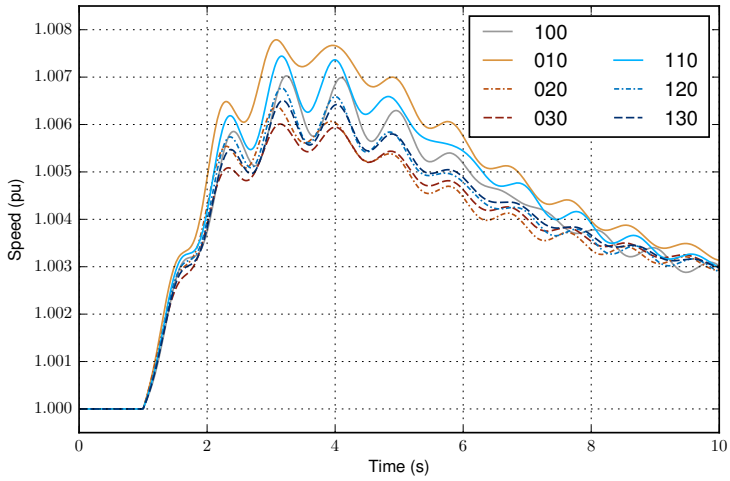


(a) Generator 3 speed.

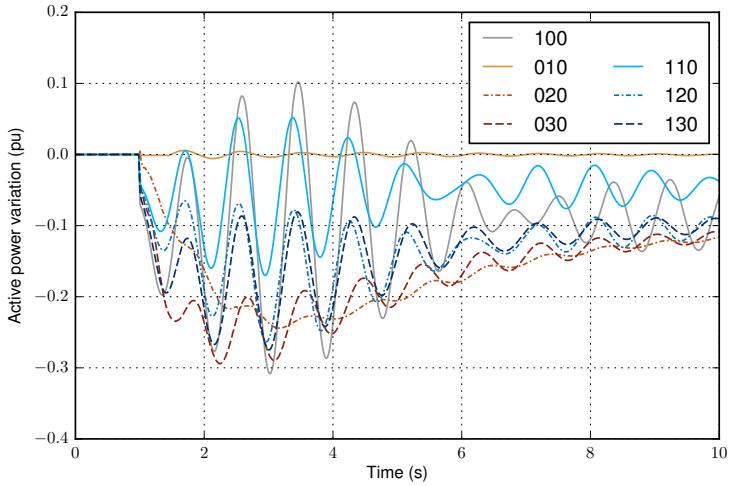


(b) Hybrid plant active power variation.

Fig. 7.16. 12-bus system response to a load reduction for hybrid plant configurations 1–3.

frequency events.

When the BESS is considered, as in Fig. 7.18, there are also slight differences among controllers and configurations. The cases with a full contribution by the PV plant, with the SPC and droop, result in faster and larger active power responses of the hybrid plant and slight reductions of the maximum frequency deviation; whereas

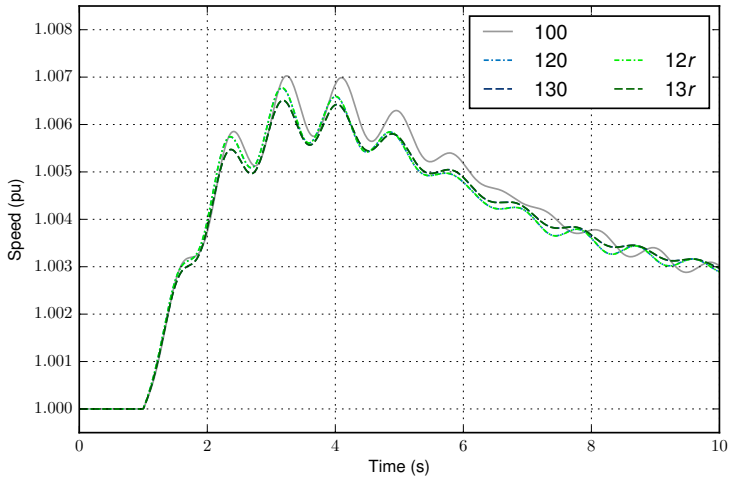


(a) Generator 3 speed.

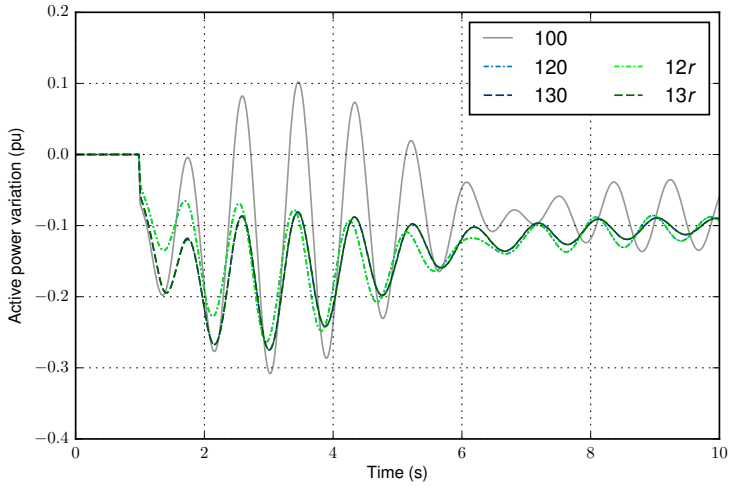


(b) Hybrid plant active power variation.

Fig. 7.17. 12-bus system response to a load reduction considering PV active power reserve.

the cases considering only droop differ from the previous during the first 2 s after the event, but follow a similar evolution afterwards. Midway between these two types of response, it is possible to find scenario 143, with a large initial contribution that later decays as the droop is provided by the BESS instead of the PV plant. Finally, the cases considering a constant PV injection and contribution only from the BESS

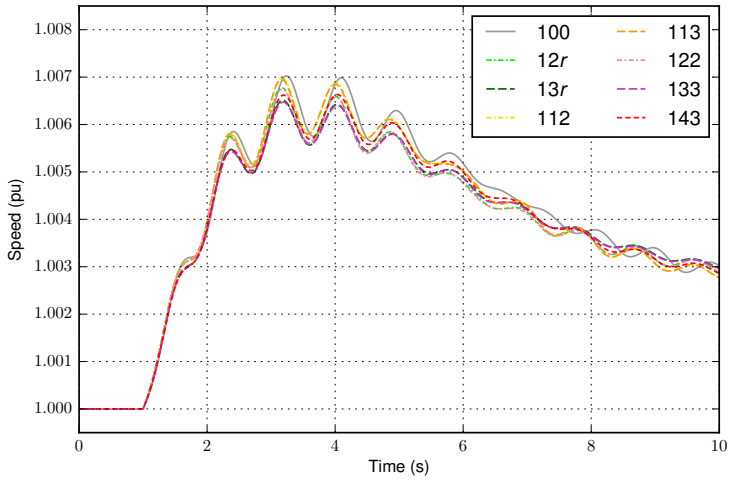


(a) Generator 3 speed.

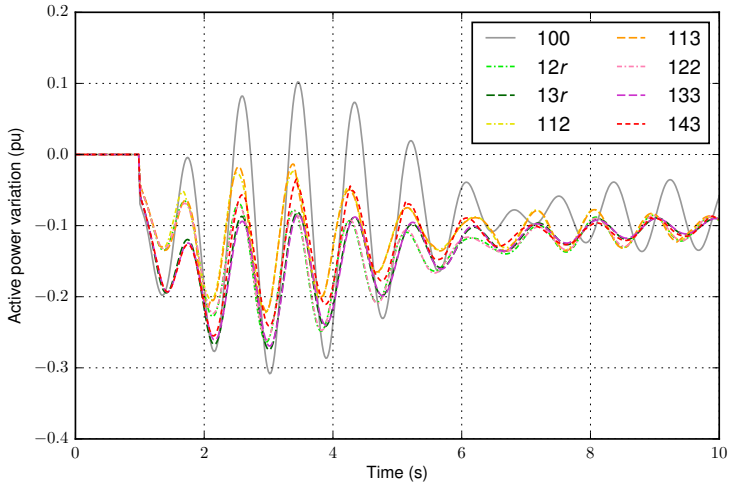


(b) Hybrid plant active power variation.

Fig. 7.18. 12-bus system response to a load reduction considering the BESS.

have a weaker response, but are still able to improve the response of the purely synchronous configuration 1 slightly.

The low incidence of the availability of reserves can be seen in Fig. 7.19. The main differences are due to the employed controller, but the configuration of the hybrid plant does not introduce appreciable variations. In fact, the only visible dif-

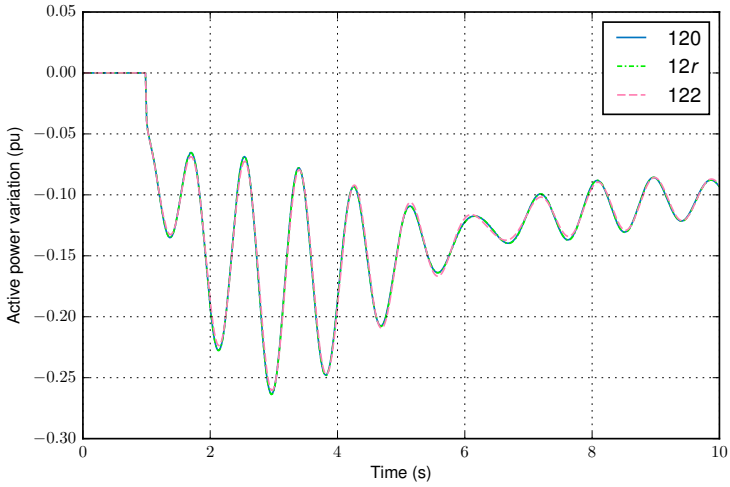


(a) Employing droop.

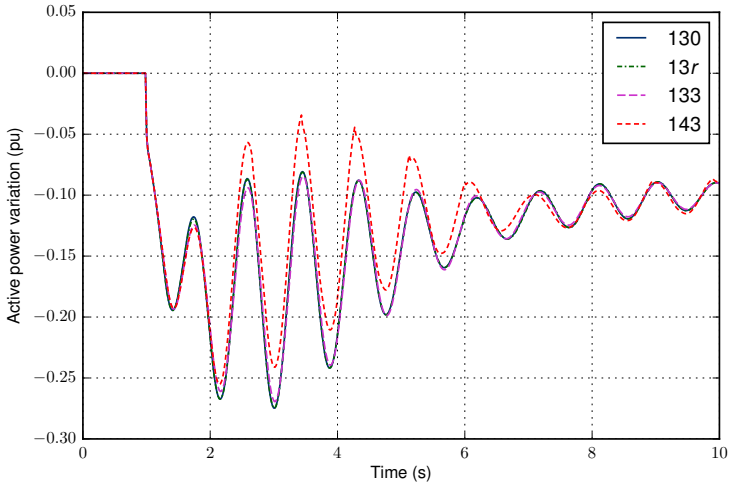


(b) Employing the SPC.

Fig. 7.19. Hybrid power plant active power variation after a load reduction considering different controllers and configurations.

ferences when a same controller is used arise in scenario 143, when the PV plant is controlled by the SPC, but it does not perform a frequency droop, transferring this task to the BESS. In this scenario, the initial contribution is similar to all the other cases employing the SPC. Afterwards, this effect is lost as the inertial response of the PV plant fades away and the contribution of the BESS is constrained. This is

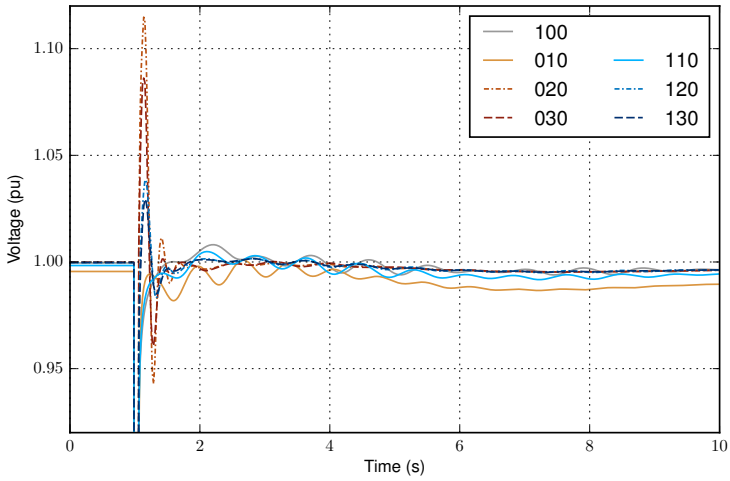


Fig. 7.20. Bus 4 voltage after a contingency on line 4-5 for hybrid plant configurations 1–3.

due to the limited size of the BESS, which does not allow reducing the total active power output of the hybrid plant as much as in the cases where the PV plant reduces its active power injection. Finally, during the last stage of the transient, the power rating of the BESS is enough to provide the expected droop response, and the total hybrid plant active power injection is similar to the other cases with the SPC.

#### 7.3.2.4 Line contingency

This event involves a short-circuit fault and the disconnection of the affected line, which affects severely the power system and modifies its topology and power transfer capability. The fault, a symmetrical short circuit to ground, takes place on line 4-5, 30 km away from bus 4, at $t = 1$ s, and is cleared 50 ms later, after the line is open at both endpoints.

The fault and the disconnection of the line cause a severe impact on the voltage at bus 4, where the hybrid plant is connected. The evolution of this voltage for configurations 1–3 can be seen in Fig. 7.20. Immediately after the line is tripped, the voltage recovers with some oscillations. When the PV plant participates in the control of the power system, this recovery results in a transient overvoltage at bus 4, greater when there is no synchronous generator and when the converter controller

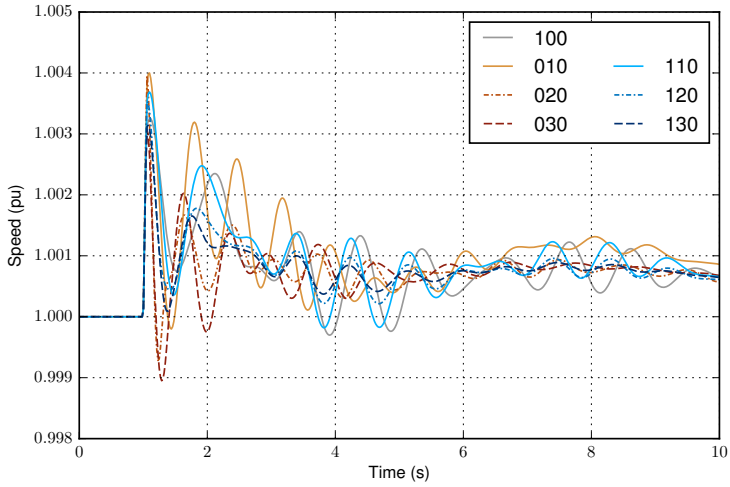


(a) Generator 3 speed.

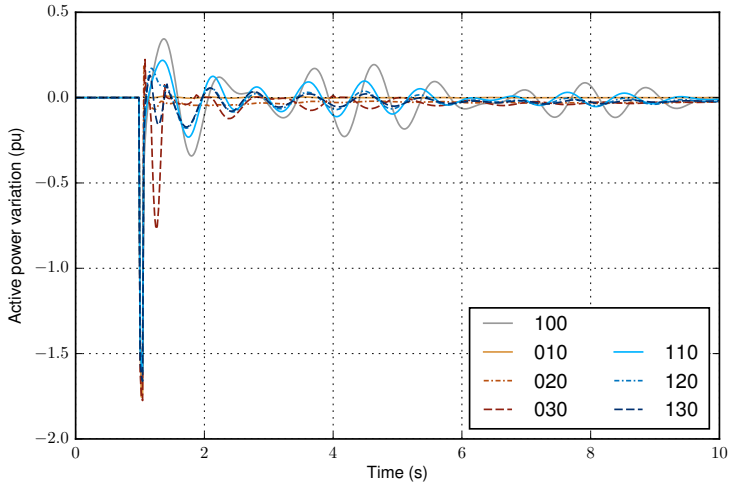


(b) Hybrid plant active power variation.

Fig. 7.21. 12-bus system response to a contingency on line 4-5 for hybrid plant configurations 1–3.

employs only droop. However, the succeeding oscillations are better damped with a grid-supporting PV plant, with better results again for the SPC.

The evolution of the system frequency, given by the speed of generator 3 in Fig. 7.21a, is defined by oscillations, which are, in agreement with the results obtained for the voltage, better damped when the PV plant contributes to the control of

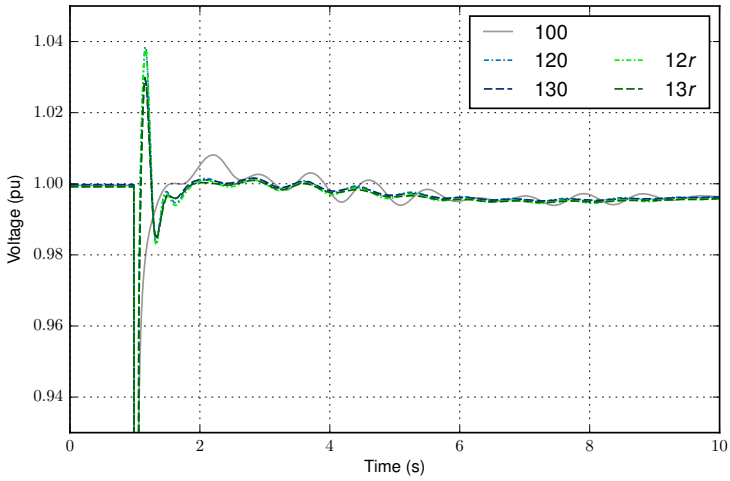


Fig. 7.22. Bus 4 voltage after a contingency on line 4-5 considering PV active power reserve.

the system. It is worth noting that hybrid plant scenarios 120 and 130 give rise to a more damped response that configurations without PV or a synchronous generator, thus showing some benefits of combining both technologies.

The active power response of the hybrid plant, which is depicted in Fig. 7.21b, shows a sharp decrease in the active power injection during the fault, due to the low voltage level. After the line is disconnected, the active power injection recovers, with some oscillations in the cases where the hybrid plant includes synchronous generation.

Once again, since the hybrid plant does not require an important additional injection of active power to respond to this event, the responses obtained when the active power reserve margin is considered are practically the same as in the scenarios without reserve. Namely, there is a small overvoltage after the fault is cleared, as shown in Fig. 7.22, and the speed of generator 3 and the active power injection by the hybrid plant experiment better damped oscillations than for configuration 1, as can be seen in Fig. 7.23.

Similar conclusions can be drawn for configuration 5, whose results are given in Figs. 7.24 and 7.25. In this case, however, there are slight differences among scenarios.

On the one hand, scenarios 112 and 113, with a passive PV plant, show a visibly

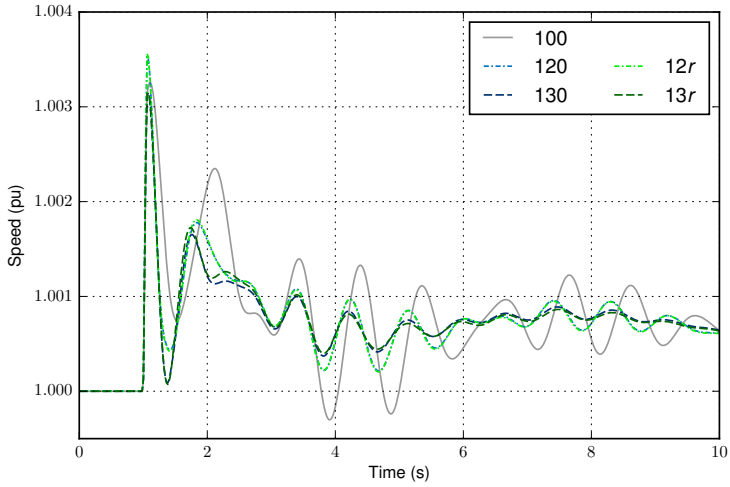


(a) Generator 3 speed.

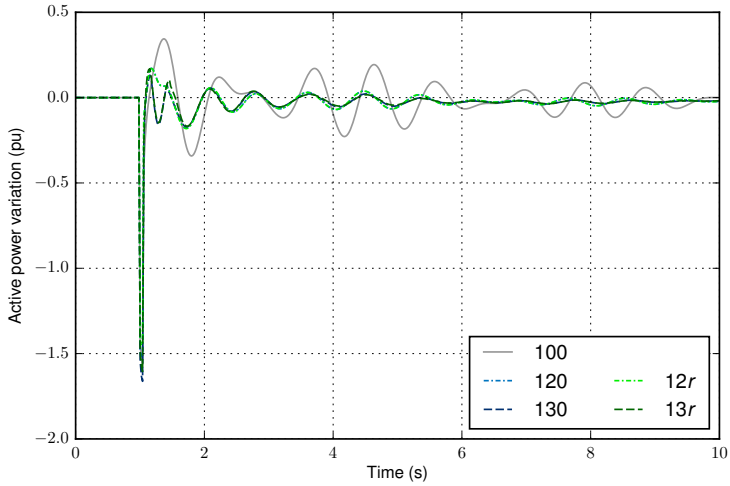


(b) Hybrid plant active power variation.

Fig. 7.23. 12-bus system response to a contingency on line 4-5 considering PV active power reserve.

different behavior, with less damping, especially in the case of the system frequency. Additionally, scenarios considering the BESS exhibit some differences with respect to their corresponding ones considering an active power reserve margin for the PV plant. Basically, the first swing of the speed of generator 3 is similar for corresponding scenarios, but the oscillations that follow are slightly less damped when the PV

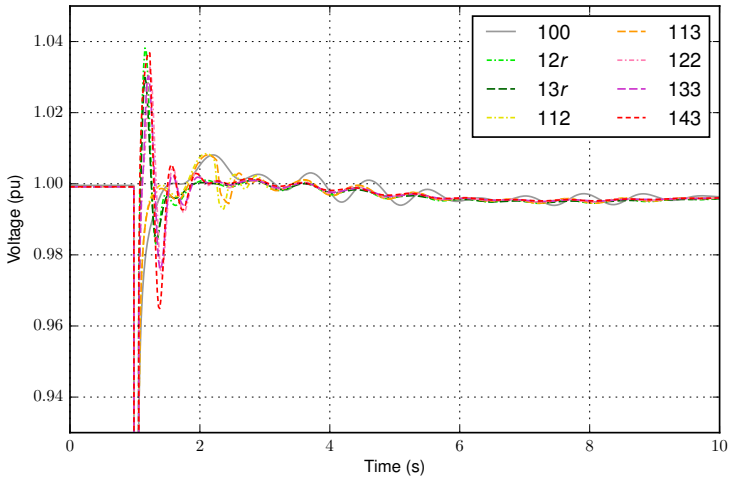


Fig. 7.24. Bus 4 voltage after a contingency on line 4-5 considering the BESS.

plant reserve is replaced by the BESS.

This can be seen in more detail in Figs. 7.26 and 7.27, where different configurations employing the same controllers are compared.

Thus, in Fig. 7.26a, the voltage at bus 4 shows a similar behavior for scenarios 120 and 12*r*, both of them considering only a synchronous machine and the PV plant, but no BESS, and with the only difference of the initial active power injection of the PV plant. However, this measurement changes when the BESS is connected in scenario 122. Initially, the connection of the BESS is able to limit the maximum voltage, but this is done at the expense of a larger amplitude of oscillations afterwards. In any case, these oscillations are faster and soon fade away, resulting in a similar response two seconds after the event takes place.

When the SPC is used, as in Fig. 7.26b, the connection of the BESS does not achieve the same improvement in reducing the overvoltage. In scenario 133, where the PV plant still develops the full SPC response with droop, the maximum voltage is delayed for a few instants, but larger amplitude, fast oscillations occur once more. In scenario 143, where the PV plant emulates inertia but does not perform a droop response, the maximum voltage increases, and so does the amplitude of the oscillations that follow, which are nonetheless well damped.

The active power injection by the hybrid plant also shows a different behav-

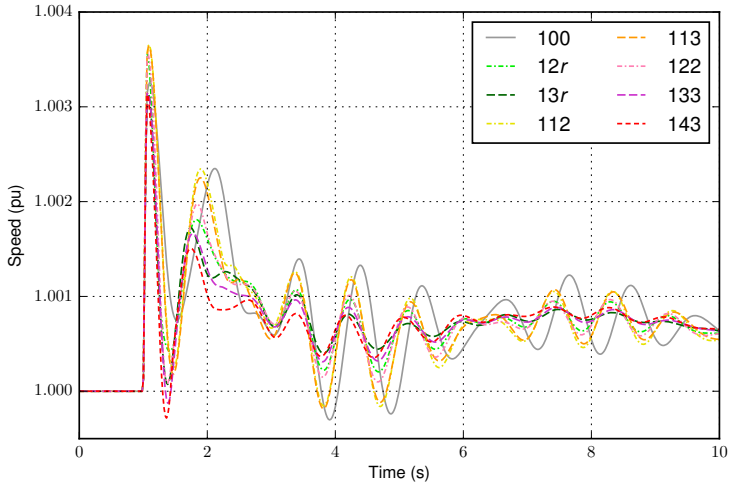


(a) Generator 3 speed.

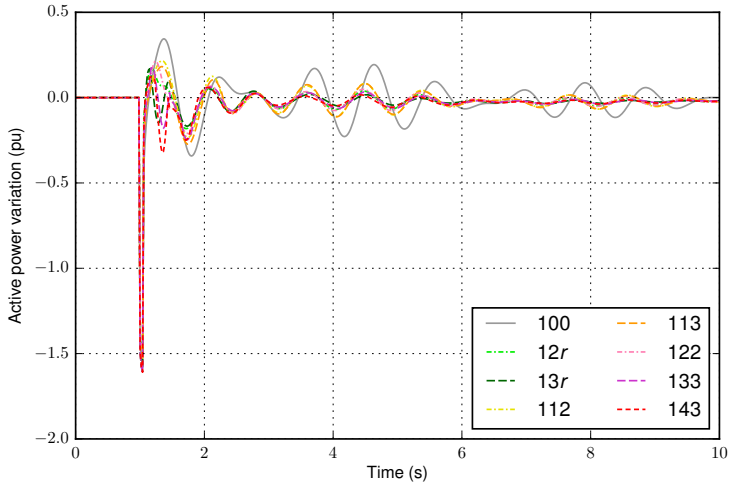


(b) Hybrid plant active power variation.

Fig. 7.25. 12-bus system response to a contingency on line 4-5 considering the BESS.

ior during the first second after the short circuit occurs. For the cases considering droop, this can be seen in Fig. 7.27a, where scenario 122 exhibits a more oscillating behavior of the plant during the first two swings.

The cases with the SPC show a greater variety of responses in Fig. 7.27b. First, it is possible to identify slight differences between scenarios 130 and 13*r*, i.e., a slight

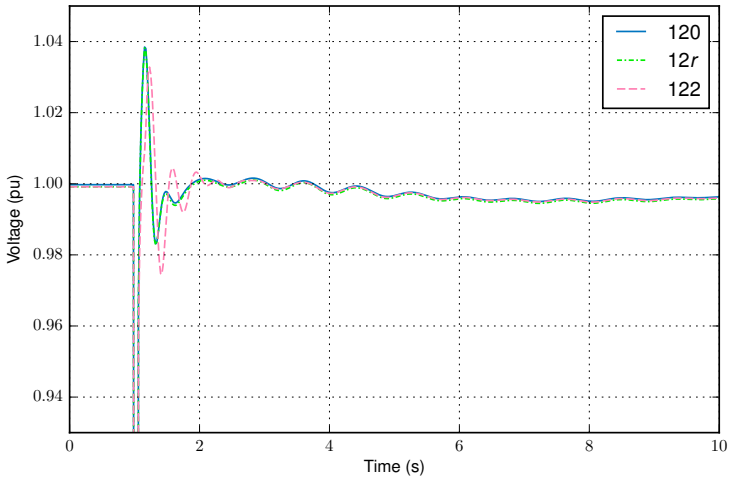


(a) Employing droop.

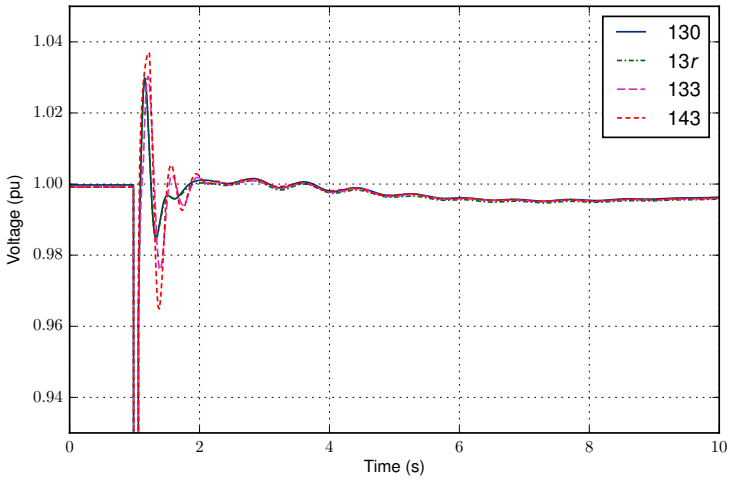


(b) Employing the SPC.

Fig. 7.26. Bus 4 voltage after a contingency on line 4-5 considering different controllers and configurations.

influence of the active power reserve. Namely, when the PV plant has a reserve margin, it is able to increase its active power output around the maximum of the oscillation, whereas it becomes constrained by the dc voltage controller in case there is no reserve.

Furthermore, adding the BESS also enables this active power increase, but it is

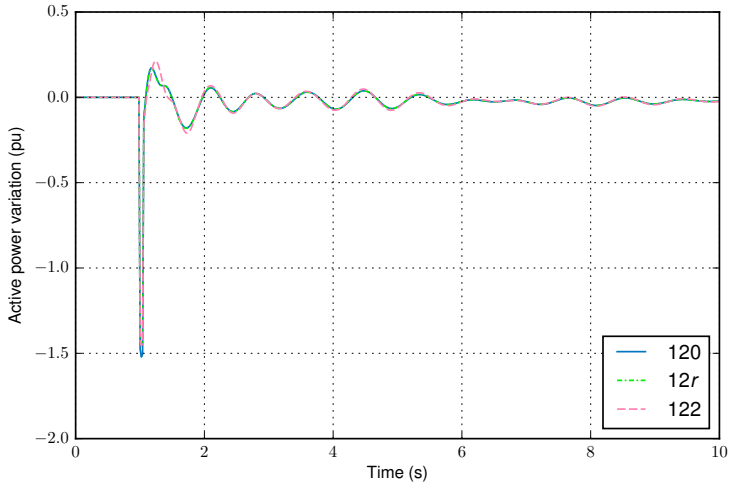


(a) Employing droop.

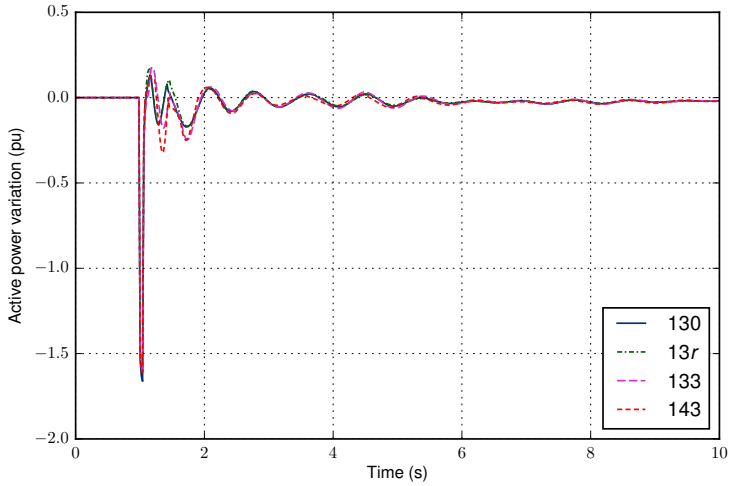


(b) Employing the SPC.

Fig. 7.27. Hybrid power plant active power variation after a contingency on line 4-5 considering different controllers and configurations.

accompanied by a delay in the maximum active power injection which is also seen in the following minimum. Afterwards, the hybrid plant does not recover the same active power level, and the second minimum is lower. In scenario 143, for which the PV does not provide frequency regulation, the hybrid plant oscillates at a lower level with respect to all the other scenarios during the first second after the event.

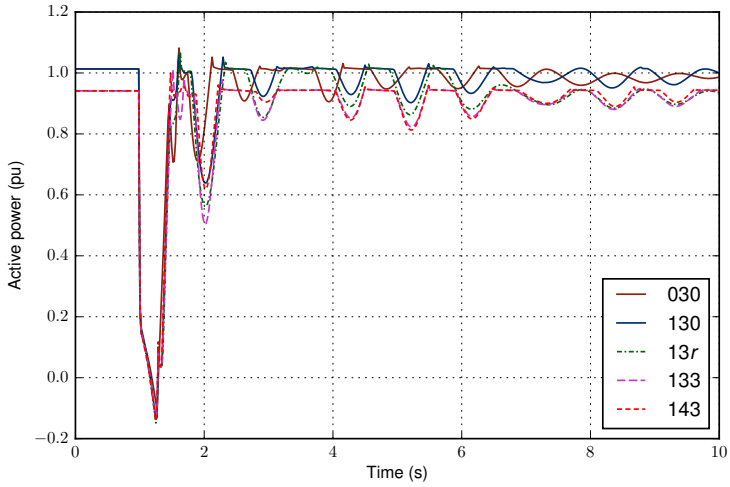


(a) 275 ms.

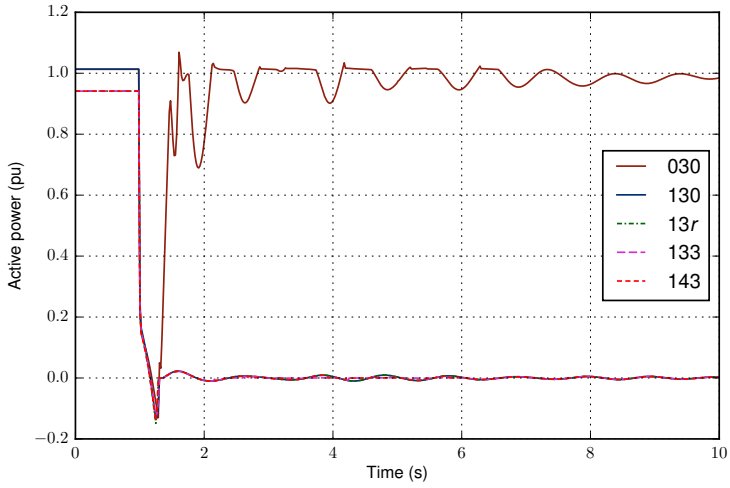


(b) 290 ms.

Fig. 7.28. PV power plant active power employing the SPC after a contingency on line 4-5 for different short-circuit clearing times.

Additionally, for an event of this kind, it is worth studying the impact of the clearing time on the response of the system, and especially, of the power plants. In this case, the stability of the synchronous generators in the system and the hybrid plant does not seem severely affected by the duration of fault. However, the PV plant suffers certain problems when the SPC is used, as shown in Fig. 7.28.

For a short-circuit clearing time of 275 ms, as in Fig. 7.28a, the PV plant sees its active power injection reduced. In fact, during the last part of the event, it starts absorbing active power, which charges the dc link capacitor. However, this voltage is kept within safe limits and the PV plant is able to continue operating after the fault is cleared, rapidly increasing its active power output, and reacting with the typical oscillations of a synchronous machine.

Nevertheless, when this clearing time is increased to 290 ms, as in Fig. 7.28b, the fault is too long and the PV plant equivalent converter is tripped because its dc voltage reaches its maximum operating voltage. Scenario 030, where the PV plant does not work in conjunction with a synchronous machine, withstands this event, but cannot do it for clearing times of 350 ms or longer.

On the other hand, as shown in Fig. 7.29 for a clearing time of 350 ms, the PV plant is able to survive long short circuits when other controllers are used. With a conventional controller injecting constant power, the PV plant reduces its output, but it is constantly over zero, so no overvoltage is generated in the dc side, and the PV plant soon recovers its initial injection, almost with no oscillations.

The response during the fault is similar when the droop is considered, as depicted in Fig. 7.29b, and the PV plant is also able to remain connected. However, with this controller, the PV plant does not recover its initial injection immediately, but it follows a steady recovery with over-imposed oscillations.

These results indicate that the SPC may induce an undesired behavior during a voltage sag, overcharging the dc capacitor. Thus, adequate measures to avoid this should be considered in the control loop, and the model should reach this degree of detail if reliable conclusions about the response of the plant to this type of events are to be drawn. Furthermore, it is worth noting that the models of the conventional controllers employed in this analysis are very simple and assume an ideal synchronization with the grid. Therefore, a detailed comparison of the response of the PV plant during voltage sags should also include the dynamics of the PLL or FLL by the conventional controller.

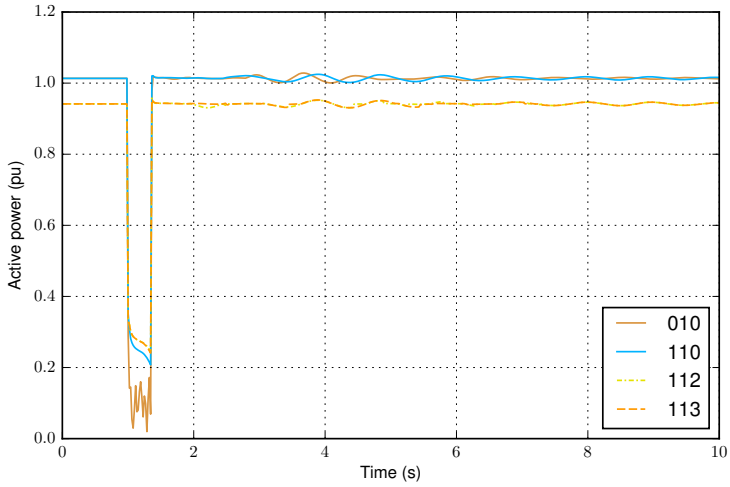


(a) Constant PV.

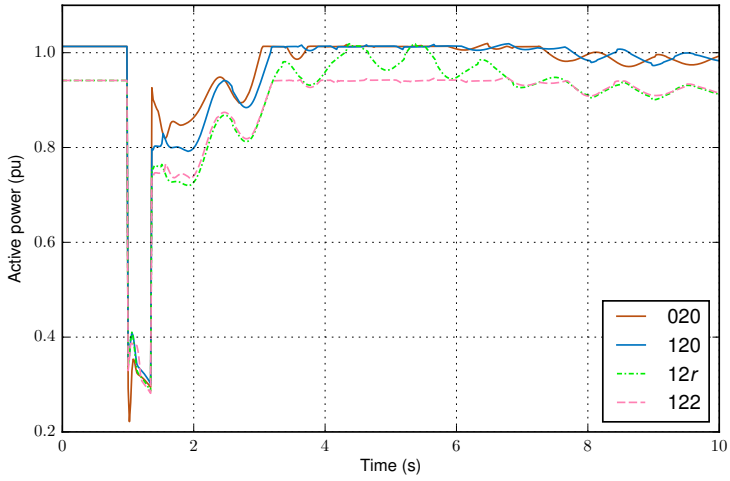


(b) Employing droop.

Fig. 7.29. PV power plant active power employing different controllers after a contingency on line 4-5 with a short-circuit clearing time of 350 ms.

#### 7.3.2.5 Voltage surge

Finally, the consequences of a voltage surge are analyzed. The disturbance is caused by the connection of a 120 Mvar capacitor at bus 4 for 2 s, starting at $t = 1$ s. As shown in Fig. 7.30, this causes two transients. First, the voltage rises sharply and

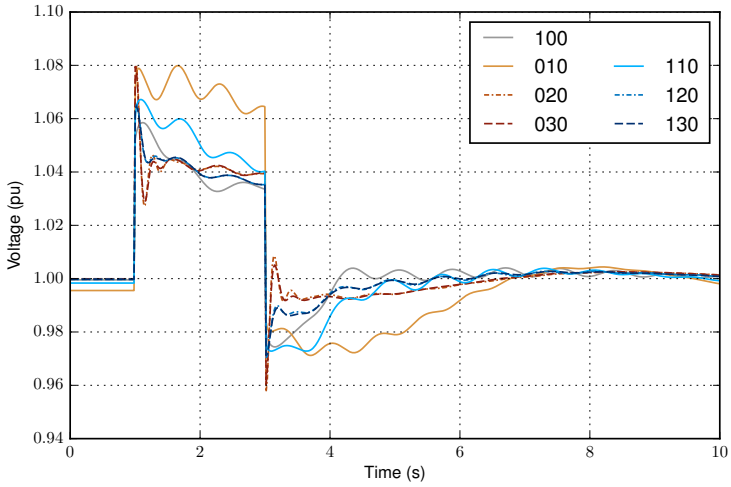


Fig. 7.30. Bus 4 voltage after a voltage surge for hybrid plant configurations 1–3.

reaches a maximum around 1.08 p.u., and it slowly tends towards a lower value which depends on the hybrid plant configuration. Thus, for scenario 100 and those considering a PV plant that participates in the control of the grid, the voltage oscillates around 1.04 p.u.; whereas this value, and the amplitude of the oscillations, are greater when the PV does not contribute to the control of the system, especially if no other generating units are considered as in case 010.

Further conclusions can be drawn from the study of the system response, in particular, the speed of generator 3 depicted in Fig. 7.31a. The larger voltage variations observed when the PV plant provides a constant power injection result in larger load variations, which, together with the reduced participation by the hybrid plant, contribute to greater frequency deviations. On the other hand, the PV converter controller or the hybrid plant configuration appear to have only a slight influence on the system frequency, and the results are very similar to those obtained when the plant consists only of synchronous machines.

The active power of the hybrid plant, shown in Fig. 7.31b, oscillates for the scenarios including a synchronous machine, but it remains constant during the period when the capacitor remains connected when it is formed only by a PV plant. This is due to the lack of active power reserve of this plant. When the capacitor is removed, the SPC induces a fast response of the PV plant, and this response is slower when

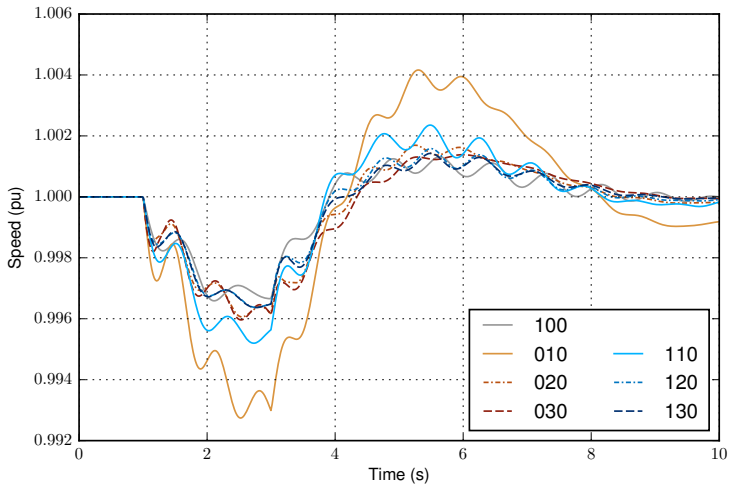


(a) Generator 3 speed.

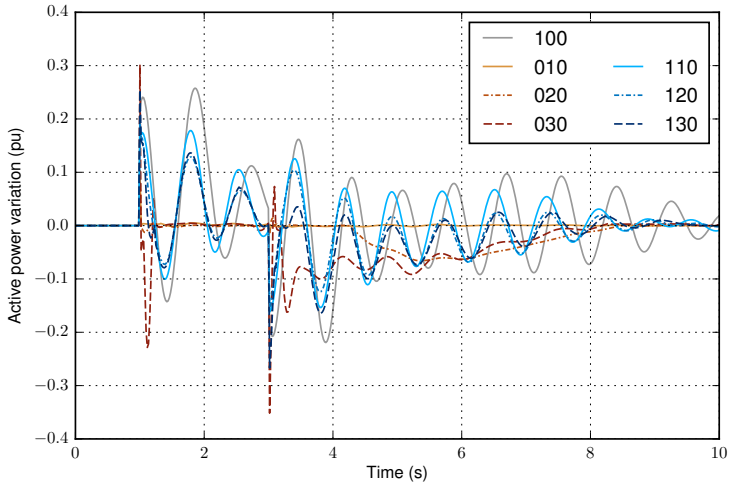


(b) Hybrid plant active power variation.

Fig. 7.31. 12-bus system response to a voltage surge at bus 4 for hybrid plant configurations 1–3.

only droop is considered. In scenario 010, with a non-reacting PV plant, the hybrid plant active power remains almost constant. In the cases considering an actually hybrid configuration, the participation of the PV plant in the control allows reducing the oscillations of the whole plant, slightly more effectively when the SPC is considered.

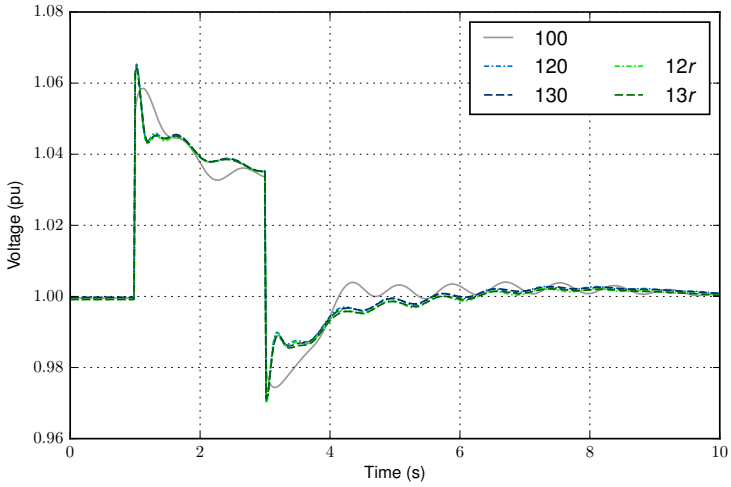


Fig. 7.32. Bus 4 voltage after a voltage surge considering PV active power reserve.

For this event, the comparison of configurations 3 and 4 is more interesting than for the previous two. On the one hand, the reserve margin does not seem to have a visible influence on the evolution of the voltage at bus 4 in Fig. 7.32. In fact, both controllers, droop and SPC, give rise to a very similar evolution of the voltage, which only differs from the response of the synchronous machine because the damping of the latter is weaker.

On the other hand, the availability of this active power reserve margin produces certain differences in the speed of the system and the active power response of the hybrid plant, which could be expected taking into account the stronger relation between active power and frequency than it has with voltage.

The differences in the speed of generator 3 in Fig. 7.33a are more significant during the first 2 s of the transient. During this period, the voltage increases, and so does the load. The frequency decreases, which would require an active power increase from the hybrid plant. However, in scenarios 120 and 130, this increase is limited because the PV plant is operating around its maximum power point. This is not the case, when the PV plant has certain reserve margin, enabling its contribution to limiting the frequency deviation. Furthermore, the SPC achieves a slight improvement in the maximum deviation with respect to the droop controller.

After the capacitor is disconnected again, the responses for different configura-

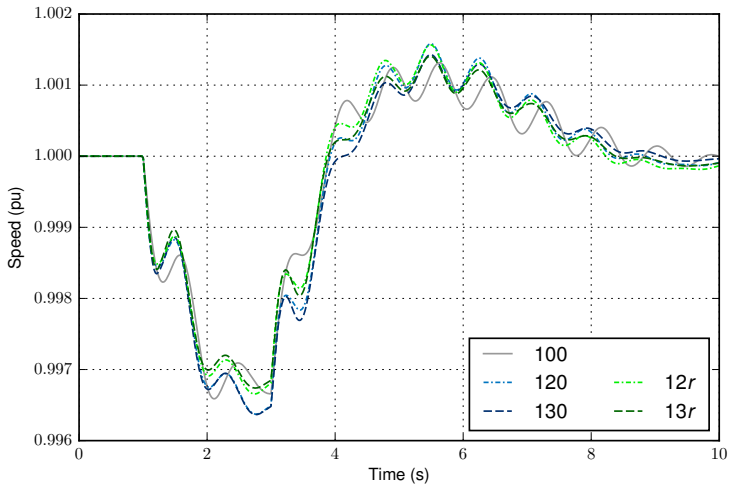


(a) Generator 3 speed.

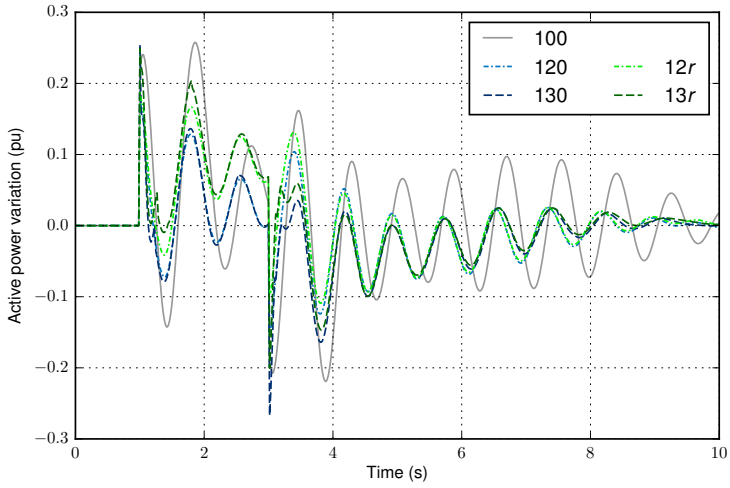


(b) Hybrid plant active power variation.

Fig. 7.33. 12-bus system response to a voltage surge at bus 4 considering PV active power reserve.

tions are more similar, and the main differences are due to the employed controller. Namely, the SPC is able to achieve slight improvements of the damping that results in a small reduction of the maximum overfrequency.

The hybrid plant active power response explaining the differences in the system frequency evolution is shown in Fig. 7.33b. During the first 2 s, the hybrid plant

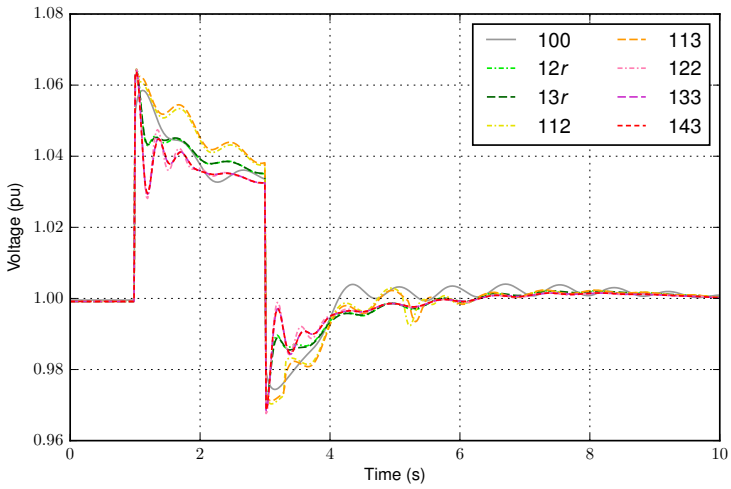


Fig. 7.34. Bus 4 voltage after a voltage surge at considering the BESS.

considering PV reserve is able to contribute more active power, and the SPC naturally provides an additional contribution during the first second, in such a way that both factors mitigate the frequency decrease. After the capacitor is disconnected, both configurations allow the PV plant to react in the same way, since the response expected from the plant is a reduction in the active power injection. In fact, after the first instants in which the responses with a same controller are different due to the previous evolution of the active power injected by the plant with different configurations, they follow very similar trajectories, and the main differences are dictated by the controller choice, with larger oscillations when the droop controller is employed.

The introduction of the BESS gives rise to a wider range of different responses, as can be seen in Fig. 7.34. Its presence allows reducing the voltage after the connection of the capacitor, with a slightly better damped response when the SPC is employed. These two effects, however, require the PV plant to participate in the control of the power system. In scenarios 112 and 113, where the BESS is the only power electronics device performing this task, the voltage is higher than in all the other scenarios considered in Fig. 7.34.

This phenomenon is seen again after the disconnection of the capacitor. The BESS, in cooperation with the PV plant, allows reducing the initial reduction of voltage and driving it faster and with small oscillations towards its original level.

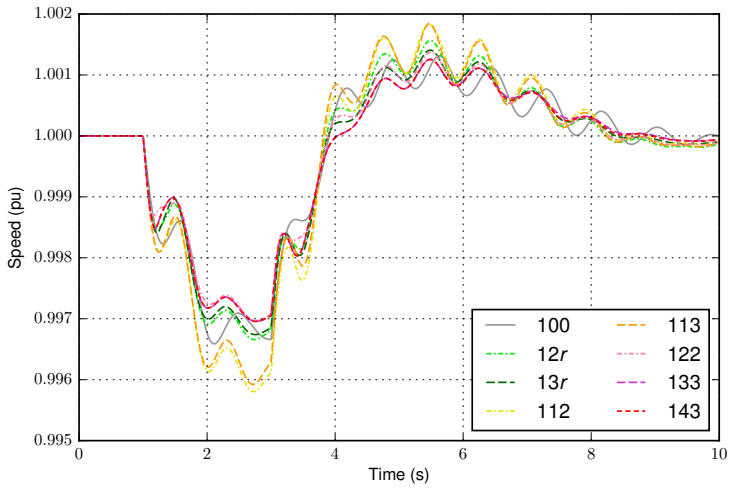


(a) Generator 3 speed.

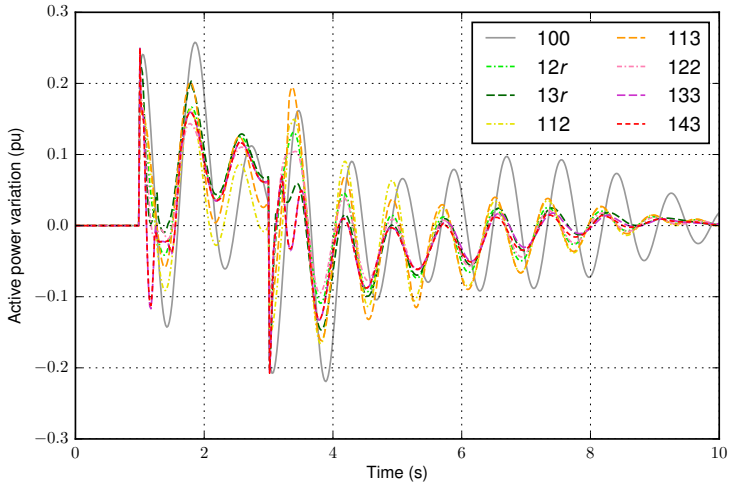


(b) Hybrid plant active power variation.

Fig. 7.35. 12-bus system response to a voltage surge at bus 4 considering the BESS.

However, when the PV plant injects constant power, the voltage requires a longer recovery period and exhibits more oscillations.

Similar effects are seen in the system frequency in Fig. 7.35a. Namely, its deviation is reduced when the BESS is connected, obtaining very similar responses for both the SPC and the droop, but it is increased when the PV plant is given a constant

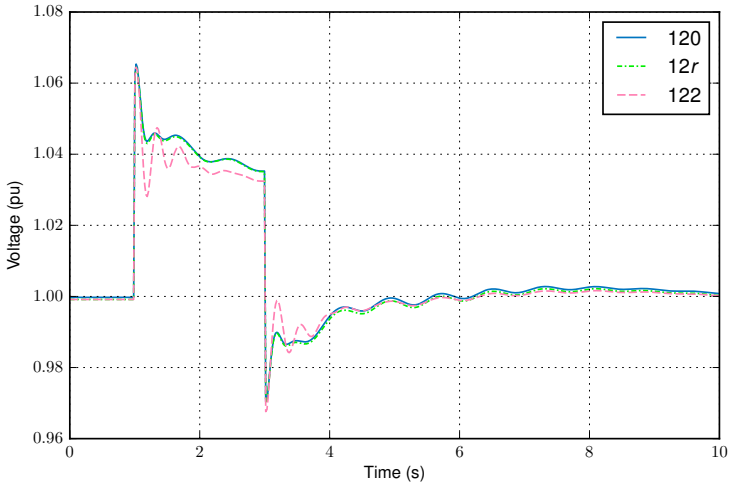


(a) Employing droop.

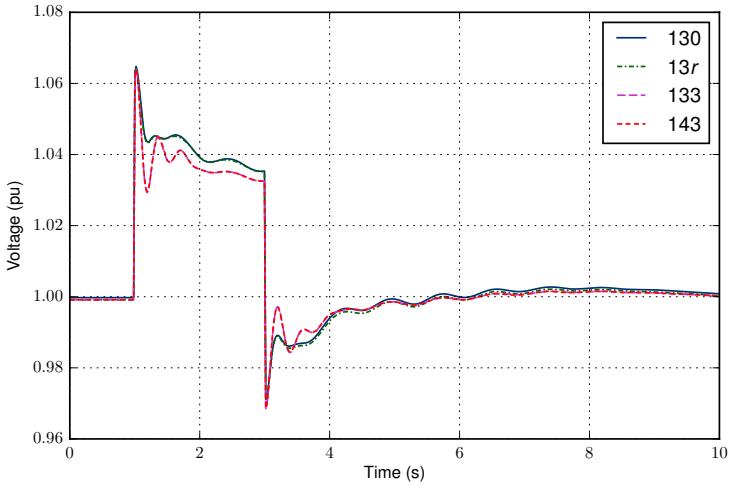


(b) Employing the SPC.

Fig. 7.36. Bus 4 voltage after a voltage surge considering different controllers and configurations.

grid-feeding control, with slightly better results when the BESS employs the SPC. After the capacitor is disconnected, the opposite trend is seen. Furthermore, in this case there is a visible reduction of the maximum frequency deviation when both hybrid plant sections use the SPC.

In Fig. 7.36, the evolution of the system voltage with the same controller for

different hybrid plant configurations can be seen. In this case, the influence of the BESS is evident again, and it is the only factor causing any differences among the responses. In both cases, it gives rise to fast but well damped oscillations immediately after the capacitor is connected or disconnected, that do not appear without the BESS, and it also reduces the high voltage level slightly.

On the other hand, the active power injected by the hybrid plant shows more differences depending on the configuration, as can be seen in Fig. 7.37. This is especially remarkable during the first 2 s of the event, when the plan is required to increase its active power after the increase in voltage and load. Without reserve nor a BESS, the response of the hybrid plant is limited to the response of the synchronous generator in scenarios 120 and 130. However, when reserve is considered, its contribution increases through the PV plant, opposing to the system frequency variations. Lastly, in the cases with a BESS, the maximum contribution of the hybrid plant is reduced. This reduction is not caused by a limitation of the hybrid plant; instead, the necessary contribution is reduced by the effect of the BESS on the control of the voltage, which allows reducing the frequency deviation, as observed in Fig. 7.35a. During the last part of the transient, after the capacitor is disconnected, these differences are not so evident, and the main change is an increase of the damping of the oscillations as more devices contribute to the control.

## 7.4 Impact on Kundur's test system

Kundur's test power system, presented in [29, pp. 831–816], has a simpler topology than the 12-bus system and is more prone to instability due to the presence of an extremely weakly damped oscillatory mode. Therefore, it can be employed to further analyze the impact of hybrid plants on power systems, and to compare the results for those obtained with power plants consisting exclusively of PV for different penetration levels.

This system consists of 11 buses with a linear topology, four generators, two loads, and two shunt capacitors boosting the voltage at the load buses. A diagram of the system is given in Fig. 7.38, indicating the length of the lines and the reactive power rating of the shunt capacitors. The initial operating point, summarized

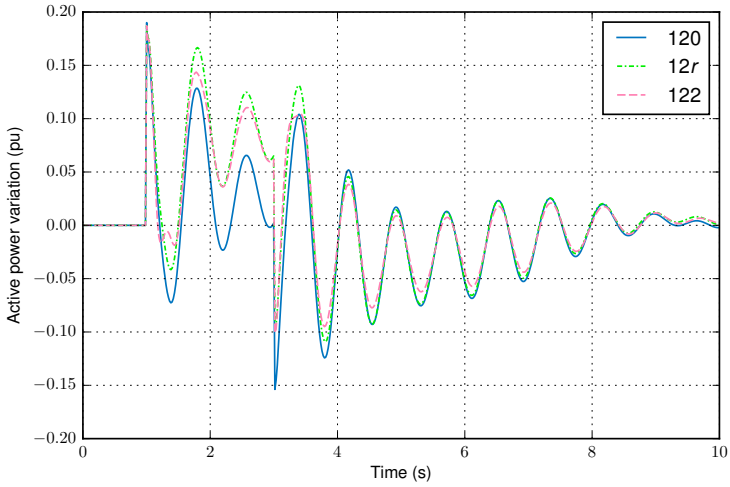


(a) Employing droop.

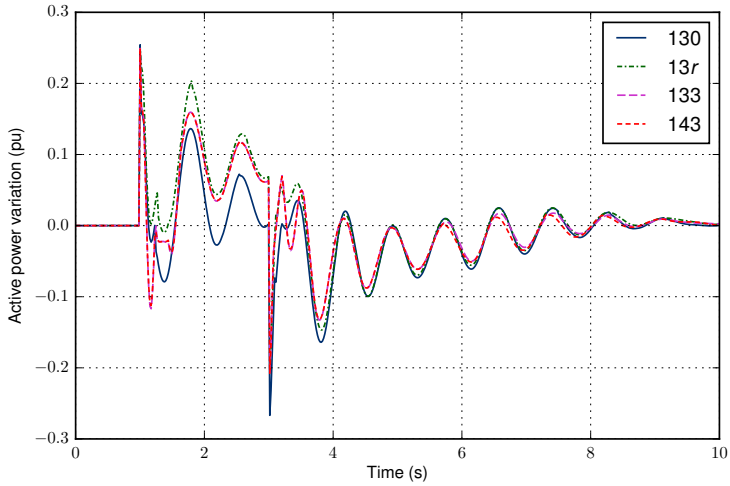


(b) Employing the SPC.

Fig. 7.37. Hybrid power plant active power variation after a voltage surge at bus 4 considering different controllers and configurations.

in Table 7.5, defines a similar active power injection from each of the generators, with G3, which is chosen as the reference machine, compensating the losses in the system. Furthermore, the different consumption at buses 7 and 9 causes an active power flow of approximately 400 MW between these two buses.

Complete data of line impedance, generators, and control systems are given

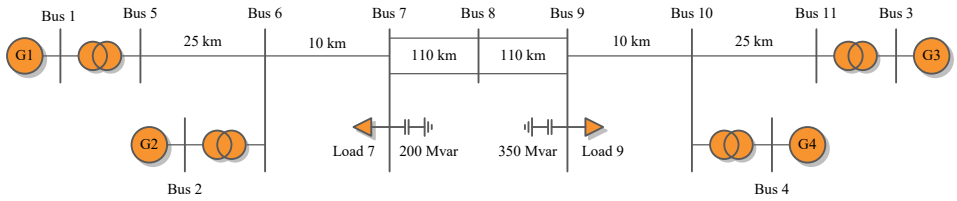


Fig. 7.38. Kundur's test system diagram [29].

Table 7.5. Initial operating point parameters for Kundur's test system [29].

| Element | P (p.u.) | Q (p.u.) | V (p.u.) |
|---|---|---|---|
| G1 | 7.00 | 1.85 | 1.03 |
| G2 | 7.00 | 2.35 | 1.01 |
| G3 | 7.19 | 1.76 | 1.03 |
| G4 | 7.00 | 2.02 | 1.01 |
| Load 7 | 9.67 | 1.00 | - |
| Load 9 | 17.67 | 1.00 | - |

in [29, pp. 813–814]. In this analysis, the thyristor exciter with transient gain, which gives rise to very weakly damped modes is considered, whereas the PSS described in [29, p. 814] is defined for G4 in order to employ it selectively in different study cases. Furthermore, in order to obtain a realistic response to frequency variations, the control systems of the synchronous generators are completed with a typical speed governor for large generating units; namely, governor *F20* in [155, apdx. D] is used. The main parameters describing the generators and their controllers are summarized in Table 7.6. To this respect, it is worth noting that generators G1 and G2 have an inertia constant of 6.5 s, whereas the value of 6.175 s corresponds to G3 and G4.

### 7.4.1 Scenarios

The scenarios considered in Kundur's test system are simpler than those defined in Section 7.3 for the 12-bus system. In this case, only PV systems are added to the sys-

Table 7.6. Main parameters of the synchronous generators in Kundur's test system.

| Parameter | Symbol | Value |
|---|---|---|
| Rated power | $S_r$ | 900 MVA |
| Rated voltage | $V_r$ | 20 kV |
| Inertia constant | $H$ | 6.5 s / 6.175 s |
| Droop slope | $R_f$ | 5% |
| Voltage controller proportional gain | $k_{AVR}$ | 200 p.u. |

tem, and they replace the synchronous machines in the original scenario, inheriting the corresponding initial active power injection, apparent power rating, and inertia constant. Namely, one or two synchronous generators among G1, G2, and G4, are replaced in different scenarios; this allows assessing the impact of the PV plants depending on their location and total penetration. Furthermore, an additional case is considered in which G4 is downsized to a 450 MVA machine, and a 450 MVA PV plant, is connected at bus 10, thus defining a hybrid power plant connected at this bus. In all cases, the active power reference of the PV plants is limited to 0.9 p.u. in its local per-unit system, and its maximum power point corresponds to a slightly higher value.

For clarity, the results discussed next focus on a reduced number of scenarios, including the base case and the following three scenarios with PV plants:

1. G4 is replaced by plant PV4.
2. G1 and G4 are respectively replaced by plants PV1 and PV4.
3. G4 is downsized to 450 MVA and a 450 MVA plant PV4 is connected at bus 10, forming a hybrid plant H4 (scenario label: *h*).

In the base scenario (scenario label: *0*), two cases are considered for comparison purposes. In the first one, the control systems of the synchronous machines include voltage regulators and speed governors, but no PSS. In the second one, the control of G4 includes a PSS; this stabilizer is not considered for any other scenario, i.e., in

the scenarios with PV plants, no PSS is considered. On the other hand, the control of the PV converters considers again the same three types as in Section 7.3: constant PV injection (case label: *ctt*), droop (*dro*), and SPC (*spc*). The comparison among scenarios focuses on the cases considering SPC-based PV power plants.

### 7.4.2 Results

The main results concerning the effect of the PV and hybrid plants on the eigenvalues and time-domain response of Kundur's test power system are presented in this section.

#### 7.4.2.1 Eigenvalue analysis

In the analysis of Kundur's test system presented in [29], this system has three critical modes whose damping depends on the controllers of the synchronous machines [29, pp. 813–816]. The scenarios considered here are built upon one of the worst cases considered in [29], the one employing high gain exciters, which results in an unstable mode and two other modes with a damping ratio around 7%. Additionally, the scenarios employed in the present analysis include speed governors that were not defined in [29]. Nevertheless, this variation does not affect the modes significantly, and these modes are only slightly affected, with a small increase in their damping that does not alter their unstable or weakly damped nature.

On the other hand, the presence of PV and the dynamics introduced by the controllers of these alternative generators have a significant impact on these modes. The results obtained for the scenarios defined in Section 7.4.1 are summarized in the eigenvalue plot in Fig. 7.39.

Each of these three modes exhibits a particular behavior under scenario variations. Thus, the local mode concerning interactions between generators G1 and G2, whose corresponding eigenvalue is close to $-0.6 \pm j7.0$, is practically identical for all the cases shown, with the exception of scenario 2. In this scenario, G1 is replaced by PV1 and the weakly damped mode associated to the oscillations between G1 and G2 disappears.

The other local mode, associated to the interactions between generators G3 and G4 is affected more severely by a similar phenomenon. Namely, it is present only

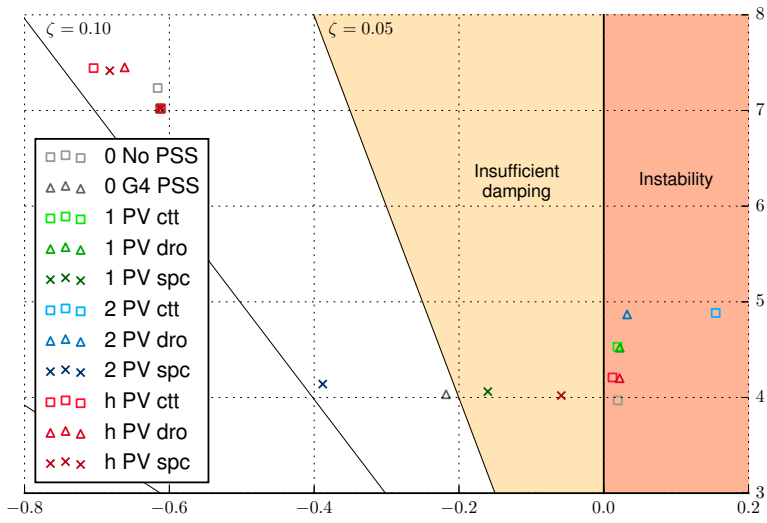


Fig. 7.39. Kundur's system eigenvalue plot considering different scenarios with PV.

for scenarios 0 and *h*, i.e., when G4 is connected to the system. Furthermore, when G4 equips a PSS in the base case, its damping ratio increases significantly over 10%. For scenario *h*, as a result of the connection of the PV plant next to one of the machines interacting through this mode, the frequency of the mode is increased, and the PV converter controller gives rise to visible variations in its damping. Thus, a non-participating PV achieves a maximum damping ratio close to 10%, and a PV employing droop has less damping than with the other two controllers, but still more than the base case.

Lastly, the inter-area mode representing the interaction between G1 and G2 on the one hand, and G3 and G4 on the other, has the most diverse behavior of these three mode depending on the scenario and the PV controller. First, it must be noted that the mode is unstable in the base case, whereas it becomes stable and sufficiently damped when G4 equips a PSS. The addition of PV has an important effect, which also depends on the controller. In scenario *h*, which corresponds to the lowest PV penetration level, the frequency of the mode increases for constant and droop controllers, remaining in the unstable region, whereas this frequency is practically unaffected by the SPC; quite the opposite, this controller increases the damping of the mode, making it positive, although still very low. As the PV penetration grows,

in scenario 1, the effect of the controllers aggravates. Thus, the constant injection and droop controllers further increase the frequency of the unstable mode, whereas the SPC increases its damping, almost reaching the 5% damping ratio requirement. Finally, when two PV plants are connected, the frequency of this mode is maximum for the conventional controllers, with a significant increase of the real part in the constant PV case, whereas the SPC is able to boost the damping of the mode, reaching almost a 10% damping ratio.

#### 7.4.2.2 Load increase contingency

This event allows studying the response of the power system to a frequency event requiring an increase of the generated active power. It is caused by load 7, whose active power increases 300 MW, without affecting its reactive power consumption, at $t = 1$ s.

This disturbance has a different impact depending on the scenarios and the controllers considered. Fig. 7.40 shows the evolution of the system frequency, represented by the speed of the reference machine G3, and the response of the PV plant connected at bus 10 for scenario 1, i.e., when PV4 is the only PV plant in the system. The speed of G3 is clearly unstable when the PV plant is controlled in order to inject constant active and reactive power. Due to the lack of response from the PV, it falls deeper than with the other two controllers and, furthermore, growing oscillations are superimposed on this trend, with a period around 1.5 s, matching the eigenvalues obtained for this case. On the other hand, the droop and SPC, after reaching a minimum and experimenting some oscillations, are able to drive the system to a steady state. As expected, the system frequency presents some oscillations that are damped after several seconds when the SPC is employed. When the PV plant controller is based only on droop, these oscillations are also damped away, although more slowly. However, this contradicts the results of the modal analysis, which predict an unstable behavior through growing oscillations. This discrepancy might be caused by the modification of the operating point after the load increase, and the effect of nonlinear dynamics that are not included in the modal analysis.

The active power variation of the PV plant, shown in Fig. 7.40b, responds to the frequency changes. With a constant injection controller, the plant maintains its

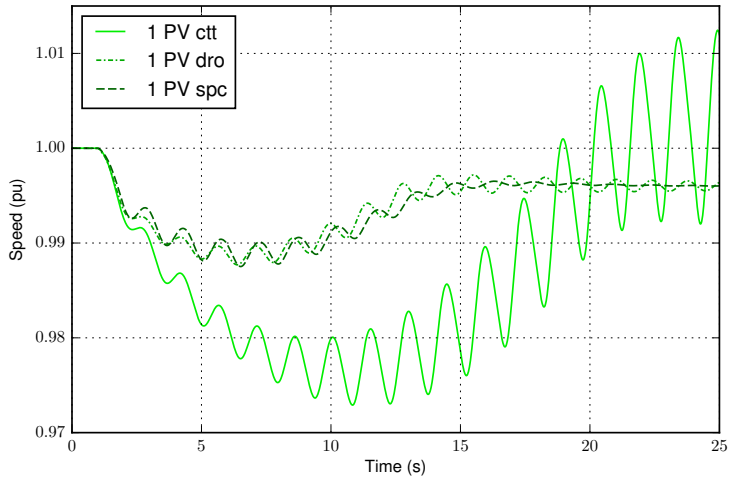


(a) G3 speed.

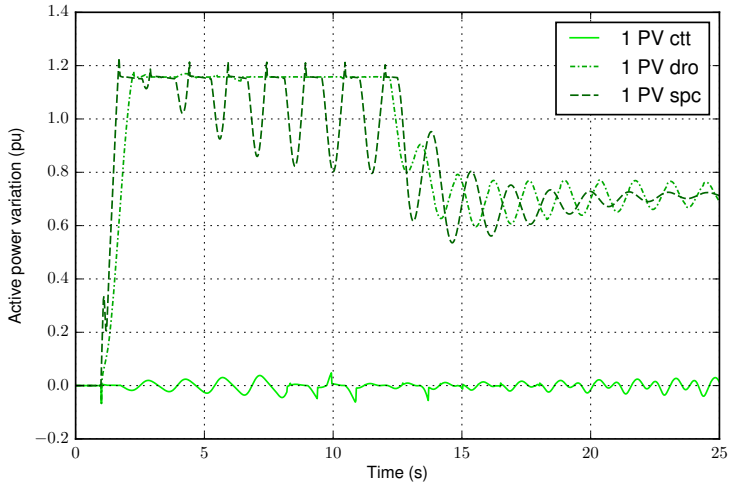


(b) PV4 active power variation.

Fig. 7.40. Kundur's system response to a load increase in scenario 1.

active power around the original value, with oscillations around this point due to the growing instability in the system. In the other two cases, the PV plant adapts its output to regulate the frequency, reaching its maximum power point and saturating during 10 s when the frequency is lowest. Furthermore, when the SPC is used, the PV plant exhibits a fast inertial reaction anticipating the droop reference variation,

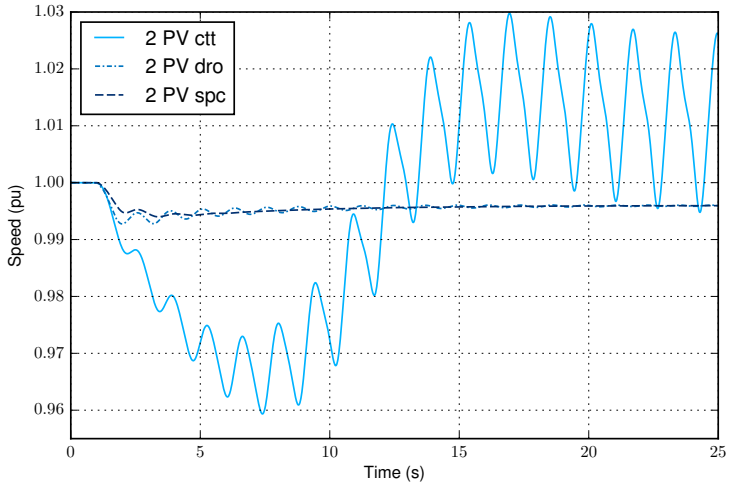


(a) G3 speed.

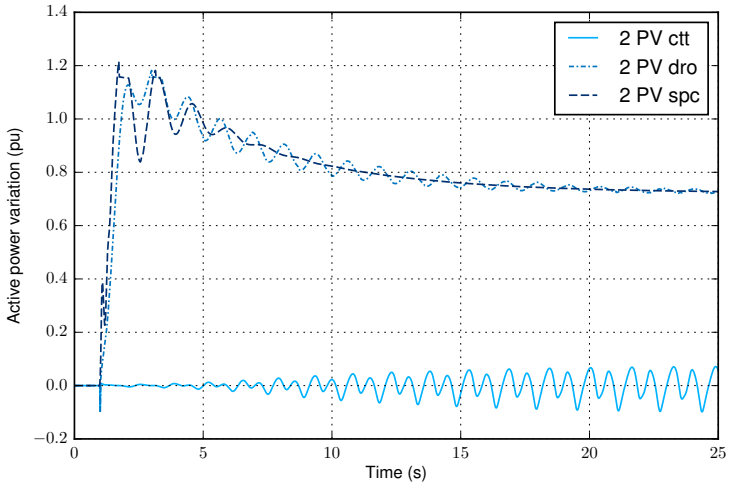


(b) PV4 active power variation.

Fig. 7.41. Kundur's system response to a load increase in scenario 2.

and it absorbs active power oscillations in order to increase the damping of the system.

The differences among controllers are accentuated when two PV plants are connected. The speed of generator G3 in Fig. 7.41a shows a larger fall of the system frequency in the case with constant PV, and also larger oscillations when it becomes

unstable. On the contrary, the maximum frequency deviation stays around 0.995 p.u. for both the droop and the SPC, which present fewer oscillations. Once again, the droop results in a stable system, contradicting the results of the modal analysis. The PV plant response, depicted in Fig. 7.41b, shows more visible oscillations for the case with constant injection, as a result of the larger oscillations suffered by the whole power system, but also a softer response when the other two controllers are used. This is due to the faster reaction of the PV plants compared to the synchronous machines, given the ability of power converters to modify not only active power but also reactive power injections in a timely manner. The efficient damping achieved by the SPC allows it to reduce the active power oscillations to be absorbed by the PV plant.

Finally, the results of the hybrid case are shown in Fig. 7.42. The loss of controllability, compared to the previous scenarios, is obvious in this figure. Despite the frequency of the system does not fall as deep as in the other scenarios when the PV does not participate in its control, the growing oscillations eventually render the system unstable. With the other two controllers, the oscillations are larger and worse damped than before, but they are still able to achieve a steady state. This oscillating behavior of the frequency is translated into the combined output of G4 and PV4 depicted in Fig. 7.42b.

Given the fact that the constant injection controller gives rise to an unstable response, and the response of the droop and SPC have a similar impact on the system, with a damping advantage for the SPC, the following analysis focuses on the response achieved with the SPC for different scenarios. In this analysis, *H4* will be used to refer also to G4 and PV4 when only one of these generating units is connected to the system.

Fig. 7.43 allows comparing the response of the system for different scenarios. Namely, it depicts the evolution of the system for the base case considering no PSS, its variation including a PSS for G4, and scenarios 1, 2, and $h$ for PV plants using the SPC. The speed of generator G3, representing the system frequency, can be seen in Fig. 7.43a. After the load increase, it decreases sharply for a few seconds. In the base case without PSS, it continues falling, reaching a minimum at around $t = 9\,\mathrm{s}$, which is followed by a slow recovery. Furthermore, growing oscillations build and

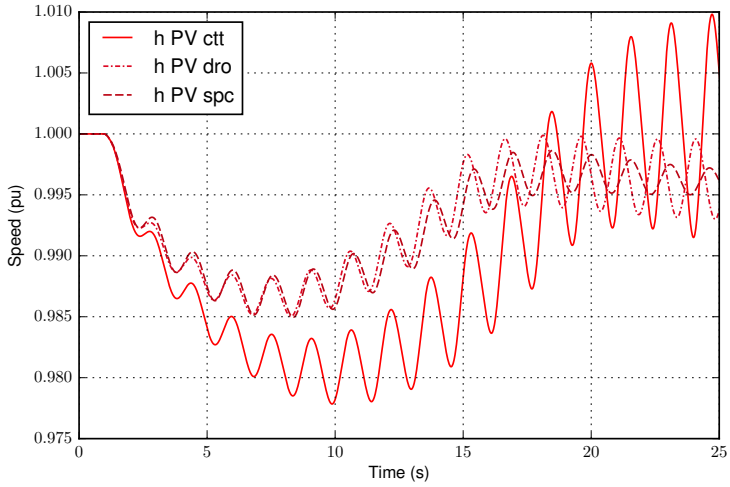


(a) G3 speed.

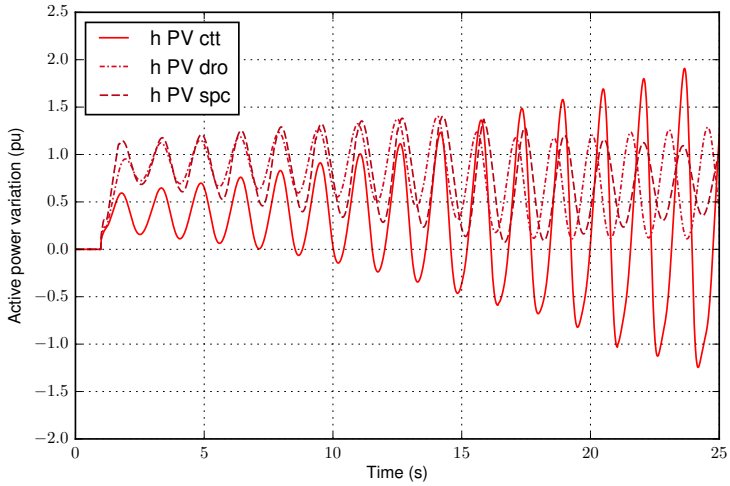


(b) H4 active power variation.

Fig. 7.42. Kundur's system response to a load increase in scenario 3.

eventually render the system unstable.

As PV replaces part of the synchronous generators in the system, the behavior of the frequency improves. Thus, when the hybrid plant is considered, it achieves a reduction of the maximum frequency deviation and a slight improvement in the speed of recovery; more importantly, the PV plant SPC is able to add enough damp-

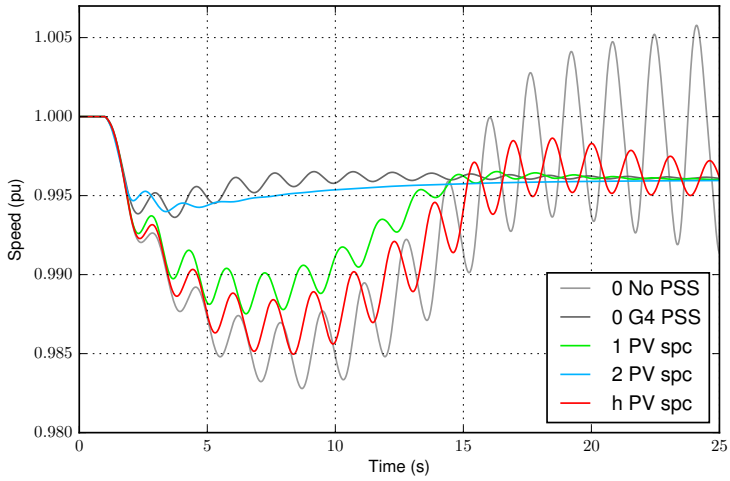


(a) G3 speed.

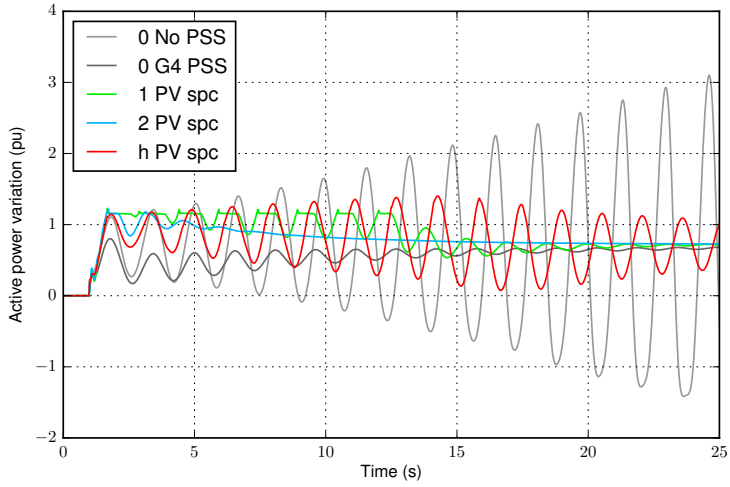


(b) H4 active power variation.

Fig. 7.43. Kundur's system response to a load increase for different scenarios.

ing to make the oscillations fade away slowly and avoid instability. These effects are stronger when G4 is totally replaced by PV4, with a further reduction in the frequency deviation, a faster recovery, and better damped oscillations. Lastly, the replacement of a second synchronous machine results in a significant improvement of the system performance. The frequency fall is quickly stopped, reducing the

maximum frequency deviation to approximately one third of the value in the base case, and making it similar to the steady-state value after the transient, with small oscillations only during the first 6 s after the event takes place. A similar response, however more oscillating, can be obtained in the base scenario if G4 employs a PSS. Therefore, the connection of two PV plants with the SPC allows the frequency of the system to experiment a similar response to the case with purely synchronous generation with a PSS, and, additionally, it improves the damping.

The response of the plant connected at bus 10, H4, is seen in Fig. 7.43b. The initial response of the plant is almost identical in all scenarios, regardless of the nature of the generating unit being used, but for the case in which a PSS is considered. Afterwards, the plant oscillates, as a synchronous machine would do, but the damping of the oscillations increases with the penetration of PV, like in the case of the frequency. It is worth noting that in scenarios 1 and 2, where this plant is formed exclusively by PV, the maximum active power injection is attained during certain intervals, but the plant is correctly controlled and this does not harm the stability of the system.

The study of the reactive power injected by G3 and H4 provides further insight into the response of the system, especially when G4 employs a PSS. The reactive power response of these units is shown in Fig. 7.44. Apart from the oscillatory behavior already observed in the frequency and the active power injected by H4, Fig. 7.44 allows observing the significant changes in the reactive power injected by these units when the PSS is connected. Thus, with a PSS, G4 reacts to the disturbance with a fast reactive power reduction, which is compensated by the injection from G3. Therefore, the improvement achieved with the connection of the PSS comes at the expense of a larger effort in the management of reactive power. On the other hand, in the scenarios considering PV, the reactive power injection is initially similar to the base case without PSS, and differences appear as the effect of the damping becomes evident.

#### 7.4.2.3 Load decrease contingency

The disturbance considered in this case is a 300 MW of the active power consumed by load 7 at $t = 1$ s. This allows studying the response of the system to an over-

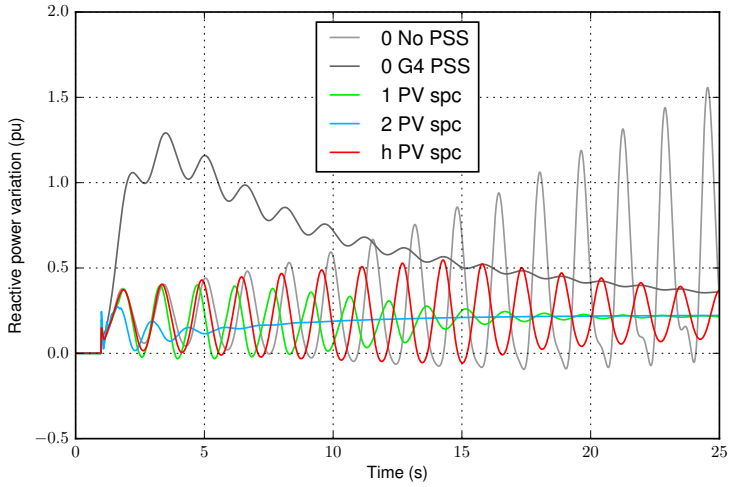


(a) G3.

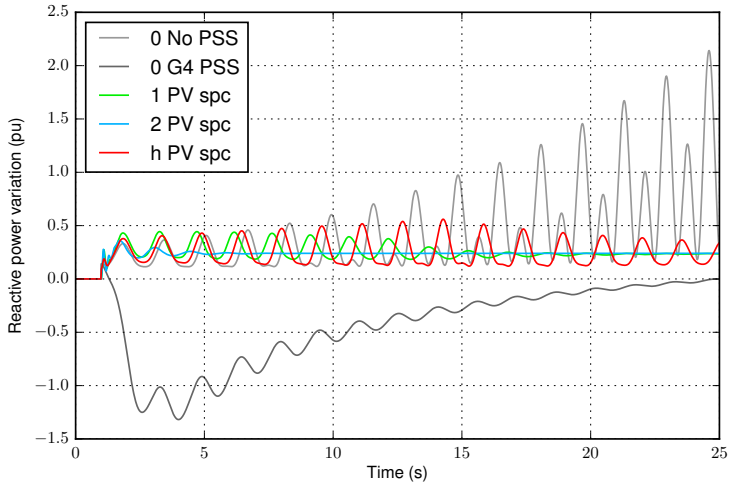


(b) H4.

Fig. 7.44. Reactive power variation after a load increase for different scenarios.

frequency, thus requiring a reduction of the generated active power, which is not so constrained by the plant capability limits.

The power system response can be seen in Fig. 7.45. As in the previous case, there is a fast initial frequency variation, and its maximum deviation decreases as the PV penetration grows and when the PSS is enabled. However, there are visible

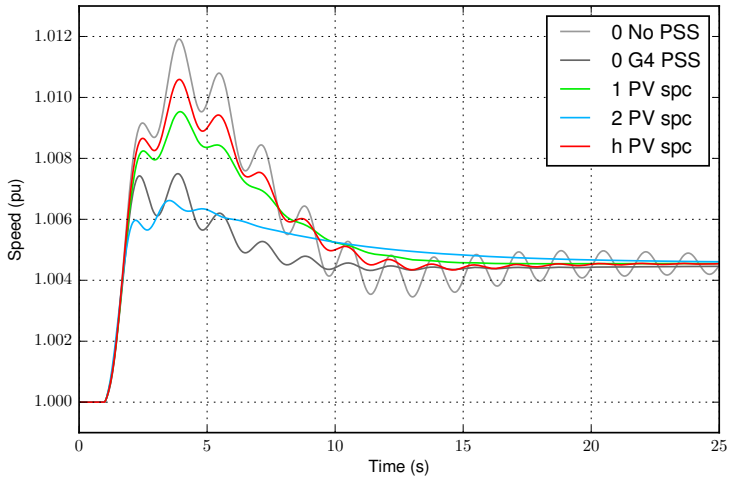


(a) G3 speed.

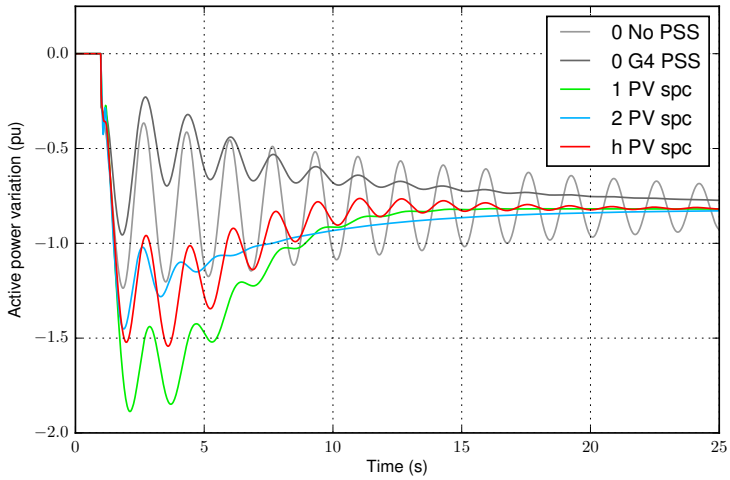


(b) H4 active power variation.

Fig. 7.45. Kundur's system response to a load reduction for different scenarios.

differences in the oscillatory behavior, and the load reduction results in a more stable state with reduced oscillations. In fact, the base case without PSS has weakly damped oscillations, but tends towards a steady state.

The response of H4 is depicted in Fig. 7.45b. In the base case, there is a sharp active power reduction followed by slow-decaying oscillations. Both the amplitude

of the initial active power reduction and the oscillations are significantly reduced when the PSS is employed. Furthermore, this response has an interesting evolution as the PV penetration grows. In the hybrid case *h*, there is a larger contribution to frequency control from H4 than in the cases without PV; additionally, the combined response of H4 exhibits certain oscillations due to the synchronous machine. In scenario 1, the reaction of the plant is stronger, and its oscillations are better damped. Finally, in scenario 2, as the amount of fast-responding PV plants increases, the individual effort to be done by each of these plants decreases, and the contribution by H4 is back at the level of scenario *h*, but with the best damping of all the considered cases.

Once again, it is worth observing the reactive power injected by G3 and H4 in Fig. 7.46. In all the scenarios without PSS, G3 reacts to the event with a small reactive power reduction; however, when the PSS of G4 is enabled, it responds with a fast reduction of reactive power that slowly tends towards a similar steady-state value. On the other hand, G4 provides an opposing reactive power injection when its PSS is enabled; in the remaining scenarios, it does a minimal contribution, with small oscillations like those seen in the frequency.

#### 7.4.2.4 Line contingency

The effect of a short circuit is studied here. The fault affects line 9-10, whose midpoint is connected to ground at $t = 1$ s, and is cleared 100 ms later without tripping the line.

The voltage at one of the endpoints of the affected line, and with close generators, bus 10, is shown in Fig. 7.47. The first seconds after the disturbance can be seen in greater detail in Fig. 7.47a. Basically, during the fault, the voltage at this bus falls around 0.2 p.u. and below, and it recovers quickly after the fault is cleared, with certain overshoot. This overshoot is larger when all the generators are synchronous machines, is reduced when a hybrid plant is considered, and is further limited in scenarios 1 and 2, when G4 is replaced by PV4. The longer-term evolution of this voltage, focusing on the surroundings of the initial value, can be seen in Fig. 7.47b. The base case with no PSS leads again to growing oscillations, which are mitigated when the PSS is enabled or PV is considered, especially in scenarios 1 and 2.

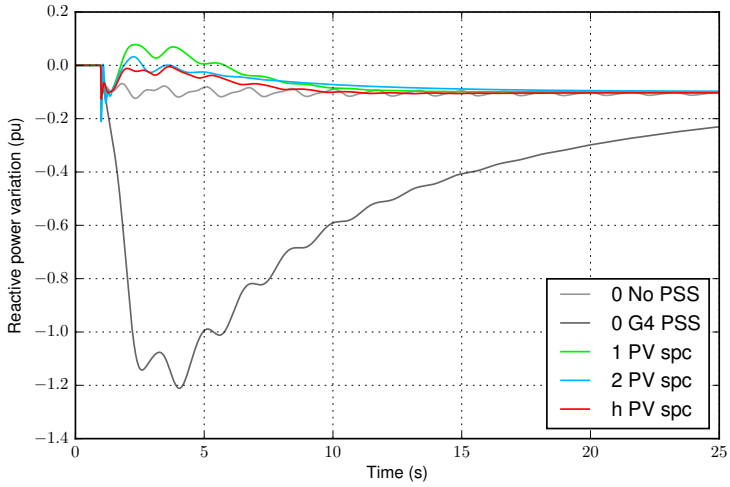


(a) G3.

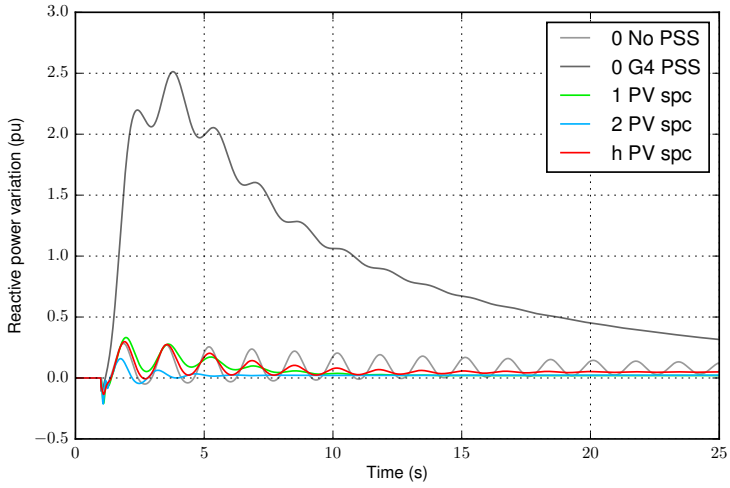


(b) H4.

Fig. 7.46. Reactive power variation after a load reduction for different scenarios.

The frequency of the system is given in Fig. 7.48a through the speed of G3. The short circuit does not cause a large imbalance that affects the mean value of the frequency of the system, but it gives rise to important oscillations. In the base case with no PSS enabled, they lead to instability, but this is prevented in the other cases. In scenario *h*, the oscillations are weakly damped but eventually fade away; whereas

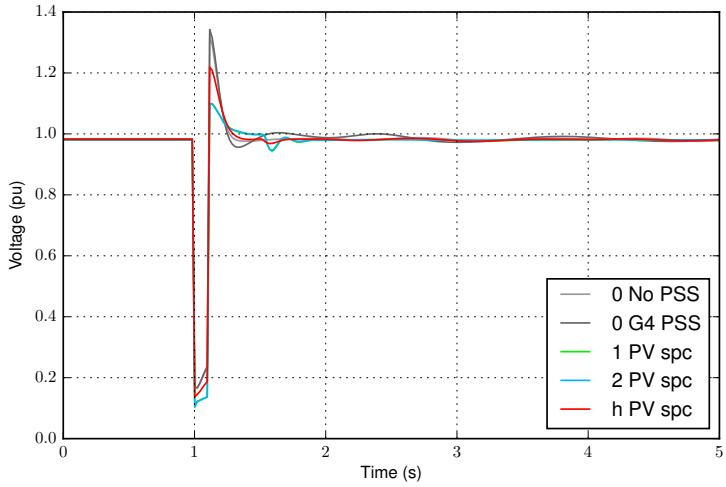


(a) Initial transient.

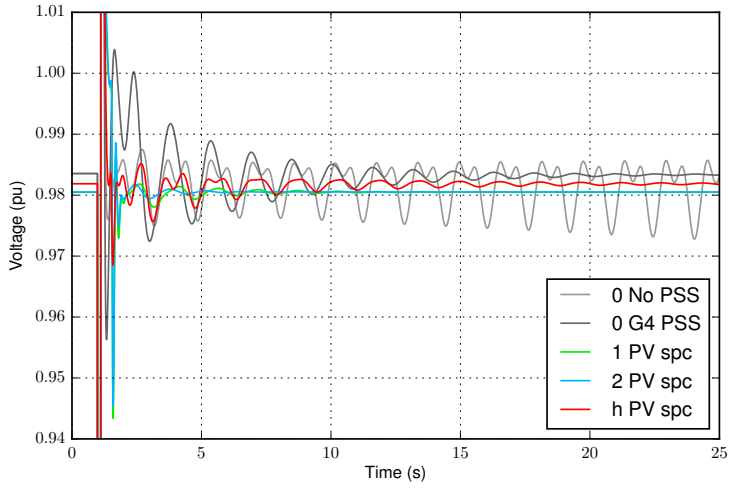


(b) Detailed view.

Fig. 7.47. Voltage at bus 10 after a 100 ms short circuit for different scenarios.

the use of the PSS in the base case results in a slightly better damping. When G4 is replaced by a full PV plant in scenarios 1 and 2, the damping of the system further improves. In this case, the active power response of the plant, limited during the fault due to the low voltage, does not require a fast reaction in terms of large active power injection, and the main contribution of the plant is related to the damping

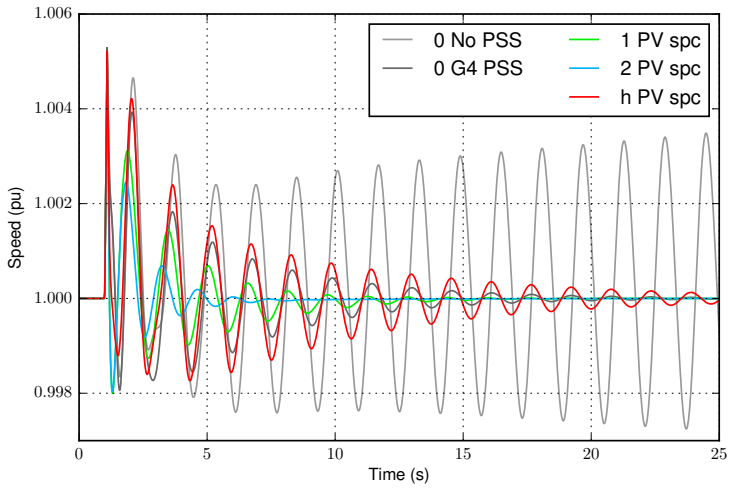


(a) G3 speed.

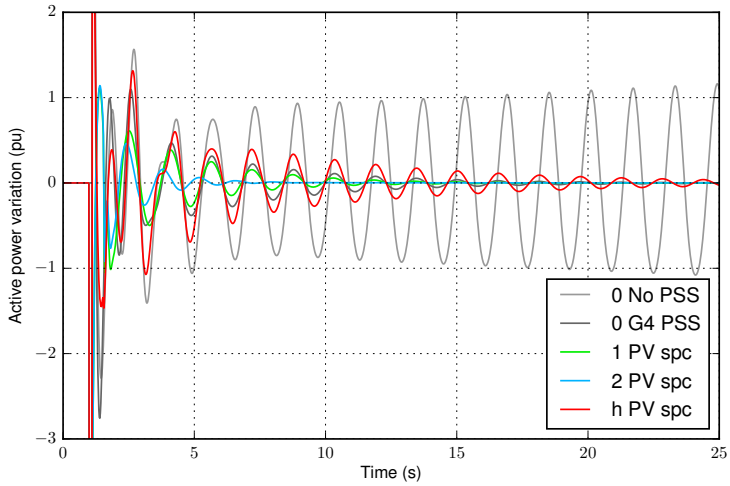


(b) H4 active power variation.

Fig. 7.48. Kundur's system response to a 100 ms short circuit for different scenarios.

after the short circuit is cleared, as shown in Fig. 7.48b. The observed oscillations agree with those seen in the frequency.

For this event, the presence of the PSS does not induce important changes in the reactive power injected by G3 and H4, as can be seen in Fig. 7.49. Once again, the main differences among scenarios are seen in the oscillations. Nonetheless, it is

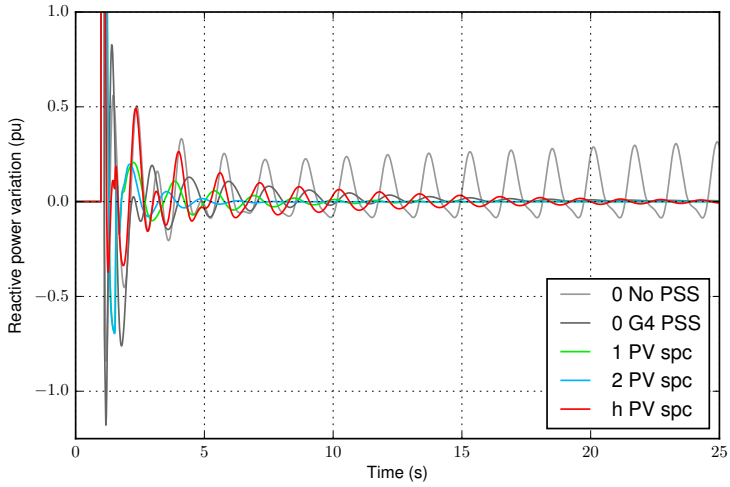


(a) G3.

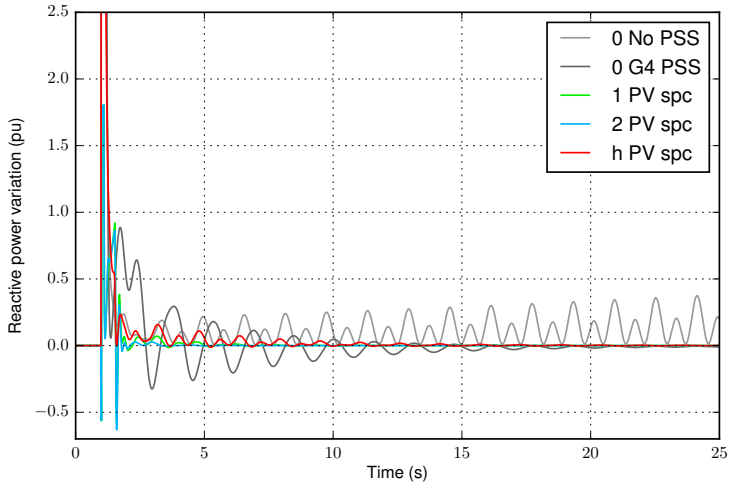


(b) H4.

Fig. 7.49. Reactive power variation after a 100 ms short circuit for different scenarios.

worth observing the response of H4 during the fault. In scenarios 0 and *h*, for which H4 consists of at least one synchronous machine, this plant increases significantly its reactive power output during the fault, in an effort to boost the voltage at its connection bus. This is possible due to the high short-circuit capability of synchronous machines. However, in scenarios 1 and 2, when the only plant connected at bus

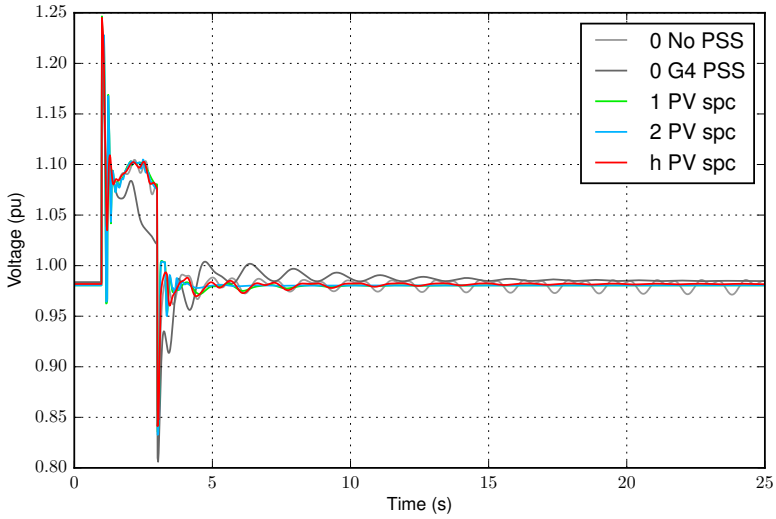


Fig. 7.50. Voltage at bus 10 after a voltage surge for different scenarios.

10 is PV4, its reactive injection during the fault increases more modestly. This is a consequence of the limited current capability of power electronics, which constrains the reactive power that can be injected during a voltage sag.

#### 7.4.2.5 Voltage surge

In addition to voltage sags, power plants must be able to withstand and mitigate voltage sags that may occur in their surroundings. The capability of the studied plants to do so is studied here by means of the connection of a 1000 Mvar capacitor at bus 10. Despite the proximity of generating units controlling the voltage at close buses, such a capacitor is able to increase the voltage at this bus 0.1 p.u. In this case, the capacitor is connected at $t = 1$ s and disconnected at $t = 3$ s. Thus, not only does the capacitor increase the voltage in the meantime, but it also causes two transients that excite the oscillatory modes of the system.

The voltage at bus 10 is depicted in Fig. 7.50. The connection of the capacitor causes a sudden voltage surge with a peak around 1.25 p.u. After the initial stage of the transient, the voltage oscillates between 1.07 p.u and 1.10 p.u., or slightly lower values when the PSS is employed. Before the voltage has completely stabilized, the disconnection of the capacitor takes place, forcing a sudden voltage reduction,

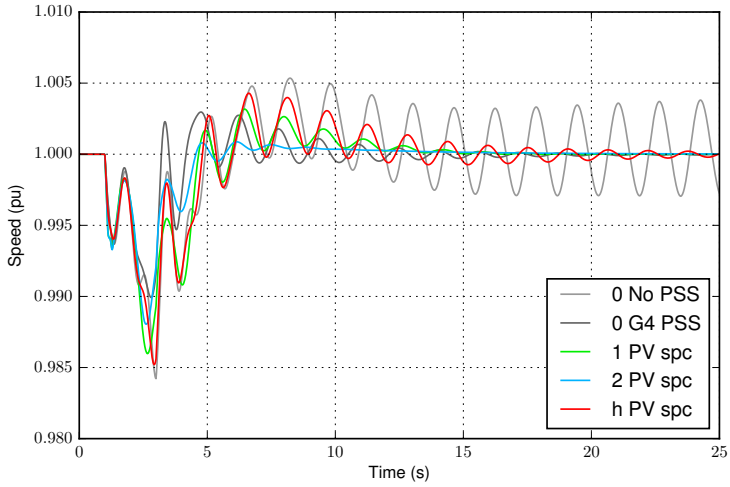


(a) G3 speed.

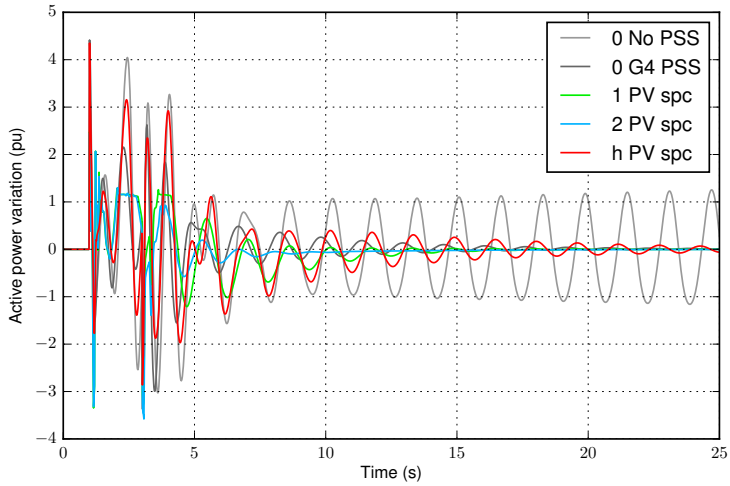


(b) H4 active power variation.

Fig. 7.51. Kundur's system response to a voltage surge for different scenarios.

with a minimum value between 0.80 p.u. and 0.85 p.u. depending on the scenario. Afterwards, it recovers the initial value with some oscillations, more slowly in the case with a PSS. These oscillations are sustained in the base case considering no stabilizer, and are better damped in the scenarios with PV.

The variations in the voltage affect the consumption of close loads, such as

load 9, which in turn alters the active power balance in the system and its frequency. Thus the voltage surge causes a frequency reduction, which can be inferred from the speed of G3 in Fig. 7.51a. This is mitigated more effectively as the PV penetration grows, or with the PSS. After the disconnection of the capacitor, the speed recovers, exhibiting the usual oscillations in this system. Once again, the connection of two PV plants proves to be the best solution to increase the damping of the system, followed by the base scenario with a PSS acting on G4, and the other cases with PV. In the base case with no PSS, it is possible to see sustained oscillations.

The main trait of the active power response of H4, shown in Fig. 7.51b, is its oscillatory behavior, which agrees with the results previously analyzed. However, it is also possible to distinguish an increase of the average power output while the capacitor is connected. In fact, this increases saturates the PV plant in scenarios 1 and 2.

In this case, as a reaction to the voltage surge, both G3 and H4 reduce their reactive power injection and start absorbing reactive power, as can be seen in Fig. 7.52. With the PSS, this reaction is weaker for G3 and stronger for G4, and visible, but well damped, oscillations appear. Furthermore, in scenarios 1 and 2, PV4 reaches its maximum current for a short interval. Thus, both its active and reactive power injection are limited, but this does not compromise the stability of the system.

#### 7.4.2.6 Angle variation

Finally, the response of the system to a sudden voltage angle variation is studied. The disturbance is caused by a 400 MW, -200 Mvar load switched on at bus 10 at $t = 1$ s, and switched off at $t = 6$ s. The connection of this load decreases the angle of G3 and G4 approximately 20° with respect to the other two synchronous machines in the system.

The impact of this disturbance on the speed of G3 can be seen in Fig. 7.53a. With the connection of the load, the speed falls, and the first swing of the machine is similar for all the scenarios. However, differences are found in the subsequent swings. Thus, the base case with no PSS, and scenarios 1 and $h$ exhibit similar oscillations and reach a minimum frequency around 0.99 p.u., whereas the base case with PSS reduces the frequency deviation and the amplitude of the oscillations, and

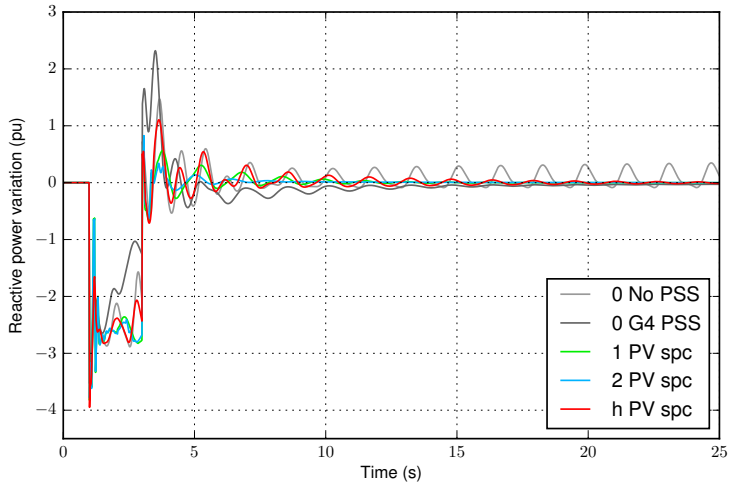


(a) G3.

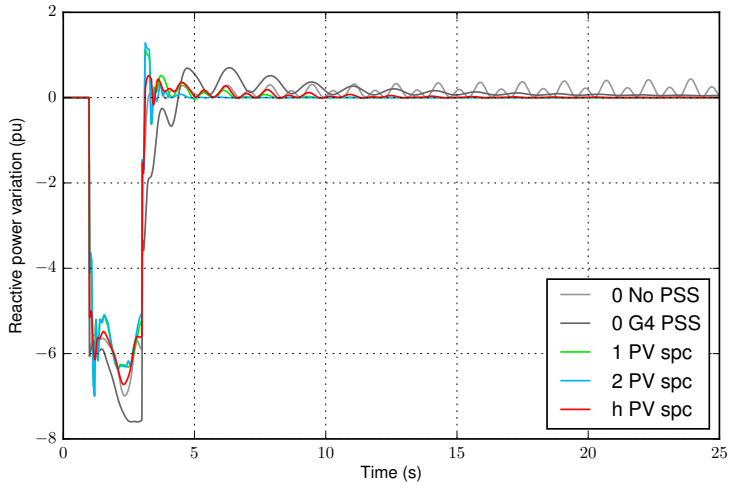


(b) H4.

Fig. 7.52. Reactive power variation after a voltage surge for different scenarios.

scenario 2 cuts the frequency deviation down by about one half and practically prevents oscillations. When the load is disconnected, the rated speed is soon recovered in average, but the oscillatory effects are aggravated, with scenario 2 providing the best performance in terms of system frequency, and scenario 1 showing also a good damping of oscillations.

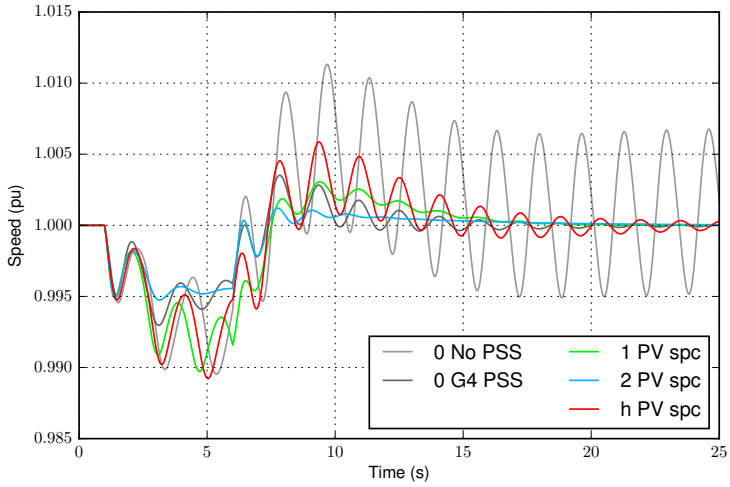


(a) G3 speed.

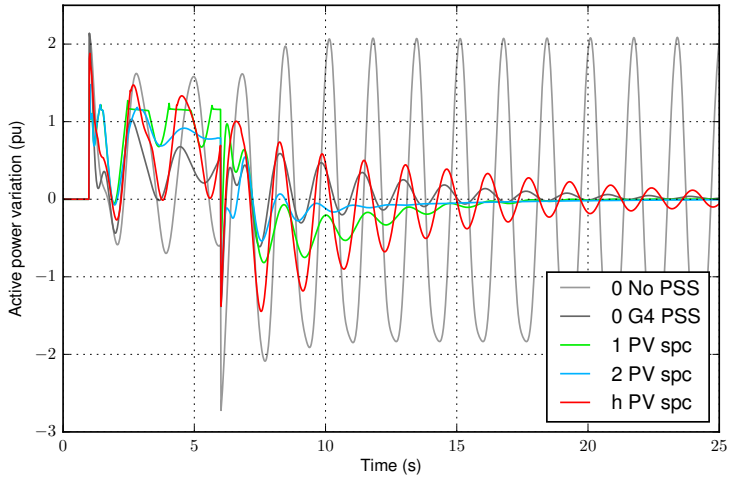


(b) H4 active power variation.

Fig. 7.53. Kundur's system response to a voltage surge for different scenarios.

The evolution of the active power injected by H4 in Fig. 7.53b is affected by the same kind of oscillations. Furthermore, the required active power increase during the interval when the load is connected causes the PV plant to saturate in scenarios 1 and 2. Once again, this saturation does not harm the stability of the system, and it occurs only for very short intervals in scenario 2, which shows a great ability to

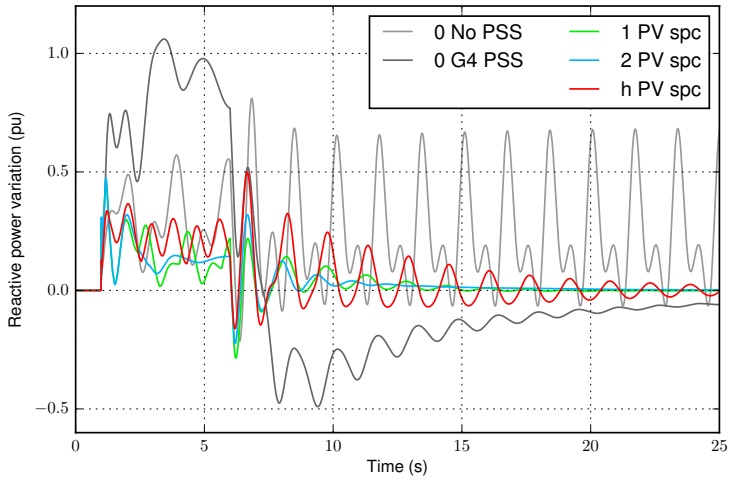


(a) G3.

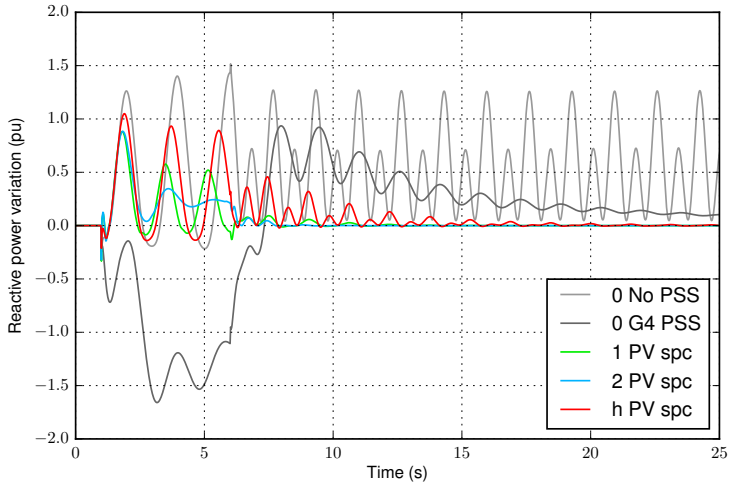


(b) H4.

Fig. 7.54. Reactive power variation after a voltage surge for different scenarios.

counter both the frequency variation and its oscillations.

As in previous cases concerning the active power balance of the system, the response of G3 and H4 is also determined by their reactive power injection, which is depicted in Fig. 7.54. Thus, G3 increases its reactive power injection during the connection of the load in all scenarios, with a significantly larger contribution

when the PSS is enabled. Afterwards, its reactive power returns to the initial value with some oscillations. As in other cases, the damping of these oscillations is best for scenario 2, followed by scenario 1, whereas the base case with no PSS gives rise to sustained oscillations. H4 also increases its reactive power production for all the scenarios not considering a PSS, with a different performance regarding the damping of the system. However, when the PSS is connected, its reactive power is significantly reduced, thus inducing G3 to provide the large injection seen in Fig. 7.54a.

Chapter
8.

# Conclusions and future work

## 8.1 Conclusions

The increasing penetration of renewable energy sources connected to power systems through power electronics converters brings new challenges to the design and operation of electricity networks. Power system operators are concerned by the reduced contribution of this type of generating units to the control of the power system, especially in the case of frequency regulation, and the fact that they replace conventional generators usually performing these tasks. Furthermore, the possible adverse effects are aggravated by the loss of inertia in the power system, as synchronous machines naturally contribute to limiting frequency excursions, whereas power electronics converters replacing these machines do not respond to disturbances in a harmonious way unless explicitly programmed to do so.

This has attracted the attention of, not only system operators, but also generation companies and academia, and different controllers aiming at reproducing some of the features of synchronous machines have been proposed. However, in most cases, the behavior of power converters employing these new controllers has been studied in particular cases considering a single power converter connected to a strong grid, or a small microgrid with few devices; whereas the impact of large penetrations of power electronics converters with this type of controllers has not received much

attention.

In this context, the work presented in this thesis, partially developed within an industrial PhD project in Abengoa, arises from the interest in exploiting the features of these controllers in commercial PV power plants with a power rating in the range of hundreds of megawatts, and aims at analyzing the impact of such plants on transmission power systems.

Therefore, the first step could be no other than studying the control system of power converters providing advanced control functions that reproduce certain aspects of the response of synchronous machines. This study included a wide range of control systems, from the modulation and current controllers that constitute the lower control layers of a power converters, to power system control functions such as frequency primary and secondary regulation, but focusing on the synchronous power controller that gives the power plants under analysis their advanced features. This was later extended to other power controllers with similar objectives, whose definitions and main properties had been presented, and sometimes reviewed, in the literature, but which had not been systematically classified and compared. Covering this gap, a classification of advanced controllers taking into account the design of their constituting blocks was defined, and the main implementations were critically reviewed and compared both analytically and through time-domain simulation. The resulting classification and the main results of the comparison are given in Chapter 3. In general, as they partially reproduce the model of synchronous machines, these controllers are inspired by similar equations describing the inertia or damping introduced by these machines. However, the details of the implementation define certain aspects of the response of these controllers and capabilities such as operation without an ancillary synchronization system, current limitation, or harmonics mitigation.

After studying the power converter control, it was possible to develop an adequate model for power system stability analysis which considered the power converter as a controlled current source. This enabled the construction of the model of an actual 100 MW PV power plant in *DIgSILENT PowerFactory*®, as explained in Chapter 4. Furthermore, since a fully detailed model is not necessary in power system stability studies, and the computational burden would hinder the analysis, a

method to obtain equivalent models of such a power plant was derived. By means of this method, several equivalent models of the studied PV plant, with different degrees of detail, were obtained. The ability of these models to reproduce the response of the detailed model under different situations, and to reduce initialization and simulation times was also proven in that chapter.

Once the main tool for power system stability analysis, i.e., this power plant model, was available, it was possible to start analyzing the impact of this kind of power plants on power systems. The first analysis was carried out in a test power system consisting of 12 buses and four generators, and adapted for renewable energy penetration studies addressing dynamic and transient stability. As covered in Chapter 5, this analysis considered several PV penetration levels, ranging from a base case with no renewable generation to a futuristic case with 50% solar penetration, and employed an early version of the plant model that did not include the full model of the PV resource, but only an active power limitation. Furthermore, it allowed comparing the performance of plants using the SPC with a more conventional control technique considering only primary regulation. The results obtained show great improvements in the damping of the critical modes when the SPC is employed, which become more evident as the solar penetration grows. This damping improvement mitigates the stress suffered by the synchronous machines in the system when there is a disturbance, reducing their active power oscillations. Moreover, the emulation of inertia allows the SPC to limit maximum frequency deviations more efficiently than the conventional controller; this is more evident for overfrequency events, during which the PV plant response is not constrained by its active power limit as the plants only require decreasing the active power output.

Afterwards, the PV plant model was completed with the inclusion of the dc side and PV source model, and further analyses were carried out letting the PV plants some headroom to respond to events requiring additional active power injections. In these analyses, the number of scenarios with different penetration levels is reduced to two cases, which allow verifying which effects are magnified as PV penetration grows. Chapter 6 presents the main results of these analyses. First, a new test in the 12-bus system with the complete model confirmed the results obtained with the simpler model with respect to the plant contribution to damping and frequency

excursion mitigation. This test was followed by a detailed study of the impact of the actual 100 MW PV power plant on the power system of northern Chile, which also included a scenario with 800 MW of PV for comparison purposes. In this case, the power system exhibits a good damping of oscillatory modes in all scenarios, and the PV plants have little influence on the associated eigenvalues. The dynamic response, however, shows more differences. Namely, the SPC is able to compensate the loss of inertia that occurs with the conventional power controller as more plants using power electronics are connected, as can be seen in the system frequency during the first seconds after a large disturbance occurs. This also has an effect on the maximum frequency deviation and the instant when it takes place, and this effect becomes more evident as PV penetration grows.

Lastly, the impact of hybrid power plants considering a PV system and a synchronous generator, optionally with an additional battery storage system, was studied. Before starting the power system stability analyses, the ability of the battery storage system to reproduce the response of a larger system, like a PV plant, including its synthetic inertial response, was assessed. This allowed verifying which factors define the response, and finding the large influence of the total connection impedance when the whole loop including the swing equation is considered. Thus, it was considered that the inertia constant of the storage system would be in accordance with its power rating, and would not try to reproduce the total inertia of a larger system. The stability analysis, which can be found in Chapter 7, was divided in two parts. The first one was carried out in the 12-bus test system, and considered different configurations with and without PV active power reserve, with and without an energy storage system, and with different controllers. The PV plant proves to be able to respond correctly to usual events affecting the bulk power balance of the system in all cases, and the results show again the ability of the SPC to increase the damping. On the other hand, the second part focused on comparing different configurations in Kundur's test power system, considering the case of a hybrid plant, a 25% penetration of PV plants, and a 50% penetration, without severe active power constraints in any case. In this test system, the usual damping improvement when the SPC is considered is especially remarkable in the 50% penetration case, where the PV plants are able to suppress power oscillations more effectively than a PSS.

Furthermore, this oscillation mitigation occurs more naturally, and does not require an additional effort in terms of reactive power injection as the PSS requires from the synchronous machines in its surroundings.

In general, PV plants with synchronous power controllers contribute to increasing the damping of the power system, thus reducing the oscillations suffered by other synchronous machines, as well as reducing maximum frequency deviations and delaying the moment when these maximum values take place after a disturbance, which would reduce the speed requirements for other generating units. The effects observed become more important as the relative size of the PV plants and their total penetration in the system increase; additionally, the plant location and the existence of critical modes in the base case also play an important role on the effects observed on the damping, as occurs for other devices aiming at mitigating oscillations, such as a PSS. Furthermore, PV plants with synchronous power controllers can safely operate at their maximum power point as long as their converter control systems include correct protections for extended voltage sags; in this operating point, these plants cannot contribute significant amounts of active power during underfrequency events, but they are still able to reduce the oscillations in the power system in those circumstances, while providing an enhanced response for other types of events.

## 8.2 Future work

Although the study of the impact of PV plants with synchronous power controllers on the stability of power systems carried out in this thesis has provided a wide range of results and conclusions pointing to a beneficial effect of this kind of power plants, more research is needed in this and related subjects. Some topics that deserve further attention in order to achieve an optimal integration of renewable energy sources in power systems are described here.

An aspect that was left out of the scope of this thesis, as it focused on the dynamic response of the plants and their effect on the response of the power system under large active power imbalances affecting the system frequency, is the response of the PV plants using synchronous power controllers to prolonged voltage sags.

The response of these plants, both with the SPC and conventional controllers, to short-circuit faults should be analyzed in detail considering all the hardware and control elements that may have an influence in this response; namely, synchronization systems employed by conventional controllers should be included. This analysis probably requires a model adapted for electromagnetic transient analysis and allowing the study of asymmetric faults, and, depending on the action of the plant voltage controller, may consider a reduced number of power converters. In any case, this analysis should provide feedback about the performance of the SPC during voltage sags, especially those with an extended duration, and it should evaluate controller enhancements to overcome the issues generated by this kind of faults.

Further studies should be devoted to the optimization of the plant controller parameter tuning. The presence of the SPC gives rise to an increased flexibility, allowing to set the virtual machine inertia constant, damping coefficient, and grid-interface impedance in addition to other controller parameter often employed to shape the response of generating units, such as voltage regulator gains. Adequate tuning methods considering both the dynamics of the power system and the plant capabilities should be derived, based on a solid theoretical framework, and supported by results. Furthermore, the optimization could be extended to the design of the power plant, taking into account the tradeoff between increased plant performance and increased cost due to the oversizing of certain elements such as the power converters or their dc capacitors.

Additionally, the internal behavior of the plant should be analyzed, taking into account the contribution of each device for given responses at the point of connection of the plant, and also the response of these devices to disturbances taking place both outside the power plant and within its internal network. This analysis might render further constraints on the power plant controller parameters. Moreover, as in the previous case, it can also be extended to an economic optimization of the design of the power plant, considering the power rating of different devices, or the need for PV reserve or storage. In fact, taking into account that the availability of storage would allow the PV plant to provide its services throughout the day, it would be interesting to study whether oversizing the PV field for reserve or including storage is more profitable. The complexity of this analysis increases if different storage

configurations are considered, from a centralized approach with dedicated power converters, to a fully distributed solution where the storage elements are connected to the dc side of PV converters.

Other analyses may consider the effect of higher-level plant controllers that determine how references are shared among units, or system controllers such as automatic generation control. These controllers usually have longer time constants; thus, they would not normally interact with the dynamics of power converter controllers like the SPC. However, in a context of larger and faster active power variations due to the variability of the employed energy sources, the speed of these higher-level controllers could be increased, and this could lead to new interactions among different controllers and devices. Furthermore, it may be interesting to design new controllers that take into account the characteristics of modern power systems.

Moving away from bulk power systems, microgrids have attracted the attention of many researchers. Indeed, microgrids are another interesting field where the application of advanced power controllers could have an important impact, as they usually constitute weak power systems with large amounts of renewable energy and power electronics converter. Thus, in this context of reduced inertia, and taking into account the trend observed as PV penetration grows, the emulation of synchronous generator features could play an important role in these systems that is worth analyzing in detail.

Finally, the results of the analyses have to be validated with experiments. These tests must include the actual primary resource and the dynamics of the power system, and could employ hardware-in-the-loop techniques or, ideally, field tests. The latter is more feasible in the case of a microgrid, or studying the short-circuit response of a single converter, than when the response of a large power plant connected to a transmission system is assessed.

# References


[1] "International Energy Outlook 2016," U.S. Energy Information Administration, Washington, DC, Tech. Rep., May 2016. [Online]. Available: http://www.eia.gov/outlooks/ieo/pdf/0484(2016).pdf

[2] "ENTSO-E network code for requirements for grid connection applicable to all generators," ENTSO-E AISBL, Brussels, Tech. Rep., March 2013. [Online]. Available: https://www.entsoe.eu/fileadmin/user_upload/_library/resources/RfG/130308_Final_Version_NC_RfG.pdf

[3] "IEEE standard for interconnecting distributed resources with electric power systems," *IEEE Std 1547-2003*, pp. 1–28, July 2003.

[4] "IEEE 1547 and 2030 standards for distributed energy resources interconnection and interoperability with electricity grid," National Renewable Energy Laboratory, Golden, CO, Tech. Rep., December 2014. [Online]. Available: http://www.nrel.gov/docs/fy15osti/63157.pdf

[5] "IEEE standard for interconnecting distributed resources with electric power systems - Amendment 1," *IEEE Std 1547a-2014 (Amendment to IEEE Std 1547-2003)*, pp. 1–16, May 2014.

[6] N. Mohan, T. M. Undeland, and W. P. Robbins, *Power Electronics: Converters, Applications and Design*. John Wiley & Sons, 2003.

[7] R. Teodorescu, M. Liserre, and P. Rodriguez, *Grid Converters for Photovoltaic and Wind Power Systems*. Wiley, 2011.

[8] J. Rodriguez, J.-S. Lai, and F. Z. Peng, "Multilevel inverters: A survey of topologies, controls, and applications," *IEEE Transactions on Industrial Electronics*, vol. 49, no. 4, pp. 724–738, Aug 2002.

[9] F. Z. Peng, "A generalized multilevel inverter topology with self voltage balancing," *IEEE Transactions on Industry Applications*, vol. 37, no. 2, pp. 611–618, Mar 2001.

[10] A. K. Sahoo, R. Otero-De-Leon, and N. Mohan, "Review of modular multilevel converters for teaching a graduate-level course of power electronics in power systems," in *North American Power Symposium (NAPS)*, Sept 2013, pp. 1–6.

[11] J. Wang, R. Burgos, and D. Boroyevich, "A survey on the modular multilevel converters: Modeling, modulation and controls," in *IEEE Energy Conversion Congress and Exposition (ECCE)*, Sept 2013, pp. 3984–3991.

[12] S. Buso and P. Mattavelli, *Digital Control in Power Electronics*. Morgan & Claypool, 2006.

[13] F. Blaabjerg, R. Teodorescu, M. Liserre, and A. V. Timbus, "Overview of control and grid synchronization for distributed power generation systems," *IEEE Transactions on Industrial Electronics*, vol. 53, no. 5, pp. 1398–1409, Oct 2006.

[14] A. Luna, J. Rocabert, G. Vazquez, P. Rodríguez, R. Teodorescu, and F. Corcoles, "Grid synchronization for advanced power processing and FACTS in wind power systems," in *IEEE International Symposium on Industrial Electronics (ISIE)*, July 2010, pp. 2915–2920.

[15] D. N. Zmood and D. G. Holmes, "Stationary frame current regulation of PWM inverters with zero steady-state error," *IEEE Transactions on Power Electronics*, vol. 18, no. 3, pp. 814–822, May 2003.

[16] R. Teodorescu, F. Blaabjerg, M. Liserre, and P. C. Loh, "Proportional-resonant controllers and filters for grid-connected voltage-source converters," *IEE Proceedings - Electric Power Applications*, vol. 153, no. 5, pp. 750–762, September 2006.

[17] P. Rodriguez, A. Luna, I. Candela, R. Mujal, R. Teodorescu, and F. Blaabjerg, "Multiresonant frequency-locked loop for grid synchronization of power converters under distorted grid conditions," *IEEE Transactions on Industrial Electronics*, vol. 58, no. 1, pp. 127–138, Jan 2011.

[18] P. Rodriguez, A. Luna, R. S. Muñoz-Aguilar, I. Etxeberria-Otadui, R. Teodorescu, and F. Blaabjerg, "A stationary reference frame grid synchronization system for three-phase grid-connected power converters under adverse grid conditions," *IEEE Transactions on Power Electronics*, vol. 27, no. 1, pp. 99–112, Jan 2012.

[19] F. J. Rodriguez, E. Bueno, M. Aredes, L. G. B. Rolim, F. A. S. Neves, and M. C. Cavalcanti, "Discrete-time implementation of second order generalized integrators for grid converters," in *2008 34th Annual Conference of IEEE Industrial Electronics*, Nov 2008, pp. 176–181.

[20] S. D'Arco and J. A. Suul, "Equivalence of virtual synchronous machines and frequency-droops for converter-based microgrids," *IEEE Transactions on Smart Grid*, vol. 5, no. 1, pp. 394–395, Jan 2014.

[21] J. Rocabert, A. Luna, F. Blaabjerg, and P. Rodriguez, "Control of power converters in ac microgrids," *IEEE Transactions on Power Electronics*, vol. 27, no. 11, pp. 4734–4749, Nov 2012.

[22] M. C. Chandorkar, D. M. Divan, and R. Adapa, "Control of parallel connected inverters in standalone ac supply systems," *IEEE Transactions on Industry Applications*, vol. 29, no. 1, pp. 136–143, Jan 1993.

[23] J. C. Vasquez, J. M. Guerrero, M. Savaghebi, J. Eloy-Garcia, and R. Teodorescu, "Modeling, analysis, and design of stationary-reference-frame droop-

controlled parallel three-phase voltage source inverters," *IEEE Transactions on Industrial Electronics*, vol. 60, no. 4, pp. 1271–1280, April 2013.

[24] J. M. Guerrero, J. Matas, L. Garcia de Vicuña, M. Castilla, and J. Miret, "Wireless-control strategy for parallel operation of distributed-generation inverters," *IEEE Transactions on Industrial Electronics*, vol. 53, no. 5, pp. 1461–1470, Oct 2006.

[25] K. D. Brabandere, B. Bolsens, J. V. den Keybus, A. Woyte, J. Driesen, and R. Belmans, "A voltage and frequency droop control method for parallel inverters," *IEEE Transactions on Power Electronics*, vol. 22, no. 4, pp. 1107–1115, July 2007.

[26] K. De Brabandere, "Voltage and frequency droop control in low voltage grids by distributed generators with inverter front-end," Dr.-Ing. dissertation, Katholieke Universiteit Leuven, Leuven, Belgium, 2006.

[27] L. Zhang, L. Harnefors, and H. P. Nee, "Power-synchronization control of grid-connected voltage-source converters," *IEEE Transactions on Power Systems*, vol. 25, no. 2, pp. 809–820, May 2010.

[28] P. Mitra, L. Zhang, and L. Harnefors, "Offshore wind integration to a weak grid by VSC-HVDC links using power-synchronization control: A case study," *IEEE Transactions on Power Delivery*, vol. 29, no. 1, pp. 453–461, Feb 2014.

[29] P. Kundur, *Power System Stability and Control*. McGraw-Hill, 1994.

[30] J. Driesen and K. Visscher, "Virtual synchronous generators," in *IEEE PES General Meeting*, July 2008.

[31] K. Visscher and S. de Haan, "Virtual synchronous machines (VSG's) for frequency stabilisation in future grids with a significant share of decentralized generation," in *CIRED Seminar SmartGrids for Distribution (IET-CIRED)*, June 2008.

[32] M. P. N. Van Wesenbeeck, S. W. H. De Haan, P. Varela, and K. Visscher, "Grid tied converter with virtual kinetic storage," in *IEEE PowerTech*, Bucharest, June 2009.

[33] V. Karapanos, S. de Haan, and K. Zwetsloot, "Real time simulation of a power system with VSG hardware in the loop," in *Annual Conference of IEEE Industrial Electronics Society (IECON)*, Nov 2011, pp. 3748–3754.

[34] V. Karapanos, S. W. H. de Haan, and K. H. Zwetsloot, "Testing a virtual synchronous generator in a real time simulated power system," in *International Conference on Power Systems Transients (IPST)*, Jun 2011.

[35] V. Van Thong, A. Woyte, M. Albu, M. Van Hest, J. Bozelie, J. Diaz, T. Loix, D. Stanculescu, and K. Visscher, "Virtual synchronous generator: Laboratory scale results and field demonstration," in *IEEE PowerTech*, Bucharest, June 2009.

[36] T. Van, K. Visscher, J. Diaz, V. Karapanos, A. Woyte, M. Albu, J. Bozelie, T. Loix, and D. Federenciuc, "Virtual synchronous generator: An element of future grids," in *IEEE PES Innovative Smart Grid Technologies Conference Europe (ISGT Europe)*, Oct 2010.

[37] M. Albu, J. Diaz, V. Thong, R. Neurohr, D. Federenciuc, M. Popa, and M. Calin, "Measurement and remote monitoring for virtual synchronous generator design," in *IEEE International Workshop on Applied Measurements For Power Systems (AMPS)*, Sept 2010, pp. 7–11.

[38] A. Vassilakis, P. Kotsampopoulos, N. Hatziargyriou, and V. Karapanos, "A battery energy storage based virtual synchronous generator," in *IREP Symposium Bulk Power System Dynamics and Control - Optimization, Security and Control of the Emerging Power Grid (IREP)*, Aug 2013.

[39] M. Torres and L. A. C. Lopes, "Virtual synchronous generator control in autonomous wind-diesel power systems," in *IEEE Electrical Power Energy Conference (EPEC)*, Oct 2009.

[40] ——, "Frequency control improvement in an autonomous power system: An application of virtual synchronous machines," in *IEEE International Conference on Power Electronics and ECCE Asia (ICPE & ECCE)*, May 2011, pp. 2188–2195.

[41] N. Miller and K. Clark, "Advanced controls enable wind plants to provide ancillary services," in *IEEE PES General Meeting*, July 2010.

[42] N. Miller, K. Clark, and M. Shao, "Frequency responsive wind plant controls: Impacts on grid performance," in *IEEE PES General Meeting*, July 2011.

[43] N. Miller, R. W. Delmerico, K. Kuruvilla, and M. Shao, "Frequency responsive controls for wind plants in grids with wind high penetration," in *IEEE PES General Meeting*, July 2012.

[44] L. Ruttledge, N. W. Miller, J. O'Sullivan, and D. Flynn, "Frequency response of power systems with variable speed wind turbines," *IEEE Transactions on Sustainable Energy*, vol. 3, no. 4, pp. 683–691, Oct 2012.

[45] F. Gonzalez-Longatt, E. Chikuni, and E. Rashayi, "Effects of the synthetic inertia from wind power on the total system inertia after a frequency disturbance," in *IEEE International Conference on Industrial Technology (ICIT)*, Feb 2013, pp. 826–832.

[46] H.-P. Beck and R. Hesse, "Virtual synchronous machine," in *IEEE International Conference on Electrical Power Quality and Utilisation (EPQU)*, Oct 2007.

[47] R. Hesse, D. Turschner, and H.-P. Beck, "Micro grid stabilization using the virtual synchronous machine (VISMA)," in *International Conference on Renewable Energies and Power Quality (ICREPQ)*, Apr 2009.

[48] Y. Chen, R. Hesse, D. Turschner, and H.-P. Beck, "Dynamic properties of the virtual synchronous machine (VISMA)," in *International Conference on Renewable Energies and Power Quality (ICREPQ)*, Apr 2011.

[49] ——, "Improving the grid power quality using virtual synchronous machines," in *IEEE International Power Engineering, Energy and Electrical Drives (POWERENG)*, May 2011.

[50] ——, "Investigation of the virtual synchronous machine in the island mode," in *IEEE PES International Conference and Exhibition on Innovative Smart Grid Technologies (ISGT Europe)*, Oct 2012.

[51] ——, "Comparison of methods for implementing virtual synchronous machine on inverters," in *International Conference on Renewable Energies and Power Quality (ICREPQ)*, Mar 2012.

[52] K. Sakimoto, Y. Miura, and T. Ise, "Stabilization of a power system with a distributed generator by a virtual synchronous generator function," in *IEEE International Conference on Power Electronics and ECCE Asia (ICPE & ECCE)*, May 2011, pp. 1498–1505.

[53] T. Shintai, Y. Miura, and T. Ise, "Reactive power control for load sharing with virtual synchronous generator control," in *IEEE International Power Electronics and Motion Control Conference (IPEMC)*, vol. 2, June 2012, pp. 846–853.

[54] J. Alipoor, Y. Miura, and T. Ise, "Distributed generation grid integration using virtual synchronous generator with adoptive virtual inertia," in *IEEE Energy Conversion Congress and Exposition (ECCE)*, Sept 2013, pp. 4546–4552.

[55] K. Sakimoto, Y. Miura, and T. Ise, "Stabilization of a power system including inverter-type distributed generators by a virtual synchronous generator," *Electrical Engineering in Japan*, vol. 187, pp. 341–349, May 2014.

[56] T. Shintai, Y. Miura, and T. Ise, "Oscillation damping of a distributed generator using a virtual synchronous generator," *IEEE Transactions on Power Delivery*, vol. 29, no. 2, pp. 668–676, April 2014.

[57] Q.-C. Zhong and G. Weiss, "Synchronverters: Inverters that mimic synchronous generators," *IEEE Transactions on Industrial Electronics*, vol. 58, no. 4, pp. 1259–1267, April 2011.

[58] G. Weiss and Q.-C. Zhong, "Static synchronous generators," International Patent WO 2010/055 322 A2, May 20, 2010, Priority date: Nov 12, 2008.

[59] P.-L. Nguyen, Q.-C. Zhong, F. Blaabjerg, and J. Guerrero, "Synchronverter-based operation of STATCOM to mimic synchronous condensers," in *IEEE Conference on Industrial Electronics and Applications (ICIEA)*, July 2012, pp. 942–947.

[60] Q.-C. Zhong, P.-L. Nguyen, Z. Ma, and W. Sheng, "Self-synchronized synchronverters: Inverters without a dedicated synchronization unit," *IEEE Transactions on Power Electronics*, vol. 29, no. 2, pp. 617–630, Feb 2014.

[61] C.-H. Zhang, Q.-C. Zhong, J.-S. Meng, X. Chen, Q. Huang, S.-H. Chen, and Z.-P. Lv, "An improved synchronverter model and its dynamic behaviour comparison with synchronous generator," in *Renewable Power Generation Conference (RPG 2013), 2nd IET*, Sept 2013, pp. 1–4.

[62] S. D'Arco, J. A. Suul, and O. B. Fosso, "Control system tuning and stability analysis of virtual synchronous machines," in *IEEE Energy Conversion Congress and Exposition (ECCE)*, Sept 2013, pp. 2664–2671.

[63] ——, "Small-signal modelling and parametric sensitivity of a virtual synchronous machine," in *IEEE Power Systems Computation Conference (PSCC)*, Aug 2014.

[64] S. D'Arco and J. A. Suul, "A synchronization controller for grid reconnection of islanded virtual synchronous machines," in *IEEE International Symposium on Power Electronics for Distributed Generation Systems (PEDG)*, June 2015.

[65] J. A. Suul, S. D'Arco, and G. Guidi, "Virtual synchronous machine-based control of a single-phase bi-directional battery charger for providing vehicle-to-grid services," *IEEE Transactions on Industry Applications*, vol. 52, no. 4, pp. 3234–3244, July 2016.

[66] P. Rodriguez Cortés, J. I. Candela García, J. Rocabert Delgado, and R. Teodorescu, "Synchronous power controller for a generating system based

on static power converters," International Patent WO 2012/117 131 A1, Sept 7, 2012, Priority date: Feb 18, 2011, Licensed by: Abengoa, S.A.

[67] P. Rodriguez, I. Candela, C. Citro, J. Rocabert, and A. Luna, "Control of grid-connected power converters based on a virtual admittance control loop," in *European Conference on Power Electronics and Applications (EPE)*, Sept 2013.

[68] P. Rodriguez, I. Candela, and A. Luna, "Control of PV generation systems using the synchronous power controller," in *IEEE Energy Conversion Congress and Exposition (ECCE)*, Sept 2013, pp. 993–998.

[69] B. Orlik, M. Schmidt, and F. Fein, "Control of a wind power station with the strategy of a conventional power plant: Assigning synchronous machine behavior on a full inverter based wind power station," in *11th International Conference on Electrical Power Quality and Utilisation*, Oct 2011, pp. 1–7.

[70] K.-I. Sakimoto, K. Sugimoto, and Y. Shindo, "Low voltage ride through capability of a grid connected inverter based on the virtual synchronous generator," in *IEEE International Conference on Power Electronics and Drive Systems (PEDS)*, April 2013, pp. 1066–1071.

[71] Y. Xiang-Zhen, S. Jian-Hui, D. Ming, L. Jin-Wei, and D. Yan, "Control strategy for virtual synchronous generator in microgrid," in *IEEE International Conference on Electric Utility Deregulation and Restructuring and Power Technologies (DRPT)*, July 2011, pp. 1633–1637.

[72] J. Zhu, C. Booth, G. Adam, A. Roscoe, and C. Bright, "Inertia emulation control strategy for VSC-HVDC transmission systems," *IEEE Transactions on Power Systems*, vol. 28, no. 2, pp. 1277–1287, May 2013.

[73] H. Bevrani, T. Ise, and Y. Miura, "Virtual synchronous generators: A survey and new perspectives," *Electrical Power and Energy Systems*, vol. 54, pp. 244–254, 2014.

[74] S. D'Arco and J. A. Suul, "Virtual synchronous machines – Classification of implementations and analysis of equivalence to droop controllers for microgrids," in *IEEE PowerTech*, Grenoble, June 2013.

[75] G. Andersson, *Power System Analysis*. ETH Zürich, 2012. [Online]. Available: http://www.eeh.ee.ethz.ch/fileadmin/user_upload/eeh/studies/courses/modelling_and_analysis_of_power_networks/Documents/PSA_skript12.pdf

[76] F. Milano, *Power System Modelling and Scripting*. Springer, 2010.

[77] F. C. Schweppe and E. J. Handschin, "Static state estimation in electric power systems," *Proceedings of the IEEE*, vol. 62, no. 7, pp. 972–982, July 1974.

[78] A. Abur and A. Gómez Expósito, *Power System State Estimation*. Marcel Dekker, 2004.

[79] A. Gomez-Exposito, A. Abur, A. de la Villa Jaen, and C. Gomez-Quiles, "A multilevel state estimation paradigm for smart grids," *Proceedings of the IEEE*, vol. 99, no. 6, pp. 952–976, June 2011.

[80] J. Machowski, J. W. Bialek, and J. R. Bumby, *Power System Dynamics: Stability and Control*. John Wiley & Sons, 2008.

[81] A. Gómez Expósito, A. J. Conejo, and C. Cañizares, *Electric Energy Systems. Analysis and Operation*. Taylor & Francis, 2008.

[82] B. C. Babu and S. Gurjar, "A novel simplified two-diode model of photovoltaic (PV) module," *IEEE Journal of Photovoltaics*, vol. 4, no. 4, pp. 1156–1161, July 2014.

[83] A. J. Germond and R. Podmore, "Dynamic aggregation of generating unit models," *IEEE Transactions on Power Apparatus and Systems*, vol. PAS-97, no. 4, pp. 1060–1069, July 1978.

[84] D. Hussein, M. Matar, and R. Iravani, "A type-4 wind power plant equivalent model for the analysis of electromagnetic transients in power systems," *IEEE Transactions on Power Systems*, vol. 28, no. 3, pp. 3096–3104, Aug 2013.

[85] D.-E. Kim and M. El-Sharkawi, "Dynamic equivalent model of wind power plant using an aggregation technique," *IEEE Transactions on Energy Conversion*, vol. 30, no. 4, pp. 1639–1649, Dec 2015.

[86] R. Nazim and T. Runolfsson, "Analysis of wind farm dynamics using multiple doubly fed induction generators," in *IEEE PES General Meeting*, July 2014, pp. 1–5.

[87] L. Fernandez, C. Garcia, F. Jurado, and J. Saenz, "Aggregation of doubly fed induction generators wind turbines under different incoming wind speeds," in *IEEE PowerTech*, June 2005, pp. 1–6.

[88] H. Liu and Z. Chen, "Aggregated modelling for wind farms for power system transient stability studies," in *IEEE Asia-Pacific Power and Energy Engineering Conference (APPEEC)*, March 2012, pp. 1–6.

[89] E. Muljadi, C. Butterfield, A. Ellis, J. Mechenbier, J. Hochheimer, R. Young, N. Miller, R. Delmerico, R. Zavadil, and J. Smith, "Equivalencing the collector system of a large wind power plant," in *IEEE PES General Meeting*, 2006, pp. 1–9.

[90] E. Muljadi, S. Pasupulati, A. Ellis, and D. Kosterov, "Method of equivalencing for a large wind power plant with multiple turbine representation," in *IEEE PES General Meeting*, July 2008, pp. 1–9.

[91] "WECC wind power plant dynamic modeling guide," WECC Renewable Energy Modeling Task Force, Tech. Rep., April 2014. [Online]. Available: www.wecc.biz/Reliability/WECC%20Wind%20Plant%20Dynamic%20Modeling%20Guidelines.pdf

[92] M. Elizondo, S. Lu, N. Zhou, and N. Samaan, "Model reduction, validation, and calibration of wind power plants for dynamic studies," in *IEEE Power and Energy Society General Meeting*, July 2011, pp. 1–8.

[93] J. Brochu, C. Larose, and R. Gagnon, "Validation of single- and multiple-machine equivalents for modeling wind power plants," *IEEE Transactions on Energy Conversion*, vol. 26, no. 2, pp. 532–541, June 2011.

[94] E. Cari, J. Neto, I. Erlich, and J. Rueda, "A methodology for parameter estimation of equivalent wind power plant," in *Annual Conference of the IEEE Industrial Electronics Society (IECON)*, Nov 2013, pp. 1804–1808.

[95] R. Castro and J. Ferreira De Jesus, "A wind park reduced-order model using singular perturbations theory," *IEEE Transactions on Energy Conversion*, vol. 11, no. 4, pp. 735–741, Dec 1996.

[96] A. Morton, "Model aggregation of wind farms and other ensemble systems," in *Australasian Universities Power Engineering Conference (AUPEC)*, Dec 2007, pp. 1–5.

[97] M. Ali, I.-S. Ilie, J. Milanovic, and G. Chicco, "Probabilistic clustering of wind generators," in *IEEE Power and Energy Society General Meeting*, July 2010, pp. 1–6.

[98] M. Ali, J. V. Milanovic, I.-S. Ilie, and G. Chicco, "Comparison of wind farm aggregate models for transient stability studies," in *17th Power Systems Computation Conference (PSCC)*, 2011, pp. 1–7.

[99] A. Bonfiglio, F. Delfino, M. Invernizzi, R. Procopio, and P. Serra, "Criteria for the equivalent modeling of large photovoltaic power plants," in *IEEE PES General Meeting*, July 2014, pp. 1–5.

[100] S. Soni, G. G. Karady, M. Morjaria, and V. Chadliev, "Comparison of full and reduced scale solar PV plant models in multi-machine power systems," in *IEEE PES T&D Conference and Exposition*, April 2014, pp. 1–5.

[101] "WECC PV power plant dynamic modeling guide," WECC Renewable Energy Modeling Task Force, Tech. Rep., April 2014. [Online]. Available: www.wecc.biz/Reliability/WECC%20Solar%20Plant%20Dynamic%20Modeling%20Guidelines.pdf

[102] "Renewable energy medium-term market report 2016: Executive summary," International Energy Agency, Paris, Tech. Rep., 2016. [Online]. Available: http://www.iea.org/Textbase/npsum/MTrenew2016SUM.pdf

[103] J. Kabouris and F. D. Kanellos, "Impacts of large-scale wind penetration on designing and operation of electric power systems," *IEEE Transactions on Sustainable Energy*, vol. 1, no. 2, pp. 107–114, July 2010.

[104] E. Vittal and A. Keane, "Identification of critical wind farm locations for improved stability and system planning," *IEEE Transactions on Power Systems*, vol. 28, no. 3, pp. 2950–2958, Aug 2013.

[105] S. Eftekharnejad, G. T. Heydt, and V. Vittal, "Optimal generation dispatch with high penetration of photovoltaic generation," *IEEE Transactions on Sustainable Energy*, vol. 6, no. 3, pp. 1013–1020, July 2015.

[106] S. Martín-Martínez, E. Gómez-Lazaro, A. Molina-Garcia, and A. Honrubia-Escribano, "Impact of wind power curtailments on the Spanish power system operation," in *IEEE PES General Meeting*, July 2014, pp. 1–5.

[107] W. A. Omran, M. Kazerani, and M. M. A. Salama, "Investigation of methods for reduction of power fluctuations generated from large grid-connected photovoltaic systems," *IEEE Transactions on Energy Conversion*, vol. 26, no. 1, pp. 318–327, March 2011.

[108] M. I. Hossain, R. Yan, and T. K. Saha, "Investigation of the interaction between step voltage regulators and large-scale photovoltaic systems regarding voltage regulation and unbalance," *IET Renewable Power Generation*, vol. 10, no. 3, pp. 299–309, 2016.

[109] A. Chidurala, T. K. Saha, and N. Mithulananthan, "Harmonic impact of high penetration photovoltaic system on unbalanced distribution networks – learning from an urban photovoltaic network," *IET Renewable Power Generation*, vol. 10, no. 4, pp. 485–494, 2016.

[110] K. Kawabe and K. Tanaka, "Impact of dynamic behavior of photovoltaic power generation systems on short-term voltage stability," *IEEE Transactions on Power Systems*, vol. 30, no. 6, pp. 3416–3424, Nov 2015.

[111] M. Edrah, K. L. Lo, and O. Anaya-Lara, "Impacts of high penetration of DFIG wind turbines on rotor angle stability of power systems," *IEEE Transactions on Sustainable Energy*, vol. 6, no. 3, pp. 759–766, July 2015.

[112] M. Yagami, N. Kimura, M. Tsuchimoto, and J. Tamura, "Power system transient stability analysis in the case of high-penetration photovoltaics," in *IEEE PowerTech*, June 2013, pp. 1–6.

[113] D. Gautam, V. Vittal, and T. Harbour, "Impact of increased penetration of DFIG-based wind turbine generators on transient and small signal stability of power systems," *IEEE Transactions on Power Systems*, vol. 24, no. 3, pp. 1426–1434, Aug 2009.

[114] Z. Miao, "Impact of unbalance on electrical and torsional resonances in power electronic interfaced wind energy systems," *IEEE Transactions on Power Systems*, vol. 28, no. 3, pp. 3105–3113, Aug 2013.

[115] S. Eftekharnejad, V. Vittal, G. T. Heydt, B. Keel, and J. Loehr, "Impact of increased penetration of photovoltaic generation on power systems," *IEEE Transactions on Power Systems*, vol. 28, no. 2, pp. 893–901, May 2013.

[116] N. Nguyen and J. Mitra, "An analysis of the effects and dependency of wind power penetration on system frequency regulation," *IEEE Transactions on Sustainable Energy*, vol. 7, no. 1, pp. 354–363, Jan 2016.

[117] R. Yan, T. K. Saha, N. Modi, N.-A. Masood, and M. Mosadeghy, "The combined effects of high penetration of wind and PV on power system frequency response," *Applied Energy*, vol. 145, pp. 320–330, 2015.

[118] A. Ghafouri, J. Milimonfared, and G. B. Gharehpetian, "Coordinated control of distributed energy resources and conventional power plants for frequency control of power systems," *IEEE Transactions on Smart Grid*, vol. 6, no. 1, pp. 104–114, Jan 2015.

[119] G. Delille, B. Francois, and G. Malarange, "Dynamic frequency control support by energy storage to reduce the impact of wind and solar generation on

isolated power system's inertia," *IEEE Transactions on Sustainable Energy*, vol. 3, no. 4, pp. 931–939, Oct 2012.

[120] Z. H. Rather, Z. Chen, and P. Thogersen, "Impact of wind energy integration on reactive power reserve and its smart solution: A Danish power system case study," in *IEEE International Conference on Power System Technology (POWERCON)*, Oct 2012, pp. 1–6.

[121] Y. V. Makarov, C. Loutan, J. Ma, and P. de Mello, "Operational impacts of wind generation on California power systems," *IEEE Transactions on Power Systems*, vol. 24, no. 2, pp. 1039–1050, May 2009.

[122] A. Helander, H. Holttinen, and J. Paatero, "Impact of wind power on the power system imbalances in Finland," *IET Renewable Power Generation*, vol. 4, no. 1, pp. 75–84, January 2010.

[123] Y. Wang, V. Silva, and M. Lopez-Botet-Zulueta, "Impact of high penetration of variable renewable generation on frequency dynamics in the continental Europe interconnected system," *IET Renewable Power Generation*, vol. 10, no. 1, pp. 10–16, 2016.

[124] S. Eftekharnejad, V. Vittal, G. T. Heydt, B. Keel, and J. Loehr, "Small signal stability assessment of power systems with increased penetration of photovoltaic generation: A case study," *IEEE Transactions on Sustainable Energy*, vol. 4, no. 4, pp. 960–967, Oct 2013.

[125] E. H. Kim, J. H. Kim, S. H. Kim, J. Choi, K. Y. Lee, and H. C. Kim, "Impact analysis of wind farms in the Jeju Island power system," *IEEE Systems Journal*, vol. 6, no. 1, pp. 134–139, March 2012.

[126] C. Han, A. Q. Huang, M. E. Baran, S. Bhattacharya, W. Litzenberger, L. Anderson, A. L. Johnson, and A. A. Edris, "STATCOM impact study on the integration of a large wind farm into a weak loop power system," *IEEE Transactions on Energy Conversion*, vol. 23, no. 1, pp. 226–233, March 2008.

[127] W. Zhang, A. M. Cantarellas, J. Rocabert, A. Luna, and P. Rodriguez, "Synchronous power controller with flexible droop characteristics for renewable

power generation systems," *IEEE Transactions on Sustainable Energy*, vol. 7, no. 4, pp. 1572–1582, Oct 2016.

[128] D. Wu, F. Tang, J. C. Vasquez, and J. M. Guerrero, "Control and analysis of droop and reverse droop controllers for distributed generations," in *IEEE International Multi-Conference on Systems, Signals Devices (SSD)*, Feb 2014.

[129] M. Torres, J. Espinoza, L. Moran, J. Rohten, and P. Melin, "Integration of a large-scale photovoltaic plant using a multilevel converter topology and virtual synchronous generator control," in *IEEE International Symposium on Industrial Electronics (ISIE)*, June 2014, pp. 2620–2624.

[130] M. Datta, H. Ishikawa, H. Naitoh, and T. Senjyu, "LFC by coordinated virtual inertia mimicking and PEVs in power utility with MW-class distributed PV generation," in *IEEE Workshop on Control and Modeling for Power Electronics (COMPEL)*, June 2012.

[131] T. K. Vrana and C. Hille, "A novel control method for dispersed converters providing dynamic frequency response," *Electrical Engineering*, vol. 93, no. 4, pp. 217–226, 2011.

[132] K. Koyanagi, Y. Hida, Y. Ito, K. Yoshimi, R. Yokoyama, M. Inokuchi, T. Mouri, and J. Eguchi, "A smart photovoltaic generation system integrated with lithium-ion capacitor storage," in *IEEE International Universities' Power Engineering Conference (UPEC)*, Sept 2011.

[133] R. Hesse, H.-P. Beck, and D. Turschner, "Conditioning device for energy supply networks," US Patent US 8,510,090 B2, Aug. 13, 2013, Priority date: Oct 6, 2006.

[134] E. Brown and G. Weiss, "Using synchronverters for power grid stabilization," in *IEEE Convention of Electrical Electronics Engineers in Israel (IEEEI)*, Dec 2014.

[135] S. Dong, Y. Chi, and Y. Li, "Active voltage feedback control for hybrid multiterminal HVDC system adopting improved synchronverters," *IEEE Transactions on Power Delivery*, vol. 31, no. 2, pp. 445–455, April 2016.

[136] C. F. dos Santos, F. B. Grigoletto, and M. Stefanello, "Power quality improvement in a grid connected voltage source inverter using the concept of virtual synchronous machine," in *IEEE Brazilian Power Electronics Conference and Southern Power Electronics Conference (COBEP/SPEC)*, Nov 2015, pp. 1–5.

[137] J. Alipoor, Y. Miura, and T. Ise, "Power system stabilization using virtual synchronous generator with alternating moment of inertia," *IEEE Journal of Emerging and Selected Topics in Power Electronics*, vol. 3, no. 2, pp. 451–458, June 2015.

[138] ——, "Voltage sag ride-through performance of virtual synchronous generator," in *IEEE International Power Electronics Conference (IPEC)*, May 2014, pp. 3298–3305.

[139] S. M. Ashabani and Y. A. R. I. Mohamed, "General interface for power management of micro-grids using nonlinear cooperative droop control," *IEEE Transactions on Power Systems*, vol. 28, no. 3, pp. 2929–2941, Aug 2013.

[140] M. Ashabani and Y. A. R. I. Mohamed, "Novel comprehensive control framework for incorporating VSCs to smart power grids using bidirectional synchronous-VSC," *IEEE Transactions on Power Systems*, vol. 29, no. 2, pp. 943–957, March 2014.

[141] M. Ashabani, Y. A. R. I. Mohamed, M. Mirsalim, and M. Aghashabani, "Multivariable droop control of synchronous current converters in weak grids/microgrids with decoupled dq-axes currents," *IEEE Transactions on Smart Grid*, vol. 6, no. 4, pp. 1610–1620, July 2015.

[142] M. Ashabani and Y. A. R. I. Mohamed, "Integrating VSCs to weak grids by nonlinear power damping controller with self-synchronization capability," *IEEE Transactions on Power Systems*, vol. 29, no. 2, pp. 805–814, March 2014.

[143] M. Guan, W. Pan, J. Zhang, Q. Hao, J. Cheng, and X. Zheng, "Synchronous generator emulation control strategy for voltage source converter (VSC) sta-

tions," *IEEE Transactions on Power Systems*, vol. 30, no. 6, pp. 3093–3101, Nov 2015.

[144] D. Remon, A. M. Cantarellas, M. A. A. Elsaharty, C. Koch-Ciobotaru, and P. Rodriguez, "Synchronous PV support to an isolated power system," in *IEEE Energy Conversion Congress and Exposition (ECCE)*, Sept 2015, pp. 1982–1987.

[145] P. Rodriguez, C. Citro, I. Candela, J. Rocabet, and A. Luna, "Flexible grid connection and islanding of SPC-based PV power converters," in *IEEE Energy Conversion Congress and Exposition (ECCE)*, Sept 2015, pp. 450–459.

[146] C. Li, R. Burgos, I. Cvetkovic, D. Boroyevich, L. Mili, and P. Rodriguez, "Analysis and design of virtual synchronous machine based statcom controller," in *IEEE Workshop on Control and Modeling for Power Electronics (COMPEL)*, June 2014.

[147] D. Remon, A. Cantarellas, E. Rakhshani, I. Candela, and P. Rodriguez, "An active power synchronization control loop for grid-connected converters," in *IEEE PES General Meeting*, July 2014.

[148] "Generic solar photovoltaic system dynamic simulation model specification," WECC Renewable Energy Modeling Task Force, Tech. Rep., Sept 2012. [Online]. Available: www.wecc.biz/Reliability/WECC%20Solar%20PV%20Dynamic%20Model%20Specification%20-%20September%202012.pdf

[149] P. Rodriguez, J. Pou, J. Bergas, J. Candela, R. Burgos, and D. Boroyevich, "Decoupled double synchronous reference frame PLL for power converters control," *IEEE Transactions on Power Electronics*, vol. 22, no. 2, pp. 584–592, March 2007.

[150] S. Jiang, U. D. Annakkage, and A. M. Gole, "A platform for validation of FACTS models," *IEEE Transactions on Power Delivery*, vol. 21, no. 1, pp. 484–491, Jan 2006.

[151] A. Adamczyk, M. Altin, O. Goksu, R. Teodorescu, and F. Iov, "Generic 12-bus test system for wind power integration studies," in *IEEE European Conference on Power Electronics and Applications (EPE)*, Sept 2013, pp. 1–6.

[152] Coordinador Eléctrico Nacional - SING. Sistema Interconectado Norte Grande. [Online]. Available: http://cdec2.cdec-sing.cl/pls/portal/cdec.pck_web_coord_elec.sp_pagina?p_id=4

[153] ——. (2016, March) Sistema Interconectado Norte Grande - Esquema Geográfico. [Online]. Available: http://cdec2.cdec-sing.cl/pls/portal/cdec.pck_web_coord_elec.sp_pagina?p_palabra=mapa+sing&p_id=1

[154] ——. Base de datos del SING. [Online]. Available: http://cdec2.cdec-sing.cl/pls/portal/cdec.pck_web_coord_elec.sp_pagina?p_id=1087

[155] P. M. Anderson and A. A. Fouad, *Power System Control and Stability*. Wiley-Interscience, 2003.